Analytical modeling of Cosmic Winds and Jets

Nektarios Vlahakis

Ph.D. thesis
University of Crete
Heraklion 1998

Αναλυτικά μοντέλα αστροφυσικών ανέμων και πιδάκων πλάσματος

Νεκτάριος Βλαχάκης

Διδακτορική διατριβή
Πανεπιστήμιο Κρήτης
Ηράκλειο 1998

Επιβλέπων καθηγητής:
Τσίγκανος Κανάρης, καθηγητής

Επιτροπή αξιολόγησης:
Τσίγκανος Κανάρης, καθηγητής
Βεντούρα Ιωσήφ, καθηγητής
Κυλάφης Νικόλαος, καθηγητής
Οικονόμου Ελευθέριος, καθηγητής
Τομαράς Θεόδωρος, καθηγητής
Μουσσάς Ξενοφών, αναπληρωτής καθηγητής
Χαλδούπης Χρήστος, αναπληρωτής καθηγητής.

Πρόλογος

Το φαινόμενο των εκκροών από αστρικά αντικείμενα - άστρα και γαλαξίες - είναι γενικό. Κάθε κοσμικό αντικείμενο χάνει μάζα με μορφή ανέμου και μαζί μ' αυτόν στροφορμή. Το κοντινότερο παράδειγμα είναι βέβαια ο ήλιος. Είναι γνωστά τα φαινόμενα που οφείλονται σε σωματίδια που έρχονται από τον ήλιο στην ατμόσφαιρα της γής (πολικό σέλας, προβλήματα στις επικοινωνίες κατά την διάρκεια των ηλιακών καταιγίδων). Το διαστημόπλοιο Οδυσσέας - το πρώτο που ταξίδεψε έξω από το επίπεδο της εκλειπτικής - μας έδειξε ότι ο ηλιακός άνεμος μεταβάλεται αρκετά καθώς κινούμαστε από τον ισημερινό προς τους πόλους. Το διαστημικό τηλεσκόπιο Hubble έχει παρατηρήσει πλήθος εκκροών από σχεδόν όλα τα είδη αστρικών αντικειμένων (πρωτοαστέρες, δραστήρια κέντρα γαλαξιών κ.λ.π.). Οι πιο πολλές από αυτές έχουν την μορφή πίδακα πλάσματος, εστιασμένης εκκροής που εκτείνεται σε αποστάσεις χιλιάδων αστρονομικών μονάδων από το κεντρικό σώμα, τα jets.

Παρά την πληθώρα αυτών των εκκροών, πολλά ερωτήματα που συνδέονται με τον σχηματισμό τους, τους μηχανισμούς επιτάχυνσης της ύλης μέσα σε αυτά, της εστίασης και της μεταφοράς ενέργειας, δεν έχουν πλήρως απαντηθεί. Μια από τις δυσκολίες είναι ότι θεωρητικά αυτή η μορφή ύλης - το πλάσμα - περιγράφεται από το -ακόμα και σε πρώτη τάξη - πολύπλοκο σύστημα των εξισώσεων της μαγνητοϋδροδυναμικής. Όπως είναι γνωστό, είναι μη γραμμικό σύστημα διαφορικών εξισώσεων με μερικές παραγώγους, οι λύσεις του οποίου απαιτείται να περνούν από διάφορες κρίσιμες επιφάνειες. Λίγες κλάσσεις αξισυμμετρικών, στάσιμων λύσεων έχουν βρεθεί, υποθέτοντας κάποιο χωρισμό μεταβλητών στις σημαντικότερες άγνωστες συναρτήσεις. Αυτή η μέθοδος - αποκαλείτε αυτοομοιότητα - μας επιτρέπει να οδηγήσουμε το σύστημα σε διαφορικές εξισώσεις με ολικές παραγώγους, οι οποίες είναι δυνατόν να αντιμετωπιστούν υπολογιστικά. Η επιλογή χωρισμού μεταβλητών επιλέγεται με βάση το συγκεκριμένο αστροφυσικό πρόβλημα. Μέχρι τώρα, όλες οι λύσεις που έχουν βρεθεί ανήκουν σε δυο κλάσσεις αυτοομοιότητας: την μεσημβρινή (Parker 1958, Tsinganos & Trussoni 1991, Sauty & Tsinganos 1994) και την ακτινική (Blandford & Payne 1982, Contopoulos & Lovelace 1994). Με συστηματικό τρόπο, σ' αυτή τη διατριβή βρέθηκαν όλες οι λύσεις αυτών των κλάσσεων καθώς και μια τρίτη κλάσση, αυτή της γενικής αυτοομοιότητας. Επίσης έχει αναλυθεί ο παραμετρικός χώρος σε κάποιες από αυτές τις λύσεις και έχει μελετηθεί η ασυμπτωτική τους συμπεριφορά.

Τα συμπεράσματα και η εμπειρία που αποκτήθηκε, βοηθά στην καλύτερη κατανόηση της φυσικής που ισχύει στο περιβάλλον συμπαγών βαρυτικών σωμάτων.

Abstract

A widespread phenomenon in astrophysics is the outflow of plasma from the environment of stellar or galactic objects. This plasma outflows range from nonuniform winds to highly collimated jets which are common to many stages of stellar evolution. For example, collimated outflows are found around young stars (e.g., as in HH 30), older mass losing stars (as in η-Carinae), symbiotic stars (e.g. in R Aqr), planetary nebulae nuclei (as in the hourglass nebula), black hole X-ray transients (as in GRS 1915+105 and GRO J1655-40), low- and high-mass X-ray binaries and recently also in cataclysmic variables (e.g. T Pyxidis). Similarly, they are also found emerging from the nuclei of many radio galaxies and quasars.

Nevertheless, despite their abundance the questions of the formation, acceleration and propagation of nonuniform winds and jets have not been fully resolved. One of the main difficulties in dealing with the theoretical problem posed by cosmical outflows is that their dynamics needs to be described - even to lowest order - by the highly intractable set of the MHD equations. As is well known, this is a nonlinear system of partial differential equations with several critical points, and only very few classes of solutions are available for axisymmetric systems obtained by assuming a separation of variables in several key functions. This hypothesis allows an analysis in a 2-D geometry of the full MHD equations which reduce then to a system of ordinary differential equations.

By a systematic method we construct general classes of exact and self-consistent axisymmetric MHD solutions.

The unifying scheme contains three large groups of exact MHD outflow models, (I) meridionally self-similar ones with *spherical* critical surfaces, (II) radially self-similar models with *conical* critical surfaces and (III) generalized self-similar models with arbitrary shape critical surfaces. This classification includes known polytropic models, such as the classical Parker description of a stellar wind and the Blandford and Payne (1982) model of a disk-wind; it also contains nonpolytropic models, such as those of winds/jets in Sauty and Tsinganos (1994), Lima et al (1996) and Trussoni et al (1997). Besides the unification of all known cases under a common scheme, several new classes emerge and some are briefly analyzed; they could be explored for a further understanding of the physical properties of MHD outflows from various magnetized astrophysical rotators.

We also propose a new class of exact and self-consistent MHD solutions which describe steady and axisymmetric hydromagnetic outflows from the magnetized atmosphere of a rotating gravitating central object with possibly an orbiting accretion disk. The plasma is driven by a thermal pressure gradient, as well as by magnetic rotator and radiative forces. At the Alfvénic and fast critical points the appropriate criticality conditions are applied. The outflows start almost radially but after the Alfvén transition and before the fast critical

surface is encountered the magnetic pinching force bends the poloidal streamlines into a cylindrical jet-type shape. The terminal speed, Alfvén number, cross-sectional area of the jet, as well as its final pressure and density obtain uniform values at large distances from the source. The goal of the study is to give an analytical discussion of the two-dimensional interplay of the thermal pressure gradient, gravitational, Lorentz and inertial forces in accelerating and collimating an MHD flow. A parametric study of the model is given, as well as a brief sketch of its applicability to a self-consistent modeling of collimated outflows from various astrophysical objects. For example, the obtained characteristics of the collimated outflow in agreement with those in jets associated with YSO's.

General theoretical arguments and various analytic self-similar solutions have recently shown that magnetized and rotating astrophysical outflows may become asymptotically cylindrical, in agreement with observations of cosmical jets. A notable common feature in all such self-consistent, self-similar MHD solutions is that before final cylindrical collimation is achieved, the jet passes from a stage of oscillations in its radius, Mach number and other physical parameters. It is shown that under rather general assumptions this oscillatory behaviour of collimated outflows is not restricted to the few specific models examined so far, but instead it seems to be a rather general physical property of an MHD outflow which starts noncylindrically before it reaches collimation. It is concluded thence that astrophysical jets are topologically stable to small amplitude, time-independent perturbations in their asymptotically cylindrical shape. Also, similarly to the familiar fluid instabilities these oscillations may give rise to brightness enhancements along jets.

Contents

Chapter 1

Introduction

In this Chapter we briefly review the available observations for the various classes of cosmic jets. Then, we discuss the numerical and analytical related studies with emphasis on the models which have been proposed so far for their theoretical description.

1.1 Observed classes of cosmic jets

Outflows from astrophysical objects have been known since the beginning of this century. The first highly collimated outflow (or jet) associated with an astrophysical object, was observed on 1917. It was "a line of matter connected to the elliptical galaxy M87" [Cur18].
Much later, it was discovered that the nearest star, our sun, possesses an extended atmosphere, visible only during eclipses, the solar corona. The first question about the solar corona was how far away it extends from the sun. The idea of a hydrostatic extension of the solar atmosphere [Cha57], gives a pressure at infinity that is much larger than the expected pressure of the interstellar medium (ISM). Parker [Par58], was the first to answer this question correctly: the solar corona undergoes a magnetohydrodynamic expansion, the so called solar wind. This idea of the solar wind, is supported by the fact that comet tails are oriented radially away from the sun. Furthermore, the solar wind was confirmed in the early 1960s, by "in situ" measurements of the plasma and magnetic properties of the interplanetary medium, obtained from instruments onboard spacecrafts. Thus, Parker was the first to show how cosmic outflows can be described correctly by using magnetohydrodynamics (MHD).
To this day, the high resolution of the modern instruments, has enabled astronomers to observe in the sky many similar outflows. Most of them are visible due to the emission of lines of various common elements, such as hydrogen, oxygen and sulfur.

The problem of how astrophysical jets are formed, has exercised the minds of astrophysicists for nearly two decades [LB96]. The most acceptable theory

today to describe the closest and better studied jets associated with young stellar objects, is the following:
The outflow has two components, one from the disc of gas which surrounds the stellar (or galactic) object (disc jet) and the other from the central object (stellar jet). For the first, there is a magnetic field which has a strong poloidal component pointing away from the disc plane. The field is tied to the disc owing to the high conductivity of the inner disc material. Thus, the base of the field is approximately in Keplerian rotation around the star (or galaxy). The magnetized fluid is then magnetocentrifugally driven along the field lines, as a bead on a wire [BP82]. The initial outflow speed is low and the plasma moves along the magnetic field lines. In doing so, the fluid gains angular momentum effectively until it reaches the Alfvén surface, where its kinetic energy exceeds the magnetic energy. Then, near the rotation axis, the inertia of the rotating wind enhances the toroidal component of the field to a point where it is capable of collimating the outflow into a jet. Away from the rotation axis, the wind expands freely outward, removing angular momentum from the disc. Of course thermal phenomena are important, at least near the disc [OL98]. The pressure gradient force, helps the gas to escape from the equatorial plane. Mass loss rates 10^{-6} to $10^{-8} M_{\odot} yr^{-1}$ are typical for this component of the outflow [PL95].

For the second component of the outflow, which has its origin at the stellar surface, the explanation is similar. This component is believed to have higher velocities (of order of the escape speed from the surface of the star) and lower mass loss rates than the previous, the one from the disc.

In the last few years, an increasing number of YSO jets has been found where the optical jet structures are associated with Herbig-Haro objects (HH). Almost fifty years ago, George Herbig and Guillermo Haro independently discovered a number of compact nebulae (shock-excited nebulae). By the early 1980s, several HH objects were shown to be of partially ionized plasma moving away from the energy source at speeds of 100 to over 1000 km/s [BMR]. They are formed in molecular clouds containing young low-mass stars, and are considered as important signposts of very resent star formation [RBG+86]. Most often the energy source, if found, is deeply embedded in the molecular cloud (only in a few cases, an optically visible star has been identified as the driving source). Millimeter wavelength observations of carbon monoxide (CO) revealed many molecular outflows, of velocities 3 to 100 km/s. Astrophysicists now believe that HH objects and CO outflows are different manifestations of the mass and angular momentum loss phenomenon during star formation. Observations indicate that jets ejected by young stars are the energy source for HH objects. When such jets interact with CO molecular outflow, they accelerate the later. In some cases, shock surfaces are formed by the interaction of faster jet fluid elements moving into the slower molecular fluid elements. These may be the so called molecular "bullets" [BMR].

Jets have ejection velocities of order of several hundred kilometers per second for low mass stars, and in excess of 10^3 km/s for high luminosity sources. Jet densities vary from 10^2 to over 10^5 cm^{-3}.

In the last few years, Hubble Space Telescope (HST) has been used to observe

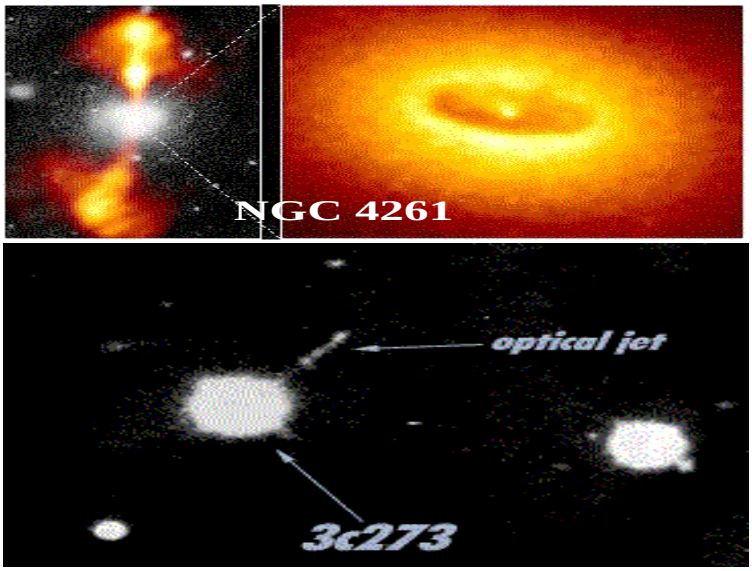

Figure 1.1: Jets from AGN, quasars.

several jets in the sky (in particular inside our galaxy). Up to now, highly collimated jets have been observed from a wide variety of astrophysical objects:

- *active galactic nuclei (AGN) & quasars*, e.g., M87, 3C273, NGC 4261, etc.
- *young stellar objects (YSOs)*, e.g., HH30, HH34, HH111, etc.
- *planetary nebulae nuclei (PNN)*, e.g., the Egg Nebula, etc
- *high- mass X ray binaries (HMXBs)*, e.g., SS433, etc.
- *low- mass X ray binaries (LMXBs)*, e.g., GRO J1655-40, GRO J0422+32, etc.
- *symbiotic stars*, e.g., R Aquarii, CH Cygni, etc.
- *black hole X-ray transients or microquasars*, e.g., GRS 1915+105, etc.
- *cataclysmic variables (CVs)*, e.g., T Pyxidis, etc.
- *super soft X-ray sources (SSSs)*, e.g., CAL 83, 87, etc.

Next we briefly describe jets from these objects.

1.1.1 Jets from AGN

One of the most interesting objects in the universe is the active galactic nucleus, which is generally believed to consist of a supermassive black hole

($M \gtrsim 10^9 M_\odot$) and an accretion disk which surrounds it [LB69]. Then the huge amounts of energy released will build up a pressure so great that it forces away matter residing close to the black hole. The matter is forced away in the directions offering less resistance, i.e. the directions normal to the accretion disk. The out-thrown matter forms usually two streams. Some AGN have jets which extend to a few megaparsec scales beyond the host galaxies. Their velocities cover a wide range, from a few hundred kilometers per second to nearly the speed of light [BBR84]. AGN jets are effectively adiabatic [Ray98]. They shine via synchrotron emission from the most energetic electrons, which have Lorentz factors $\gamma \gtrsim 10^3$ [Bir96]. A typical example of an AGN jet is NGC 4261 and a jet associated with a QSO is 3C273, (Fig. 1.1).

1.1.2 Jets from YSOs

Stellar jets in the HST era can be used as "laboratories" to verify our models of the MHD evolution of jets by direct comparison with observations. Stellar jets are sufficiently near, so that we can measure proper motions, radial velocities and the location of components on the plane of the sky with high angular resolution.

Jets from YSOs (e.g., from T Tauri stars) are highly supersonic, with Mach numbers $\gtrsim 20$, and are very well collimated, at least several hundred AU from their source. Their total length varies from a few hundred AU to several tenths of a parsec. The jet is initially poorly focused before being asymptotically collimated into a "column" with diameter of order a few tens of AU. The initial opening angle is very large ($\gtrsim 60^o$ for the HH 30 jet) [RMD+96]. Observations show that most jets from YSOs are associated with accretion disks. The radius of the disk is about 100 AU, the disk magnetic field ≈ 0.1 G and the mass loss rate from the disk is $\approx 10^{-7} M_\odot yr^{-1}$ [KT88]. Jet velocities are usually in the range 200-1000 km/s. Typical examples of such jets are HH30, HH34, HH47, HH111 (Figs. 1.2-1.5).

1.1.3 Jets associated with PNN

Almost 95 % of all stars that we see in our own galaxy, including the sun, will become one day "planetary nebulae". The other 5 % (those with masses larger than 8 $M_\odot$) will end their lives as supernovae.
The name "planetary nebulae" is a misnomer; it arose when over a century ago astronomers saw these objects as compact, green-coloured objects that reminded them the view of Uranus. These objects are not made of planets. They are the gaseous and dusty material expelled by a geriatric star just before death.
The commonly accepted model for the formation of planetary nebulae is the interacting stellar winds model. A solar mass star, while on the asymptotic giant branch, losses mass steadily through a "superwind" with a velocity of 10 km/sec and mass loss rate 10^{-4} to $10^{-5} M_\odot yr^{-1}$. Toward the end of the asymptotic giant branch stage the star switches to loosing mass in the form of a fast wind with a velocity rising up to 2000 km/sec, albeit with a lower mass-loss rate

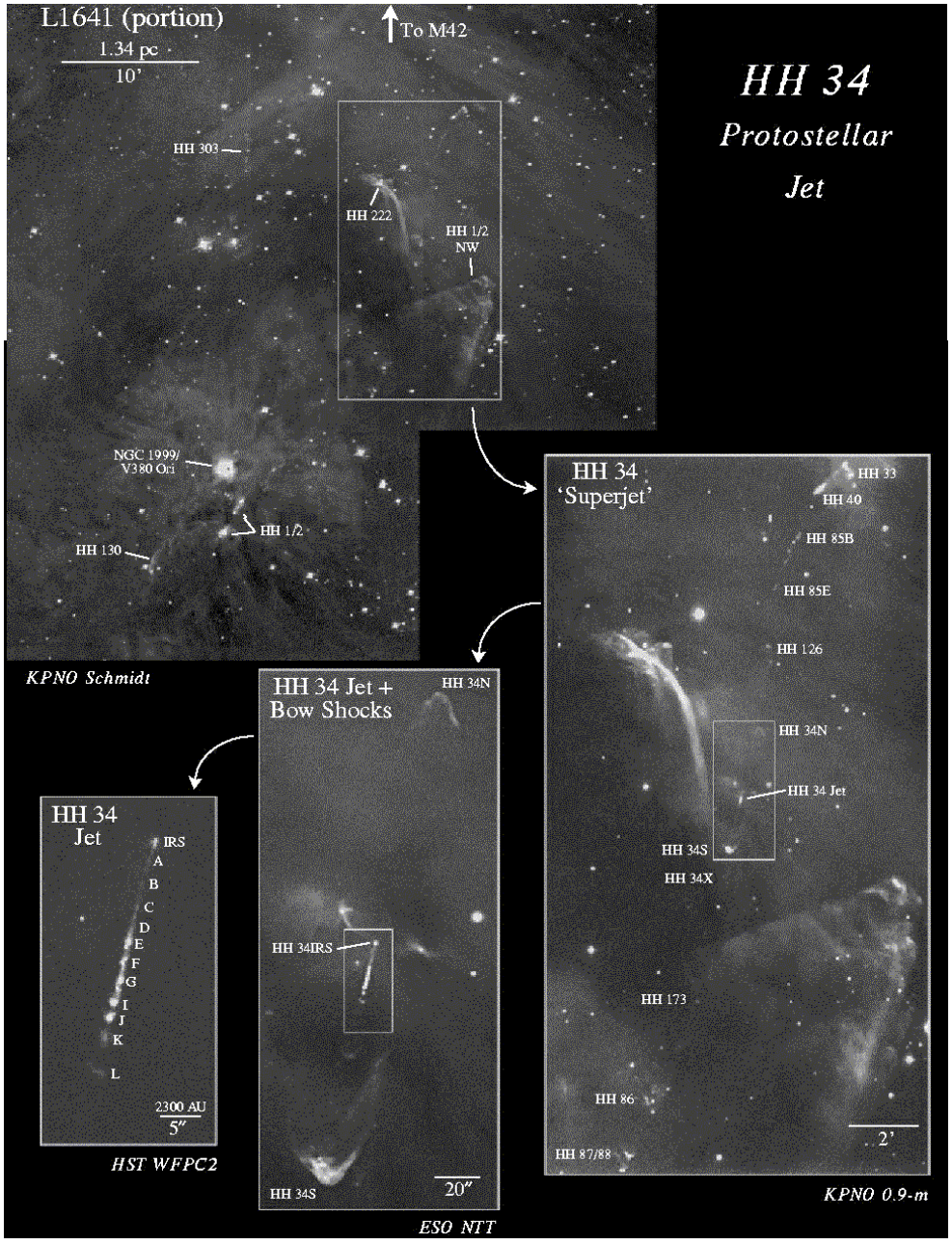

Figure 1.2: Ground based and HST images in $H\alpha + [S\ II]$ of the HH 34 system. A scale indicates the relative size of each frame. *Upper left.* KPNO 0.6 m Schmidt. *Lower right.* KPNO 0.9 m. *Lower middle.* ESO 3.5 m NTT. *Lower left.* HST WFPC2.

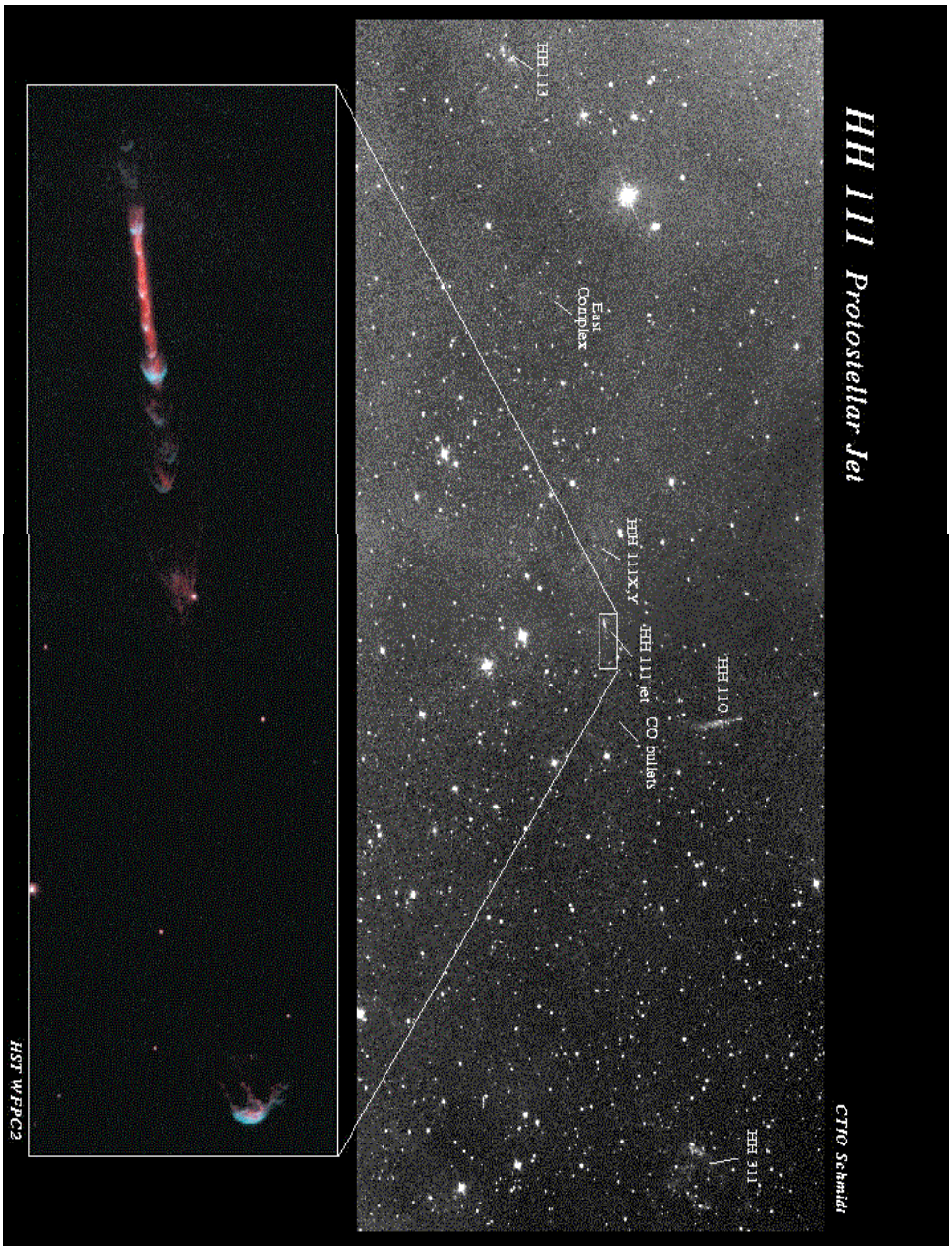

Figure 1.3: The HH 111 system. The top panel shows a 1 degree field of view CTIO 0.6 m Curtis Schmidt image that shows the terminal bow shocks (HH 113 and HH311) at the ends of the outflow. The location of HH 111 is indicated by the rectangle near the middle of the image. The bottom panel shows the HST image of the HH 111 jet. In the colour image $[S\ II]$ is red and $H\alpha$ is cyan.

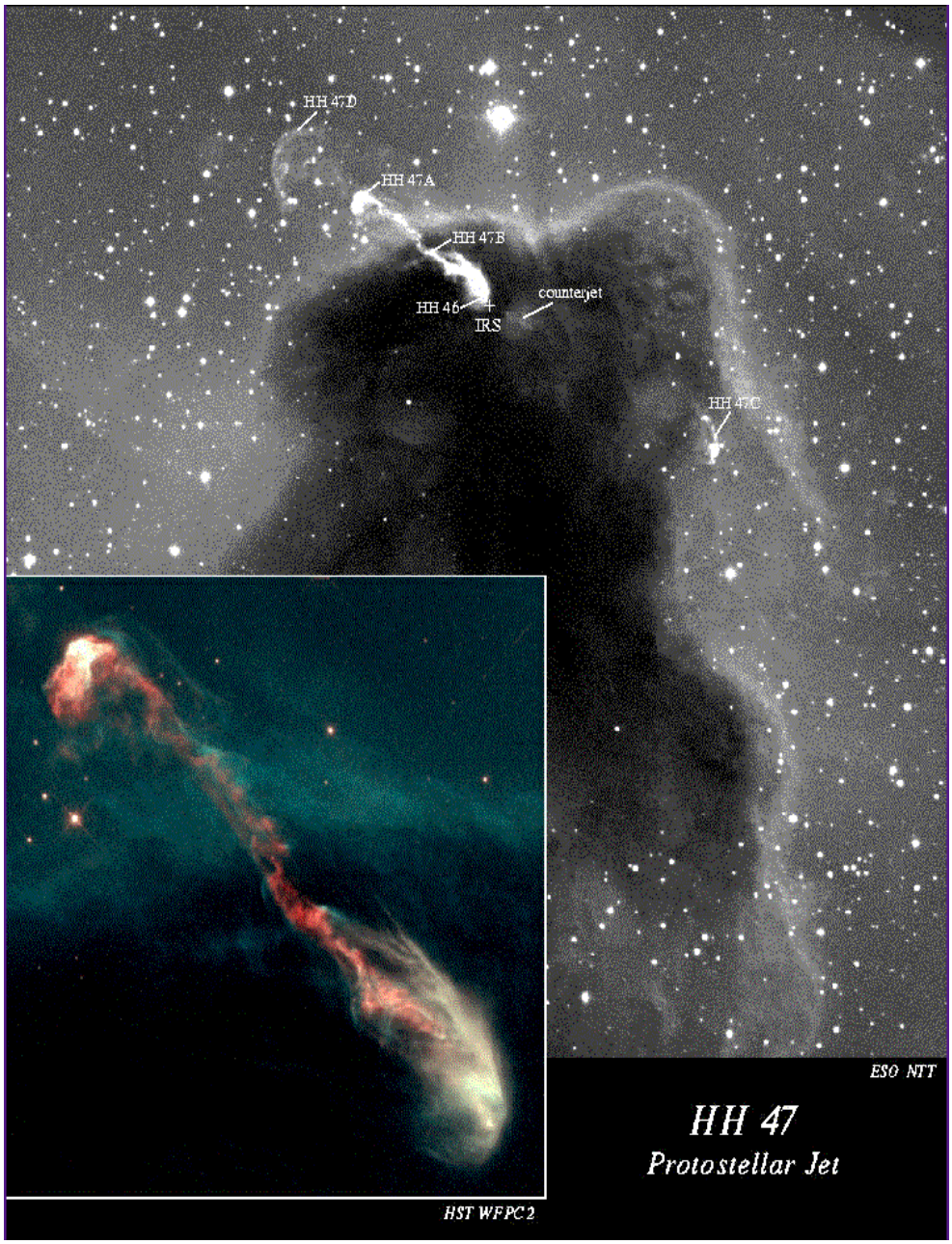

Figure 1.4: Ground based and HST images of the HH 46/47 system. *Background.* 3.5 m ESO NTT. *Foreground.* HST WFPC2. In the colour image $[S\ II]$ is red and $H\alpha$ is cyan.

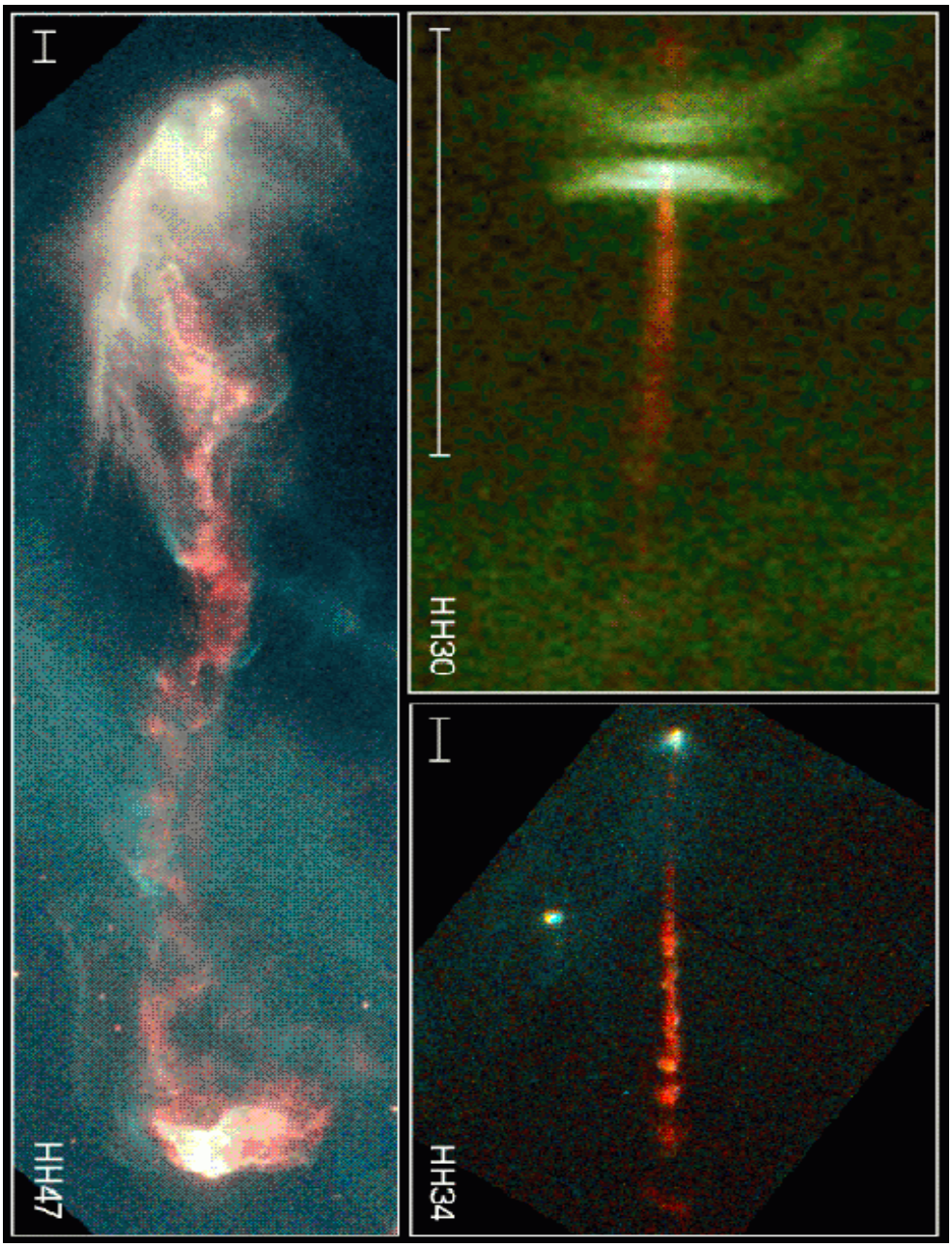

Figure 1.5: **HH30**: The newly forming star is hidden behind the densest parts of the disk. This protostar is 450 light-years away in the constellation of Taurus. **HH34**: This protostar is 1500 light-years away in the vicinity of the Orion Nebulae. **HH47**: The HH 47 system is 1500 light-years away, and lies at the edge of the Gum Nebulae, possibly an ancient supernova remnant which can be seen from Earth's southern hemisphere.
The scale on the bottom left corner of each picture represents 1000 AU. All images were taken with the Wide Field Planetary Camera 2 (WFPC2) in visible light.

10^{-8} to $10^{-6} M_{\odot} yr^{-1}$. The fast wind catches up with the slow wind and drives a shocked shell through it. A contact discontinuity is formed at the interface between the shocked slow and fast winds. The slow wind shell is identified with the visible boundary of the planetary nebulae. The outer edge of the shell is the outward moving shock, whereas the contact discontinuity separates the shell from the shocked fast wind material.
Deviations from sphericity are normally attributed to a nonuniformity in the slow "superwind", which leads to an asymmetry in the shape of the shell [VCB96, Che88]. See also [BK95]. Typical examples are the Egg Nebula, the Siamese Squid Nebula, etc (Fig. 1.6).

1.1.4 Jets from X-ray binaries

X-ray binaries [1] are binary stellar systems which are extremely bright at X-ray wavelengths. They consist of an ordinary star circling around a collapsed, relativistic object: a neutron star or a black hole [KK96]. A typical mass for this object is one solar mass and a typical radius about 15 km. The gravity at the surface of this object is enormous, so if any matter falls onto the surface, it produces an enormous amount of energy, which we see as X-rays.
The companion star (a supergiant of approximately ten solar masses) is very close to the compact object: typically its period is only a few hours. This massive primary star usually possesses a strong stellar wind. The gravitational pull of the compact object will lead to the capture of some fraction of this stellar wind. This means that some matter spills off the surface, forms an accretion disk and falls into the compact object, producing X-rays.
In some cases, the surface of the primary star, is near the Roche lobe of the compact object. Then, the wind-supplied accretion will be augmented by a tidal stream.
In every case when an accretion disk exists, a jet is usually observed. The prototype of jets from such X-ray binaries is the famous SS433 wherein the velocity of the ejected material is about $0.26\,c$.

1.1.5 Jets from symbiotic binaries

Symbiotic binaries are composed of two stars that orbit each other with a period of one year or more. One star is a red giant with mass approximately one solar mass but of course much bigger radius than the sun. The other star is a white dwarf (a very compact and hot star). Our Sun will eventually become a red giant, and later on a white dwarf, so symbiotic binaries tell us about the future of our own star. The red giant is loosing material via a stellar wind, and this is lit up by the nearby white dwarf. The system creates both the nebula and the jet. A typical example of this kind of binary system, is R Aquarii. The jet from this binary has been examined by many authors [KHM83, DBL+95, Kaf96]. Optical images show two knots of emission (C_1 , C_2) which consist of several discrete

[1] High- or Low- mass X-ray binaries; it depends on the mass of the ordinary star [UKG98].

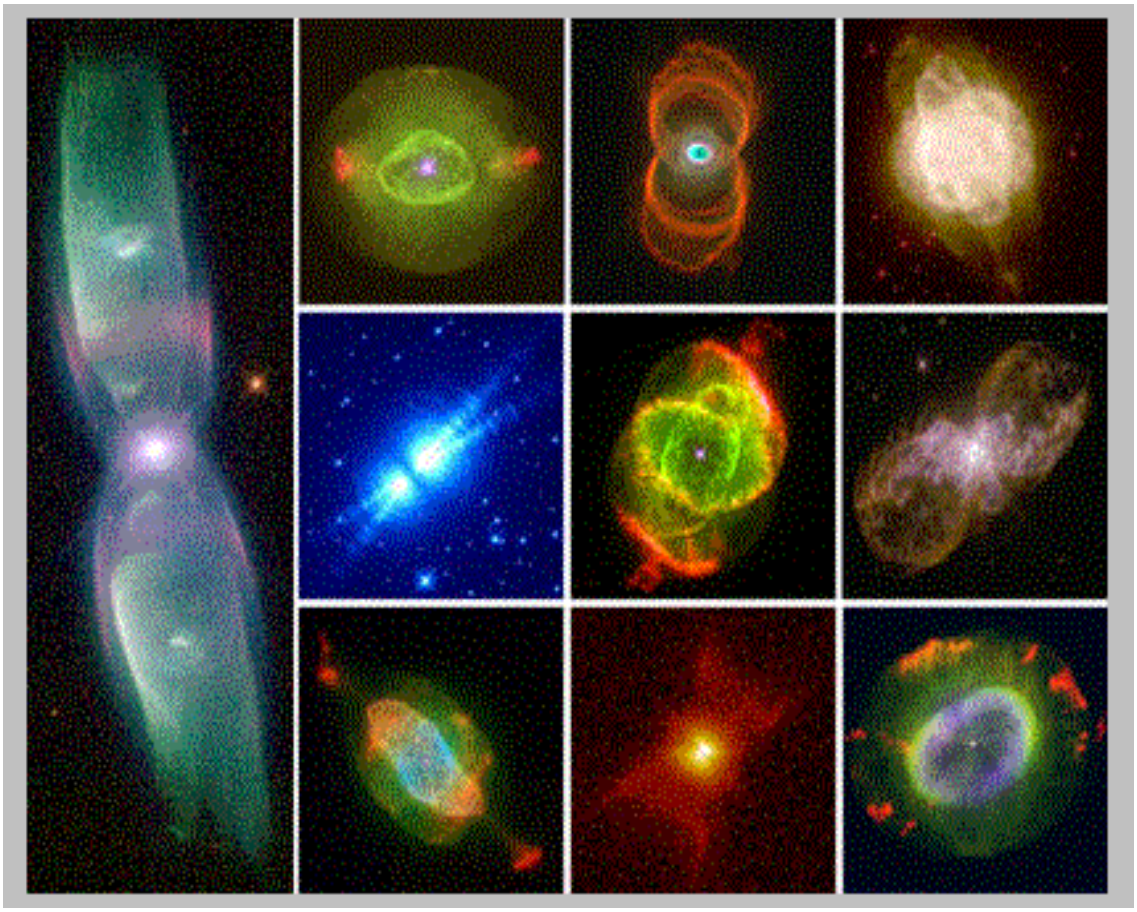

Figure 1.6: A montage of images of planetary nebulae made with the HST. These illustrate the various ways in which dying stars eject their outer layers as highly structured nebulae. In the left panel, the
M2-9 "Siamese Squid Nebula" or "Twinjet Nebula" while the other nine from left to right and from top to bottom are
NGC 6826 "Blinking Eye Nebula"
MyCn 18 "Hourglass Nebula"
NGC 3918
CRL 2688 "Egg Nebula"
NGC 6543 "Cat's Eye Nebula"
"Hubble's Double Bubble" (from the dying star Eta Carinae)
NGC 7009 "Saturn Nebula"
"Red Rectangle"
NGC 7662 "Blue Snowball Nebula".

features, which are part of a continuous, well collimated stream of material. It is now thought that these discrete features are condensations associated with the expanding "inner" nebula which have been shock excited by a highly collimated, supersonic wind (with velocity 400-600 km/s) from the binary system [Sol92].

1.1.6 Jets from black hole X-ray transients

The well known example of this category, is GRS 1915+105, a superluminal source. It is the first source where the proper motions of both the approaching and receding condensations can be detected and measured [2]. It is commonly believed that in these accretion-powered X-ray sources, the acceleration and the collimation of the ejection material is magnetohydrodynamic. Observations suggest that this superluminal motion corresponds to actual bulk motions of massive plasma clouds rather than the propagation of shocks [MR96]. In the later case, one would expect more erratic fluctuations in the proper motions than the observed ones. The velocity of the ejected material is highly relativistic $V \approx 0.92\ c$.

1.1.7 Jets from cataclysmic variables

Cataclysmic variables are characterized by their eruptive behaviour, induced by mass transfer between two stars. The secondary star is typically a Main Sequence star that is less massive than its compact companion, which is filling its Roche Lobe and transferring mass to the primary. These systems have small orbits, with orbital periods typically ten hours. The first observed collimated jet associated with a CV is in the nova T Pyxidis [SLSC97]. Typically, outflows from CVs are observed to have velocities in the range 3000-5000 km/s (measured by the Doppler shifted emission lines); these are of the order of the escape velocity from the central object.

1.1.8 Jets from SSSs

They consist of a white dwarf which accretes mass from an evolved companion at high rates ($\gtrsim 10^{-7} M_{\odot}\, yr^{-1}$), that hydrogen burns steadily on the white dwarf surface [vdHBNR92]. This is the energy source which is always needed in order to have collimated outflows [Liv97]. From the blue- and red- shifted emission lines the jet velocities are of the order of 10^3 km/sec.

1.2 The MHD theoretical description

Among the main goals of research on jets associated with YSOs is to probe the nature of the physical processes that operate within several Astronomical Units

[2] In the case of quasars, only the proper motions of the approaching condensation have been measured.

(AUs) of a young star, to learn about the potential existence of physical conditions that might lead to the formation of planets, and to understand how stars and planetary systems form. The interplay between models and observations may help us in estimating quantities for the star itself, or in understanding the energy transfer mechanisms which is a yet unresolved problem in astrophysics. Analogously, the research on jets from compact objects and AGN is aiming at understanding the extreme physical conditions prevailing around stellar or galactic black holes. In all cases, jets can be regarded as probes for understanding what is happening in exotic and enigmatic environments directly inaccessible to present day observations.

In the various mechanisms which are currently being investigated for accelerating and collimating astrophysical outflows in galactic and extragalactic scales, magnetic rotator forces seem to play a rather dominant and crucial role [LB96]. *First*, thermal gas pressure driven models are based on the *de Laval nozzle* analogy of the solar wind [Par63, LS97]. This requires temperatures of order 10^6 K to drive the observed several 100 km s^{-1} flows in YSO jets. However, if the temperature in the source region of YSO jets is also 10^4 K as observed along the jets, these temperatures are two orders of magnitude lower than required. Of course this limitation does not apply to the X-ray emitting coronae around stars and AGN. *Second*, magnetic pressure driven models are based on the *uncoiling spring* analogy and have been examined by Draine [Dra83] and Uchida & Shibata [US85] (see also Contopoulos [Con95]). There, it is assumed that a toroidal magnetic field B_ϕ is created and highly amplified by the winding-up of its field lines by a radially collapsing and non-Keplerian rotating disk. Plasma is then accelerated from the disk in the poloidal direction by the action of the resulting torsional Alfvén waves. A critique usually attributed to these models of transient bipolar outflows has to do with the Parker instability of the accumulated strong azimuthal magnetic field [Par66, MHSH88]. *Third*, magnetocentrifugally driven outflow models are based on the classical *bead on a rotating rigid wire* analogy [BP82, PP92, CL94]. There, the magnetized fluid is flung out from the surface of the accretion disk, provided that the poloidal field lines are inclined by less than 60° from the disk midplane, although in a relativistic treatment outflows very close to a sufficiently fast rotating Kerr black hole will be launched even when the initial angle is close to 90° [Cao97]. An idealized situation would have the poloidal field lines perpendicular to a thin disk. For distances further away and for not a very rapid rotation, the less than 60° angle requirement would not be satisfied, as noted by Blandford & Payne [BP82], not to mention other inherent difficulties of these self similar models, such as the pinching off in the jet radius at finite vertical heights and the singular electric current density at the symmetry axis.

In another type of model, the interaction of magnetosphere with its surrounding accretion disk, results in the opening of some of the magnetospheric field lines. Thus the disk-magnetosphere boundary creates a stellar wind, the so called "X-wind" [SLRN88, SNO+94, NS94].

Heyvaerts and Norman [HN89] have been shown that polytropic outflows either become cylindrical at large distances from the source or parabolic, de-

pending on whether they carry an electric current to infinity or not.

Definitely, magnetic fields play an important role in the described outflows. The part of physics which describes this kind of matter is magnetohydrodynamics. As we may see in the next Chapters, it consists of a system of partial differential equations (PDE). Up to now, researchers follow two different approaches to solve the MHD equations:

1. Solve the time-dependent problem. To find a steady state is a difficult task. Instead they follow the evolution in time of some initial configurations. They choose an initial state and numerically find a steady state (if exists). For example Bogovalov [Bog96, BT99] studies what happens if plasma is outflowing in a rotating monopole-like field. Some researchers have developed the PPM numerical code [Bod98, CW84]. However, some of these studies have problems in satisfying Maxwell's equation $\vec{\nabla}\cdot\vec{B}=0$. For time dependent numerical simulations see also [SU90, WS93, GWB97].

2. Solve the time-independent problem. The steady state equations, which we try to solve in the following Chapters of this thesis, are rather difficult to be solved due to the fact that the equation for the poloidal magnetic field is a mixed elliptic-hyperbolic partial differential equation (PDE). Also there are various singular points, the position of which is not known a-priori, but can be determined only simultaneously with the solution. These steady state equations have not be solved yet numerically.
   Here, we shall solve them quasi-analytically, i.e. after a judicious separation of the variables we solve numerically the resulting ordinary differential equations (ODE).
   We concentrate on the dynamics of the flow and not on the energetics, since the later is not known yet (even for the sun, we don't know how the solar corona is heated to high temperatures).

1.2.1 The hypothesis of self similarity

The investigation of plasma equilibria is one of the most important problems in magnetohydrodynamics (MHD), and arise in a variety of fields, such as thermonuclear fusion, astrophysics and solar physics, to mention just a few.

At present, difficulties associated with describing fully three-dimensional (3-D) equilibrium configurations are far from being resolved. For that reason, considering configurations with additional symmetries is imperative from the mathematical point of view. Fortunately, these configurations are the most interesting and important ones from the physical viewpoint as well. In many astrophysical situations (solar wind, outflows from YSOs, AGN, etc.) and in thermonuclear fusion (tokamaks) axial symmetry is appropriate, in solar physics (evolution of solar arcades) translational symmetry is a dominant one, etc.

As with any fully MHD approach and despite of the simplifications of steadiness and the axisymmetric geometry, several approximations are still unavoidable in order to obtain exact solutions useful for an understanding of the MHD

mechanism for the initial acceleration and final collimation of astrophysical outflows. Thus, one simple analytical way out is the use of self similarity. This hypothesis allows an analysis in a 2-D geometry of the full MHD equations which reduce then to a system of ordinary differential equations. The basis of the self similarity treatment is the assumption of a scaling law of one of the variables as function of one of the coordinates. The choice of the scaling variable depends on the specific astrophysical problem.

Several models self similar in the radial direction have been investigated to analyze the structure of winds from accretion disks [BP82, CL94, LCB92, Li95, Li96, Fer97, Ost97]. In these models that cannot account however for the flow along the polar axis, the driving force and the collimation derive from a combination of the magnetic and centrifugal forces. The absence of an exact crossing of all the existing critical points in the solutions presented in these papers prevents from considering their conclusions as definitive.

In a series of studies, solutions of the MHD equations that are self similar in the meridional direction have been also analyzed [TT90, TT91, TS92, TS92, TT93, ST94, TTS97]. Such a treatment allows to study the physical properties of the outflow close its rotational axis. As in this region the contribution to acceleration of the magnetocentrifugal forces is small, the effect of a thermal driving force is essential. This implies also that the structure of the gas pressure in the flow is essential.

Two main classes of these self similar solutions exist depending on whether the components of the pressure gradient along the radial and meridional directions are or not related. In this second case the shape of the streamlines and fieldlines is prescribed 'a priori', and the main features of the dynamical variables are deduced from the integration. In particular, it has been shown that acceptable solutions for magnetized flows with asymptotic superAlfvénic velocity exist only when rotation is included [TT91, TT93, TTS97]. As a consequence of this study it seems that even pressure confined jets from slow magnetic rotators need magnetic fields and rotation. In the other case, in which the two components of the gas pressure are related, the structure of the streamlines is deduced as a self consistent solution of the MHD equations.

The solutions which we examine in the rest of this thesis, are steady, axisymmetric, nonrelativistic and can be used in order to describe jets from YSOs and PNN. They may also be used in addition to understanding key-elements in the physics of MHD outflows, as initial states for a perturbation analysis, or, to test numerical codes.

Bibliography

[BBR84] M. C. Begelman, R.D. Blandford, and M.J. Rees, Rev. Mod. Phys. **56** (1984), 265.

[Bir96] T. Biretta, *in Solar and Astrophysical MHD Flows*, K. Tsinganos (ed.), Kluwer Academic Publishers, p. 357, 1996.

[BK95] L. Burderi and A.R. King, MNRAS **276** (1995), 1141.

[BMR] J. Bally, J. Morse, and B. Reipurth, *in Science with the Hubble Space Telescope - II*, P. Benvenuti, F. D. Macchetto, E. J. Schreier (eds.).

[Bod98] G. Bodo, *in Astrophysical Jets - open problems*, Massaglia S., Bodo G. (eds.), Gordon and Breach Science Publishers, p. 161, 1998.

[Bog96] S.V. Bogovalov, *in Solar and Astrophysical MHD Flows*, K. Tsinganos (ed.), Kluwer Academic Publishers, p. 411, 1996.

[BP82] R.D. Blandford and D.G. Payne, MNRAS **199** (1982), 883.

[BT99] S.V. Bogovalov and K. Tsinganos, MNRAS (1999), in press.

[Cao97] X. Cao, MNRAS **291** (1997), 145.

[Cha57] S. Chapman, Smithsonian Contr. Ap. **2** (1957), 1.

[Che88] R. A. Chevalier, Nat **332** (1988), 514.

[CL94] J. Contopoulos and R.V.E. Lovelace, ApJ **429** (1994), 139.

[Con95] J. Contopoulos, ApJ **450** (1995), 616.

[Cur18] H. D. Curtis, Publ. Lick. Obs. **13** (1918), 9.

[CW84] P. Colella and P. R. Woodward, J. Comp. Phys. **54** (1984), 174.

[DBL+95] S. M. Dougherty, M. F. Bode, H. M. Lloyd, R. J. Davis, and S. P. Eyres, MNRAS **272** (1995), 843.

[Dra83] B. T. Draine, ApJ **270** (1983), 519.

[Fer97] J. Ferreira, A&A **319** (1997), 340.

[GWB97] A.P. Goodson, R.M. Winglee, and K.H. Bohm, ApJ **489** (1997), 199.

[HN89] J. Heyvaerts and C.A. Norman, ApJ **347** (1989), 1055.

[Kaf96] M. Kafatos, *in Solar and Astrophysical MHD Flows*, K. Tsinganos (ed.), Kluwer Academic Publishers, p. 585, 1996.

[KHM83] M. Kafatos, J. M. Hollis, and A. G. Michalitsianos, ApJ **267** (1983), L103.

[KK96] T. Kudoh and O. Kaburaki, ApJ **460** (1996), 199.

[KT88] J. Kwan and E. Tademaru, ApJ **332** (1988), L41.

[LB69] D. Lynden-Bell, Nature **262** (1969), 649.

[LB96] D. Lynden-Bell, MNRAS **279** (1996), 389.

[LCB92] Z.-Y Li, T. Chiueh, and M.C. Begelman, ApJ **394** (1992), 459.

[Li95] Z.-Y Li, ApJ **444** (1995), 848.

[Li96] Z.-Y Li, ApJ **465** (1996), 855.

[Liv97] M. Livio, *in IAU Colloq. 163, Accretion Phenomena and Related Outflows*, D.T. Wickramasinghe, L. Ferrario, & G.V. Bicknel (eds.), ASP: San Francisco, 1997.

[LS97] K. Liffman and A. Siora, MNRAS **290** (1997), 629.

[MHSH88] R. Matsumoto, T. Horiuchi, K. Shibata, and T. Hanawa, PASJ **40** (1988), 171.

[MR96] I.F. Mirabel and L.F. Rodriguez, *in Solar and Astrophysical MHD Flows*, K. Tsinganos (ed.), Kluwer Academic Publishers, p. 683, 1996.

[NS94] J. Najita and F. H. Shu, ApJ **429** (1994), 808.

[OL98] G. I. Ogilvie and M. Livio, ApJ **499** (1998), 329.

[Ost97] E. C. Ostriker, ApJ **486** (1997), 306.

[Par58] E.N. Parker, ApJ **128** (1958), 664.

[Par63] E.N. Parker, *in: Interplanetary Dynamical Processes*, Interscience Publishers, New York, 1963.

[Par66] E.N. Parker, ApJ **145** (1966), 811.

[PL95] J. C. B. Papaloizou and D. N. C. Lin, Annu. Rev. Astron. Astrophys. **33** (1995), 505.

[PP92] G. Pelletier and R.E. Pudritz, ApJ **394** (1992), 117.

[Ray98] T.P. Ray, *in Astrophysical Jets - open problems*, Massaglia S., Bodo G. (eds.), Gordon and Breach Science Publishers, p. 173, 1998.

[RBG+86] B. Reipurth, J. Bally, J. A. Graham, A. P. Lane, and W. J. Zealey, A&A **164** (1986), 51.

[RMD+96] T. P. Ray, R. Mundt, J. E. Dyson, S. A. E. Falle, and A. C. Raga, ApJ **468** (1996), L103.

[SLRN88] F. H. Shu, S. Lizano, S. Ruden, and J. Najita, ApJ **328** (1988), L19.

[SLSC97] T. Shahbaz, M. Livio, K.A. Southwell, and P.A. Charles, ApJ **484** (1997), L59.

[SNO+94] F. H. Shu, J. Najita, E. Ostriker, F. Wilkin, S. Ruden, and S. Lizano, ApJ **429** (1994), 781.

[Sol92] J. Solf, A&A **257** (1992), 228.

[ST94] C. Sauty and K. Tsinganos, A&A **287** (1994), 893.

[SU90] K. Shibata and Y. Uchida, Publ. Astron. Soc. Japan **42** (1990), 39.

[TS92a] K. Tsinganos and C. Sauty, A&A **255** (1992), 405.

[TS92b] K. Tsinganos and C. Sauty, A&A **257** (1992), 790.

[TT90] K. Tsinganos and E. Trussoni, A&A **231** (1990), 270.

[TT91] K. Tsinganos and E. Trussoni, A&A **249** (1991), 156.

[TT93] E. Trussoni and K. Tsinganos, A&A **269** (1993), 589.

[TTS97] E. Trussoni, K. Tsinganos, and C. Sauty, A&A **325** (1997), 1099.

[UKG98] V. Urpin, D. Konenkov, and U. Geppert, MNRAS **299** (1998), 73.

[US85] Y. Uchida and K. Shibata, Publ. Astron. Soc. Japan **37** (1985), 515.

[VCB96] Dwarkadas. V. V., R. A. Chevalier, and J. M. Blondin, ApJ **457** (1996), 773.

[vdHBNR92] E. P. J. van den Heuvel, D. Bhattacharga, K. Nomoto, and S. A. Rappaport, A&A **262** (1992), 97.

[WS93] H. Washimi and K. Shibata, MNRAS **262** (1993), 936.

Chapter 2

MHD equations

In this Chapter we derive the basic equations which describe plasma outflows from various astrophysical objects, as those discussed in the previous Chapter. Matter is regarded to be fully ionized and nonrelativistic while quantum phenomena are negligible. Examination of the outflows in terms of particle orbit theory is useful in certain situations; however, it is adequate only when the number density of particles is low enough for their interaction to be ignored. On the other hand, when collisional effects are not negligible we use instead the magnetohydrodynamic (MHD) approach which we shall invoke in all this thesis. The MHD description of the plasma essentially describes how inertial, electromagnetic, gravitational and pressure gradient forces interact in a fluid. When we assume the fluid approximation we mean that a given particle remains reasonably close to its neighbouring particles during time scales of interest, so we may divide the plasma into small fluid elements and examine the motion of these "particles".
In this approximation we get equations for the basic physical quantities of the plasma (including the observable ones). One of the principal goals of this thesis is then to find analytical solutions of these equations.

2.1 Deriving the equations

The sun and the other stars are hot enough to be almost completely ionized.

The interstellar gas and the various outflows in the ISM are also ionized, due to the action of stellar radiation. This means that almost the whole universe (about 99 %) can be regarded to be in the plasma state. The plasma state is usually called the fourth state of matter (the other three being the solid, liquid and gaseous).
By a plasma state, we mean a partially or fully ionized gas which contains enough free, charged particles for its dynamical behaviour to be dominated by electromagnetic forces [BS69].
In Fig. 2.1 it is shown the area occupied by classical plasmas which is bounded

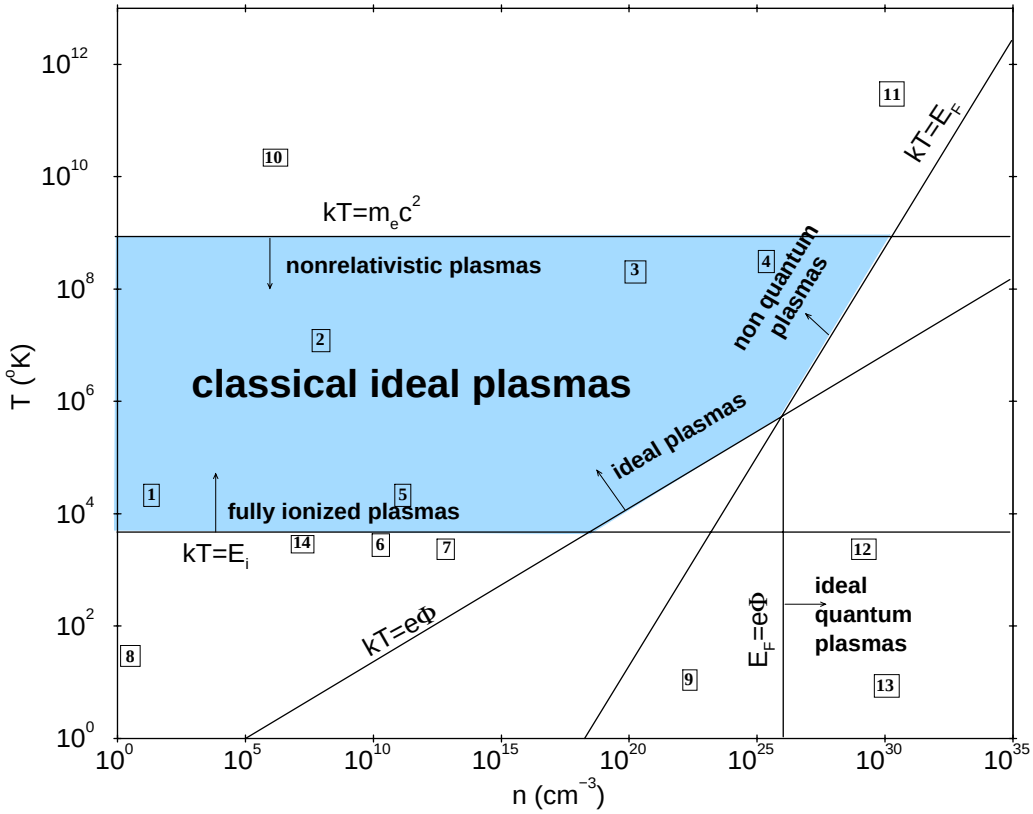

1: Solar wind
2: Solar corona
3: Tokamak
4: Thermonuclear fussion
5: Gas discharge tubes
6: Chromosphere
7: Photosphere
8: Interstellar medium (ISM)
9: Electron gas in metals
10: Pulsar magnetospheres
11: H-bomb
12: Interior of Jupiter
13: White dwarfs
14: Ionosphere

Figure 2.1: Classification of plasmas in a density-temperature plane. The various plasmas in our universe occupy the area indicated by the corresponding number.

by some curves indicating the validity of the corresponding governing equations. In this $n-T$ plane we distinguish the following domains:

- $kT \ll m_e c^2$, i.e., the plasma is nonrelativistic.
- $kT \gg E_i$, i.e., the plasma is almost completely ionized (from the Saha equation the number density of the ions divided by the number density of the hydrogen atoms is proportional to $e^{-E_i/kT}$ where E_i is the ionization energy of the atom).
- $kT \gg e\Phi$, i.e., the plasma is ideal. This means that the Coulomb interaction potential Φ is negligible compared to the thermal energy of the particles. This also means that nl_D^3, the number of particles into the Debye sphere is large, $nl_D^3 \gg 1$.
- $kT \gg E_F$, where E_F is the Fermi energy.
  This means that quantum phenomena are negligible because the mean distance between the particles is much larger than the de-Broglie wavelength $h/m_e\,(2kT/m_e)^{1/2}$.

From Fig. 2.1 it follows that this region of classical plasmas contains almost all non-relativistic gases in the atmospheres of stars and galaxies. In order to derive the relations between the observable quantities (which are functions of space and time), first we remark that matter exhibits a fluid behaviour (the collisions are not negligible so the orbit theory is not valid here). This fluid contains two species: electrons with number density n_e, and ions (protons) with number density n_i. Approximately this fluid is neutral, so $n_e \approx n_i$ (only in spheres with radius smaller than the Debye length l_D, which is much less than the length scale of the fluid, the electric potential Φ is not zero).
The basic description of a classical plasma is given by the kinetic theory of gases which uses statistical mechanics. For each of the species we define the distribution function $f_{e,i}\,(\vec{r},\vec{v},t)$ such that the quantity $f_{e,i}(\vec{r},\vec{v},t)d\vec{r}d\vec{v}$ represents the probability of finding particles (protons for the "i" and electrons for the "e") within the 6-dimensional volume element $d\vec{r}d\vec{v}$, which contains the point $(\vec{r},\vec{v})$ in coordinate and velocity space (phase space) [BS69, Fre82, Tsi92].
The mean value of each quantity can be found if we know this distribution function. For example, the number density of particles in a 3-dimensional volume element $d\vec{r}$ is

$$n_{e,i}\,(\vec{r},t) = \iiint f_{e,i}\,(\vec{r},\vec{v},t)\,d\vec{v}$$

where the integration is in all $\vec{v}$ space, and the mean velocities for ions and electrons are

$$\vec{V}_{e,i}\,(\vec{r},t) = \frac{1}{n_{e,i}} \iiint \vec{v} f_{e,i}\,(\vec{r},\vec{v},t)\,d\vec{v}\,.$$

The total derivative of this function $f_{e,i}$ with respect to time is not zero due to collisions :

$$\frac{df_{e,i}}{dt} = \left(\frac{\partial f_{e,i}}{\partial t}\right)_C \text{, or, } \frac{\partial f_{e,i}}{\partial t} + \left(\vec{v}\cdot\vec{\nabla}\right) f_{e,i} + \left(\frac{\vec{F}_{e,i}}{m_{e,i}}\cdot\vec{\nabla}_{\vec{v}}\right) f_{e,i} = \left(\frac{\partial f_{e,i}}{\partial t}\right)_C$$

where $\vec{F}_{e,i}$ is the total force acting on electrons and ions (Lorentz force, gravitational force, ratiative force e.t.c.). This equation is the kinetic equation in its most general form.
If the collision term (the RHS of the previous equation) is given on the basis of the two-body interaction [BS69] we obtain the Boltzmann equation. By taking various velocity moments of this equation we obtain relations between functions of space and time only (like the observable quantities). In particular, the zero-order moment of the distribution function corresponds to the number density, the first-order moment to the mean velocity, the second-order moment to the pressure and temperature and the third-order moment to the heat flux. The scalar pressure can be defined by $P_{e,i} = \frac{m_{e,i}}{3} \iiint v^2 f_{e,i}\left(\vec{r}, \vec{v}, t\right) d\vec{v}$. It must be noted that $f_{e,i}$ in general may not be isotropic in velocity space, in which case the concept of a scalar pressure may be inappropriate. In this case we must take into account all the components of the pressure tensor [Tsi92, GR95]. But these equations are not all very useful because there is a closure problem involving moments of higher order: there is always one more variable than there are equations. An approximate solution to this problem is the ideal MHD description we discuss in the following.
First we introduce single-fluid variables:
$P = P_e + P_i$, total pressure,
$\rho = n_e m_e + n_i m_i \approx n_i m_i$, total mass density,
$\vec{V} = \left(n_e m_e \vec{V}_e + n_i m_i \vec{V}_i\right) / \left(n_e m_e + n_i m_i\right) \approx \vec{V}_i$, (because $m_i \gg m_e$ while as we shall discuss later $\vec{V}_i \approx \vec{V}_e$), bulk flow speed (momentum of the fluid),
$\delta = n_e q_e + n_i q_i = \left(n_i - n_e\right) \mid e \mid$, total charge density, and
$\vec{J} = n_e q_e \vec{V}_e + n_i q_i \vec{V}_i$, current density.
Next, if we assume that the distribution function is close to a Maxwellian one, (collisions, being a random process, tend to smooth out any anisotropies so that within a few collision times the local distribution functions for both, ions and electrons, approach Maxwellian distributions), we get to the lowest order the equations (for Maxwellian distributions, $P_e \approx P_i \approx P/2$):

$$\left(\frac{\partial}{\partial t} + \vec{V} \cdot \vec{\nabla}\right) \rho + \rho \vec{\nabla} \cdot \vec{V} = 0 \text{ (continuity equation)},$$

$$\rho \left(\frac{\partial}{\partial t} + \vec{V} \cdot \vec{\nabla}\right) \vec{V} = -\vec{\nabla} P + \delta \vec{E} + \frac{1}{c} \vec{J} \times \vec{B} - \rho \vec{\nabla} \mathcal{V} + \vec{F}_{rad} \text{ (momentum equation)}$$

where $\mathcal{V}$ is the gravitational potential and $\vec{F}_{rad}$ is the volumetric force due to radiation (this equation is often called the Euler equation-Euler(1755)),

$$\rho \left(\frac{\partial}{\partial t} + \vec{V} \cdot \vec{\nabla}\right) \frac{P}{\left(\Gamma - 1\right) \rho} + P \vec{\nabla} \cdot \vec{V} = q \text{ (energy equation)}$$

with Γ the ratio of the specific heats of the gas: $\Gamma = c_p / c_v$. The volumetric heating rate q is the sum of all heating sources. There are heating fluxes due to particle conduction, due to the net radiation, to the nuclear reactions, to

viscous and wave heating, ohmic dissipation etc.
Using the continuity equation, the last relation is equivalent with to first law of thermodynamics

$$q = \frac{\rho^{\Gamma}}{\Gamma - 1}\frac{d}{dt}\left(\frac{P}{\rho^{\Gamma}}\right) = \rho\left[\frac{d}{dt}\left(\frac{P}{(\Gamma-1)\,\rho}\right) + P\frac{d}{dt}\left(\frac{1}{\rho}\right)\right] .$$

Note that the comoving derivative $d/dt = \partial/\partial t + \vec{V}\cdot\vec{\nabla}$ for each function of space and time, represents the temporal changes within an element moving with velocity $\vec{V}$.
These equations together with Maxwell's equations and Ohm's law

$$\vec{\nabla}\cdot\vec{B} = 0 \text{ (no magnetic monopoles exist)}$$

$$\vec{\nabla}\cdot\vec{E} = 4\pi\delta \text{ (Gauss law)}$$

$$\vec{\nabla}\times\vec{B} = \frac{4\pi}{c}\vec{J} + \frac{1}{c}\frac{\partial\vec{E}}{\partial t} \text{ (Ampere's law)}$$

$$\vec{\nabla}\times\vec{E} = -\frac{1}{c}\frac{\partial\vec{B}}{\partial t} \text{ (Faraday's law)}$$

$$\vec{E} = -\frac{1}{c}\vec{V}\times\vec{B} \text{ (Ohm's law for a perfect conductor)}$$

form a closed system (for a known volumetric heating rate q). The fields $\vec{E}\,,\vec{B}$ are in inertial frame.

In these equations, because $n_e \approx n_i\,,\delta \approx 0$ (quasi-neutrality of plasma), the force associated with the electric field in the momentum equation is negligible (it is much smaller than the Lorentz force).
Because the distribution functions for ions and electrons are almost equal to each other (both are close to Maxwellian distributions), the velocities $\vec{V}_e \approx \vec{V}_i$: this is the reason why we may see the motion of a plasma as the motion of a neutral gas with velocity $\vec{V}$. Though these velocities are close to each other, they are not equal, and a nonzero current density is produced.

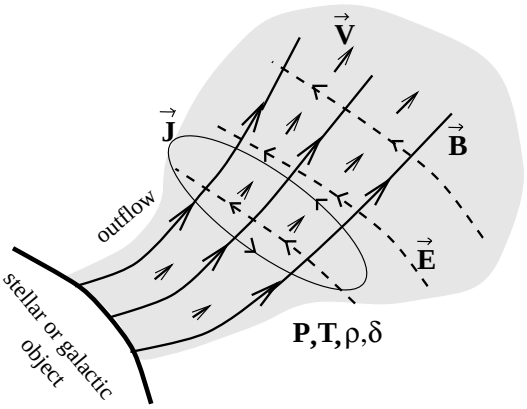

Figure 2.2: Plasma outflow from a cosmic object

2.2 Integrals for steady flows with an ignorable coordinate

In this section we present the Euler-Maxwell equations for the steady state case (which means that all procedures are exactly the same in all times) and when one coordinate of the system $(x_1\,,x_2\,,x_3)$ (say x_3) is ignorable (which means that all physical quantities depend on $(x_1\,,x_2)$ alone). For example, if the outflow is steady and axisymmetric, then the coordinate ϕ is ignorable and all quantities depend on $(\varpi\,,z)$ in cylindrical coordinates $(z\,,\varpi\,,\phi)$, or on $(r\,,\theta)$ in spherical coordinates $(r\,,\theta\,,\phi)$.

With $\dfrac{\partial}{\partial t}=0$ the MHD equations are:

$$\vec{E}=-\frac{1}{c}\vec{V}\times\vec{B} \tag{2.1}$$

$$\vec{J}=\frac{c}{4\pi}\vec{\nabla}\times\vec{B} \tag{2.2}$$

$$\delta=\frac{1}{4\pi}\vec{\nabla}\cdot\vec{E} \tag{2.3}$$

$$\vec{\nabla}\cdot\vec{B}=0 \tag{2.4}$$

$$\vec{\nabla}\cdot\left(\rho\vec{V}\right)=0 \tag{2.5}$$

$$\vec{\nabla}\times\left(\vec{V}\times\vec{B}\right)=0 \tag{2.6}$$

$$\rho\left(\vec{V}\cdot\vec{\nabla}\right)\vec{V}=-\vec{\nabla}P+\frac{1}{4\pi}\left(\vec{\nabla}\times\vec{B}\right)\times\vec{B}-\rho\vec{\nabla}\mathcal{V}+\vec{F}_{rad} \tag{2.7}$$

$$\rho\vec{V}\cdot\left[\vec{\nabla}\left(\frac{P}{(\Gamma-1)\,\rho}\right)+P\vec{\nabla}\left(\frac{1}{\rho}\right)\right]=q\,, \tag{2.8}$$

with $\dfrac{\partial}{\partial x_3}=0$. From Eq. (2.4), there is a function $A\,(x_1\,,x_2)$ such that $\vec{B}=\vec{\nabla}A\times\vec{\nabla}x_3+\vec{B}_3=\vec{\nabla}\times\left(A\vec{\nabla}x_3\right)+\vec{B}_3$. Similarly, from Eq. (2.5) there exist a function $\Psi\,(x_1\,,x_2)$ such that $4\pi\rho\vec{V}=\vec{\nabla}\Psi\times\vec{\nabla}x_3+4\pi\rho\vec{V}_3$. From Eq. (2.6) there exist a function Φ_0 such that

$$\vec{V}\times\vec{B}=\vec{\nabla}\Phi_0 \tag{2.9}$$

(this function is proportional to the electric potential since $\vec{E}=-\dfrac{1}{c}\vec{V}\times\vec{B}=-\vec{\nabla}\left(\Phi_0/c\right)$). From the $\hat{x}_3$ component of Eq. (2.9) (if we assume that $\dfrac{\partial\Phi_0}{\partial x_3}=0$ or equivalently $E_3=0$, [1] such that there is no electric field in the ignorable direction) we have $\Psi=\Psi\,(A)$. If this is the case, the components of $\vec{V}$ and $\vec{B}$

[1] In [Con94] the axisymmetric case with $E_3\neq 0$ is examined.

on the plane $(x_1\,,x_2)$ (which are usually called the poloidal components, $\vec{V}_p\,,\vec{B}_p$ respectively) are parallel to each other : $\vec{V}_p//\vec{B}_p$. Next Eq. (2.9) together with the $\hat{x}_3$ component of Eq. (2.7) gives that

$$\Phi_0=\Phi_0\left(A\right)\ \text{From now on we put}\ \frac{d\Phi_0}{dA}=\Omega\left(A\right)\,, \tag{2.10}$$

$$\vec{B}_3=\vec{\nabla}x_3\frac{h_3^2\Omega\Psi_A-L\Psi_A}{1-\Psi_A^2/4\pi\rho}\,, \tag{2.11}$$

$$\vec{V}_3=\vec{\nabla}x_3\frac{h_3^2\Omega-L\Psi_A^2/4\pi\rho}{1-\Psi_A^2/4\pi\rho}\,, \tag{2.12}$$

with $L=L\left(A\right)\,,\Psi_A\equiv\dfrac{d\Psi\left(A\right)}{dA}$ and $h_3\left(x_1\,,x_2\right)$ the line element of the coordinate system associated with the x_3- coordinate.
So from these integrations we have

$$\vec{B}=\vec{\nabla}A\times\vec{\nabla}x_3+\vec{\nabla}x_3\frac{h_3^2\Omega\Psi_A-L\Psi_A}{1-\Psi_A^2/4\pi\rho}\,, \tag{2.13}$$

$$\vec{V}=\frac{\Psi_A}{4\pi\rho}\vec{\nabla}A\times\vec{\nabla}x_3+\vec{\nabla}x_3\frac{h_3^2\Omega-L\Psi_A^2/4\pi\rho}{1-\Psi_A^2/4\pi\rho}\,, \tag{2.14}$$

together with the $\hat{x}_1\,,\hat{x}_2$ components of Eq. (2.7) and Eq. (2.8).
The vector Eq. (2.7) leads to two scalar equations in any two independent directions $(\hat{x}_1\,,\hat{x}_2)$ on the poloidal plane. We symbolize the $\hat{x}_1$ component (which contains the derivative $\partial P\left(x_1\,,x_2\right)/\partial x_1$) with $\mathcal{M}_{x_1}=0$ and the $\hat{x}_1$ component with $\mathcal{M}_{x_2}=0$. So the momentum equation can be written in the form $\mathcal{M}_{x_1}\vec{\nabla}x_1+\mathcal{M}_{x_2}\vec{\nabla}x_2=0$.
If we know the volumetric heating rate q or the relation of q with the functions $\rho\,,A\,,P$ and the integrals $\Psi_A\,,L\,,\Omega$ then the previous equations may in general be solved to give $\rho\,,A\,,P$.
The integrals $\Psi_A\,,L\,,\Omega$, in the axisymmetric case where the ignorable coordinate is ϕ and $\vec{\nabla}\phi=\hat{\phi}/\varpi\,,h_3=\varpi=r\sin\theta$, have a special physical meaning :

- first A is the magnetic flux function, which means that the magnetic field-lines in the poloidal plane $(r\,,\theta)$ or $(\varpi\,,z)$ are the lines where the function A is constant
- near the stellar surface when the density is big enough, so $\Psi_A^2/4\pi\rho\ll1$ we have $V_\phi=\varpi\Omega$, so Ω is the angular velocity at the stellar base. If Ω depends on A then we have a differential rotation (each line A=constant has different angular velocity $\Omega=\Omega\left(A\right)$). In general,
  $\vec{V}=\dfrac{\Psi_A}{4\pi\rho}\vec{B}+(\Omega\hat{z})\times\vec{r}=\dfrac{\Psi_A}{4\pi\rho}\vec{B}+\Omega\varpi\hat{\phi}$.
- Ω is related with the electric field: $\vec{E}=-\dfrac{1}{c}\vec{V}\times\vec{B}=-\dfrac{1}{c}\Omega\vec{\nabla}A$.

- L is the total angular momentum carried by the fluid and the electromagnetic field, since $L = \varpi\,(V_\phi - B_\phi/\Psi_A)$.
- Ψ_A is the mass to magnetic flux ratio.

Note that $V_1/B_1 = V_2/B_2 = V_p/B_p = \dfrac{\Psi_A}{4\pi\rho}$ where $V_p\,, B_p$ are the poloidal components of $\left(\vec{V}\,, \vec{B}\right)$ respectively.
The ratio $\Psi_A^2/4\pi\rho$ is the square of the Alfvén Much number M^2, since $M^2 = V_p^2/V_{A,p}^2 = \Psi_A^2/4\pi\rho$ with $V_{A,p} = B_p/\sqrt{4\pi\rho}$ the poloidal Alfvén velocity.

2.2.1 Other forms

The MHD equations can be also derived

- from the covariant differentiation $T^{\alpha\beta}_{;\beta} = 0$ of the energy-momentum tensor $T^{\alpha\beta} = T^{\alpha\beta}_{fluid} + T^{\alpha\beta}_{em}$ where $T^{\alpha\beta}_{fluid} = (e+P)\,u^\alpha u^\beta - P g^{\alpha\beta}$ and $T^{\alpha\beta}_{em}$ are the stress tensors for the fluid and electromagnetic field respectively (in the limit $V/c \ll 1$).
  e is the proper internal energy density, P is the proper pressure, $g^{\alpha\beta}$ is the metric tensor and u^α is the fluid 4-velocity [LL75, Cam86, LMMS86, BT99]
- as the minimizing Euler-Lagrange equations, from a single variational principle [HO78, RP94, GL96].

2.3 Appendix 2.A: Alternative forms of reduced MHD equations

2.3.1 General forms

Assume a generalized curvilinear orthogonal coordinate system $(x_1\,, x_2\,, x_3)$, with line elements $h_i\,(x_1\,, x_2)\;, i = 1, 2, 3$, wherein the coordinate x_3 is ignorable. We introduce the square of the Alfvén Mach number $M^2 = \Psi_A^2/4\pi\rho$ and $\mathcal{S} = V^2/2 + \mathcal{V} - h_3\Omega B_3/\Psi_A$. Then the density is $\rho = \Psi_A^2/4\pi M^2$ while the components of velocity and magnetic field are

$$B_1 = \frac{1}{h_2 h_3}\frac{\partial A}{\partial x_2}\,, B_2 = -\frac{1}{h_1 h_3}\frac{\partial A}{\partial x_1}\,, B_3 = \frac{\Psi_A}{h_3}\frac{h_3^2\Omega - L}{1 - M^2} \text{ and} \tag{2.15}$$

$$V_1 = \frac{M^2}{\Psi_A}B_1\,, V_2 = \frac{M^2}{\Psi_A}B_2\,, V_3 = \frac{1}{h_3}\frac{h_3^2\Omega - LM^2}{1 - M^2}\,. \tag{2.16}$$

Also we assume that the radiative force is negligible compared with the other forces in the momentum equation.
The remaining equations are the $\hat{x}_1-$ and $\hat{x}_2-$ components of the momentum

equation, $\mathcal{M}_{x_1}=0$, or $\frac{\partial \mathcal{S}}{\partial x_1}=-\frac{1}{\rho}\frac{\partial P}{\partial x_1}$ and $\mathcal{M}_{x_2}=0$ or $\frac{\partial \mathcal{S}}{\partial x_2}=-\frac{1}{\rho}\frac{\partial P}{\partial x_2}$ respectively. These two equations can be manipulated in the form (using the Poisson brackets $\{f_1\,,f_2\}=\frac{\partial f_1}{\partial x_1}\frac{\partial f_2}{\partial x_2}-\frac{\partial f_1}{\partial x_2}\frac{\partial f_2}{\partial x_1}$ [Tsi82], or the Jacobian of the two functions $\mathcal{J}\left(\frac{f_1\,,f_2}{x_1\,,x_2}\right)=\frac{\partial f_1}{\partial x_1}\frac{\partial f_2}{\partial x_2}-\frac{\partial f_1}{\partial x_2}\frac{\partial f_2}{\partial x_1}$ [Tsi81])

$$\mathcal{J}\left(\frac{\mathcal{S}\,,A}{x_1\,,x_2}\right)=-\frac{1}{\rho}\mathcal{J}\left(\frac{P\,,A}{x_1\,,x_2}\right)\qquad\left(\text{or }\rho=-\frac{\partial P\left(A\,,\mathcal{S}\right)}{\partial \mathcal{S}}\right)\,, \tag{2.17}$$

$$\begin{aligned}0=&\frac{1}{h_1h_2h_3}\left(\frac{\partial}{\partial x_1}\frac{h_2}{h_1h_3}\frac{\partial A}{\partial x_1}+\frac{\partial}{\partial x_2}\frac{h_1}{h_2h_3}\frac{\partial A}{\partial x_2}\right)-\\&\frac{\Psi_A}{h_1h_2h_3}\left(\frac{\partial}{\partial x_1}\frac{h_2}{h_1h_3}\frac{\Psi_A}{4\pi\rho}\frac{\partial A}{\partial x_1}+\frac{\partial}{\partial x_2}\frac{h_1}{h_2h_3}\frac{\Psi_A}{4\pi\rho}\frac{\partial A}{\partial x_2}\right)+4\pi\frac{\partial P\left(A\,,\mathcal{S}\right)}{\partial A}+\\&\frac{1}{2h_3^2}\left(\frac{L-h_3^2\Omega}{1-M^2}\right)^2\frac{d\Psi_A^2}{dA}-\frac{4\pi\rho L}{h_3^2}\frac{dL}{dA}+4\pi\rho\frac{\left(L-h_3^2\Omega\right)\left(\frac{dL}{dA}-h_3^2\frac{d\Omega}{dA}\right)}{h_3^2\left(1-M^2\right)}\end{aligned} \tag{2.18}$$

Note that if we know the functional form which relates pressure and density $P=P\left(\rho\,,A\right)$ (e.g. polytropic relation), Eq. (2.17) can be integrated to give

$$\mathcal{S}+\int\frac{dP}{\rho}=E\left(A\right)\,,$$

where the integration is performed keeping A constant (this is the generalized Bernoulli integral).

In general there is an orthogonal system of coordinates $(x_1=\chi\,,x_2=\chi_\perp)$ on the poloidal plane, such that $M=M\left(\chi\right)$. Also for compressible flows (if density isn't constant on each line, $\{\rho\,,A\}\not\equiv 0\Leftrightarrow\rho\not\equiv\rho\left(A\right)$), we may regard as the coordinate system on this plane the pair $(\chi\,,A)$ (in general, a non-orthogonal system).
After introducing

$$\mathcal{F}_1=\frac{\partial A\left(\chi\,,\chi_\perp\right)}{\partial\chi}=-h_1h_3B_2\,,\ \mathcal{F}_2=\frac{\partial A\left(\chi\,,\chi_\perp\right)}{\partial\chi_\perp}=h_2h_3B_1\,,$$

we may transform from the pair $(\chi\,,\chi_\perp)$ to the pair $(\chi\,,A)$, using the elementary relations valid for each function $\mathcal{G}$:

$$\frac{\partial\mathcal{G}\left(\chi\,,\chi_\perp\right)}{\partial\chi}=\frac{\partial\mathcal{G}\left(\chi\,,A\right)}{\partial\chi}+\mathcal{F}_1\frac{\partial\mathcal{G}\left(\chi\,,A\right)}{\partial A}\,,\ \frac{\partial\mathcal{G}\left(\chi\,,\chi_\perp\right)}{\partial\chi_\perp}=\mathcal{F}_2\frac{\partial\mathcal{G}\left(\chi\,,A\right)}{\partial A}\,.$$

Then we find the equations

$$\frac{4\pi M^2}{\Psi_A^2}\frac{\partial P}{\partial\chi}+\frac{\partial\mathcal{S}}{\partial\chi}=0\,, \tag{2.19}$$

$$\frac{1}{h_1h_2h_3}\left[\frac{\partial}{\partial\chi}\left(\frac{h_2\mathcal{F}_1}{h_1h_3}\right)+\mathcal{F}_1\frac{\partial}{\partial A}\left(\frac{h_2\mathcal{F}_1}{h_1h_3}\right)+\mathcal{F}_2\frac{\partial}{\partial A}\left(\frac{h_1\mathcal{F}_2}{h_2h_3}\right)\right]-$$
$$\frac{\Psi_A}{h_1h_2h_3}\left[\frac{\partial}{\partial\chi}\left(\frac{h_2M^2\mathcal{F}_1}{h_1h_3\Psi_A}\right)+\mathcal{F}_1\frac{\partial}{\partial A}\left(\frac{h_2M^2\mathcal{F}_1}{h_1h_3\Psi_A}\right)+\mathcal{F}_2\frac{\partial}{\partial A}\left(\frac{h_1M^2\mathcal{F}_2}{h_2h_3\Psi_A}\right)\right]+$$
$$4\pi\frac{\partial P}{\partial A}+\frac{\Psi_A^2}{M^2}\frac{\partial\mathcal{S}}{\partial A}+\frac{1}{2h_3^2}\left(\frac{L-h_3^2\Omega}{1-M^2}\right)^2\frac{d\Psi_A^2}{dA}-$$
$$\frac{\Psi_A^2L}{h_3^2M^2}\frac{dL}{dA}+\frac{\Psi_A^2\left(L-h_3^2\Omega\right)\left(\dfrac{dL}{dA}-h_3^2\dfrac{d\Omega}{dA}\right)}{h_3^2M^2\left(1-M^2\right)}=0\,, \tag{2.20}$$

because $\dfrac{\partial P\left(A\,,\mathcal{S}\right)}{\partial A}=\mathcal{J}\left(\dfrac{P\,,\mathcal{S}}{A\,,\mathcal{S}}\right)=\mathcal{J}\left(\dfrac{P\,,\mathcal{S}}{A\,,\chi}\right)/\mathcal{J}\left(\dfrac{A\,,\mathcal{S}}{A\,,\chi}\right)\overset{Eq.(2.19)}{=}\dfrac{\partial P}{\partial A}+\dfrac{\Psi_A^2}{4\pi M^2}\dfrac{\partial\mathcal{S}}{\partial A}$. Note that in Eqs. (2.19),(2.20) the symbol $\partial/\partial A$ means derivative with respect to A keeping χ constant while $\partial/\partial\chi$ means derivative with respect to χ keeping A constant. For the line elements we have $h_1=1/\mid\vec{\nabla}\chi\mid$ and $h_2=1/\mid\vec{\nabla}\chi_\perp\mid$, while $h_3=1/\mid\vec{\nabla}x_3\mid$.

2.3.2 Axisymmetric case

General axisymmetric case

If the ignorable equation is the rotational angle ϕ, then $x_3=\phi\,,\vec{\nabla}\phi=\hat{\phi}/\varpi\,,h_3=\varpi=r\sin\theta$ and from the momentum equation we have [HL89]

$$\frac{1-M^2}{4\pi r^2\sin^2\theta}\left[\frac{\partial^2A}{\partial r^2}+\frac{\sin\theta}{r^2}\frac{\partial}{\partial\theta}\left(\frac{1}{\sin\theta}\frac{\partial A}{\partial\theta}\right)\right]\vec{\nabla}A+\frac{1}{4\pi r^3\sin^2\theta}\frac{\partial M^2\left(r\,,A\right)}{\partial r}\frac{\partial A}{\partial\theta}\vec{\nabla}A\times\hat{\phi}+$$
$$+M^2\vec{\nabla}\left[\frac{\left(\vec{\nabla}A\right)^2}{8\pi r^2\sin^2\theta}\right]+\rho\vec{\nabla}\mathcal{V}+\frac{B_\phi}{4\pi r\sin\theta}\vec{\nabla}\left(r\sin\theta B_\phi\right)-\frac{\rho V_\phi^2}{r\sin\theta}\vec{\nabla}\left(r\sin\theta\right)+\vec{\nabla}P=0\,. \tag{2.21}$$

From this equation we have

- in spherical coordinates $\mathcal{M}_r=0$, or

$$\frac{1-M^2}{4\pi r^2\sin^2\theta}\left[\frac{\partial^2A}{\partial r^2}+\frac{\sin\theta}{r^2}\frac{\partial}{\partial\theta}\left(\frac{1}{\sin\theta}\frac{\partial A}{\partial\theta}\right)\right]\frac{\partial A}{\partial r}+\frac{1}{4\pi r^4\sin^2\theta}\frac{\partial M^2\left(r\,,A\right)}{\partial r}\left(\frac{\partial A}{\partial\theta}\right)^2+$$
$$+M^2\frac{\partial}{\partial r}\left(\frac{\left(\dfrac{\partial A}{\partial r}\right)^2+\left(\dfrac{\partial A}{r\partial\theta}\right)^2}{8\pi r^2\sin^2\theta}\right)+\rho\frac{\partial\mathcal{V}}{\partial r}+\frac{B_\phi^2}{4\pi r}+\frac{B_\phi}{4\pi}\frac{\partial B_\phi}{\partial r}-\frac{\rho V_\phi^2}{r}+\frac{\partial P}{\partial r}=0\,, \tag{2.22}$$

and $\mathcal{M}_\theta = 0$, or

$$\frac{1-M^2}{4\pi r^2 \sin^2\theta}\left[\frac{\partial^2 A}{\partial r^2}+\frac{\sin\theta}{r^2}\frac{\partial}{\partial\theta}\left(\frac{1}{\sin\theta}\frac{\partial A}{\partial\theta}\right)\right]\frac{\partial A}{\partial\theta}-\frac{1}{4\pi r^2\sin^2\theta}\frac{\partial M^2\left(r\,,A\right)}{\partial r}\frac{\partial A}{\partial\theta}\frac{\partial A}{\partial r}+$$

$$+M^2\frac{\partial}{\partial\theta}\left(\frac{\left(\frac{\partial A}{\partial r}\right)^2+\left(\frac{\partial A}{r\partial\theta}\right)^2}{8\pi r^2\sin^2\theta}\right)+\rho\frac{\partial\mathcal{V}}{\partial\theta}+ \tag{2.23}$$

$$\frac{B_\phi^2\cos\theta}{4\pi\sin\theta}+\frac{B_\phi}{4\pi}\frac{\partial B_\phi}{\partial\theta}-\frac{\rho V_\phi^2\cos\theta}{\sin\theta}+\frac{\partial P}{\partial\theta}=0\,.$$

- in cylindrical coordinates (using the relation $\frac{1}{r}\frac{\partial A}{\partial\theta}\frac{\partial M^2\left(r\,,A\right)}{\partial r}=\frac{1}{r}\mathcal{J}\left(\frac{M^2\,,A}{r\,,\theta}\right)=\frac{1}{r}\mathcal{J}\left(\frac{z\,,\varpi}{r\,,\theta}\right)\mathcal{J}\left(\frac{M^2\,,A}{z\,,\varpi}\right)=-\frac{\partial A}{\partial z}\frac{\partial M^2\left(\varpi\,,A\right)}{\partial\varpi}$)
$\mathcal{M}_\varpi = 0$, or

$$\frac{1-M^2}{4\pi\varpi^2}\left[\varpi\frac{\partial}{\partial\varpi}\left(\frac{1}{\varpi}\frac{\partial A}{\partial\varpi}\right)+\frac{\partial^2 A}{\partial z^2}\right]\frac{\partial A}{\partial\varpi}+\frac{1}{4\pi\varpi^2}\frac{\partial M^2\left(\varpi\,,A\right)}{\partial\varpi}\left(\frac{\partial A}{\partial z}\right)^2+$$

$$+M^2\frac{\partial}{\partial\varpi}\left(\frac{\left(\frac{\partial A}{\partial\varpi}\right)^2+\left(\frac{\partial A}{\partial z}\right)^2}{8\pi\varpi^2}\right)+\rho\frac{\partial\mathcal{V}}{\partial\varpi}+\frac{B_\phi}{4\pi\varpi}\frac{\partial}{\partial\varpi}\left(\varpi B_\phi\right)-\frac{\rho V_\phi^2}{\varpi}+\frac{\partial P}{\partial\varpi}=0\,, \tag{2.24}$$

and $\mathcal{M}_z = 0$, or

$$\frac{1-M^2}{4\pi\varpi^2}\left[\varpi\frac{\partial}{\partial\varpi}\left(\frac{1}{\varpi}\frac{\partial A}{\partial\varpi}\right)+\frac{\partial^2 A}{\partial z^2}\right]\frac{\partial A}{\partial z}-\frac{1}{4\pi\varpi^2}\frac{\partial M^2\left(\varpi\,,A\right)}{\partial\varpi}\frac{\partial A}{\partial z}\frac{\partial A}{\partial\varpi}+$$

$$+M^2\frac{\partial}{\partial z}\left(\frac{\left(\frac{\partial A}{\partial\varpi}\right)^2+\left(\frac{\partial A}{\partial z}\right)^2}{8\pi\varpi^2}\right)+\rho\frac{\partial\mathcal{V}}{\partial z}+\frac{B_\phi}{4\pi}\frac{\partial B_\phi}{\partial z}+\frac{\partial P}{\partial z}=0\,, \tag{2.25}$$

An alternative form of Eq. (2.21) is [Hey96]

$$\vec{\nabla}\mathcal{S}+\frac{\vec{\nabla}P}{\rho}+\left[\frac{1}{4\pi\rho\varpi}\left(\frac{\partial}{\partial\varpi}\frac{1}{\varpi}\frac{\partial A}{\partial\varpi}+\frac{\partial}{\partial z}\frac{1}{\varpi}\frac{\partial A}{\partial z}\right)-\right.$$

$$\frac{\Psi_A}{4\pi\rho\varpi}\left(\frac{\partial}{\partial\varpi}\frac{\Psi_A}{4\pi\rho\varpi}\frac{\partial A}{\partial\varpi}+\frac{\partial}{\partial z}\frac{\Psi_A}{4\pi\rho\varpi}\frac{\partial A}{\partial z}\right)+\frac{1}{8\pi\rho\varpi^2}\left(\frac{L-\varpi^2\Omega}{1-M^2}\right)^2\frac{d\Psi_A^2}{dA}-$$

$$\left.\frac{L}{\varpi^2}\frac{dL}{dA}+\frac{\left(L-\varpi^2\Omega\right)\left(\frac{dL}{dA}-\varpi^2\frac{d\Omega}{dA}\right)}{\varpi^2\left(1-M^2\right)}\right]\vec{\nabla}A=0\ , \tag{2.26}$$

where $\mathcal{S}=V^2/2+\mathcal{V}-\dfrac{\varpi\Omega B_\phi}{\Psi_A}$.

Polytropic axisymmetric case

When the relation between P and ρ is of the form $P=Q\left(A\right)\rho^\gamma$ then force balance along poloidal fieldlines, or $\mathcal{M}_{A\perp}=0$, gives (after integration)

$$\frac{V^2}{2}+\frac{\gamma}{\gamma-1}\frac{P}{\rho}+\mathcal{V}-\frac{\varpi\Omega}{\Psi_A}B_\phi=E\left(A\right)\ . \tag{2.27}$$

Note that if $\gamma=1$ (isothermal case) the term $\dfrac{\gamma}{\gamma-1}\dfrac{P}{\rho}$ must be replaced with the term $C_s^2\left(A\right)\ln\rho$. In this case $\dfrac{P}{\rho}=Q\left(A\right)=C_s^2\left(A\right)$ is the square of the isothermal sound speed.
On the other hand, force balance across the poloidal fieldlines, or $\mathcal{M}_A=0$, gives

$$\left(1-M^2\right)\left[\vec{\nabla}\cdot\left(\frac{\vec{\nabla}A}{\varpi^2}\right)\right]-\Psi_A\left(\frac{\vec{\nabla}A}{\varpi^2}\right)\cdot\left[\left(\frac{M^2}{\Psi_A}\right)\right]+\frac{1}{2\varpi^2}\left(\frac{L-\varpi^2\Omega}{1-M^2}\right)^2\frac{d\Psi_A^2}{dA}-$$
$$\frac{4\pi\rho L}{\varpi^2}\frac{dL}{dA}+4\pi\rho\frac{\left(L-\varpi^2\Omega\right)\left(\frac{dL}{dA}-\varpi^2\frac{d\Omega}{dA}\right)}{\varpi^2\left(1-M^2\right)}+4\pi\rho\frac{dE}{dA}-4\pi\frac{\rho^\gamma}{\gamma-1}\frac{dQ}{dA}=0 \tag{2.28}$$

The last equation is the most known form of the transfield equation.
By differentiating Eq. (2.27) solving for $\vec{\nabla}\rho$ and substituting in Eq. (2.28), we get the Grad-Shafranov equation (GSE) [Sak90, TSS+96]

$$\frac{1-M^2}{\varpi^2}\left(\nabla^2A-\frac{\vec{\nabla}A\cdot\vec{\nabla}\left(\vec{\nabla}A\right)^2}{2\left(\vec{\nabla}A\right)^2}\frac{V_p^4}{V_p^4-V_p^2\left(C_s^2+V_A^2\right)+C_s^2V_{A\ ,p}^2}\right)=F_0\ , \tag{2.29}$$

where F_0 is a function of $A\ ,\vec{\nabla}A$ and ρ while C_s^2 is the square of the sound speed $C_s^2=\dfrac{\partial P\left(\rho\ ,A\right)}{\partial\rho}=\gamma\dfrac{P}{\rho}$.

Bibliography

[BS69] T. J. M. Boyd and J. J. Sanderson, *Plasma Dynamics*, Nelson, Great Britain, 1969.

[BT99] S.V. Bogovalov and K. Tsinganos, MNRAS (1999), in press.

[Cam86] M. Camenzind, A&A **162** (1986), 32.

[Con94] J. Contopoulos, ApJ **432** (1994), 508.

[Fre82] J. P. Freidberg, Rev. Mod. Phys. **54** (1982), 801.

[GL96] J. P. Goedbloed and A. Lifschitz, Astrophys. Lett. Commun. **34** (1996), 261.

[GR95] R. J. Goldston and P. H. Rutherford, *Introduction to Plasma Physics*, Institute of Physics Publishing, Brostol and Philadelphia, ch.6, 1995.

[Hey96] J. Heyvaerts, *in Plasma Astrophysics, (EADN Astrophysics School VII, San Miniato, Italy 1994)*, C. Ghiuderi & G. Einaudi (Eds.), Springer, p. 31, 1996.

[HL89] Y.Q. Hu and B.C. Low, ApJ **342** (1989), 1049.

[HO78] M. Heinemann and S. Olbert, J. Geophys. Res. **83-A6** (1978), 2457.

[LL75] L. D. Landau and E. M. Lifschitz, *Fluid Mechanics*, Pergamon Press, Oxford, ch. 15, 1975.

[LMMS86] R. V. E. Lovelace, C. Mehanian, C. M. Mobarry, and M. E. Sulkanen, APJS **62** (1986), 1.

[RP94] F. Rosso and G. Pelletier, A&A **287** (1994), 325.

[Sak90] T. Sakurai, Computer Physics Reports **12(4)** (1990), 247.

[Tsi81] K.C. Tsinganos, ApJ **245** (1981), 764.

[Tsi82] K.C. Tsinganos, ApJ **252** (1982), 775.

[Tsi92] K. Tsinganos, *in The Sun, A Laboratory for Astrophysics*, J. T. Schmelz and J. C. Brown (ed.), Kluwer Academic Publishers, p. 139, 1992.

[TSS+96] K. Tsinganos, C. Sauty, G. Surlantzis, E. Trussoni, and J. Contopoulos, *in Solar and Astrophysical MHD Flows*, K. Tsinganos (ed.), Kluwer Academic Publishers, p. 427, 1996.

Chapter 3

MHD Critical Surfaces

In this Chapter we 'll examine some generic properties of the physical solutions of the set of the MHD equations, for steady, axisymmetric flows, which we outlined in the previous Chapter 2. In particular, we investigate the role which the limiting characteristics play in selecting the appropriate solution of the MHD equations. We examine these characteristics in relation to the appropriate boundary conditions for an integration of the MHD equations, we show how they can be constructed and also give their geometrical representation. The propagation of magnetosonic waves in the various domains in which the limiting characteristics devide the solution space, is discussed in their relation to the correct number of boundary conditions. For the particular case of self similar solution, at these characteristics the component of the flow speed perpendicular to the directions of the characteristics, which are the directions of self similarity, equals to the fast/slow MHD wave speed in the same direction.

3.1 Polytropic MHD flows

In an axisymmetric system the coordinate ϕ is ignorable, so all physical quantities are functions of $(x_1\,,x_2)$ alone, where x_1 and x_2 are orthogonal coordinates on the poloidal plane (for example $x_1 = r\,, x_2 = \theta$ when we use spherical coordinates, or $x_1 = z\,, x_2 = \varpi$ when we use cylindrical coordinates). First we see that in the expressions for V_ϕ and B_ϕ we have a denominator $\Psi_A^2/4\pi\rho - 1$, or $M^2 - 1$. When this vanishes the numerator must vanishes too, in order to have finite values for V_ϕ and B_ϕ. So at the Alfvén point, where the poloidal speed is equal to the Alfvén poloidal speed (that is to say $M = 1$), we have $L = (h_3)^2_{M=1}\,\Omega$ or $L = \varpi_\alpha^2\Omega$, where $\varpi_\alpha\,(A)$ is the distance from the symmetry axis at the Alfvén point, for each line A =constant. We have seen in the previous Chapter that the full system of the MHD equations after the described integrations in case of a steady state with one ignorable coordinate, reduces to three equations: the two components of the momentum equation and the energy equation. If in addition, a polytropic relation between the pressure and

the density exists

$$P = Q\left(A\right)\rho^{\gamma}\ , \tag{3.1}$$

we need to solve only the two components of the momentum equation and the energy equation gives the function q. Equivalently, by assuming that $q = \dfrac{\gamma-\Gamma}{\Gamma-1}\dfrac{P}{\rho}\vec{V}\cdot\vec{\nabla}\rho$ then the energy equation can be integrated to give the relation between pressure and density $P = Q\left(A\right)\rho^{\gamma}$. In this case we define the square of the sound speed as the derivative of the pressure with respect to density, with constant A

$$C_s^2 = \frac{\partial P\left(\rho\,,A\right)}{\partial\rho} = \gamma\frac{P}{\rho}\,.$$

This is an effective sound speed because only if $\gamma=\Gamma$ it is isentropic, i.e., only then the entropy remains constant on each field-streamline.
If this is the case, then we may have as the two remaining equations the two components of the momentum equation parallel ($\mathcal{M}_{A\perp}=0$) and perpendicular ($\mathcal{M}_A=0$) to the field-streamlines A =constant on the poloidal plane. The first equation can be integrated at once (if the radiative force is negligible compared with the other forces in the momentum equation) to give the Bernoulli equation

$$\frac{V^2}{2}+\frac{\gamma}{\gamma-1}\frac{P}{\rho}+\mathcal{V}-\frac{\varpi\Omega}{\Psi_A}B_{\phi}=E\left(A\right)\ , \tag{3.2}$$

while the other one is called the transfield equation.
It is worth to note that the term $\dfrac{\gamma}{\gamma-1}\dfrac{P}{\rho}=\displaystyle\int\frac{dP}{\rho}$, often called the effective enthalpy, is equal with the enthalpy only for $\gamma=\Gamma$.
So the full set of the MHD equations reduces to two equations with two unknown functions, the density ρ and the flux function A. Generally speaking one may solve from the Bernoulli equation to yield ρ (this equation has only ρ and not its derivatives but unfortunately it's complex and can't be solved analytically) and then replace it in the transfield. So we'll keep in mind that with the help of numerical methods we find ρ from the Bernoulli while the derivatives of ρ can be found after the differentiation of Eq. (3.2). The resulting equation called the Grad-Shafranov equation (or GSE) is equivalent with the transfield. It is a second order partial differential equation (PDE) for the flux function A, of a mixed type (elliptic or hyperbolic). It can be written in the canonical form [HO78, LMMS86, TSS$^+$96, TSS$^+$96] (it is equivalent to Eq. (2.29)).

$$\left(1-M^2\right)\left(\frac{a}{h_1^2}\frac{\partial^2 A}{\partial x_1^2}+\frac{2b}{h_1h_2}\frac{\partial^2 A}{\partial x_1\partial x_2}+\frac{c}{h_2^2}\frac{\partial^2 A}{\partial x_2^2}+d\right)+e=0\,, \tag{3.3}$$

where

$$a=\left[V_1^4-V_1^2\left(C_s^2+V_A^2\right)+C_s^2V_{A\,,p}^2\right]V_{A\,,p}^2/V_{A\,,1}^2\,,$$

$$b=V_1V_2V_p^2\,,$$

$$c=\left[V_2^4-V_2^2\left(C_s^2+V_A^2\right)+C_s^2V_{A\,,2}^2\right]V_{A\,,p}^2/V_{A\,,2}^2\,,$$

while there are two lengthly expressions for d and e (note that in the nonrotating case the expression for e vanishes [1]). The functions $a\,,b\,,c\,,d\,,e$ have only first order derivatives of A (the density ρ, from Eq. (3.2) is a function of A and its first order derivatives).
If $V_s\,,V_f$ are the roots of the equation

$$V_{f\,,s}^4 - V_{f\,,s}^2\left(C_s^2+V_A^2\right)+C_s^2V_{A\,,p}^2=0$$

and the cusp velocity is defined by

$$V_c^2=\frac{C_s^2V_{A\,,p}^2}{C_s^2+V_A^2}=\frac{V_s^2V_f^2}{V_s^2+V_f^2}\,,$$

the expression

$$\mathcal{D}=b^2-ac=\left(V_p^2-V_s^2\right)\left(V_p^2-V_f^2\right)\left(V_p^2-V_c^2\right)\left(C_s^2+V_A^2\right) \tag{3.4}$$

determines the type of the equation. In particular if $V_c<V_p<V_s$ or $V_p>V_f$ the PDE Eq. (3.3) is hyperbolic while in the regimes where $V_p<V_c$ or $V_s<V_p<V_f$ is elliptic. Assuming that near the stellar surface $V_p<V_c$ and as the plasma flows away from the star we have certain surfaces where $V_p=V_c\,,V_p=V_s\,,V_p=V_{A\,,p}\,,V_p=V_f$. So if the flow begins from the stellar surface with subcusp velocity, then Eq. (3.3) will be elliptic until the surface $V_p=V_c$, then hyperbolic until the surface $V_p=V_s$, then again elliptic until the surface $V_p=V_f$ (this domain includes the Alfvén singular surface where $V_p=V_{A\,,p}$), and finally hyperbolic. At last, the solution maybe connected to the interstellar medium with a fast MHD shock.

3.1.1 Integration of the GSE and the characteristics surfaces

Now let's examine how we may integrate the second order PDE (3.3) for A. Let's start from some curve $x\left(\varpi\,,z\right)=constant$[2], or, parametrically $\varpi=(x,s)$ and $z=z\left(x,s\right)$ where $ds^2=d\varpi^2+dz^2$, where s is the arclength on the curve $x=$constant. We may give on this curve the function $A\left(s\right)$ and its normal derivative $N\left(s\right)=\hat{n}_0\cdot\vec{\nabla}A$, where $\hat{n}_0$ is the unit vector normal to the line $x=const$ on the poloidal plane, together with the integrals $L\,,\Omega\,,\Psi_A$. These are generalized Cauchy boundary conditions. Then we must calculate the derivatives of A and start the numerical integration of our system.
The first derivatives of A are calculated from the equations

$$N\left(s\right)=-\frac{dz}{ds}\frac{\partial A}{\partial\varpi}+\frac{d\varpi}{ds}\frac{\partial A}{\partial z}\,,$$

[1] that's why in the nonrotating case the Alfvén critical point disappear
[2] If we rotate this curve around the $\hat{z}$ axis, the characteristic surface is produced.

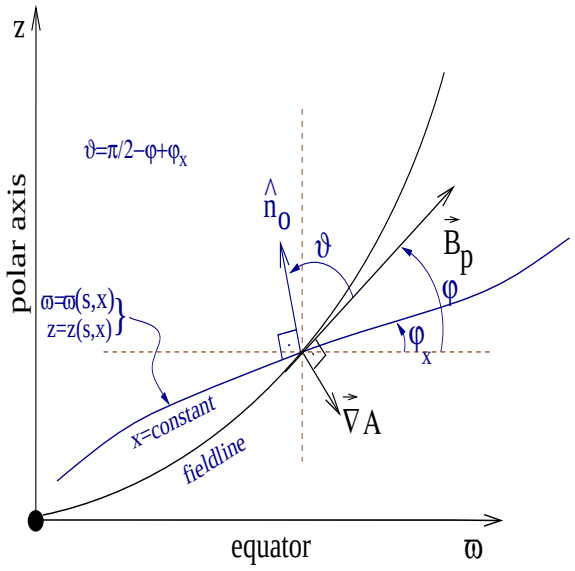

Figure 3.1: The characteristic curve x=constant. The unit vector perpendicular to this surface is $\hat{n}_o = -\sin\varphi_x\hat{\varpi} + \cos\varphi_x\hat{z}$, where $\sin\varphi_x = dz/ds$, $\cos\varphi_x = d\varpi/ds$. Note that $\hat{n}_o$ should not be confused with $\hat{n}$. The later is normal to the fieldline.

$$\frac{dA\,(s)}{ds} = \frac{d\varpi}{ds}\frac{\partial A}{\partial \varpi} + \frac{dz}{ds}\frac{\partial A}{\partial z}\,.$$

The trouble comes with the second order partial derivatives of A, or equivalently the first derivatives of the components of magnetic field. We have

$$\frac{d}{ds}\left(\frac{\partial A}{\partial \varpi}\right) = \frac{d\varpi}{ds}\frac{\partial^2 A}{\partial \varpi^2} + \frac{dz}{ds}\frac{\partial^2 A}{\partial \varpi \partial z}\,,$$

$$\frac{d}{ds}\left(\frac{\partial A}{\partial z}\right) = \frac{d\varpi}{ds}\frac{\partial^2 A}{\partial \varpi \partial z} + \frac{dz}{ds}\frac{\partial^2 A}{\partial z^2}\,,$$

together with the GSE, Eq. (3.3), in cylindrical coordinates where $x_1 = z$, $x_2 = \varpi$, $h_1 = h_2 = 1$. Altogether we have to solve the system

$$\begin{bmatrix} \frac{d\varpi}{ds} & \frac{dz}{ds} & 0 \\ 0 & \frac{d\varpi}{ds} & \frac{dz}{ds} \\ c\left(1-M^2\right) & 2b\left(1-M^2\right) & a\left(1-M^2\right) \end{bmatrix} \begin{bmatrix} \frac{\partial^2 A}{\partial \varpi^2} \\ \frac{\partial^2 A}{\partial \varpi \partial z} \\ \frac{\partial^2 A}{\partial z^2} \end{bmatrix} = \begin{bmatrix} \frac{d}{ds}\left(\frac{\partial A}{\partial \varpi}\right) \\ \frac{d}{ds}\left(\frac{\partial A}{\partial z}\right) \\ -e - d\left(1-M^2\right) \end{bmatrix}.$$

This system can be solved to give the second derivatives of A unless the determinant of the matrix is zero. This happens when (after some manipulation)

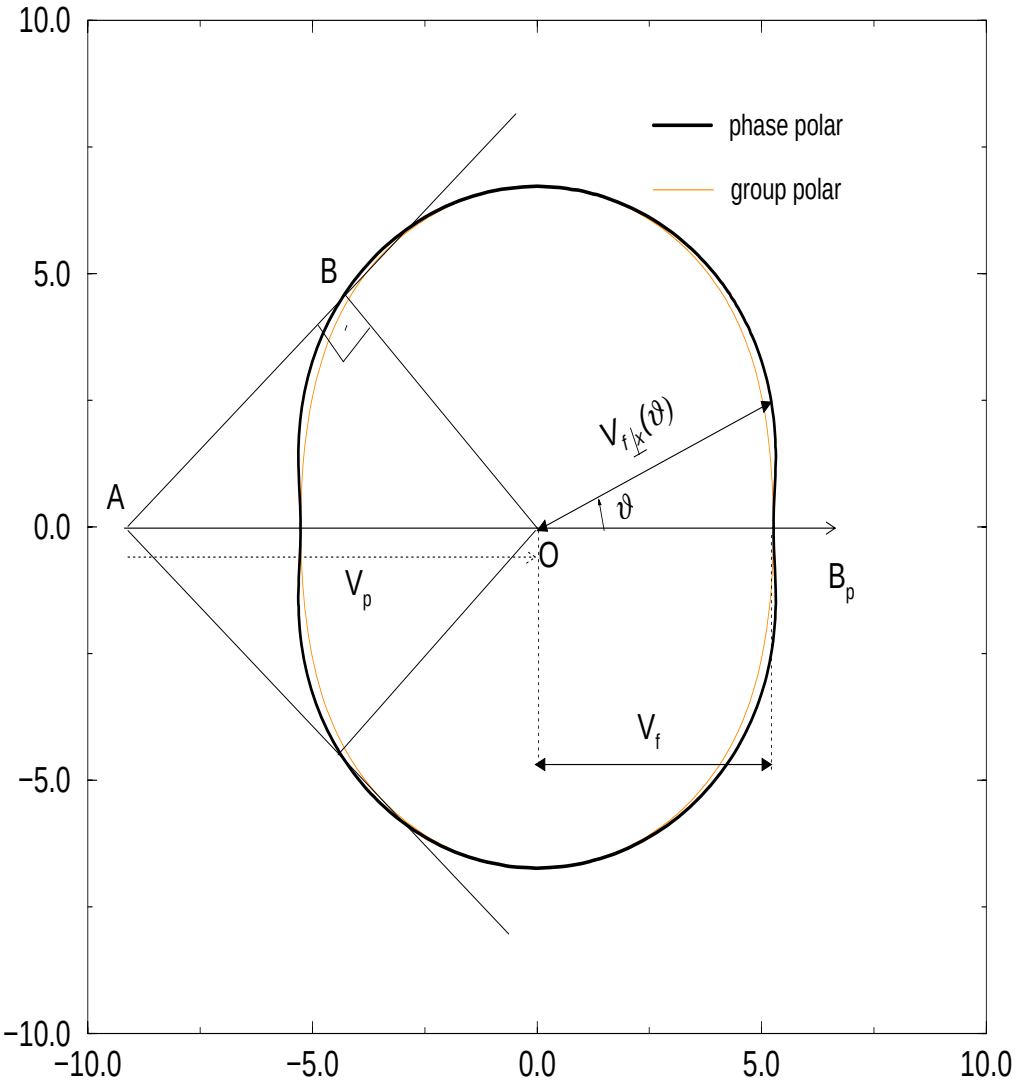

Figure 3.2: Fast phase and group polars and the characteristics. ($V_A = 5\,, V_{A\,,p} = 4.9\,, C_s = 4.5$).

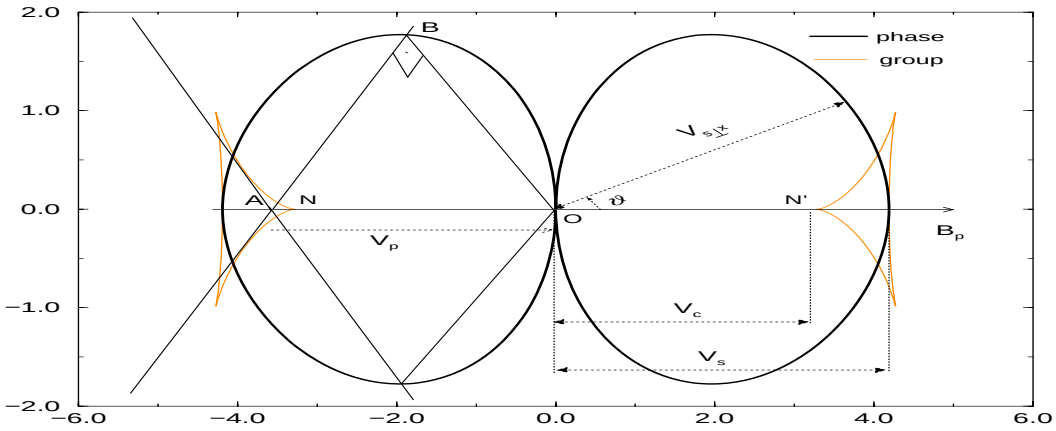

Figure 3.3: Slow phase and group polars and the characteristics. ($V_A = 5\,, V_{A\,p} = 4.9\,, C_s = 4.5$).

[Con96, STP96]

$$V_{\perp x}^4 - V_{\perp x}^2 \left(C_s^2 + V_A^2\right) + C_s^2 V_{A\perp x}^2 = 0^3\,, \tag{3.5}$$

where the sound speed

$$C_s^2 = \frac{\partial P\left(\rho\,, A\right)}{\partial \rho} = \gamma \frac{P}{\rho} \text{ and } V_{\perp x} = \vec{V} \cdot \vec{\nabla} x / \mid \vec{\nabla} x \mid$$

is the component of the flow velocity perpendicular to the surface $x = const.$ In each point of the poloidal plane, the values of $d\varpi/dz$ (or the directions of $\hat{n}_o$) which make zero the previous determinant define the directions of the characteristics. If the tangent on the surface of integration coincides with one of the characteristics, we can't integrate the system from this surface. If this is the case, we need to impose some kind of regularity condition in order that the integration proceeds through this surface. [4]

3.1.2 Construction of the characteristics

One may see in Appendix 3.A that fast and slow waves with wavevector $\vec{k} = k\hat{n}_0$ normal to the characteristic surface on the poloidal plane have phase velocities

[3] The determinant vanishes to, if $1 - M^2 = 0$,or $V_{\perp x}^2 - V_{A\perp x}^2 = 0$. This case correspond to the propagation of Alfvén waves.

[4] When $M = 1$ the determinant vanishes to, so when we reach the Alfvén surface we can't pass through it without imposing the Alfvén regularity condition (for all possible directions of tangent on the surface of integration at this point).

satisfying the equation

$$V_{f,s\perp x}^4 - V_{f,s\perp x}^2\left(C_s^2+V_A^2\right)+C_s^2V_{A\perp x}^2=0\,.$$

So one surface is characteristic, if the component of the flow velocity perpendicular to this, is equal with the phase velocity of a fast or slow magnetosonic wave with wavevector perpendicular to it: $V_{\perp x}^2=V_{f\perp x}^2$ or $V_{\perp x}^2=V_{s\perp x}^2$. This can be seen geometrically with the help of the phase-polar diagram for the wave phase speed (or the group-polar for the wave group velocity).
If we have waves in the frame of the axisymmetric equations (that is to say $\vec{k}$ is on the poloidal plane and thus the wave quantities do not depend on the angle ϕ) the phase and group polars are shown in Figs. 3.2,3.3. Let's examine the fast wave (for the slow wave we do the same). Suppose that we are in a point A of the poloidal plane. If $\vec{AO}=\vec{V}_p$, then with the origin at O we plot the phase polar diagram and we look in a direction $\vec{OB}$ such that the point B is on the phase polar and $\vec{OB}\perp\vec{AB}$. Note that in this case, $\vec{AO}//\vec{B}_p$ since $\vec{V}_p//\vec{B}_p$. Then the projection of $\vec{V}_p$ on the direction $\vec{OB}$ is equal with the phase speed in this direction. But the direction $\vec{OB}$ is perpendicular to $\vec{AB}$. Thus $\vec{AB}$ is the characteristic direction (there is another characteristic $\vec{AB}'$, in a symmetrical position with respect to the axis of $\vec{B}_p$).
Equivalently, if we plot the group polar (which is the envelope of lines AB with $\vec{OB}\perp\vec{AB}$ and B moves in all the phase polar -see Fig. 3.13, or Fig.2 in [Con96]) then the characteristics at one point A are lines which are tangent to the group polar. One can see from Figs. 3.2,3.3 that when $V_p>V_f$ there are two fast characteristics while when $V_c<V_p<V_s$ there are two slow characteristics. When $V_s<V_p<V_f$ or $V_p<V_c$ there are no characteristics [5] This is expected because only for $V_p>V_f$ and $V_c<V_p<V_s$ the PDE equation for A is hyperbolic (otherways it is elliptic and no characteristics exist).

3.1.3 Another geometrical representation of the characteristics

Let's go back to Eq. (3.5). Because $V_{\perp x}/V_{A\perp x}=M$ this can be written in the form $V_{\perp x}^2\left(V_{\perp x}^2-C_s^2-V_A^2+C_s^2/M^2\right)=0$. The vanishing of the first term $V_{\perp x}^2$ gives us two slow characteristics which correspond to a non-propagating layer (see the footnote).

On the other hand when the bracket vanishes, we have

$$V_{\perp x}^2=C_s^2+V_A^2-C_s^2/M^2 \tag{3.6}$$

(this is the solution of Eq. (3.5) equivalent to $V_{\perp x}=V_{f\perp x}$ if $V_p>V_f$ or to $V_{\perp x}=V_{s\perp x}$ if $V_c<V_p<V_s$). So another geometrical representation of characteristics is the following (see also Fig. 3.4):
Suppose that we are in a point A and $\vec{AO}=\vec{V}_p$. With center O we draw a

[5] In all cases there are two slow characteristics parallel to $\vec{B}_p$ (corresponding to tangents at points N, N') but these are degenerate since there is no slow wave traveling parallel to the fieldline on the poloidal plane (the phase speed in that direction vanishes and the wave correspond to a non-propagating layer in the moving frame) [Dra75].

circle with radius $\sqrt{C_s^2+V_A^2-C_s^2/M^2}$ (this radius depends on the fluid velocity V_p). The tangents from point A to this circle are the characteristics (since the component of V_p tangent to them, is equal with the radius of the circle). Two tangents exist when the point A is outside the circle (or $V_p^2 > C_s^2+V_A^2-C_s^2/M^2$) and the radius of the circle is real (or $C_s^2+V_A^2-C_s^2/M^2>0$). These two conditions are equivalent with $\{\left(V_p^2-V_s^2\right)\left(V_p^2-V_f^2\right)>0$ and $V_p^2>V_c^2\}$ respectively, or $\{V_p>V_f$ or $V_c<V_p<V_f\}$ as we expect.
From Fig. 3.1 we have $V_{\perp x}=V_z\cos\varphi_x-V_\varpi\sin\varphi_x=V_p\sin(\varphi-\varphi_x)$ since $V_z=V_p\sin\varphi\,,V_\varpi=V_p\cos\varphi$. So Eq. (3.6) can be rewritten in the forms

$$\sin(\varphi-\varphi_x)=\pm\frac{\sqrt{C_s^2\left(1-1/M^2\right)+V_A^2}}{V_p}\Leftrightarrow$$
$$\tan(\varphi-\varphi_x)=\pm\sqrt{\frac{\left(C_s^2+V_A^2\right)\left(V_p^2-V_c^2\right)}{\left(V_p^2-V_s^2\right)\left(V_p^2-V_f^2\right)}}\,. \qquad (3.7)$$

If we choose a system of orthogonal coordinates $(\xi\,,n)$ on the poloidal plane, such that the lines of constant ξ are the poloidal field-streamlines $(\xi=\xi(A))$ and normal to these lines the unit vector is $\hat{n}=\vec{\nabla}A/\mid\vec{\nabla}A\mid$, then $\tan(\varphi-\varphi_x)=h_n dn/h_\xi d\xi$. So the two characteristics are

$$\frac{h_n dn}{h_\xi d\xi}=\pm\sqrt{\frac{\left(C_s^2+V_A^2\right)\left(V_p^2-V_c^2\right)}{\left(V_p^2-V_s^2\right)\left(V_p^2-V_f^2\right)}} \qquad (3.8)$$

Sakurai [Sak90] has this relation with $h_n=h_\xi=1$ since he considers a local Cartesian system $(\xi\,,n)$.

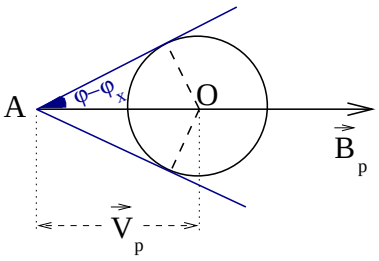

Figure 3.4: The characteristics, as tangents to a circle.

If we move from the pair $(\xi\,,n)$ to a pair of orthogonal coordinates on the poloidal plane $(x_1\,,x_2)$ then the characteristics are $h_2dx_2/h_1dx_1=\tan\varphi_{12}$ because $d\vec{r}=h_1dx_1\hat{x}_1+h_2dx_2\hat{x}_2$. Using $\varphi-\varphi_x=\varphi_{12}+\theta_{12}$ and $B_1=B_p\cos\theta_{12}\,,B_2=-B_p\sin\theta_{12}$ we get

$$\frac{h_2dx_2}{h_1dx_1}=\frac{B_1\dfrac{h_n dn}{h_\xi d\xi}+B_2}{B_1-B_2\dfrac{h_n dn}{h_\xi d\xi}}$$

or after some manipulation

$$\frac{h_2dx_2}{h_1dx_1}=\frac{b\pm\sqrt{b^2-ac}}{a}=\frac{c}{b\mp\sqrt{b^2-ac}}\,. \qquad (3.9)$$

This is the well known definition for the characteristics of a second order PDE equation like Eq. (3.3). [6] So there are two families of curves; the characteristics

[6] Without imposing the integrals $A\,,\Psi_A\,,L\,,\Omega\,,E$ we have a PDE system of seven unknowns $(\vec{V}\,,\vec{B}\,,\rho)$ and there are seven characteristics [Con96, STP96]. One of them is identical with

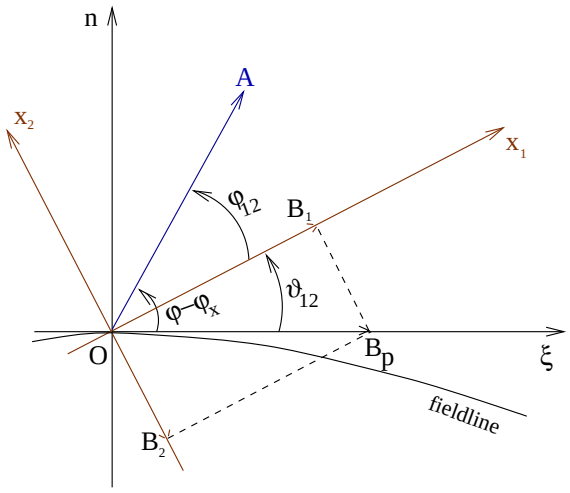

Figure 3.5: The ξ-n system of coordinates

(solutions of Eq. (3.9)) $u_+(x_1, x_2) = constant$, $u_-(x_1, x_2) = constant$ which fill all the hyperbolic domain of the solution. Note that in the non-orthogonal system of coordinates (u_+, u_-), Eq. (3.3) can be written as

$$\frac{\partial^2 A}{\partial u_+ \partial u_-} = \mathcal{L}_0$$

where $\mathcal{L}_0$ is a function containing first order derivatives of A.

3.1.4 Propagation of waves and boundary conditions

Now suppose that we know a solution of the MHD equations and look for the characteristics. First let's look about the fast ones which start from the surface $V_p = V_f$ downstream. If at this surface these curves have $dn < 0$ as in Fig. 3.6 then for the "-" sign we have $d\xi > 0$ while for the "+" sign, $d\xi < 0$ (on the surface $V_p = V_f$, $d\xi = 0^{\pm}$ from Eq. (3.8)). The sign of the slope $dn/d\xi$ is constant in each characteristic. So we can see from the geometry of the problem that the "+" characteristics which begin from the surface $V_p = V_f$ can not fill all the hyperbolic domain from this surface through infinity. The same for the curves which begin from infinity and can not intersect the surface $V_p = V_f$. Thus there is one (at least) separatrix surface (or limiting characteristic) which is the

the field-stream line on the poloidal plane (corresponding to the entropy wave). The associated Riemman invariant is the flux function A. In our case five of them (one entropy, two slow and two Alfvén characteristics) are identical and parallel to the flow in the poloidal plane. The Riemman invariants associated with them are the integrals (constants as we move parallel to the flow onto poloidal plane) while the other two are the slow or the fast characteristics (depend on magnitude of V_p).

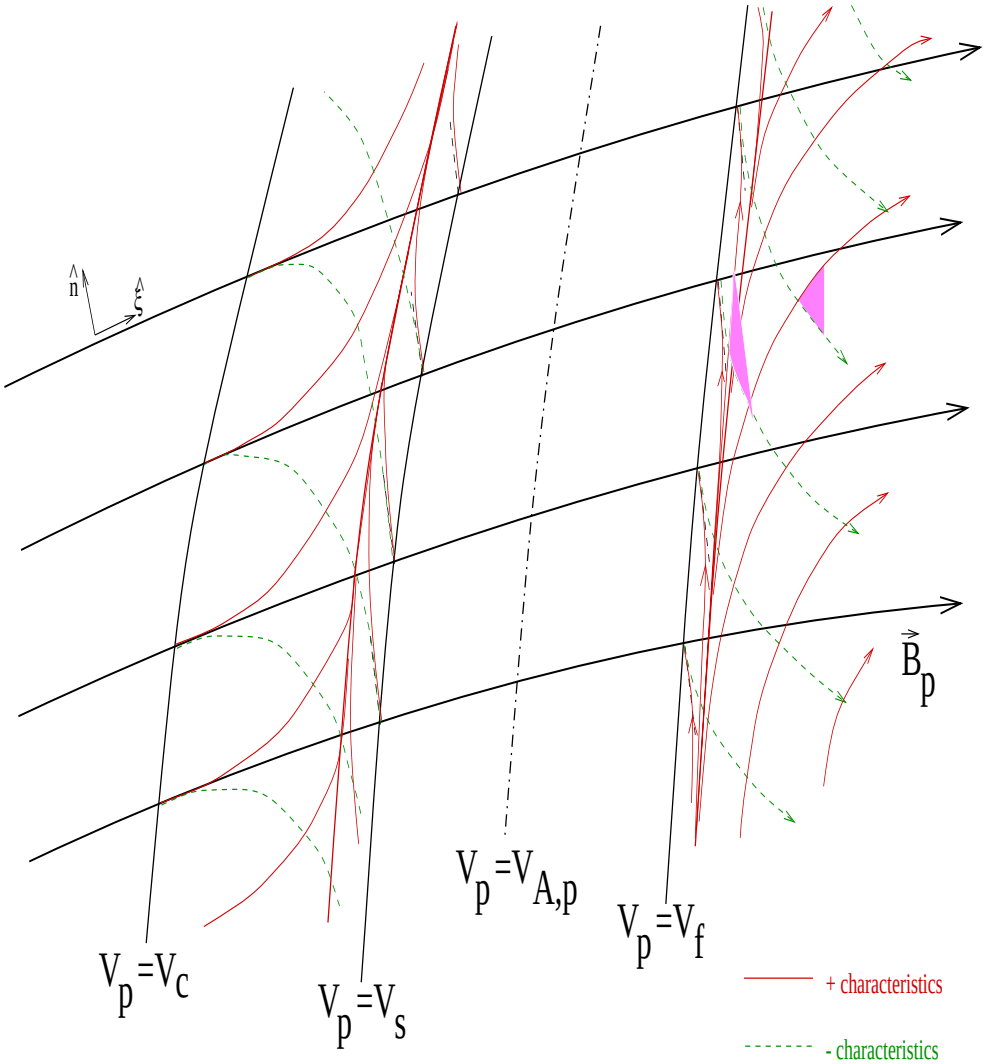

Figure 3.6: Sketch of the elliptic-hyperbolic regimes. The fast characteristics (with arrows) shows the envelope of the vectors $\vec{V}_{g\,,i}\,(\vartheta)+\vec{V}_p$ for various ϑ. The slow characteristics shows only where the Riemman invariants remain constants.

only closed characteristic in the regime $V_p > V_f$ [Sak90, TSS+96, TSS+96]. From now on we 'll call this surface fast magnetosonic separatrix surface, or FMSS [LL75a, Bog94, Bog96, Bog97].
Now let's think about the relation of characteristics with a signal traveling in a moving fluid. As it is shown in Appendix 3.A the two fast characteristics which pass through a point A, determine the part of the whole space where a signal from point A travels (as the Mach "cone" in a supersonic hydrodynamic flow). So looking at Fig. 3.6, if a signal is generated at a point in the regime downstream from the FMSS, it cannot influence points in the regime upstream from the FMSS. This is the causality principle: the flow must pass this FMSS in order to be steady. Otherways a small disturbance at "infinite" distance from the origin of the outflow will change all the solution. But if the solution pass this FMSS then any disturbance at infinity will affect the solution through a surface where a fast-shock will connect the new solution with the previous steady one in the regime downstream from the FMSS.
Now let's see about the slow characteristics in the regime $V_c < V_p < V_s$. As before, there is at least one slow magnetosonic separatrix surface (SMSS) or limiting characteristic Fig. 3.6.
But a significant difference from the previous case is occurred when we examine the propagation of waves in this regime. As it is shown in Appendix 3.A, if we make a disturbance at one point A of this regime, the signal influences this part of space which is determined from the cusp points of the slow group-polar and not from the slow characteristics. So there is no necessity for passing the solution through the SMSS (there in no relation with the causality principle on this surface). In this regime the characteristics have the meaning that on these lines the Riemman invariants remain constants.
Another important property of the characteristics is the following: Suppose that you are in some point of space and imagine a surface passing through this point. This surface separates space in two domains. Then assume that we want to answer the following question: In which domain travel the two signals with wavevectors perpendicular to the surface (for an observer without velocity with respect to the star)? The answer depends on the phase velocity of the signal (the signal moves with the group velocity but since the phase velocity depends only on the angle between $\vec{k}$ and $\vec{B}_p$, the component of the group velocity perpendicular to the surface is the phase velocity $\vec{V}_{ph} = V_{ph}\hat{k}$). So one can find the answer by looking at the phase polar diagram, which is different for various values of the poloidal speed of the flow, V_p. For the slow wave:

- If $V_p < V_c$ there is one signal traveling downstream and one upstream.
- If $V_p > V_s$ there are two signals traveling downstream.
- If $V_c < V_p < V_s$ there are two characteristic surfaces such that: if our surface is not in the domain which these two characteristics make and include the fieldline, then there is only one signal moving downstream (the other one is moving upstream) ; otherwise there are two. See Fig. 3.16 in Appendix 3.A.

Similarly for the fast and the Alfvén waves (the entropy wave is always moving with the fluid).
So in each point of the space (or for each value of V_p) when $V_p > V_f$ or $V_c < V_p < V_s$ there are two directions such that if our surface is tangent to one of them, we can't answer the previous question. These surfaces are the characteristics (lines on the poloidal plane).

3.1.5 Number of boundary conditions and characteristics

Now let's consider the boundary conditions and the integration of the GSE (in relation with the propagation of waves in the moving plasma [PD90, JT64, GH62, Gud62].)
Suppose that we start the integration downstream from the stellar surface. The number of the boundary conditions depend on the relation of V_p with $V_c\,, V_s$ and V_f. In general, if we start the integration downstream from some surface, the number of boundary conditions which we must give on this surface is equal to the number of waves which can be emitted from this surface downstream. (These waves which can propagate from a given surface are: one entropy, two Alfvén, two slow and two fast magnetosonic waves). The remaining conditions (until reach the number seven) are specified in order to pass through singular surfaces. When we pass through these closed surfaces the number of outgoing waves is changed. These surfaces are the SMSS, the Alfvén surface and the FMSS.
For example, if we begin the integration from the stellar surface with the component of the velocity perpendicular to this surface less than the corresponding component of the slow speed, then we must give four boundary conditions (related to the entropy wave, to one Alfvén, one slow and one fast wave). The other three are specified in order to pass the solution through the SMSS, the Alfvén surface (AS) and the FMSS. Totally we have seven functions that define the steady state: the integrals $L\,, \Omega\,, \Psi_A\,, Q\,, E$ and for the component of the electric field ϖE_ϕ (the last integral is usually taken to be zero, but it must be added for completeness [Con96]) together with the free functions (which define the solution of the GSE) A and $\partial A/\partial \hat{n}_0$. We see that the number of the free functions (8) is larger from the sum of the number of boundaries plus the number of regularity conditions (7). That's why one of the free functions depend on the history of the flow [Bog97]. In all this thesis we have chosen this free function to be $\varpi E_\phi = 0$.
If we begin the integration with the component of the velocity perpendicular to the stellar surface less than the same component of the Alfvén speed but greater than the same component of the slow speed, then we must give five boundary conditions (related to the entropy wave, to one Alfvén, two slow and one fast wave). We 'll come back to this issue when we 'll examine the Blanford & Payne model (in Chapter 6).
Note that, in general, the surfaces where the PDE changes character from elliptic to hyperbolic or vice-versa, (namely the surfaces where $V_p = V_c\,, V_s\,, V_f$) are

not singular. Experience shows that the solution passes through the surfaces of this kind without any difficulty while the singularities appear when the solution crosses limiting characteristics [BP82, Sak85, TT91, LCB92, TS92, Con94, ST94]. This happens if we solve the Bernoulli equation simultaneously with the transfield equation (or GSE).
It is worth to note that another approach to solve the MHD equations is the following:
One can pretend that the shape of the fieldlines on the poloidal plane is known, such that at the moment we may ignore the transfield equation. Then the flux function and its derivatives are known. Then we need to examine the Bernoulli equation in order to find the density ρ or the Alfvén Mach number $M = \sqrt{\Psi_A^2/4\pi\rho}$ as a function of the position (or function of $G = \varpi/\varpi_\alpha$) on each line A=constant. This we discuss in the following.

3.1.6 Study of the Bernoulli equation

Using variables $G = \varpi/\varpi_\alpha$, $M = \rho/\rho_\alpha$ (where ϖ_α , ρ_α are the values of ϖ , ρ on the Alfvén surface $M = 1$) Eqs. (2.13),(2.14) can be written in the forms

$$\vec{B} = \frac{1}{\varpi_\alpha G}\vec{\nabla}A \times \hat{\phi} - \hat{\phi}\varpi_\alpha \Omega \Psi_A \frac{1-G^2}{G\left(1-M^2\right)} ,$$

$$\vec{V} = \frac{M^2}{\varpi_\alpha \Psi_A G}\vec{\nabla}A \times \hat{\phi} + \hat{\phi}\varpi_\alpha \Omega \frac{G^2-M^2}{G\left(1-M^2\right)} .$$

The Bernoulli equation (3.2) is then $\mathcal{B}\left(A\,,G\,,M\right) = E\left(A\right)$ with

$$\mathcal{B}\left(A\,,G\,,M\right) = \frac{\mid \vec{\nabla}A \mid^2}{2\varpi_\alpha^2 \Psi_A^2 G^2}M^4 + \frac{\gamma}{\gamma-1}Q\rho_\alpha^{\gamma-1}M^{-2(\gamma-1)} + \\ + \frac{\varpi_\alpha^2\Omega^2}{2}\left[\frac{\left(G^2-M^2\right)^2}{G^2\left(1-M^2\right)^2} + 2\frac{1-G^2}{1-M^2}\right] + \mathcal{V} , \qquad (3.10)$$

where the terms $\mid \vec{\nabla}A \mid$ and $\mathcal{V}$ are regarded as functions of G and A only.
If we want to find M at each G and on a constant line A, we must find the intersection of the function $\mathcal{B}$ (regarded as a function of M only) with $E\left(A\right)$ [7]. For each $G \neq 1$ we have:

$$\frac{\partial \mathcal{B}\left(A\,,G\,,M\right)}{\partial M^2} = \frac{\mid \vec{\nabla}A \mid^2}{\varpi_\alpha^2 \Psi_A^2 G^2}M^2 - \gamma Q \rho_\alpha^{\gamma-1}M^{-2\gamma} + \varpi_\alpha^2\Omega^2\frac{\left(1-G^2\right)^2}{G^2}\frac{M^2}{\left(1-M^2\right)^3} ,$$

$$\frac{\partial^2 \mathcal{B}\left(A\,,G\,,M\right)}{\partial\left(M^2\right)^2} = \frac{\mid \vec{\nabla}A \mid^2}{\varpi_\alpha^2 \Psi_A^2 G^2} + \gamma^2 Q \rho_\alpha^{\gamma-1}M^{-2(\gamma+1)} + \varpi_\alpha^2\Omega^2\frac{\left(1-G^2\right)^2}{G^2}\frac{2M^2+1}{\left(1-M^2\right)^4} .$$

We see that

$$\frac{\partial^2 \mathcal{B}\left(A\,,G\,,M\right)}{\partial\left(M^2\right)^2} > 0\,,\forall\, M^2 \text{ and } \lim_{M^2\to 1^\pm}\frac{\partial^2 \mathcal{B}\left(A\,,G\,,M\right)}{\partial\left(M^2\right)^2} = +\infty .$$

So the first derivative $\dfrac{\partial \mathcal{B}\left(A\,,G\,,M\right)}{\partial M^2}$ monotonically increases from $-\infty$ (when $M^2 \to 0^+$) to ∞ (when $M^2 \to 1^-$) and from $-\infty$ (when $M^2 \to 1^+$) to ∞ (when $M^2 \to \infty$). Therefore, $\exists\, M_1^2 \in (0\,,1), M_2^2 \in (1\,,\infty)$ such that $\left(\dfrac{\partial \mathcal{B}\left(A\,,G\,,M\right)}{\partial M^2}\right)_{M^2=M_{1,2}^2} = 0.$
As we see in general there are four roots (see Fig. 3.7) which correspond to super- or sub-Alfvénic, in- or out-flow. So, as we change G the function $\mathcal{B}$ consists of two grooves which connect with each other at $G = 1$ (the singularity $M = 1$ disappears when $G = 1$) and then separate again (see Fig. 3.8). The two local minima of these grooves move, and when $\mathcal{B} = E$ at this minimum

[7] A similar analysis is presented in [HN89, Hey96].

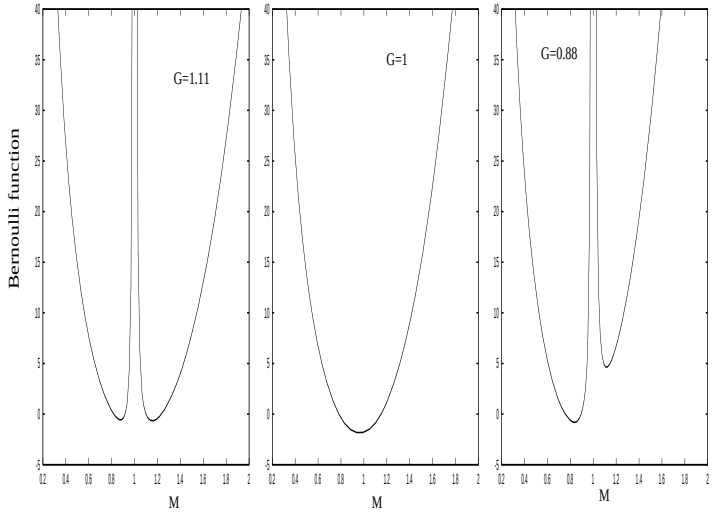

Figure 3.7: The function $\mathcal{B}$ for various values of G. The example is taken from an exact polytropic, r- self similar solution, which is analyzed in detail in Chapter 6. See also Figs. 6.7,6.8.

we have a critical point because at this point: $\partial\mathcal{B}(A\,,G\,,M)/\partial M = 0$ and $\partial\mathcal{B}(A\,,G\,,M)/\partial G = 0$ (since immediately after this point the minimum of the function $\mathcal{B}$ decreases in order to be solvable the equation $\mathcal{B} = E$). This point corresponds to a saddle point of the Bernoulli surface (Fig. 3.8).
After some manipulation, we find that
$M^2\dfrac{\partial\mathcal{B}(A\,,G\,,M)}{\partial M^2} = \dfrac{V_p^4 - V_p^2\left(C_s^2 + V_A^2\right) + C_s^2 V_{A\,,p}^2}{V_p^2 - V_{A\,,p}^2}$ [8]. So when at this point $\mathcal{B} = E$, (this minimum is a point of the solution), we have $V_p = V_s$ or $V_p = V_f$. After finding the necessary conditions in order to pass the solution for M from the two critical points $V_p = V_s\,, V_f$ (otherwise as we see from the contours in Fig. 3.8 the solution is unphysical), one must go back to the transfield equation and examine if the known fieldlines and the function M which is found from the Bernoulli equation (together with the integrals which are determined for the passing through critical points), satisfy this equation. If not we must assume another form of the lines and do the same first with the Bernoulli and secondly with the transfield until this algorithm converts to the right solution [Sak90].

[8] Note that without rotation, $\Omega = 0$, we have $M^2\dfrac{\partial\mathcal{B}(A\,,G\,,M)}{\partial M^2} = V_p^2 - C_s^2$. Thus in this case, the only critical point is the sonic point (correspond to a saddle point of the Bernoulli function, which consists of only one groove in this case.

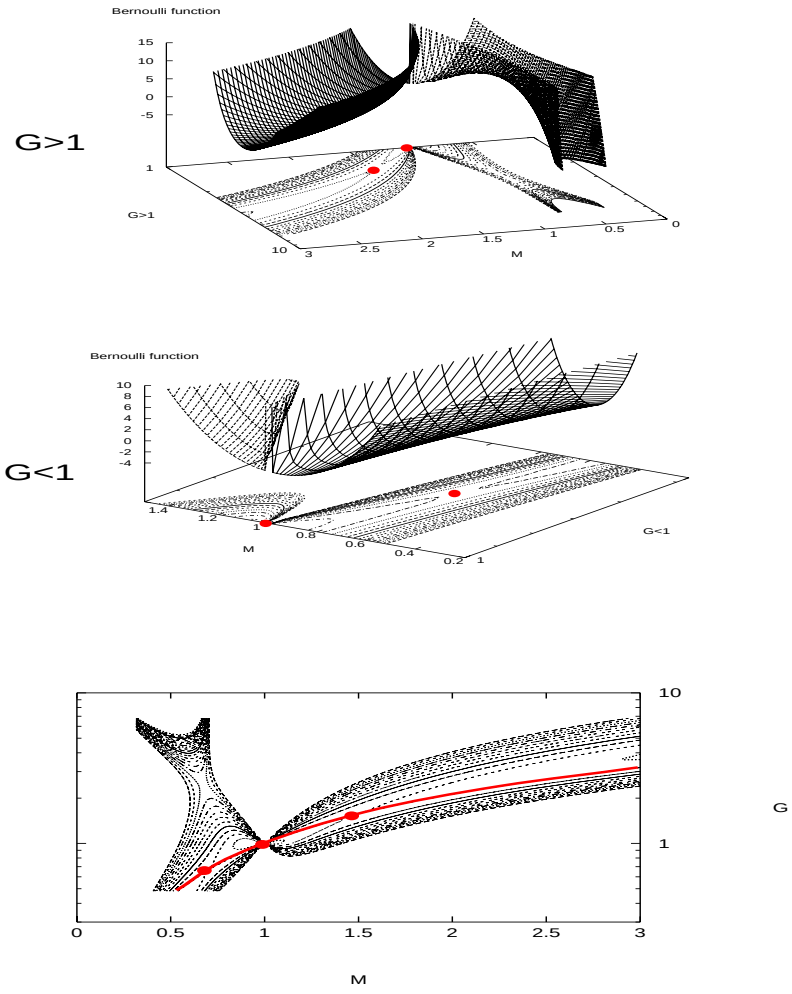

Figure 3.8: The three-dimensional diagram for the function $\mathcal{B}$, and the isocontoures on the $G\,,M$ plane. We see the critical solution (thick line) which pass through the three critical points: the slow, where $V_p = V_s$, the Alfvén, where $V_p = V_{A\,,p}$ and the fast, where $V_p = V_f$. The example is taken from an exact polytropic, r- self similar solution, which is analyzed in detail in Chapter 6 (see Figs. 6.7,6.8). Note that only if we know one exact solution of the MHD equations, we can plot this Bernoulli function. Exceptions are the models where the transfield equation is identically satisfied as in the Parker's solution and the Weber-Davis equatorial wind.

3.2 Self-similar approach

On the poloidal plane one may define a system of non-orthogonal coordinates $O\chi\psi$ such that all physical quantities are functions of χ and ψ. If we give the ψ dependence in all these quantities then PDE becomes an ordinary differential equation (ODE) with respect to the coordinate χ. This is practically done in the self similar approach. The whole problem after this assumption is simplified though it remains again very difficult due to the existence of singular surfaces (now singular points since ψ disappears from the equations) the position of which is not known *a priori* but is found simultaneously with the solution. In subsection 3.2.1 even if we have non-polytropic flows we prove that these singular surfaces are the Alfvén and the modified by the self similarity slow and fast magnetosonic critical (or singular) surfaces, where

$$V_\chi^4 - V_\chi^2 \left(C_s^2 + V_A^2\right) + C_s^2 V_{A\,,\chi}^2 = 0\,.$$

The last singular surfaces are the limiting characteristics (or separatrices). Obviously all singular surfaces in all self similar cases correspond to χ =constant. At this point we remark the difference on integration between the general solution of the MHD equations and the self similar solution. When we integrate the GSE, we must analyse with a different method the hyperbolic and elliptic regimes [Shu92a]. In elliptic regimes we may use the relaxation method. In hyperbolic regimes one way is the method of characteristics [LS96, Li96]. Another method is the integration using the $(\xi\,, n)$ coordinates [BT99]. Generaly speaking in a hyperbolic regime we begin the integration from a given surface, and we move from this to another (close to the previous) surface. Theoretically speaking we can integrate with this way the elliptic regime too. But this method is very unstable [Shu92a]. Thus, the right way for integration in an elliptic regime is to give conditions in a closed boundary (because a disturbance in one point of an elliptic regime can affect the whole elliptic regime) using the method of relaxation. Of course the difficulty is that we don't know *a priori* the end of the elliptic regime.

But in a self similar solution we integrate all regimes like the hyperbolic ones since the ODE have infinite acurracy. Thus we move from a surface $\chi = \chi_0$ to another one $\chi = \chi_0 + d\chi$, with $\mid d\chi \mid \ll \mid \chi_0 \mid$. When we pass the Alfvén surface and slow or fast limiting characteristic we can't continue the integration without imposing some regularity condition (in the next Chapters we 'll examine in detail self similar solutions).

3.2.1 Singular points in self similar flows

Using the pair $(\chi\,,A)$ as the independent coordinates on the poloidal plane, the full set of the MHD equations reduces to Eqs. (2.19),(2.20).
Next regarding each function $\mathcal{G}\,(\chi\,,A)$ of χ and A as a function of $\chi\,,A$ and M^2, we have

$$\frac{\partial \mathcal{G}\,(\chi\,,A)}{\partial \chi} \equiv \frac{\partial \mathcal{G}}{\partial \chi} = \frac{\partial \mathcal{G}\left(\chi\,,A\,,M^2\right)}{\partial \chi} + \frac{\partial \mathcal{G}\left(\chi\,,A\,,M^2\right)}{\partial M^2}\frac{dM^2}{d\chi} \text{ and}$$

$$\frac{\partial \mathcal{G}\,(\chi\,,A)}{\partial A} \equiv \frac{\partial \mathcal{G}}{\partial A} = \frac{\partial \mathcal{G}\left(\chi\,,A\,,M^2\right)}{\partial A}\,.$$

Thus, when the operator $\dfrac{\partial}{\partial \chi}$ acts on a function which may depend implicitly on M^2, generates a term, proportional to $\dfrac{dM^2}{d\chi}$. The functions $P\,,\mathcal{F}_1\,,\mathcal{F}_2$ and $\mathcal{S}$ (see their definitions in Chapter 2) may have a M^2-dependence.
Assume that this is not the case for the line elements $h_1\,,h_2$ and h_3. This is true in all the examined (until now) self similar models:

- in θ- self similarity, $\chi = r$ and $\chi_\perp = \theta$ so $h_1 = 1\,,h_2 = r$. We see that h_2 doesn't depend on $M^2\,(r)$ since it's simply equal to r.
- in r- self similarity $\chi = \theta$ and $\chi_\perp = -r$ so $h_1 = r\,,h_2 = 1$. But r is an explicit function of $\alpha\,,G\,(\theta)$ and θ as we'll see in Eq. (5.55) (we remind that the dimensionless radius $G = \varpi/\varpi_\alpha$ depend only on θ and not on M^2 although its derivative may depend on M^2).

Now collecting the terms with $\dfrac{dM^2}{d\chi}$ in Eqs. (2.19),(2.20) we end up (after some manipulation) with

$$\left[\frac{4\pi M^2}{\Psi_A^2}\frac{\partial P\left(\chi\,,A\,,M^2\right)}{\partial M^2} + \frac{\partial \mathcal{S}\left(\chi\,,A\,,M^2\right)}{\partial M^2}\right]\frac{dM^2}{d\chi} + \mathcal{G}_1\left(\chi\,,A\,,M^2\right) = 0 \text{ and} \tag{3.11}$$

$$\left[\left(1-M^2\right)\frac{\partial \mathcal{F}_1\left(\chi\,,A\,,M^2\right)}{\partial M^2} - \mathcal{F}_1\right]\frac{dM^2}{d\chi} + \mathcal{G}_2\left(\chi\,,A\,,M^2\right) = 0\,. \tag{3.12}$$

So at each point where in the derivative of M^2 the numerator and denominator simultaneously vanish, $\dfrac{dM^2}{d\chi} = \dfrac{0}{0}$ we have

$$\left[\frac{4\pi M^2}{\Psi_A^2}\frac{\partial P\left(\chi\,,A\,,M^2\right)}{\partial M^2} + \frac{\partial \mathcal{S}\left(\chi\,,A\,,M^2\right)}{\partial M^2}\right]_x = 0 \text{ and} \tag{3.13}$$

$$\left[\frac{\partial \mathcal{F}_1\left(\chi\,,A\,,M^2\right)}{\partial M^2} - \frac{\mathcal{F}_1}{1-M^2}\right]_x = 0\,. \tag{3.14}$$

A point where this happens is called singular or critical (in self similar solutions it is an isocontour χ =constant). We define the square of the sound speed as the infinitesimal change of the pressure divided by the change of density, for a disturbance in a given point of space (so from the three "variables" $\chi\,,A$ and M^2, only the third is changed)

$$C_s^2=\left(\frac{\partial P}{\partial\rho}\right)_{(\chi\,,A)}=\frac{\dfrac{\partial P\left(\chi\,,A\,,M^2\right)}{\partial M^2}}{\dfrac{\partial\rho\left(\chi\,,A\,,M^2\right)}{\partial M^2}}=-\frac{4\pi M^4}{\Psi_A^2}\frac{\partial P\left(\chi\,,A\,,M^2\right)}{\partial M^2}\,. \tag{3.15}$$

Now, using Eqs. (2.15),(2.16),(3.14), we find that if at the critical point

$$\left[\frac{\partial\mathcal{F}_2\left(\chi\,,A\,,M^2\right)}{\partial M^2}\right]_x=0\,, \tag{3.16}$$

then Eq. (3.13) is equivalent with

$$\left[V_\chi^4-V_\chi^2\left(C_s^2+V_A^2\right)+C_s^2V_{A\,,\chi}^2\right]_x=0\,. \tag{3.17}$$

Eq. (3.16) holds at every point in all known self similar models where $\chi=r$ or $\chi=\theta$ (in all these cases $\mathcal{F}_2=\alpha\dfrac{dA}{d\alpha}\dfrac{\partial\varpi^2}{\partial\chi_\perp}$ which is independent of M^2 since G is independent of M^2).
Note that a combination of Eqs. (3.11)-(3.12), at each point (not only at the critical ones) is

$$\frac{dM^2}{d\chi}=V_\chi^2\frac{\left(1-M^2\right)\mathcal{G}_1-M^4B_2^2\mathcal{G}_2/\Psi_A^2\mathcal{F}_1}{V_\chi^4-V_\chi^2\left(C_n^2+V_A^2\right)+C_s^2V_{A\,,\chi}^2} \tag{3.18}$$

where

$$C_n^2=\left(\frac{\partial P}{\partial\rho}\right)_{(\chi\,,A)}+M^2\left(\frac{\partial B_1^2/8\pi}{\partial\rho}\right)_{(\chi\,,A)}=C_s^2+M^2\frac{\dfrac{\partial B_1^2\left(\chi\,,A\,,M^2\right)}{8\pi\partial M^2}}{\dfrac{\partial\rho\left(\chi\,,A\,,M^2\right)}{\partial M^2}}\,.$$

In all known self similar models $C_n=C_s$, since $\dfrac{\partial\mathcal{F}_2\left(\chi\,,A\,,M^2\right)}{\partial M^2}=0\Leftrightarrow\dfrac{B_1\left(\chi\,,A\,,M^2\right)}{\partial M^2}=0$. From the Eq. (3.18) it is obvious that at each critical point, Eq. (3.17) holds.

3.3 Appendix 3.A: MHD wave propagation in a moving medium

3.3.1 Dispersion relations and polar diagrams

Suppose that we have a stationary axisymmetric solution of the MHD equations. Consider small axisymmetric perturbations of this system. If we consider small range disturbances, then we assume that the unperturbed solution is space independent. So we may look for perturbations having a Fourier dependence

$$e^{i\left(\omega_i t-\vec{k}\cdot\vec{r}_i\right)} ,$$

with ω_i , $\vec{k}$ being real constants, $\vec{k}$ on the poloidal plane and $\vec{r}_i$ the position vector in a frame moving with the fluid velocity. After linearizing the time-dependent MHD equations and assuming polytropic relation between pressure and density $P \propto \rho^\gamma$, we have the following types of dispersion relations (or waves) [Wei83, Pri84, Shu92b]:

- entropy wave: $\omega_i/k = \mathcal{P}_e$ where $\mathcal{P}_e = 0$
- Alfvén wave: $\omega_i/k = \mathcal{P}_A$ where $\mathcal{P}_A = V_{A\,,p} \mid \cos\vartheta \mid$ and ϑ is the angle between $\vec{B}_p$ and $\vec{k}$ (if x =constant is the line perpendicular to $\vec{k}$, on the poloidal plane, then $V_{A\perp x} = \mathcal{P}_A$).
- slow wave: $\omega_i/k = \mathcal{P}_s$ where
  $\mathcal{P}_s = \sqrt{\dfrac{C_s^2 + V_A^2 - \sqrt{\left(C_s^2 + V_A^2\right)^2 - 4C_s^2 V_{A\,,p}^2 \cos^2\vartheta}}{2}}$
  (in this case $V_{s\perp x} = \mathcal{P}_s$).
- fast wave: $\omega_i/k = \mathcal{P}_f$ where
  $\mathcal{P}_f = \sqrt{\dfrac{C_s^2 + V_A^2 + \sqrt{\left(C_s^2 + V_A^2\right)^2 - 4C_s^2 V_{A\,,p}^2 \cos^2\vartheta}}{2}}$
  (in this case $V_{f\perp x} = \mathcal{P}_f$).

The last two phase velocities satisfy the equation

$$V_{f\,,s\perp x}^4 - V_{f\,,s\perp x}^2 \left(C_s^2 + V_A^2\right) + C_s^2 V_{A\perp x}^2 = 0 .$$

In the plasma, the number of the waves with the wave vector perpendicular to a surface x =constant, is equal to the number of the parameters defining the state of the plasma. In the magnetized plasma these are the density, the pressure, three components of $\vec{V}$ and two components of $\vec{B}$ (since $\vec{\nabla}\cdot\vec{B} = 0$). Totally we have seven parameters. Correspondingly we have seven MHD waves: the entropy wave, two Alfvén waves (with $\hat{k} = \pm\vec{\nabla}x/ \mid \vec{\nabla}x \mid$), two slow and two fast magnetosound waves.

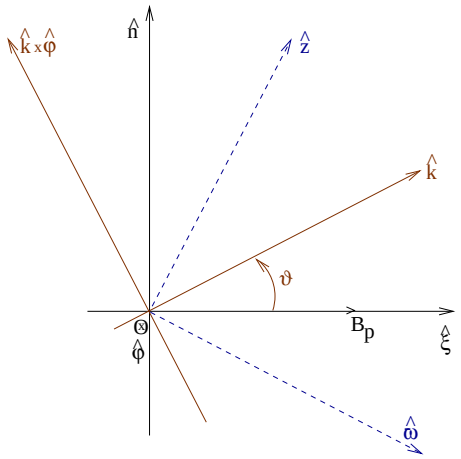

Figure 3.9: Unit vectors.

In the inertial frame (the frame of the star), we must replace ω_i with the Doppler-shifted frequency $\omega = \omega_i + \vec{V}_p \cdot \vec{k}$. The phase velocity in the moving frame is $\vec{V}_{ph\,,i} = \hat{k}\omega_i/k \equiv \hat{k}\mathcal{P}$. We see that this velocity depends only on the angle ϑ but not on the $\mid \vec{k} \mid = k$. So the group velocity in the moving frame is $\vec{V}_{g\,,i} = \vec{\nabla}_{\vec{k}}\omega_i = \hat{k} \quad \mathcal{P} + \hat{k} \times \hat{\phi} \quad d\mathcal{P}/d\vartheta$, where $\hat{k} \times \hat{\phi}$ is the unit vector on the poloidal plane, perpendicular to $\vec{k}$. In the frame of the star we have $\vec{V}_g = \vec{V}_{g\,,i} + \vec{V}_p$ and $\vec{V}_{ph} = \hat{k}\left(\mathcal{P} + \hat{k} \cdot \vec{V}_p\right)$.

Let's examine the direction of $\vec{V}_{g\,,i}$. If ϑ_g is the angle which $\vec{V}_{g\,,i}$ makes with the poloidal magnetic field $\vec{B}_p$, then

$$\tan\vartheta_g = \frac{\vec{V}_{g\,,i} \cdot \left(\vec{B}_p \times \hat{\phi}\right)}{\vec{V}_{g\,,i} \cdot \vec{B}_p} = \frac{\mathcal{P}\sin\vartheta + \mathcal{P}^{'}\cos\vartheta}{\mathcal{P}\cos\vartheta - \mathcal{P}^{'}\sin\vartheta} \,,$$

$$\sin\vartheta_g = \hat{V}_{g\,,i} \cdot \left(\hat{B}_p \times \hat{\phi}\right) \,,$$

where $\mathcal{P}^{'} \equiv d\mathcal{P}/d\vartheta$.
In the frame of the star, the phase polar depend on the poloidal velocity of the flow $\vec{V}_p$. We 'll examine only the case where $\vec{V}_p // \vec{B}_p$.

Suppose we are in a surface x =constant (line on the poloidal plane) and we examine the two waves with $\vec{k}$ perpendicular to this surface. For one $\vec{k}\,, \vartheta \in (-\pi/2\,, \pi/2)$ while for the other $\vartheta \in (-\pi\,, -\pi/2) \cup (\pi/2\,, \pi)$. (We remind that ϑ is the angle between $\vec{B}_p$ and $\vec{k}$). The phase velocity is $V_{ph} = \omega_i/k + V_p\cos\vartheta$. So for the first $\vec{k}$, the $\vec{V}_{ph}$ is on the downstream regime (note that the wave may propagate downstream or upstream, since the $\vec{V}_g$ shows the direction of propagation; $\vec{V}_{ph}$ shows as only in which midplane the wave propagates). For

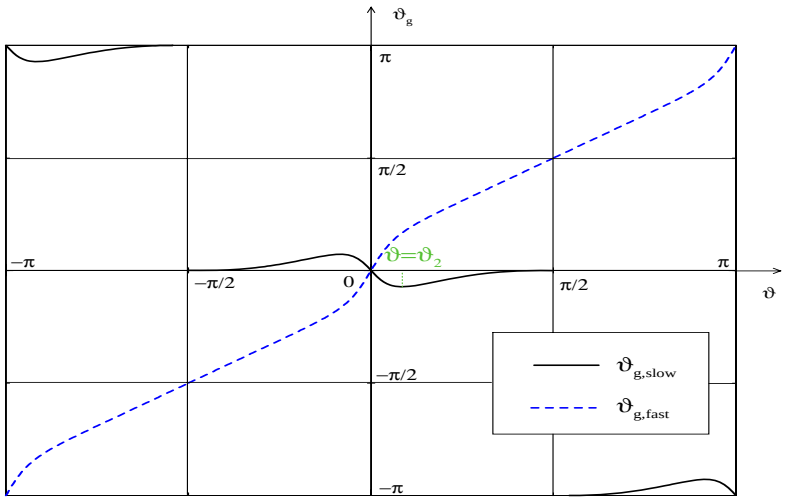

Figure 3.10: The angle of the group velocity ($V_A = 5\,, V_{A\,,p} = 4.9\,, C_s = 4.5$).

the other, $\mid \vartheta \mid > \pi/2$, and $V_{ph} = \omega_i/k + V_p \cos\vartheta = \mid \cos\vartheta \mid \left(f - V_p^2\right)\left(\sqrt{f} + V_p\right)$ where $f = \left(\omega_i/k \cos\vartheta\right)^2$. For the slow wave we see from Fig. 3.14 that:

- if $V_p < V_c$, then $f_{slow} > V_p\,, \forall\,\vartheta\,,$ so $V_{ph} > 0$ or $\vec{V}_{ph} \nearrow\!\!\nearrow \vec{k}$.
- if $V_p > V_s\,, V_{ph} < 0$ or $\vec{V}_{ph} \swarrow\!\!\nearrow \vec{k}$.
- if $V_c < V_p < V_s$, there is an angle $\vartheta_1 \in (\pi/2\,, \pi)$ such that in this direction (and in the symmetric one $\vartheta = -\vartheta_1$), $V_{ph} = 0$. For $\mid \vartheta \mid > \vartheta_1\,, V_{ph} > 0$. The lines $\vartheta = \pm\vartheta_1$ are perpendicular to the characteristics.

Similarly for the fast wave, we see from Fig. 3.14 that:

- if $V_p < V_f\,, V_{ph} > 0$
- if $V_p > V_f$, there is an angle $\vartheta_1 \in (\pi/2\,, \pi)$ such that in this direction (and in the symmetric one $\vartheta = -\vartheta_1$), $V_{ph} = 0$. For $\mid \vartheta \mid > \vartheta_1\,, V_{ph} < 0$. The lines $\vartheta = \pm\vartheta_1$ are perpendicular to the characteristics.

Fig. 3.18 shows the phase and group polars, for slow, Alfvén and fast waves (for various values of V_p).

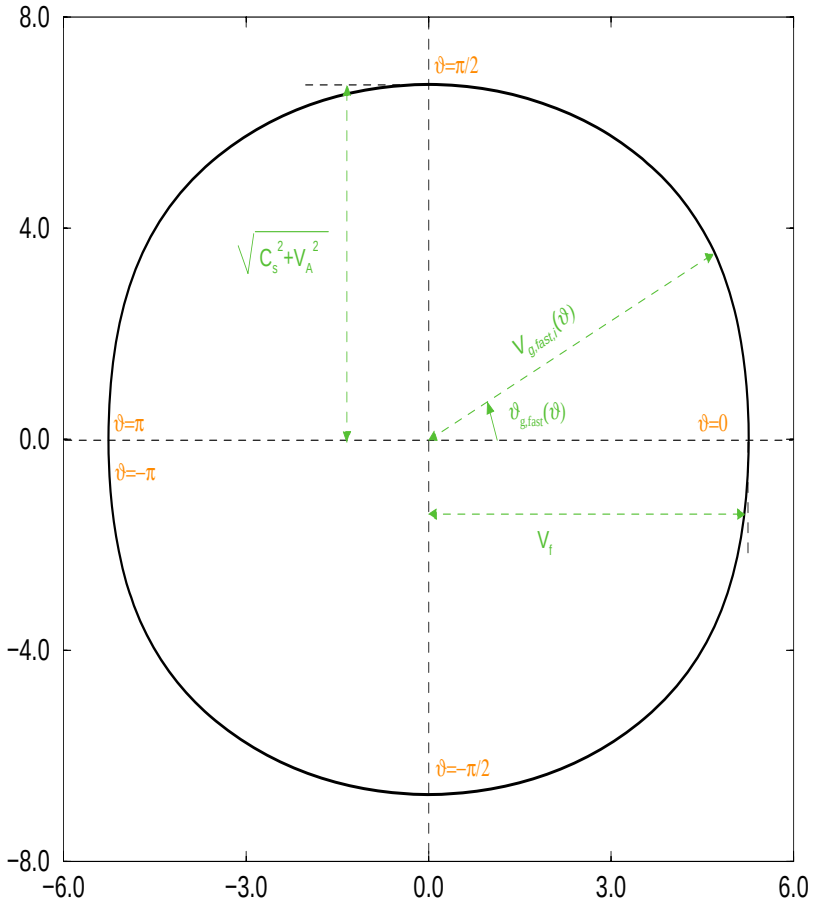

Figure 3.11: Fast wave group polar ($V_A = 5\,, V_{A\,,p} = 4.9\,, C_s = 4.5$). Parametrically, $\vec{V}_{g\,,i} \cdot \hat{B}_p = \mathcal{P}\cos\vartheta - \mathcal{P}^{'}\sin\vartheta$ and $\vec{V}_{g\,,i} \cdot \left(\hat{B}_p \times \hat{\phi}\right) = \mathcal{P}\sin\vartheta + \mathcal{P}^{'}\cos\vartheta$. This diagram is the envelope of lines AB of fig. 3.2 as point B moves on the phase polar and A moves on the axis of $\vec{B}_p$, in a way such $\vec{OB} \perp \vec{AB}$. See fig. 3.13.

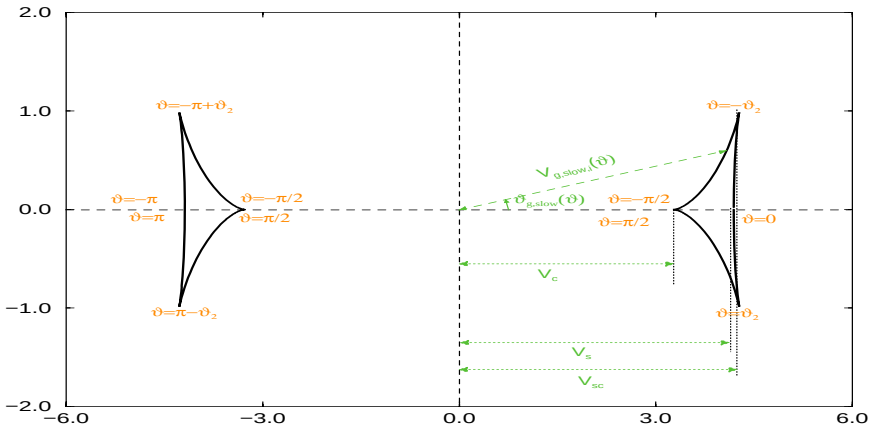

Figure 3.12: Slow wave group polar ($V_A = 5\,, V_{A\,,p} = 4.9\,, C_s = 4.5$). As in the previous figure, it is the envelope of lines AB of fig. 3.3 as point B moves on the phase polar and A moves on the axis of $\vec{B}_p$ in a way such $\vec{OB} \perp \vec{AB}$. See fig. 3.13.

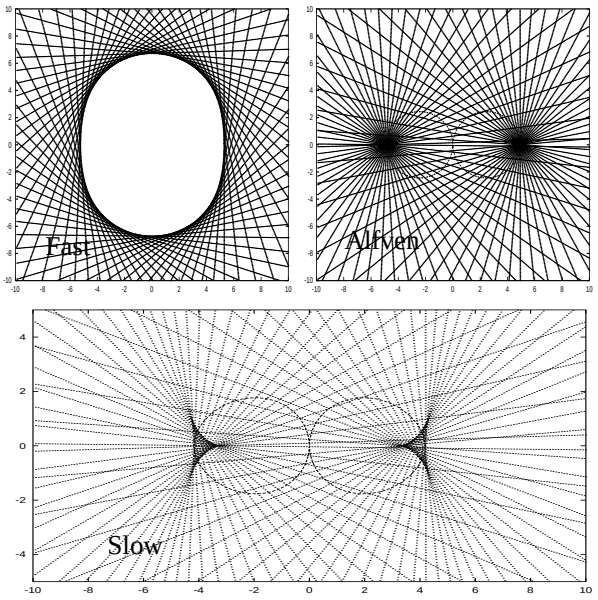

Figure 3.13: The group polars, as the envelope of lines which intersect the phase polars perpendicularly. ($V_A = 5\,, V_{A\,,p} = 4.9\,, C_s = 4.5$).

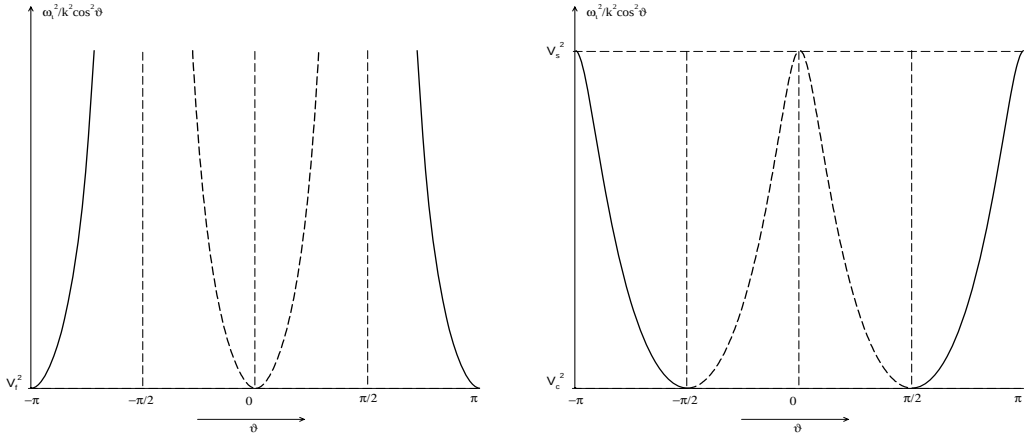

Figure 3.14: Left panel: the function f_{fast}. Right panel: the function f_{slow}. ($V_A = 5\,, V_{A\,,p} = 4.9\,, C_s = 4.5$).

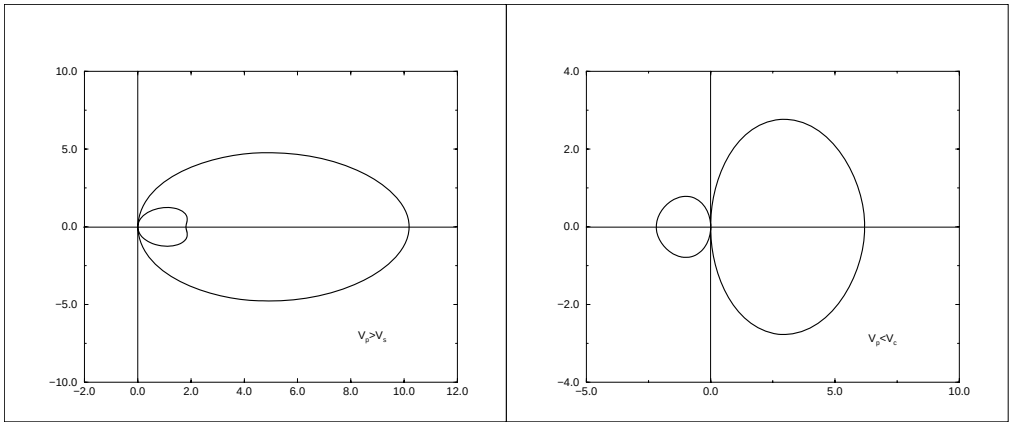

Figure 3.15: Slow wave phase polar ($V_A = 5\,, V_{A\,,p} = 4.9\,, C_s = 4.5$). Left panel: $V_p = 6 > V_s$. Right panel: $V_p = 2 < V_c$.

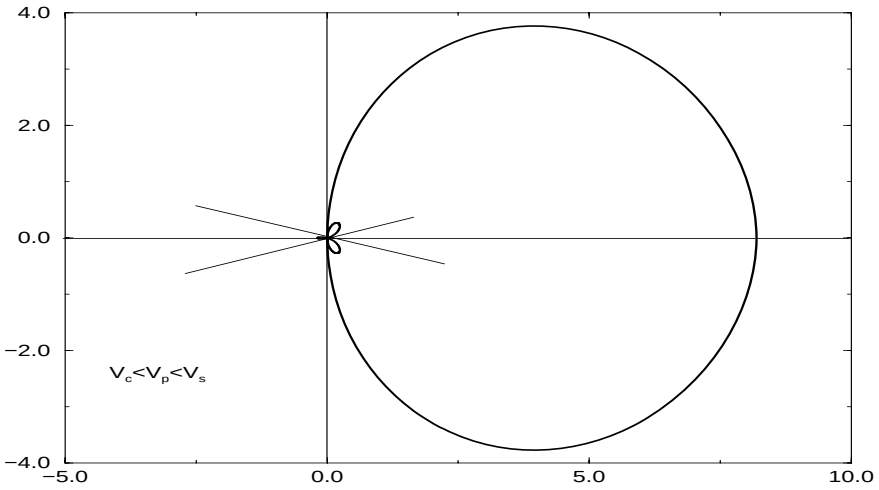

Figure 3.16: Slow wave phase polar ($V_A = 5\,, V_{A\,,p} = 4.9\,, C_s = 4.5$). In this diagram $V_p = 4$ ($V_c < V_p < V_s$). The lines $\vartheta = \pm\vartheta_1$ are shown (they are perpendicular to the characteristics).

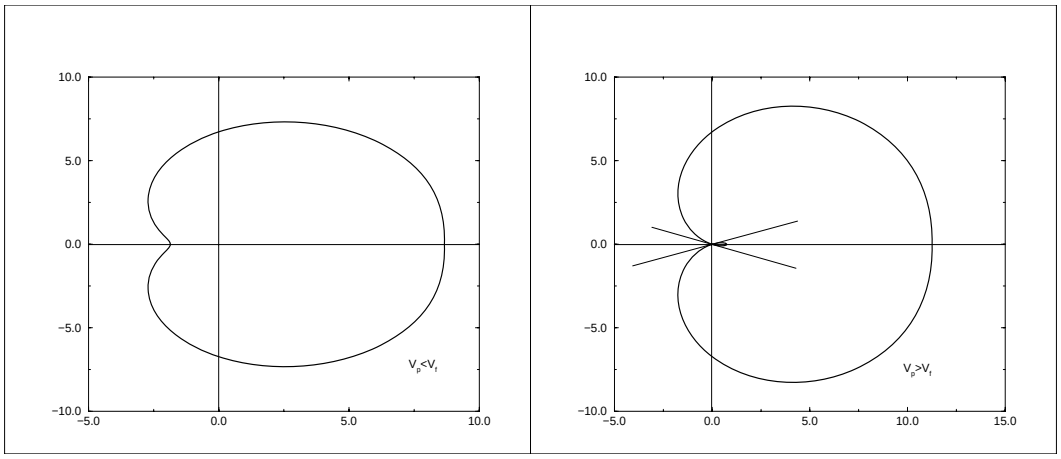

Figure 3.17: Fast wave phase polar ($V_A = 5\,, V_{A\,,p} = 4.9\,, C_s = 4.5$). Left panel: $V_p = 3.4 < V_f$. Right panel $V_p = 6 > V_f$. The lines $\vartheta = \pm\vartheta_1$ are shown.

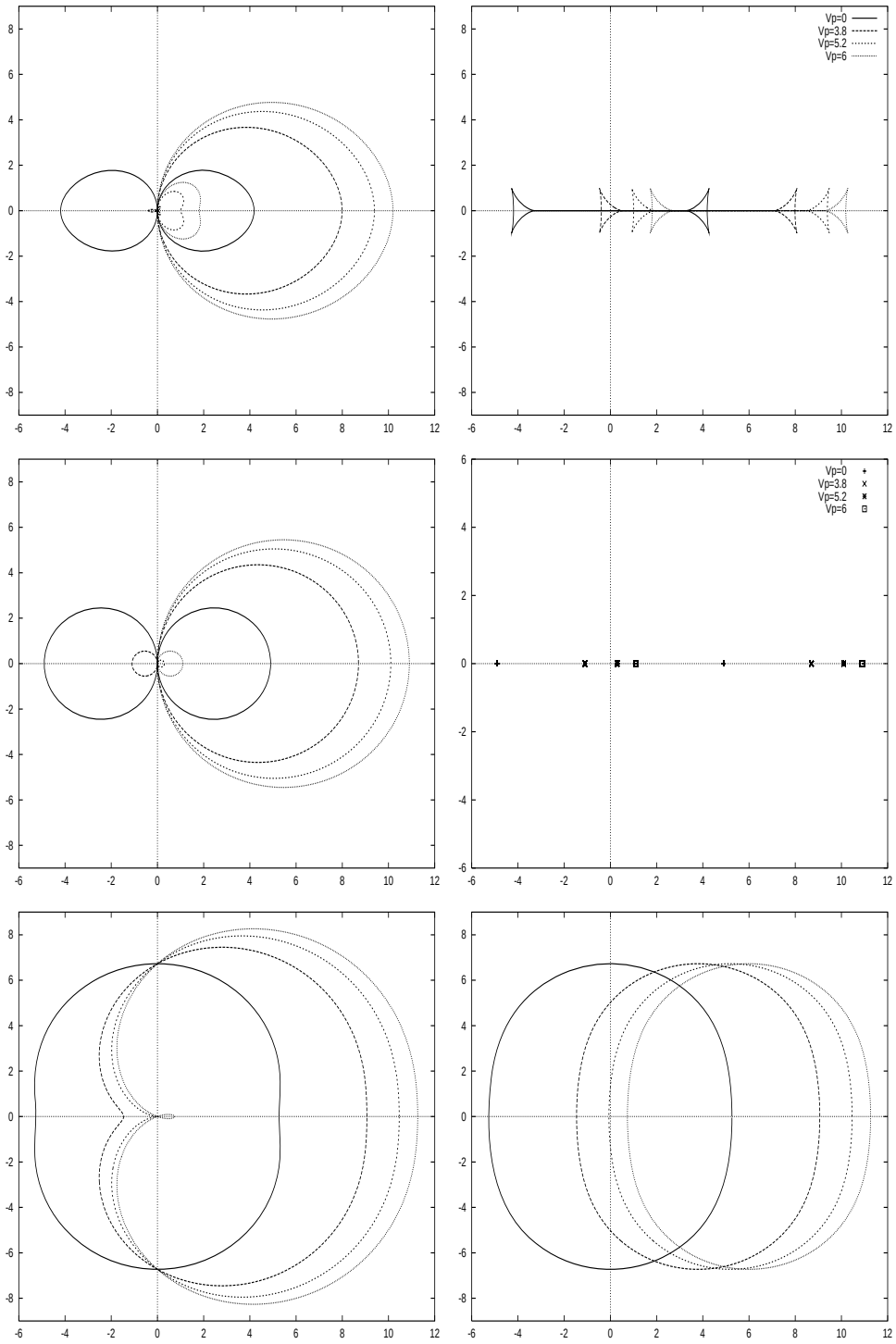

Figure 3.18: Phase (left panels) and group (right panels) polars, for the slow (top diagrams), Alfvén (diagrams in the middle) and fast (bottom diagrams) waves. In this example we choose $V_A = 5\,, V_{A\,,p} = 4.9\,, C_s = 4.5$, so $V_c = 3.278\,, V_s = 4.19\,, V_f = 5.26$. We plot the polar diagrams in the cases where $V_p = 0 < V_c\,, V_p = 3.8 \in (V_c\,, V_s)\,, V_p = 5.2 \in (V_s\,, V_f)\,, V_p = 6 > V_f$.

3.3.2 The area to which a signal may propagate

Imagine that at point A and $t = 0$ there is a small axisymmetric disturbance. This disturbance travels with velocity equal to the group velocity $\vec{V}_{g\,,i}$, with respect to the moving frame while in the frame of the star moves with velocity $\vec{V}_g = \vec{V}_{g\,,i} + \vec{V}_p$. So the components of the signal velocity in the $(\xi\,, n)$ system of coordinates (where $\hat{\xi} = \hat{B}_p\,, \hat{n} \perp \hat{\xi}$) are

$$h_\xi \frac{d\xi}{dt} = \vec{V}_{g\,,i} \cdot \hat{n} \quad \text{and} \quad h_n \frac{dn}{dt} = \vec{V}_{g\,,i} \cdot \hat{\xi} + V_p \,.$$

By eliminating the time in these two equations (divide them)

$$\frac{h_\xi d\xi}{h_n dn} = \frac{\vec{V}_{g\,,i} \cdot \hat{n}}{\vec{V}_{g\,,i} \cdot \hat{\xi} + V_p} = \frac{\mathcal{P} \sin\vartheta + \mathcal{P}^{'} \cos\vartheta}{V_p + \mathcal{P} \cos\vartheta - \mathcal{P}^{'} \sin\vartheta} \,. \tag{3.19}$$

The envelope of the family of the previous curves for various values of ϑ, is given from the system of Eq. (3.19) together with

$$0 = \frac{d}{d\vartheta} \left(\frac{\mathcal{P} \sin\vartheta + \mathcal{P}^{'} \cos\vartheta}{V_p + \mathcal{P} \cos\vartheta - \mathcal{P}^{'} \sin\vartheta} \right) \,.$$

After some manipulation this last equation yields

$$\left(\mathcal{P}^{''} + \mathcal{P} \right) \left(\mathcal{P} + V_p \cos\vartheta \right) = 0 \,. \tag{3.20}$$

- For the fast wave:
  One can prove that $\mathcal{P}_f^{''} + \mathcal{P}_f \neq 0\,, \forall\, \vartheta$ while the vanishing of the second parenthesis $\mathcal{P}_f + V_p \cos\vartheta = 0$ gives us two solutions, the $\vartheta = \pm\vartheta_1$ (see the previous subsection), which are the characteristics. For $V_p < V_f$, the envelope doesn't exist, since in this case the signal moves everywhere.
  Thus in the case of the fast wave, the situation is similar with the sound waves in hydrodynamics, where the characteristics shows the regime where the signal travel in a supersonicaly moving medium [LL75b]. Fig. 3.19 shows the propagation of a fast wave.

- For the slow wave:
  In this case, the vanishing of the second parenthesis in Eq. (3.20) gives the slow characteristics. But as we see in Figs. 3.20,3.21 the area where the wave is propagating, is determined from the vanishing of the second parenthesis in Eq. (3.20). When this happens, we have as the envelope the lines $\dfrac{h_\xi d\xi}{h_n dn} = \left(\dfrac{\mathcal{P}_s \sin\vartheta + \mathcal{P}_s^{'} \cos\vartheta}{V_p + \mathcal{P}_s \cos\vartheta - \mathcal{P}_s^{'} \sin\vartheta} \right)_{\vartheta = \vartheta_o}$, where $\left(\mathcal{P}_s^{''} + \mathcal{P}_s \right)_{\vartheta = \vartheta_o} = 0$. The solution of the last equation are the cusp points of the slow group polar, $\vartheta = \pm\vartheta_2\,, \vartheta = \pi \pm \vartheta_2$ (see Figs. 3.10,3.12).

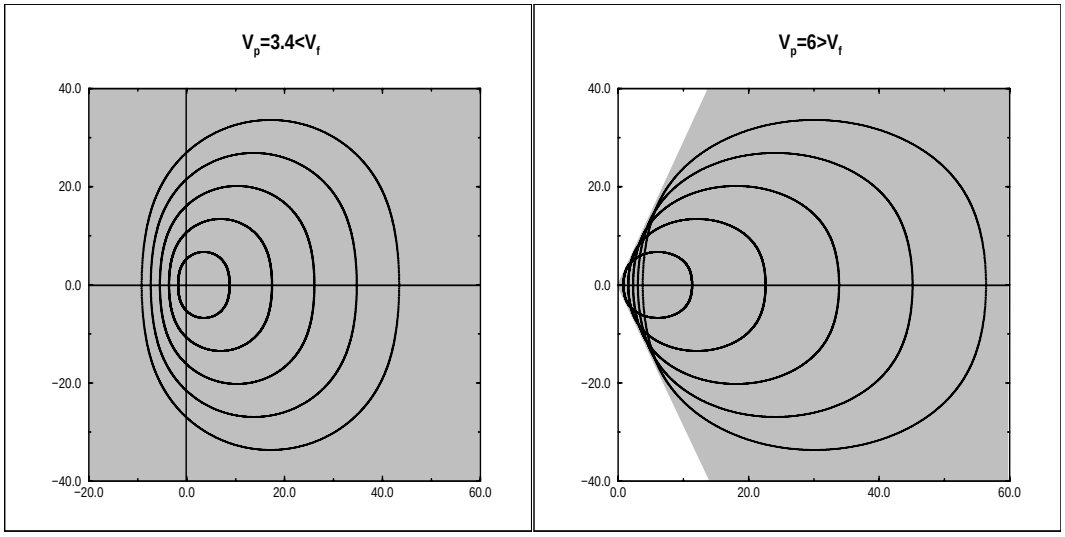

Figure 3.19: The gray area shows where the fast wave propagates. We 've plot the position of the center of the wavepacket (which travels with velocity $\vec{V}_{g\,,i}+\vec{V}_p$ at times $t = 1, 2, 3, 4, 5$. ($V_A = 5\,, V_{A\,,p} = 4.9\,, C_s = 4.5$).

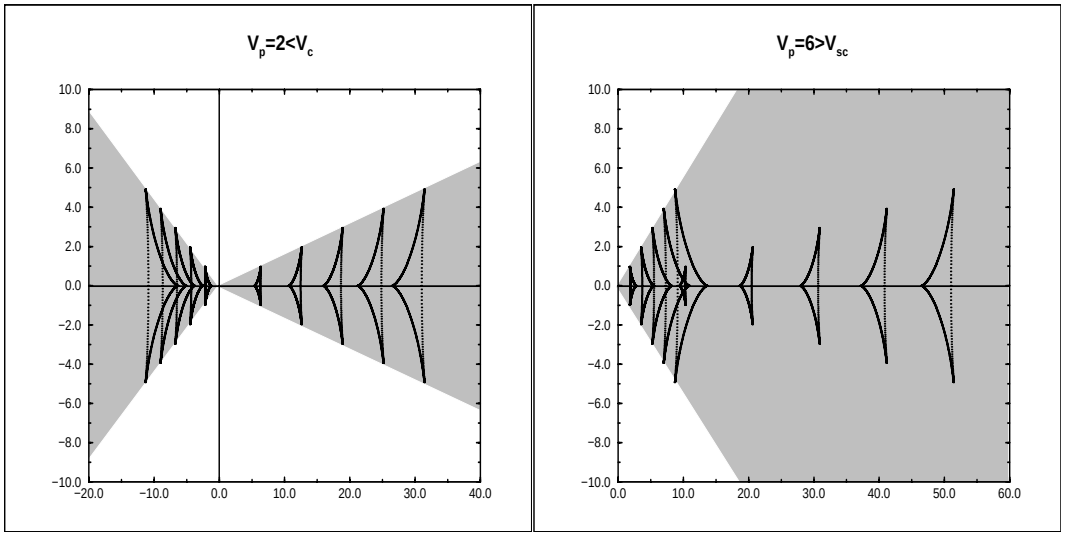

Figure 3.20: The gray area shows where the slow wave propagates. We 've plot the position of the center of the wavepacket (which travels with velocity $\vec{V}_{g\,,i} + \vec{V}_p$ at times $t = 1, 2, 3, 4, 5$. ($V_A = 5\,, V_{A\,,p} = 4.9\,, C_s = 4.5$).

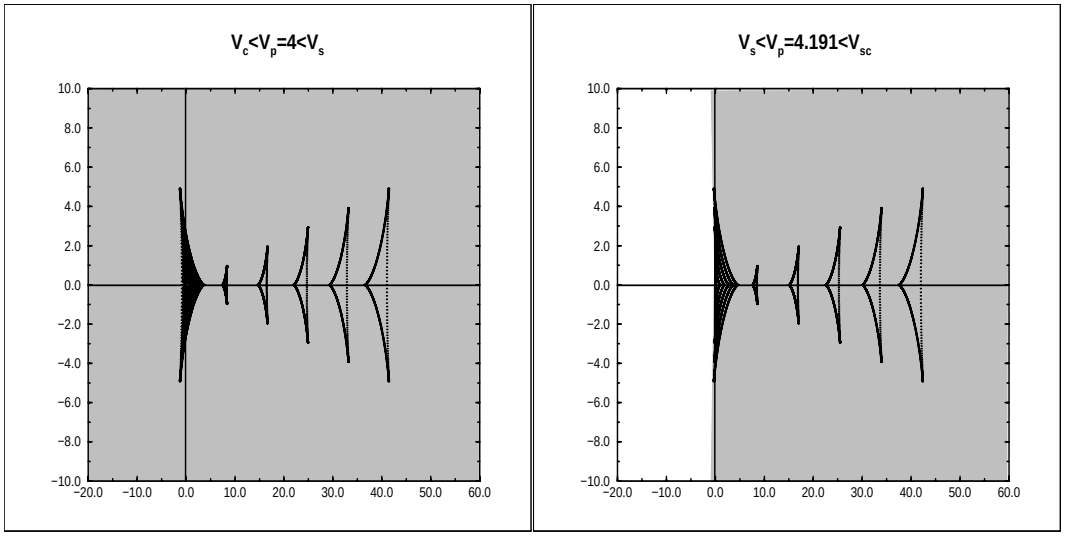

Figure 3.21: The same as the previous figure, but in the case when $V_c < V_p < V_s$ (left panel) and $V_s < V_p < V_{sc}$ (right panel).

$V_{sc} = \left(\mathcal{P}_s \cos\vartheta - \dfrac{d\mathcal{P}_s}{d\vartheta} \sin\vartheta \right)_{\vartheta = -\vartheta_2}$; see Fig. 3.12.

3.3.3 Propagation of a wave packet

Let's illustrate the meaning of the group velocity of a slow or fast MHD wave with an example. Suppose that at time $t = 0$ we have on the poloidal plane $0xy$, with $\left(\hat{x} = \vec{B}_p / B_p\right)$ a source which produces the quantity $\mathcal{G}\left(\vec{r}_i\,, t = 0\right) = e^{-x^2/2\sigma_x^2 - y^2/2\sigma_y^2} \cos\left(\vec{k}_o \cdot \vec{r}_i\right)$, where $\vec{k}_o = k_{ox}\hat{x} + k_{oy}\hat{y}$ [GR95]. It represents a wave packet with a Gaussian envelope.
We can re-express $\mathcal{G}\left(\vec{r}_i\,, t = 0\right)$ in terms of its Fourier transform:

$$\mathcal{G}\left(\vec{r}_i\,, t = 0\right) = \mathrm{Re}\left[\frac{\sigma_x \sigma_y}{2\pi} \int_{-\infty}^{-\infty}\int_{-\infty}^{-\infty} e^{i\,\vec{k}\cdot\vec{r}_i - \frac{\sigma_x^2}{2}(k_x - k_{ox})^2 - \frac{\sigma_y^2}{2}(k_y - k_{oy})^2}\, dk_x\, dk_y\right],$$

with $\vec{k} = k_x\hat{x} + k_y\hat{y}$.
If the quantity $\mathcal{G}\left(\vec{r}_i\,, t\right)$ represents a wave quantity, it must satisfy the wave equation $\frac{\omega^2}{k^2}\nabla^2\mathcal{G} = \frac{\partial^2\mathcal{G}}{\partial t^2}$. So at each time t, in order to get the time evolution, we replace $\vec{k}\cdot\vec{r}_i$ with $\vec{k}\cdot\vec{r}_i - \omega\left(\vec{k}\right)t$. The frequency ω depends on $\vec{k}$ (dispersion relation for each wave). In the case of the fast and slow MHD waves, $\omega = k\,\mathcal{P}\left(\vartheta\right)$ where $\tan\vartheta = k_y/k_x$.
So we have at each time t:

$$\mathcal{G}\left(\vec{r}_i\,, t\right) =$$

$$\mathrm{Re}\left[\frac{\sigma_x\sigma_y}{2\pi} \int_{-\infty}^{-\infty}\int_{-\infty}^{-\infty} e^{i\left[\vec{k}\cdot\vec{r}_i - \omega\left(\vec{k}\right)t\right] - \frac{\sigma_x^2}{2}(k_x - k_{ox})^2 - \frac{\sigma_y^2}{2}(k_y - k_{oy})^2}\, dk_x\, dk_y\right] . \tag{3.21}$$

For a given set of $\sigma_x\,, \sigma_y\,, k_{ox}\,, k_{oy}$ and t, we calculate numerically the quantity $\mathcal{G}$.

Figs. 3.22,3.23,3.24 for slow, and Fig. 3.22,3.25,3.26 for fast show this result.
If $k_{ox}\sigma_x + k_{oy}\sigma_y \gg 1$ (there exist many oscillations inside the initial wavepacket), we may expand the wavefrequency and keep only the first two terms

$$\omega\left(\vec{k}\right) \approx \omega\left(\vec{k}_o\right) + \left(\vec{k} - \vec{k}_o\right)\cdot\left(\vec{\nabla}_{\vec{k}}\omega\right)_{\vec{k}=\vec{k}_o} .$$

Substituting in Eq. (3.21) we get

$$\mathcal{G}\left(\vec{r}_i\,, t\right) \approx \mathrm{Re}\left[e^{-i\left[\omega\left(\vec{k}_o\right) - \vec{k}_o\cdot\left(\vec{\nabla}_{\vec{k}}\omega\right)_{\vec{k}=\vec{k}_o}\right]t} \times \right.$$

$$\left. \frac{\sigma_x\sigma_y}{2\pi} \int_{-\infty}^{-\infty}\int_{-\infty}^{-\infty} e^{i\,\vec{k}\cdot\left[\vec{r}_i - \left(\vec{\nabla}_{\vec{k}}\omega\right)_{\vec{k}=\vec{k}_o} t\right] - \frac{\sigma_x^2}{2}(k_x - k_{ox})^2 - \frac{\sigma_y^2}{2}(k_y - k_{oy})^2}\, dk_x\, dk_y\right] . \tag{3.22}$$

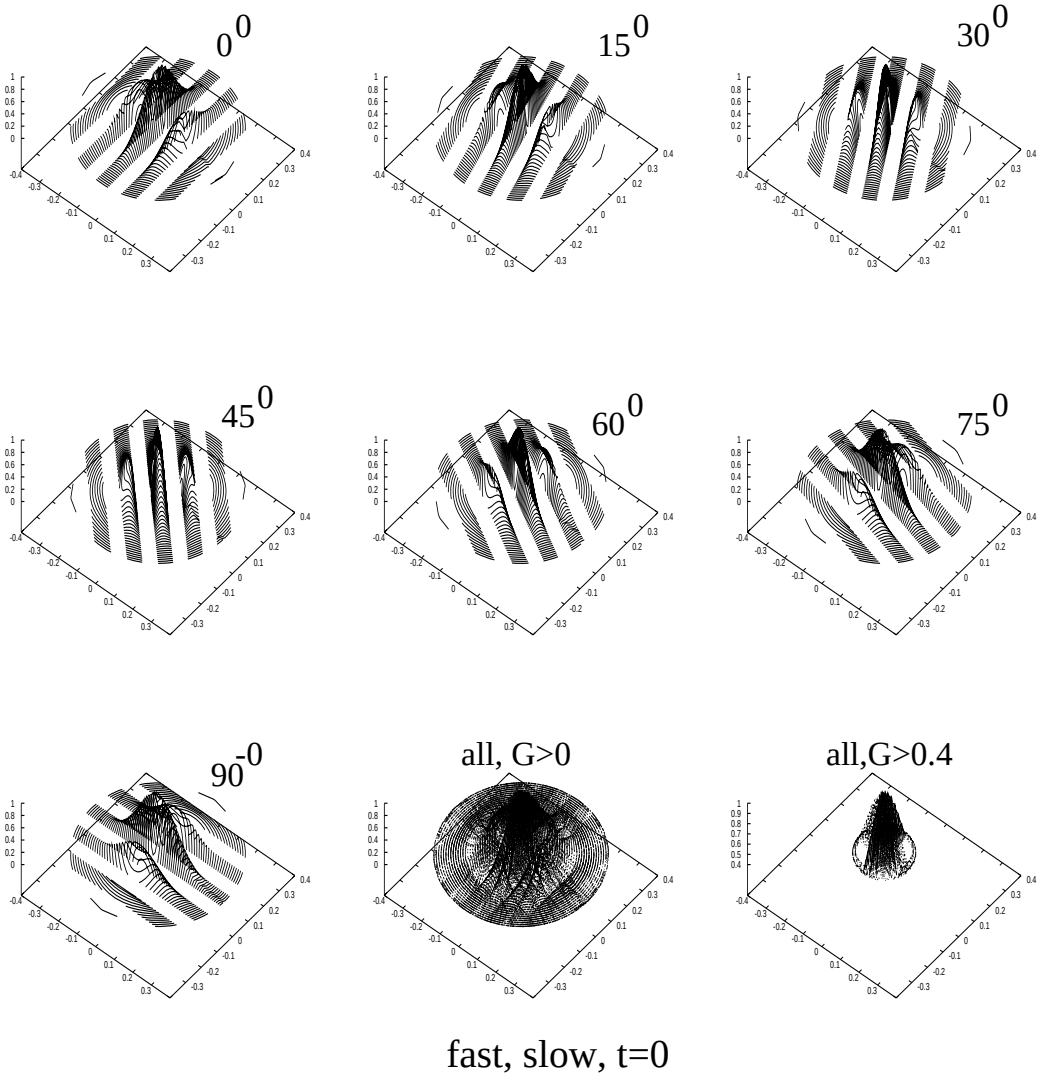

Figure 3.22: For various values of the angle between $\vec{k}_o\,,\vec{B}_p$ and time $t\,=\,0$ we've plot the quantity $\mathcal{G}$ in the midspace $\mathcal{G}\,>\,0$ as a function of the coordinates $(x\,,y)$ of the poloidal plane. In this example, $V_A\,=\,4\,,V_{A\,p}\,=\,2.5\,,C_s\,=\,3\,,\sigma_x\,=\,\sigma_y\,=\,0.1\,,k_{ox}\,=\,k_o\cos\vartheta\,,k_{oy}\,=\,k_o\sin\vartheta$, with $k_o\,=\,50$ and $\vartheta\,=\,0^o\,,15^o\,,30^o\,,45^o\,,60^o\,,75^o$ and $90^{-\,o}$. In the middle of the bottom diagrams, all packets together (the same in the right bottom, but only the values $\mathcal{G}\,>\,0.4$).

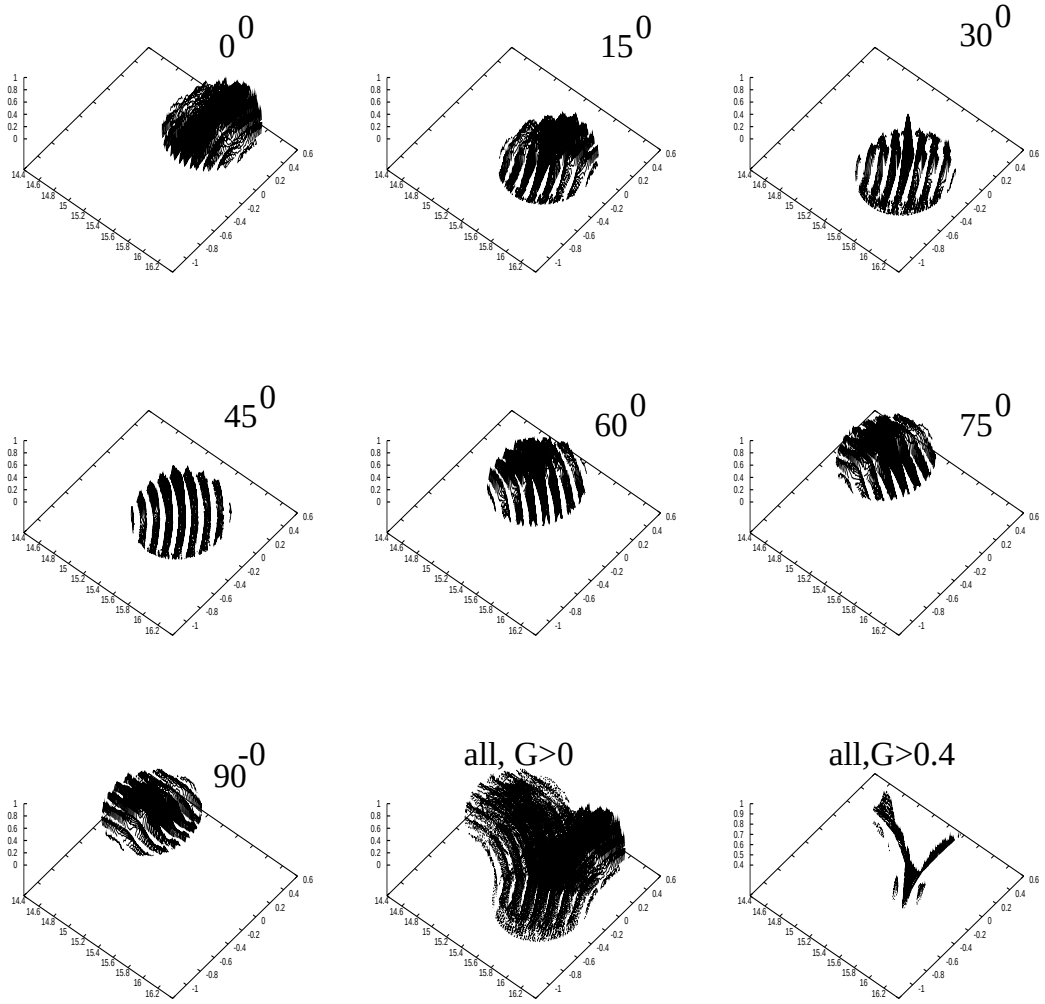

Figure 3.23: The same as in the previous figure, but only for the slow and time $t = 10$. Altogether the wave packets bring to light the half triangle-shape group polar of the slow wave.

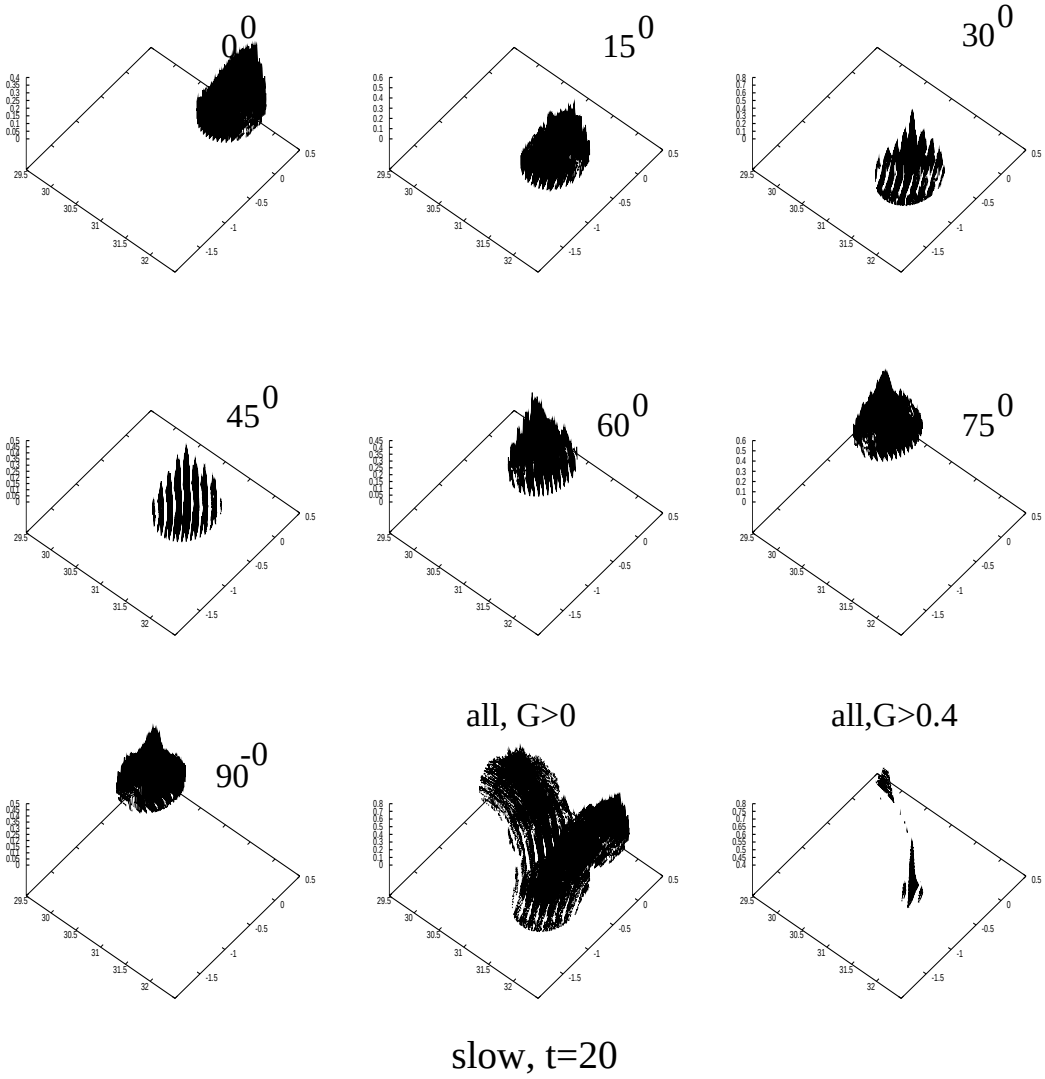

Figure 3.24: The same as in the previous figure, but for time $t = 20$. The group polar is seen very clear.

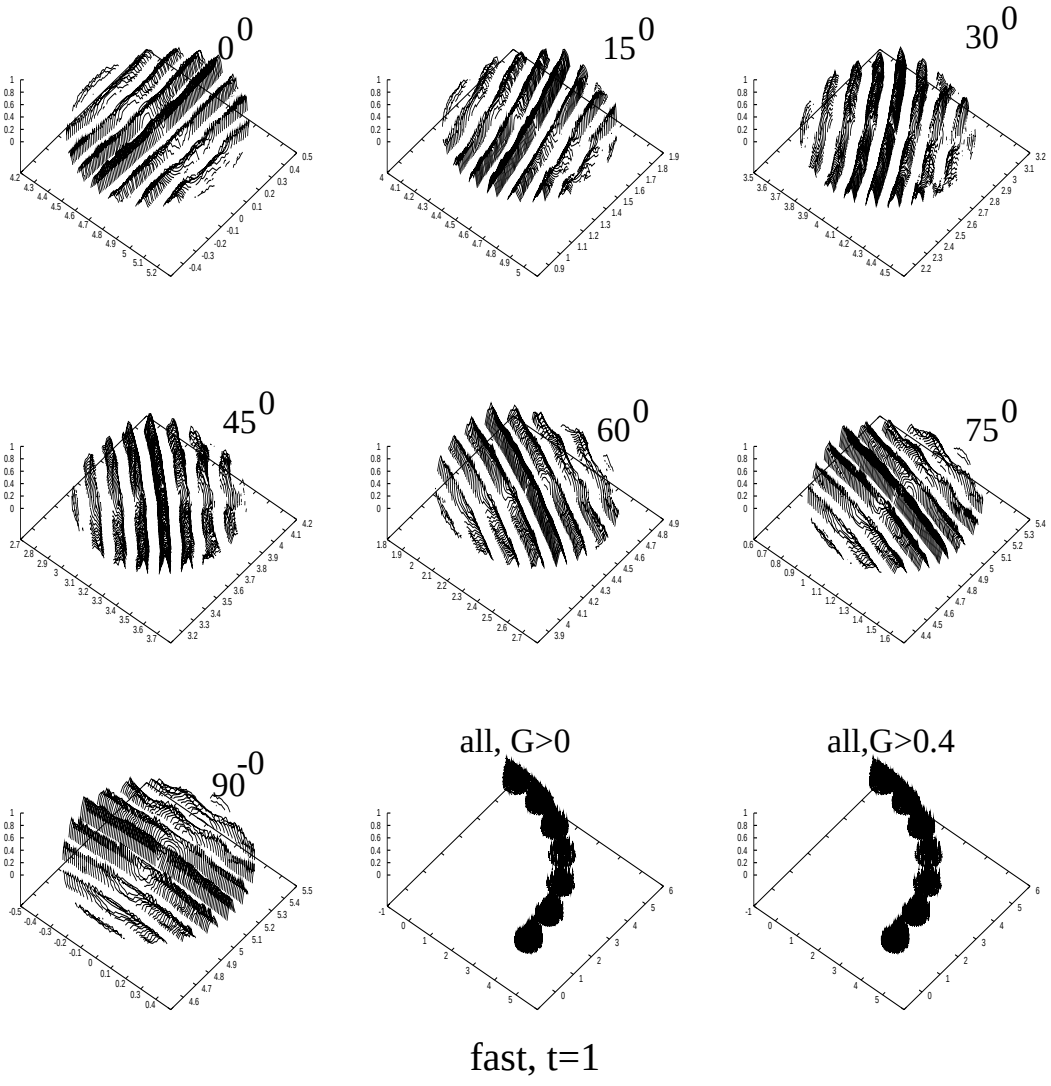

Figure 3.25: The same as in the previous figure, but for the fast and time $t = 1$.

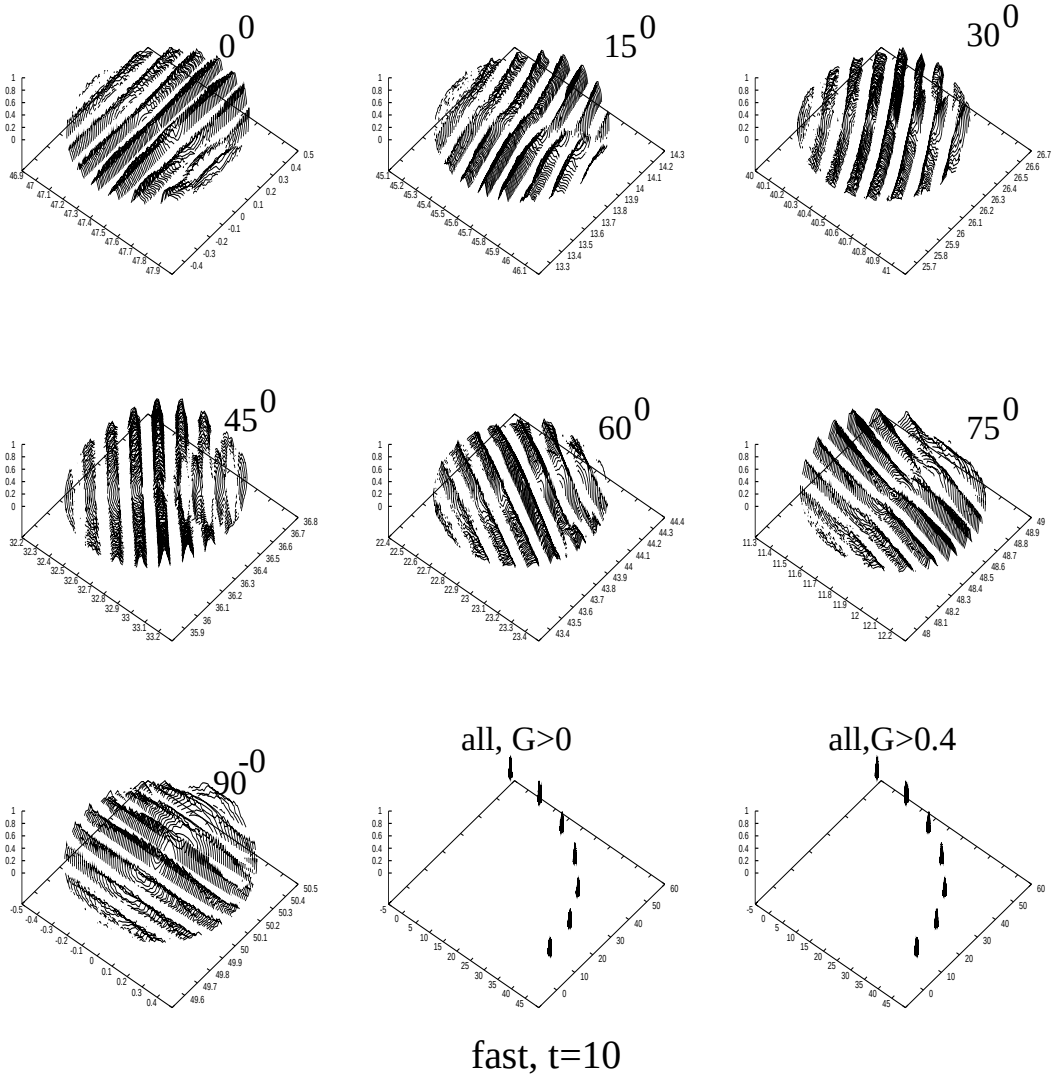

Figure 3.26: The same as in the previous figure, but for time $t = 10$.

Now the factor beginning with $\frac{\sigma_x \sigma_y}{2\pi}$ is exactly $\mathcal{G}\left(\vec{r}_i - \left(\vec{\nabla}_{\vec{k}}\omega\right)_{\vec{k}=\vec{k}_o} t\ ,0\right)$. In other words, the original packet moves with velocity $\vec{V}_{g\ ,i}\left(\vec{k}_o\right) = \left(\vec{\nabla}_{\vec{k}}\omega\right)_{\vec{k}=\vec{k}_o}$ which is called group velocity [Shu92c].
Figs. 3.22-3.26 verify this result (we see the triangle-shape slow group polar and the ellipse-shape fast group polar. The factor on the first line is an overall space-independent time oscillation corresponding to the fact that the wave fronts are propagating at the phase velocity, $\frac{\omega\left(\vec{k}_o\right)}{k_o}\hat{k}_o$, while the wave-packet moves at the group velocity, $\left(\partial\omega/\partial\vec{k}\right)_{\vec{k}=\vec{k}_o}$, not equal to $\frac{\omega\left(\vec{k}_o\right)}{k_o}\hat{k}_o$. But in the case of slow and fast MHD waves where the component of the group velocity in the direction of the vector $\vec{k}_o$ is equal with the phase speed, this factor is simply unity. So in this case, the wave-packets simply moves in space, without changing their shape. Of course if $k_{ox}\sigma_x + k_{oy}\sigma_y$ is not much larger than unity, this result is only an approximation.

Bibliography

[Bog94] S.V. Bogovalov, MNRAS **270** (1994), 721.

[Bog96] S.V. Bogovalov, MNRAS **280** (1996), 39.

[Bog97] S.V. Bogovalov, A&A **323** (1997), 634.

[BP82] R.D. Blandford and D.G. Payne, MNRAS **199** (1982), 883.

[BT99] S.V. Bogovalov and K. Tsinganos, MNRAS (1999), in press.

[Con94] J. Contopoulos, ApJ **432** (1994), 508.

[Con96] J. Contopoulos, ApJ **460** (1996), 185.

[Dra75] L. Dragos, *Magnetofluid Dynamics*, (Kent: Abacus Press), 1975.

[GH62] R. Gourant and D. Hilbert, *Methods of Mathematical Physics, Volume II*, John Wiley, New York, 1962.

[GR95] R. J. Goldston and P. H. Rutherford, *Introduction to Plasma Physics*, Institute of Physics Publishing, Brostol and Philadelphia, ch.15, 1995.

[Gud62] K. G. Guderley, *The Theory of Transonic Flow*, Addison-Wesley, Reading, 1962.

[Hey96] J. Heyvaerts, *in Plasma Astrophysics, (EADN Astrophysics School VII, San Miniato, Italy 1994)*, C. Ghiuderi & G. Einaudi (Eds.), Springer, p. 31, 1996.

[HN89] J. Heyvaerts and C.A. Norman, ApJ **347** (1989), 1055.

[HO78] M. Heinemann and S. Olbert, J. Geophys. Res. **83-A6** (1978), 2457.

[JT64] A. Jeffrey and T. Taniuti, *Nonlinear Wave Propagation with Applications to Physics and Magnetohydrodynamics*, Academic, New York, 1964.

[LCB92] Z.-Y Li, T. Chiueh, and M.C. Begelman, ApJ **394** (1992), 459.

[Li96] Z.-Y Li, ApJ **473** (1996), 873.

[LL75a] L. D. Landau and E. M. Lifschitz, *Fluid Mechanics*, Pergamon Press, Oxford, p. 444, 1975.

[LL75b] L. D. Landau and E. M. Lifschitz, *Fluid Mechanics*, Pergamon Press, Oxford, §82, 1975.

[LMMS86] R. V. E. Lovelace, C. Mehanian, C. M. Mobarry, and M. E. Sulkanen, APJS **62** (1986), 1.

[LS96] Z.-Y Li and F. H. Shu, ApJ **468** (1996), 261.

[PD90] R. V. Polovin and V. P. Demutskii, *Fundamentals of Magnetohydrodynamics*, (New York: Consultants Bureau), 1990.

[Pri84] E. R. Priest, *Solar Magnetohydrodynamics*, D. Reidal Publishing Company, Holland, ch. 4, 1984.

[Sak85] T. Sakurai, A&A **152** (1985), 121.

[Sak90] T. Sakurai, Computer Physics Reports **12(4)** (1990), 247.

[Shu92a] F. H. Shu, *The Physics of Astrophysics, Volume II: Gas Dynamics*, Univesrity Science Books, ch.13, 1992.

[Shu92b] F. H. Shu, *The Physics of Astrophysics, Volume II: Gas Dynamics*, Univesrity Science Books, ch.22, 1992.

[Shu92c] F. H. Shu, *The Physics of Astrophysics, Volume II: Gas Dynamics*, Univesrity Science Books, ch.12, 1992.

[ST94] C. Sauty and K. Tsinganos, A&A **287** (1994), 893.

[STP96] G. Surlantzis, K. Tsinganos, and E. Priest, Astrophys. Lett. Commun. **34** (1996), 251.

[TS92] K. Tsinganos and C. Sauty, A&A **255** (1992), 405.

[TSS+96a] K. Tsinganos, C. Sauty, G. Surlantzis, E. Trussoni, and J. Contopoulos, MNRAS **283** (1996), 811.

[TSS+96b] K. Tsinganos, C. Sauty, G. Surlantzis, E. Trussoni, and J. Contopoulos, *in Solar and Astrophysical MHD Flows*, K. Tsinganos (ed.), Kluwer Academic Publishers, p. 427, 1996.

[TT91] K. Tsinganos and E. Trussoni, A&A **249** (1991), 156.

[Wei83] H. Weitzner, *in Basic Plasma Physics I*, Volume editors: A.A. Galeev, R.N. Sudan, North-Holland, ch. 2.1, 1983.

Chapter 4

Asymptotic analysis of MHD outflows

General theoretical arguments and various analytic self-similar solutions have recently shown that magnetized and rotating astrophysical outflows may become asymptotically cylindrical, in agreement with observations of cosmical jets. A notable common feature in all such self-consistent, self-similar MHD solutions is that before final cylindrical collimation is achieved, the jet passes from a stage of oscillations in its radius, Mach number and other physical parameters. In this Chapter it is shown that under rather general assumptions this oscillatory behaviour of collimated outflows is not restricted to the few specific models examined so far, but instead it seems to be a rather general physical property of an MHD outflow which starts noncylindrically before it reaches collimation. It is concluded thence that astrophysical jets are topologically stable to small amplitude, time-independent perturbations in their asymptotically cylindrical shape. Also, similarly to the familiar fluid instabilities these oscillations may give rise to brightness enhancements along jets.

4.1 Introduction

Astrophysical jets are by now widely observed in several cosmical environments, from the rich variety of stellar objects to AGN and Quasars (e.g., see reviews [Bir96, FMBR96, Ray96]). Three key aspects of the theoretical problem posed by the observations of jets are (i), the construction of self-consistent dynamical equilibria describing the initial acceleration and final collimation of the outflow; (ii) examination of the stability properties of the beam and the detailed energetics of the outflow together with the *in situ* acceleration of particles and subsequent emission of radiation; and (iii) the modeling of the time-dependent problem.

Since magnetic fields seem to play a pivotal role in the acceleration, collimation and emission of radiation in jets, one may try to answer these questions

by considering to lowest approximation the magnetohydrodynamic (MHD) description. For example, in meridionally self-similar models [ST94, TST96] the outflow is accelerated by a combination of gas pressure gradients and magnetocentrifugal forces; after the outflow crosses the modified by self-similarity slow/fast magnetoacoustic surfaces [TSS$^+$96], the jet is confined either magnetically, or, by the thermal gas pressure. Similar is the situation in radially self-similar [BP82, FH96], or translationally self-similar MHD models [CH80, BC92, DZC96].

Regarding the question of classical stability of collimated outflows, it is well known that low Mach number, laboratory fluid beams maintain their directionality for relatively short distances, typically 10 times their diameter.The basic reason for beam disruption is the familiar Kelvin-Helmholtz (KH) instability due to the motion of the fluid of the beam relatively to the surrounding medium [FTZ78, FTZ81, FMBR96]. Linear KH stability analysis [FTZ78, FTZ81] predicts that the most unstable modes are of the order of the circumference of the beam times its Mach number, $\lambda_{KH} \sim 2\pi R_j M_j$ while typical times of the fastest growing modes are of the order of the ratio of the circumference of the beam to the sound or Alfvén speed times its Mach number, $\tau_{KH} \sim 2\pi (R_j/c_s) M_j$. Nevertheless, astrophysical jets firstly observed in association with extragalactic radio sources and secondly in association with young stellar objects, often extend over distances which are a much larger multiple of their width. Apart the occasional wiggles and knots of enhanced surface brightness along their length, these astrophysical jets appear to survive much longer periods than the time scales of the linear analysis of the KH instability predict that they should break up. In order to investigate possible saturation effects of the linear phase of the instability, the nonlinear evolution of the KH hydrodynamic instability has also been followed [BMFT94, BMR$^+$95]. In this case, it is found that the persistence of the jet depends principally on the density contrast with the ambient medium and the Mach number.

In addition to the KH instabilities, magnetized jets are also subject to current driven instabilities which are well known to create great difficulties in the confinement of laboratory plasmas. In superfast magnetosonic jets with speeds exceeding the fast MHD speed, the kinetic energy dominates the sum of the magnetic and thermal energies and therefore the KH instability growth rates are an order of magnitude or so, higher than the growth rates of the kink instabilities [AC92, App96]. Instead, in transfast magnetosonic jets, the current and fluid instabilities have comparable effects.

Probably related to the stability of jets, a notable aspect of available self-consistent MHD equilibrium solutions is that the beam width and other parameters undergo small amplitude oscillations which often decay with distance from the source [CH80, BC92, CL94]. These exact and quasi-analytic solutions have been obtained under specific assumptions such as the corresponding self-similarity ansatz. The subject of this Chapter is to further investigate the question which naturally arises then whether the particular feature of oscillations in the jet's width can be obtained from the general set of the MHD equations, regardless of specific models. Hence, we shall examine the *topological* stabil-

ity of an MHD outflow which is asymptotically collimated and together with its ambient medium consists of a compressible plasma of infinite conductivity. Classical stability theory addresses the question whether a given equilibrium configuration evolves away from (unstable) or back toward (stable) the initial state when perturbed. In the present context, topological stability refers to the question whether a given equilibrium state preserves its topological properties when subjected to a perturbation. We should keep in mind that topologically stable configurations may well be unstable from the classical point of view. However, since for sufficiently slow time variations, the outflow can be modeled by a sequence of quasi-static (equilibrium) states, the topological stability of a configuration may provide evidence on its classical stability.

4.2 Perturbations of collimated outflows

Consider the steady ($\partial/\partial t = 0$) hydromagnetic equations,

$$\rho\left(\vec{V}\cdot\vec{\nabla}\right)\vec{V} = \frac{\left(\vec{\nabla}\times\vec{B}\right)\times\vec{B}}{4\pi} - \vec{\nabla}P - \rho\vec{\nabla}\mathcal{V}\,, \tag{4.1}$$

$$\vec{\nabla}\cdot\vec{B} = 0\,, \quad \vec{\nabla}\cdot\left(\rho\vec{V}\right) = 0\,, \quad \vec{\nabla}\times\left(\vec{V}\times\vec{B}\right) = 0\,, \tag{4.2}$$

where $\vec{B}$, $\vec{V}$, $-\vec{\nabla}\mathcal{V}$ are the magnetic, velocity and external gravity fields, respectively while ρ and P denote the gas density and pressure. With axisymmetry ($\partial/\partial\phi = 0$), we may introduce the magnetic flux function A, such that three free integrals $\Psi(A), \Omega(A), L(A)$ exist (see Chapter 2). In terms of these integrals and the square of the poloidal Alfvén number,

$$M^2 = \frac{4\pi\rho V_p^2}{B_p^2} = \frac{\Psi_A^2}{4\pi\rho}\,, \tag{4.3}$$

the magnetic field and bulk flow speed are given in cylindrical coordinates (ϖ, ϕ, z) by the forms,

$$\begin{aligned}\vec{B} &= \frac{\vec{\nabla}A\times\hat{\phi}}{\varpi} - \frac{L\Psi_A - \varpi^2\Omega\Psi_A}{\varpi(1-M^2)}\hat{\phi}\,,\\ \vec{V} &= \frac{\Psi_A}{4\pi\rho}\frac{\vec{\nabla}A\times\hat{\phi}}{\varpi} + \frac{\varpi^2\Omega - LM^2}{\varpi(1-M^2)}\hat{\phi}\,,\end{aligned} \tag{4.4}$$

while force balance in the poloidal plane is expressed by the transfield Eq. (2.21), or

$$\begin{aligned}&\frac{\left(1-M^2\right)}{4\pi\varpi^2}\left[\varpi\frac{\partial}{\partial\varpi}\left(\frac{1}{\varpi}\frac{\partial A}{\partial\varpi}\right) + \frac{\partial^2 A}{\partial z^2}\right]\vec{\nabla}A - \frac{1}{4\pi\varpi}\frac{\partial M^2\left(\varpi, A\right)}{\partial\varpi}\frac{\partial A}{\partial z}\vec{B_p} +\\ &+M^2\vec{\nabla}\left(\frac{(\vec{\nabla}A)^2}{8\pi\varpi^2}\right) + \vec{\nabla}P + \rho\vec{\nabla}\mathcal{V} + \frac{B_\phi}{4\pi\varpi}\vec{\nabla}\left(\varpi B_\phi\right) - \hat{\varpi}\frac{\rho V_\phi^2}{\varpi} = 0\,,\end{aligned} \tag{4.5}$$

If P is related to ρ and A, for example, via a polytropic relationship with constant or variable polytropic index γ, this last vector equation leads to two scalar equations in any two independent directions on the poloidal plane for the unknowns A and M^2 (or, equivalently A and ρ). Quasi-analytical solutions of Eq. (4.5) have been found only by additionally assuming a self-similar ansatz for the dependence of the physical variables on the spherical (r,θ), or cylindrical coordinates (ϖ,z) of the poloidal plane. Thus, we have available solutions which are self-similar in (i) the cylindrical radius ϖ [CH80, BC92, DZC96], (ii) the spherical radius r [BP82, CL94, FH96] and (iii) the meridional angle θ [TT91, ST94].
In the following we shall consider an infinitely long jet where in a direction perpendicular to the flow axis, the outwards directed centrifugal force is balanced by the inwards tension of the toroidal magnetic field and gradient of the magnetic pressure, enhanced (reduced) by the gradient of the gas pressure,

$$\frac{\rho V_\phi^2}{\varpi} = \frac{\mathrm{d}}{\mathrm{d}\varpi}\left(\frac{B^2}{8\pi}+P\right)+\frac{B_\phi^2}{4\pi\varpi}\,, \tag{4.6}$$

where ϖ is the cylindrical distance in spherical coordinates (r,θ,ϕ), $\varpi = r\sin\theta$. In such a case of an asymptotically $(r\longrightarrow\infty)$ collimated outflow (jet) [HN89], the magnetic flux function A_∞, Alfvén number M_∞ and gas pressure P_∞ all become functions of the cylindrical distance ϖ at large radial distances r (in comparison to the Alfvén radius $r_\star$) from the source of the outflow where we may neglect the gravitational field,

$$A_\infty = A_\infty(\varpi)\ ,\ M_\infty^2 = M_\infty^2(\varpi)\ ,\ P_\infty(\varpi) = \int \mathcal{F}_0 d\varpi\,, \tag{4.7}$$

where the pressure gradient $\mathcal{F}_0$ is given in Appendix 4.A. For example, in the cases of cylindrical collimation of [ST94] and [CL94], $M_\infty(\varpi) = \text{const.}$ while $A_\infty(\varpi)\propto\varpi^2$, or, $A_\infty(\varpi)\propto\varpi^x$, for a constant x, in [ST94] and [CL94], respectively.
In the following we shall investigate the *topological* or structural stability of such collimated solutions. Namely, we are interested to check whether there exist small amplitude steady and axisymmetric perturbations in the streamline shape, Alfvén number and pressure, which satisfy Eq. (4.5). We are interested to derive the dependence of these perturbations on the radial distance from the central object. Consider then a solution which is topologically close to one describing a collimated outflow, Eq. (4.7),

$$\begin{aligned} &A = A_\infty(\varpi)(1+\varepsilon)\,,\quad M^2 = M_\infty^2(\varpi)(1+\varepsilon_1)\,,\\ &P = P_\infty(\varpi)+\delta P, \end{aligned} \tag{4.8}$$

where all functions $\mid\varepsilon\mid,\mid\varepsilon_1\mid$ and $\mid\delta P/P_\infty\mid \ll 1$. Substituting Eqs. (4.8) into Eq. (4.5) and by assuming that the derivatives of $\varepsilon,\varepsilon_1$ are also very small (so that we may ignore squares and products of the perturbation quantities), we obtain from the $\hat{z}$ and $\hat{\varpi}$ components of the momentum Eq. (5.1) two equations

which the perturbations ε, ε_1 and δP satisfy,

$$\delta P = \mathcal{F}_1\varepsilon + \mathcal{F}_2\varepsilon_1 + \mathcal{F}_3\frac{\partial\varepsilon}{\partial\varpi} \tag{4.9}$$

$$\frac{\partial\delta P}{\partial\varpi} = \left(\mathcal{F}_1^{'} + \mathcal{G}_1\mathcal{G}_0\right)\varepsilon + \left(\mathcal{F}_2^{'} + \mathcal{G}_2\mathcal{G}_0\right)\varepsilon_1 + \mathcal{G}_3\frac{\partial\varepsilon}{\partial\varpi} + \mathcal{G}_4\frac{\partial\varepsilon_1}{\partial\varpi} + \mathcal{G}_5\frac{\partial^2\varepsilon}{\partial\varpi^2} + \mathcal{G}_0\frac{\partial^2\varepsilon}{\partial z^2} \tag{4.10}$$

or (because of Eq. (4.9)), [1]

$$\frac{\partial^2\varepsilon}{\partial z^2} + \frac{\partial^2\varepsilon}{\partial\varpi^2} + \left(\frac{2A^{'}}{A} - \frac{1}{\varpi}\right)_\infty\frac{\partial\varepsilon}{\partial\varpi} - \left(\frac{M^2}{1-M^2}\frac{A^{'}}{A}\right)_\infty\frac{\partial\varepsilon_1}{\partial\varpi} + \mathcal{G}_2\varepsilon_1 + \mathcal{G}_1\varepsilon = 0 \tag{4.11}$$

The perturbations ε, ε_1 and δP satisfy the above equations containing the lengthy general expressions $[\mathcal{F}_1(\varpi),\ \mathcal{F}_2(\varpi),\ \mathcal{F}_3(\varpi)]$ and $[\mathcal{G}_0(\varpi),\ \mathcal{G}_1(\varpi),\ \mathcal{G}_2(\varpi),\ \mathcal{G}_3(\varpi),\ \mathcal{G}_4(\varpi),\ \mathcal{G}_5(\varpi)]$ which are all given in Appendix 4.A.
The previous analysis is independent of a specific polytropic relationship between pressure and density, some particular dependence of the perturbations ε, ε_1 and δP on their variables, as well as of any special choice of the free integrals $\Psi_A(A)$, $L(A)$ and $\Omega(A)$. In order to get some insight into the behaviour of the perturbations, one should analyze the above general nonlinear equation. This is however a formidable mathematical task and instead it occurred to us that some physical understanding of the physical trends of the perturbations can be gained by examining separately, (a) the case where the perturbations in streamline shape and Alfvén number are related, (b) the case where the perturbations in streamline shape and Alfvén number are unrelated, and (c) the case where a *constant* index polytropic relation between pressure and density is assumed. In each of the above cases (a), (b) or (c), we shall further examine separately the various cases where a separation of the variables in the perturbations ε and ε_1 is possible. Finally, in each such subcase, we shall apply the results of our analysis to the few examples where special sets of the free integrals $\Psi_A(A)$, $L(A)$ and $\Omega(A)$ have provided known quasi-analytical solutions.

4.3 Linearly related perturbations, $\varepsilon_1 = \lambda_0(\varpi)\,\varepsilon$

In order to make further progress, we shall first examine the case where the perturbations ε and ε_1 are linearly related,

$$\varepsilon_1 = \lambda_0(\varpi)\,\varepsilon\,. \tag{4.12}$$

No specific polytropic relationship between pressure and density is imposed at this stage where the pressure perturbation is given by Eq. (4.9) while ε and

[1] If we write the differential equation for the perturbation $A_\infty\varepsilon$ then the A_∞ disappear (consistent with the initial equations where only derivatives of A appears).

$\lambda_0(\varpi)$ satisfy Eq. (4.11) which now becomes,

$$\frac{\partial^2\varepsilon}{\partial z^2}+\frac{\partial^2\varepsilon}{\partial\varpi^2}+\left[\frac{A^{'}}{A}\left(2-\frac{\lambda_0 M^2}{1-M^2}\right)-\frac{1}{\varpi}\right]_\infty\frac{\partial\varepsilon}{\partial\varpi}+$$
$$\left[\mathcal{G}_1+\lambda_0\mathcal{G}_2-\lambda_0^{'}\frac{M^2}{1-M^2}\frac{A^{'}}{A}\right]_\infty\varepsilon=0\,. \tag{4.13}$$

The above equation obtained by substituting Eq. (4.12) into Eq. (4.11), relate the two unknown functions ε and λ_0 and their derivatives. However, it is still complicated for a general analysis; in the following, we shall analyze Eq. (4.13) in some special cases where the variables of the perturbations can be separated in various coordinates of the poloidal plane.

4.3.1 Perturbations separable in $\varpi\,, r$

Assume that the variables of the cylindrical and radial distances, (ϖ, r) are separable in ε,

$$\varepsilon=f\,(\varpi)\,g\,(r)\;,\qquad\qquad \mid g\mid\ll 1\,. \tag{4.14}$$

Then Eq. (4.13) gives,

$$g^{''}+\frac{g^{'}}{r}\left\{2\varpi\frac{f^{'}}{f}+\varpi\frac{A^{'}}{A}\left(2-\frac{\lambda_0 M^2}{1-M^2}\right)\right\}_\infty+g\left\{\frac{f^{''}}{f}+\right.$$
$$\left.\left[\frac{A^{'}}{A}\left(2-\frac{\lambda_0 M^2}{1-M^2}\right)-\frac{1}{\varpi}\right]\frac{f^{'}}{f}+\mathcal{G}_1+\lambda_0\mathcal{G}_2-\frac{\lambda_0^{'}M^2}{1-M^2}\frac{A^{'}}{A}\right\}_\infty=0 \tag{4.15}$$

Therefore (Appendix 4.B), there are constants (s, k) such that:

$$g^{''}+2s\frac{g^{'}}{r}+k^2 g=0\,, \tag{4.16}$$

or,

$$x^2\frac{d^2y}{dx^2}+x\frac{dy}{dx}+\left[x^2-\left(s-\frac{1}{2}\right)^2\right]y=0\,,$$
$$x=kr\,,\qquad y=gx^{s-\frac{1}{2}}\,. \tag{4.17}$$

The last differential equation is the familiar Bessel differential equation with the solution

$$y=D_1 J_{s-\frac{1}{2}}(x)+D_2 Y_{s-\frac{1}{2}}(x). \tag{4.18}$$

In the limit $x\to\infty$, Bessel's functions become,

$$J_\nu(x)\overset{x\gg 1}{\approx}\frac{1}{\sqrt{x}}\cos\left(x-\frac{\nu\pi}{2}-\frac{\pi}{4}\right),$$
$$Y_\nu(x)\overset{x\gg 1}{\approx}\frac{1}{\sqrt{x}}\sin\left(x-\frac{\nu\pi}{2}-\frac{\pi}{4}\right), \tag{4.19}$$

and therefore the solution of (4.16) is

$$g = \frac{D}{r^s}\sin(kr + \phi_0)\,. \tag{4.20}$$

Finally, Eq. (4.15) gives two conditions relating the functions of ϖ:

$$\left\{2\varpi\frac{f'}{f} + \varpi\frac{A'}{A}\left(2 - \frac{\lambda_0 M^2}{1-M^2}\right)\right\}_\infty = 2s \tag{4.21}$$

and

$$\left\{\frac{f''}{f} + \left[\frac{A'}{A}\left(2 - \frac{\lambda_0 M^2}{1-M^2}\right) - \frac{1}{\varpi}\right]\frac{f'}{f}\mathcal{G}_1 + \lambda_0\mathcal{G}_2 - \frac{\lambda_0' M^2}{1-M^2}\frac{A'}{A}\right\}_\infty = k^2\,. \tag{4.22}$$

Note that for $k = 0\,, g \propto r^{1-2s}$ while for $k^2 < 0\,, g \propto e^{-|k|r}/r^s$, cases which apply to non-oscillating solutions.
In the following we shall test our analysis by comparing it with available exact solutions of analytical models of outflows which exhibit an oscillatory behaviour.

Example 1

We may start with the simplest case wherein M_∞, λ_0, f, $\mathcal{G}_1$ and $\mathcal{G}_2$ are constants and $A_\infty(\varpi) \propto \varpi^2$. Indeed this case has been studied in [ST94] (see also [TST96]). They considered the following expressions of the free integrals,

$$A = \frac{r_\star^2 B_\star}{2}\alpha(R,\theta), \quad \Psi_A(\alpha) = \frac{4\pi\rho_\star V_\star}{B_\star}\sqrt{1+\delta\alpha},$$
$$\alpha = \frac{\varpi^2}{r_\star^2 G^2(R)}\,, \quad R = \frac{r}{r_\star}\,, \tag{4.23}$$

$$L(\alpha) = \lambda r_\star V_\star\frac{\alpha}{\sqrt{1+\delta\alpha}}\,, \qquad \Omega(\alpha) = \frac{\lambda V_\star}{r_\star}\frac{1}{\sqrt{1+\delta\alpha}}\,, \tag{4.24}$$

where $G(R)$ is the radius of the jet in units of the Alfvén radius and λ, δ and $G(R \to \infty) = G_\infty$ are constants, while the starred quantities refer to values at the Alfvén radius $r_\star$. Writing down the expressions of the perturbations for this case we have,

$$\varepsilon(r) = \frac{G_\infty^2}{G^2(r)} - 1\,, \qquad \varepsilon_1(r) = \frac{M^2(r)}{M_\infty^2} - 1\,. \tag{4.25}$$

It follows from Eqs. (4.21–4.22) that $f(\varpi) = 1$ while λ_0 is a constant which furthermore can be calculated at $r = r_\star$,

$$\lambda_0 \equiv -|\lambda_0| = -\frac{M_\infty^2 - 1}{M_\infty^2(G_\infty^2 - 1)}\,. \tag{4.26}$$

This is the same result with that in the study of [ST94] although the surface $r = r_\star$ is not always in the asymptotic regime where gravity is negligible. The

functions $\mathcal{G}_1$ and $\mathcal{G}_2$ given in Appendix 4.A are constants in this model and from Eqs. (4.21–4.22) the corresponding expressions for s and k are,

$$s = 2 + \frac{\lambda_0 M_\infty^2}{M_\infty^2 - 1} \tag{4.27}$$

$$k^2 \equiv \frac{4\pi^2}{\Lambda_{osc}^2} = \frac{2\lambda^2}{r_\star^2 \left(1 - M_\infty^2\right)^2} \left[2 - \lambda_0 \frac{\left(2M_\infty^2 - 1\right) G_\infty^4 - M_\infty^4}{M_\infty^2 \left(1 - M_\infty^2\right)} \right] . \tag{4.28}$$

The wavelength of the oscillations grows quadratically with the Alfvén number, $\Lambda_{osc}/r_\star \propto M_\infty^2$, while the amplitude of the oscillations drops with distance as $r^{-(2-|\lambda_0|)}$, as found in [ST94] (their Figs. 2, 8, 10). For example, as the magnitude of the asymptotic Alfvén number M_∞ increases by a factor of about 10 when the energetic parameter ϵ in the [ST94] notation decreases from $\epsilon = 10$ to $\epsilon = 1$, Λ_{osc} increases accordingly by a factor of about 100. Similarly, the amplitude of the oscillations Λ_{osc} in the width of the jet and the Alfvén number drops with radial distance as r^{-s}, where $1 < s < 2$ with its exact value $s = 2 - |\lambda_0|$ depending on M_∞ and G_∞, according to Eq. (4.27).

Example 2

Another more general class of solutions can be generated by the following set of free integrals [VT98],

$$\begin{aligned} A &= \frac{r_\star^2 B_\star}{2} \alpha(R,\theta),\ \Psi_A(\alpha) = \frac{4\pi\rho_\star V_\star}{B_\star} \sqrt{1 + \delta\alpha + \mu\delta_0\alpha^\epsilon}, \\ \alpha &= \frac{\varpi^2}{r_\star^2 G\left(R\right)^2}\ , \quad L(\alpha) = r_\star V_\star \alpha \sqrt{\frac{\xi + \mu\alpha^{\epsilon-1}}{1 + \delta\alpha + \mu\delta_0\alpha^\epsilon}}\ , \\ \Omega(\alpha) &= \frac{V_\star}{r_\star} \sqrt{\frac{\xi + \mu\alpha^{\epsilon-1}}{1 + \delta\alpha + \mu\delta_0\alpha^\epsilon}}\ . \end{aligned} \tag{4.29}$$

where μ, ϵ, δ_0,ξ are constants, in addition to the ones introduced in the previous example. If M_∞ , λ_0 and f are constants then,

$$k^2 = \frac{2\xi\left(\epsilon - 1\right)\left(G_\infty^4 - M_\infty^2\right)}{r_\star^2 M_\infty^2 \left(1 - M_\infty^2\right)^2} \approx \frac{2\xi\left(1 - \epsilon\right)}{r_\star^2 M_\infty^4} \tag{4.30}$$

because $M_\infty^2 \gg 1$,

$$\lambda_0 = \left[\left(\epsilon + 1\right) M_\infty^2 - \left(\epsilon - 1\right) G_\infty^4\right] \frac{1 - M_\infty^2}{\left(2M_\infty^2 - 1\right) G_\infty^4 - M_\infty^4}, \tag{4.31}$$

and

$$s = 2 + \frac{\lambda_0 M_\infty^2}{M_\infty^2 - 1} \approx \epsilon + 3\,. \tag{4.32}$$

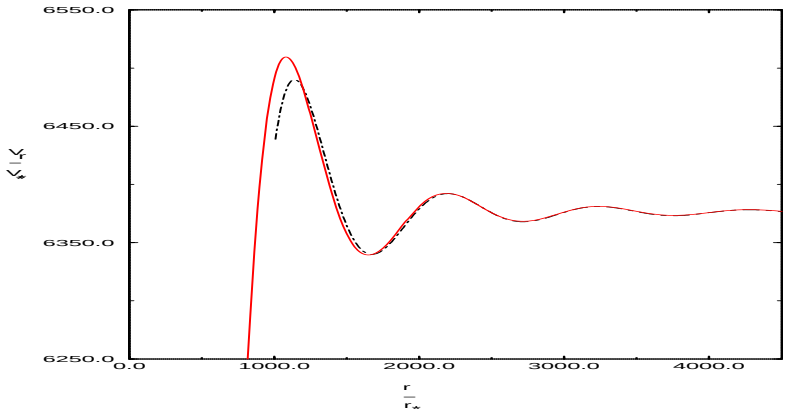

Figure 4.1: Dimensionless radial velocity V_r on the rotation/magnetic axis *vs.* dimensionless radial distance R. The solid curve indicates the super-fast exact solution of the model of example 2 for the following set of parameters: $\epsilon = 0.1$, $\delta = 0.35$, $\delta_0 = 0.01$, $\xi = 5$, $\mu = 0.01$, $2\mathcal{GM}/r_\star V_\star^2 = 10$. From the integration of the MHD Eq. (5) we find that $M_\infty^2 = 490.24$, $G_\infty^2 = 0.0769$. The dotted line indicates the corresponding solution which emerges from the perturbation analysis with $D_0 = 2.79 \times 10^7, \phi_0 = 0.46$).

Substituting in Eq. (4.8) the above expressions for k and s we find the perturbed form of the streamfunction,

$$A \approx \frac{B_\star \varpi^2}{2G_\infty^2}\left[1 + \frac{D_0}{R^{\epsilon+3}}\sin\left(\frac{\sqrt{2\xi\,(1-\epsilon)}}{M_\infty^2}R + \phi_0\right)\right]\,. \tag{4.33}$$

A comparison of the oscillatory behaviour of a solution obtained by this *perturbative* analysis with the corresponding *exact* solution obtained by an integration of the MHD equations and selecting a super-fast solution crossing the modified by self-similarity fast critical point is shown in Figs. 4.1,4.2. In Fig. 4.1 the dimensionless radial speed oscillates with the dimensionless radial distance while in Fig. 4.2 the shape of the streamlines in the poloidal plane shows a similar behaviour. Since by assumption the present perturbation analysis applies to large distances where gravity is negligible and the jet starts approaching its cylindrical shape, such a comparison is meaningful far away from the Alfvén surface, $r \gg r_\star$. Then, the purpose of Figs. 4.1,4.2 is to show by a specific example that in such distances the perturbation analysis gives results which compare rather well with the corresponding exact solution. And with the perturbation analysis being independent of any specific model, this comparison shows that the effect of the oscillations is rather model-independent, as discussed in the last section.

For the specific example shown in Figs. 4.1,4.2, the amplitude of the oscillations in the strength of the radial speed is rather low, at the 3% level. However,

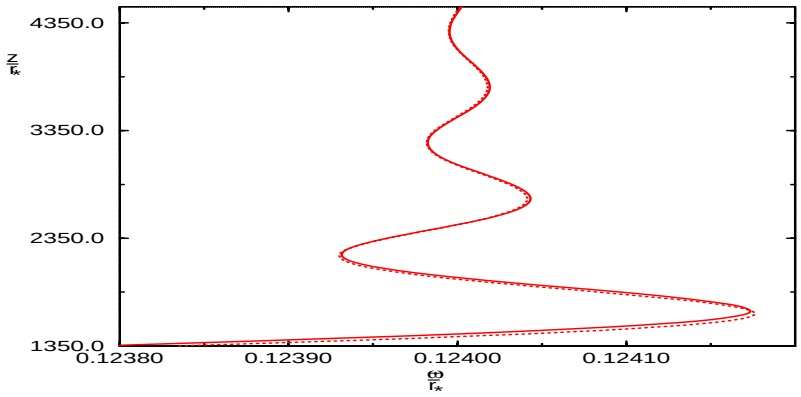

Figure 4.2: Shape of the streamline on the poloidal plane for the model of example 2, as emerges from the perturbation analysis ($D_0 = 2.79 \times 10^7, \phi_0 = 0.46$). With dotted line an exact solution is shown for the model of example 2 where gravity is included.

the same oscillatory behaviour has also been found for other parameters yielding larger amplitudes of the oscillations close to the 10 % level [VT98], similarly to the [ST94] solution (see Chapter 7). However, a peculiarity of the present model Eq. (4.29) is that the crossing of the critical point becomes numerically rather difficult for parameters giving larger amplitude oscillations. And such a crossing of the critical point is the main difficulty for obtaining exact solutions [TSS+96]. Hence, in the illustration shown in Figs. 4.1,4.2 we have been restricted to a case with an unambiguous crossing of the critical point. In other words, numerical difficulties prohibit the construction of exact solutions with larger amplitudes of oscillations, unlike the case of [ST94]. Nevertheless and as it is discussed in the last session, the physics of the oscillations remains the same.

4.3.2 Perturbations separable in ϖ, θ

Assume next that the variables of the cylindrical distance and meridional angle (ϖ, θ), are separable in ε,

$$\varepsilon = f(\varpi)\, g(\theta) \ , \qquad |\, g \,| \ll 1 \, . \tag{4.34}$$

Then Eq. (4.13) gives,

$$0 = \sin^2\theta\, g^{''} + \sin\theta\cos\theta\, g^{'} \left\{ 2\frac{\varpi f^{'}}{f} + \frac{\varpi A^{'}}{A}\left(2 - \frac{\lambda_0 M^2}{1-M^2}\right) - 1 \right\}_{\infty} +$$

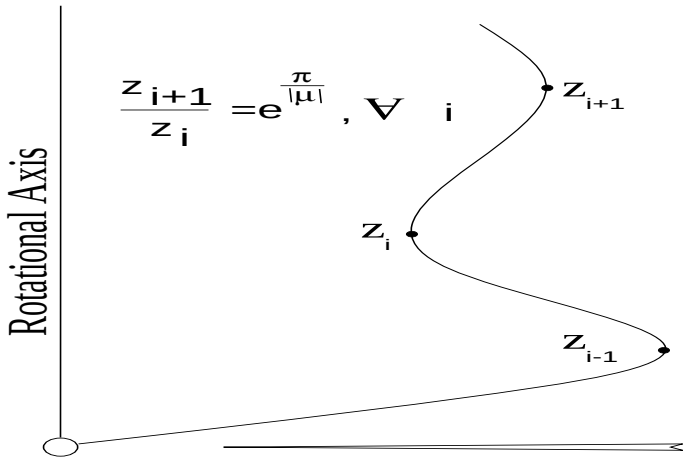

Figure 4.3: Sketch of an oscillating streamline on the poloidal plane in this case. We see that the wavelength increases logarithmicaly such that $\frac{z_{i+1}}{z_i}$ =constant $\forall i$.

$$g\left\{\frac{\varpi^2 f''}{f}+\left[\frac{\varpi A'}{A}\left(2-\frac{\lambda_0 M^2}{1-M^2}\right)-1\right]\frac{\varpi f'}{f}+\varpi^2\mathcal{G}_1+\lambda_0\varpi^2\mathcal{G}_2-\frac{\varpi\lambda_0' M^2}{1-M^2}\frac{\varpi A'}{A}\right\}_{\infty} \quad (4.35)$$

Therefore (Appendix 4.B), there are constants μ, ν such that:

$$\sin^2\theta g'' + (2\nu+1)\sin\theta\cos\theta g' + \left(\nu^2-\mu^2\right)g = 0\,, \quad (4.36)$$

or,

$$\left(1-x^2\right)\frac{d^2y}{dx^2} - 2x\frac{dy}{dx} + \left[\nu(\nu+1) - \frac{\mu^2}{1-x^2}\right]y = 0\,, \quad (4.37)$$

where

$$x = \cos\theta, \qquad y = g\sin^{\nu}\theta\,. \quad (4.38)$$

The last differential equation is the associated Legendre equation and the solution is given in terms of the associated Legendre functions $P_\nu^\mu(x)$ and $Q_\nu^\mu(x)$

$$y = D_1 P_\nu^\mu(x) + D_2 Q_\nu^\mu(x)\,. \quad (4.39)$$

For $\mu^2 < 0$ as $\theta \to 0$ the solutions of the associated Legendre equation are $\theta^{\pm\mu}$, or $\sin(\mid\mu\mid\ln\theta)$, $\cos(\mid\mu\mid\ln\theta)$ [AS72] and therefore the solution of Eq. (4.35) is

$$g = D\theta^{-\nu}\cos(\mid\mu\mid\ln\theta + D_0) \Leftrightarrow g = D\left(\varpi/z\right)^{-\nu}\cos\left(\mid\mu\mid\ln\frac{\varpi}{z} + D_0\right)\,.$$

We see an oscillatory behaviour in the angle $\theta(x)$ similar to the Bessel functions of the previous section (with the wavelength logarithmically increased - see Fig.

4.3).
Furthermore, Eq. (4.35) gives two conditions for the functions of ϖ,

$$\left\{ 2\varpi \frac{f^{'}}{f} + \varpi \frac{A^{'}}{A} \left(2 - \frac{\lambda_0 M^2}{1-M^2} \right) \right\}_{\infty} = 2\nu + 2 \tag{4.40}$$

and

$$\left\{ \frac{f^{''}}{f} + \left[\frac{A^{'}}{A} \left(2 - \frac{\lambda_0 M^2}{1-M^2} \right) - \frac{1}{\varpi} \right] \frac{f^{'}}{f} + \mathcal{G}_1 + \lambda_0 \mathcal{G}_2 - \frac{\lambda_0^{'} M^2}{1-M^2} \frac{A^{'}}{A} \right\}_{\infty} = \frac{\nu^2 - \mu^2}{\varpi^2} \tag{4.41}$$

It is worth to note that the Eqs. (4.40–4.41) are identical to the corresponding Eqs. (4.21–4.22) except the factor ϖ^2 in the denominator of Eqs. (4.41). The wavelength of the oscillations was found constant in section (4.3.1) while now it varies with distance (it grows logarithmically).

4.3.3 Perturbations separable in $\varpi\,, z$

Assume finally that the variables of the cylindrical and axial distances, (ϖ, z) are separable in ε,

$$\varepsilon = f(\varpi)\, g(z)\,, \qquad |\, g\,| \ll 1\,. \tag{4.42}$$

Then Eq. (4.13) gives,

$$g^{''} + g \left\{ \frac{f^{''}}{f} + \left[\frac{A^{'}}{A} \left(2 - \frac{\lambda_0 M^2}{1-M^2} \right) - \frac{1}{\varpi} \right] \frac{f^{'}}{f} + \mathcal{G}_1 + \lambda_0 \mathcal{G}_2 - \frac{\lambda_0^{'} M^2}{1-M^2} \frac{A^{'}}{A} \right\}_{\infty} = 0 \tag{4.43}$$

Proceeding as before (Appendix 4.B), it follows that there is constant k such that:

$$g^{''} + k^2 g = 0 \Leftrightarrow g = D \sin(kz + \phi_0)\,, \tag{4.44}$$

and the oscillations are undamped in this case. This result should be expected because now the radial distance r with its associated scale $r = r_\star$ does not enter directly into the analysis while with the neglect of gravity the distance z along the jet does not have any associated scale.

4.4 Unrelated perturbations

Nonoscillating jet-type solutions have been also found recently (Trussoni et al 1996) and they also emerge from this topological stability analysis by considering the case where the perturbations in the streamline shape and Alfvén number are uncoupled. Assume for simplicity that $\varepsilon = g(r)$ and $\varepsilon_1 = g_1(r)$. For $A_\infty = \lambda_A \varpi^2$, $\lambda_A = constant$ and $M_\infty^{2'} = 0$, Eq. (4.11) takes the form:

$$g^{''} + 4\frac{g^{'}}{r} - \frac{2M_\infty^2}{1-M_\infty^2} \frac{g_1^{'}}{r} + \mathcal{G}_1 g + \mathcal{G}_2 g_1 = 0\,. \tag{4.45}$$

Then (Appendix 4.B), there are constants c_1, c_2 such that,

$$g^{''} + 4\frac{g^{'}}{r} - \frac{2M_\infty^2}{1-M_\infty^2}\frac{g_1^{'}}{r} + c_1 g + c_2 g_1 = 0\,. \tag{4.46}$$

Comparing this with Eq. (4.45) it follows that,

$$(\mathcal{G}_1 - c_1)\, g + (\mathcal{G}_2 - c_2)\, g_1 = 0\,. \tag{4.47}$$

From this last equation two possibilities emerge. The *first*, where g and g_1 are proportional to each other, has been already studied in Sec. (4.3.1) and it was found to give an oscillatory behaviour. The *second* one corresponds to setting $\mathcal{G}_1 = c_1$ and $\mathcal{G}_2 = c_2$. By solving these equations we find then the following general expressions,

$$\left(\frac{L\Psi_A}{A}\right)_\infty^2 = c_0 \frac{2M_\infty^2 - 1}{\lambda_A^2 M_\infty^4} A_\infty^{-2\frac{2M_\infty^2-1}{M_\infty^2-1}} + \frac{c_1\left(1-M_\infty^2\right)^2}{\lambda_A^2}, \tag{4.48}$$

$$(\Omega\Psi_A)_\infty^2 = c_0 A_\infty^{-2\frac{2M_\infty^2-1}{M_\infty^2-1}} + \frac{M_\infty^2\left(1-M_\infty^2\right)^2}{2M_\infty^2-1}\left[c_1 M_\infty^2 - 2c_2\lambda_A^2\left(1-M_\infty^2\right)\right] \tag{4.49}$$

where c_0 is a constant. In other words, if the functions of A $L\Psi_A/A$ and $\Omega\Psi_A$ are given by Eqs. (4.48 – 4.49) the corresponding solutions may not exhibit an oscillatory behaviour. In other words, the above conditions are the necessary (but not sufficient) conditions for the appearance of oscillations in the asymptotic regime of collimated outflows, if ε and ε_1 are functions only of r.

Examples

For the case which has been studied by Trussoni et al (1996) the free integrals are given be Eqs. (4.23) with $\lambda_A = B_\star/2G_\infty^2$. Their non-oscillating solutions there correspond in the notation of the previous section to,

$$c_0 = 0, \quad c_2 = -2\lambda^2\frac{\left(2M_\infty^2-1\right)G_\infty^4 - M_\infty^4}{r_\star^2 M_\infty^2\left(1-M_\infty^2\right)^3},$$
$$c_1 = \frac{\lambda^2 B_\star^2}{r_\star^2 G_\infty^4\left(1-M_\infty^2\right)^2}. \tag{4.50}$$

Another general class of solutions can be generated by the set of the free integrals given by Eqs. (4.29). Non-oscillating solutions also exist within this model for the following values of the constants,

$$c_0 = \frac{\lambda^2 B_\star^2}{r_\star^2\left(\frac{B_\star r_\star^2}{2}\right)^{\epsilon-1}}, c_2 = 0, c_1 = \frac{\mu\lambda^2 B_\star^2}{r_\star^2 G_\infty^4\left(1-M_\infty^2\right)^2}\,, \tag{4.51}$$

$$M_\infty^2 = \frac{\epsilon+1}{\epsilon+3}, \quad G_\infty^4 = \frac{(\epsilon+1)^2}{(\epsilon-1)(\epsilon+3)}\,. \tag{4.52}$$

4.5 Polytropic models

Assume now that there exists a polytropic relation between density and pressure

$$P \propto \rho^{\gamma} \,, \qquad \text{or} \,, \qquad P M^{2\gamma} = Q\left(A\right) \,, \tag{4.53}$$

for some constant index γ. For a small perturbation this relation becomes,

$$\left(P_{\infty} + \delta P\right) M_{\infty}^{2\gamma} \left(1+\varepsilon_1\right)^{\gamma} = Q_{\infty} + \delta Q \,, \tag{4.54}$$

with

$$Q_{\infty}\left(\varpi\right) = P_{\infty} M_{\infty}^{2\gamma} \,, \tag{4.55}$$

and

$$\delta Q = \left(\frac{dQ}{dA}\right)_{\infty} A_{\infty} \varepsilon = \frac{Q_{\infty}^{'} A_{\infty}}{A_{\infty}^{'}} \varepsilon \,. \tag{4.56}$$

Substituting the pressure perturbation from Eqs. (4.54–4.56) in Eq. (4.9) gives,

$$\left(\mathcal{F}_2 + \gamma P_{\infty}\right) \varepsilon_1 = \left[\frac{A}{A^{'}}\left(\mathcal{F}_0 + \gamma \frac{P_{\infty} M^{2'}}{M^2}\right) - \mathcal{F}_1\right]_{\infty} \varepsilon - \mathcal{F}_3 \frac{\partial \varepsilon}{\partial \varpi} \,. \tag{4.57}$$

We shall distinguish two cases:

$$\begin{aligned} &\text{(a)} \qquad \mathcal{F}_2 + \gamma P_{\infty} = 0 \,, \\ &\mathcal{F}_3 \frac{\partial \varepsilon}{\partial \varpi} = \left[\frac{A}{A^{'}}\left(\mathcal{F}_0 + \gamma \frac{P_{\infty} M^{2'}}{M^2}\right) - \mathcal{F}_1\right]_{\infty} \varepsilon \,, \end{aligned} \tag{4.58}$$

and

$$\text{(b)} \qquad \mathcal{F}_2 + \gamma P_{\infty} \neq 0 \,, \qquad \varepsilon_1 = \mathcal{K}_1 \varepsilon + \mathcal{K}_2 \frac{\partial \varepsilon}{\partial \varpi} \,. \tag{4.59}$$

In case (a), we may solve Eq. (4.58) and get for each of the particular dependence of ε, the three following cases:

(i) for $\varepsilon = f\left(\varpi\right) g\left(r\right)$,

$$\varepsilon = e^{\left[-\left(\frac{r}{r_0}\right)^2\right]} e^{\left[\left(\frac{\varpi}{r_0}\right)^2\right]} e^{\int \frac{\left[\frac{A}{A^{'}}\left(\mathcal{F}_0 + \gamma \frac{P_{\infty} M^{2'}}{M^2}\right) - \mathcal{F}_1\right]_{\infty}}{\mathcal{F}_3} d\varpi} \,, \tag{4.60}$$

(ii) for $\varepsilon = f\left(\varpi\right) g\left(\theta\right)$,

$$\varepsilon = \left(\tan\theta\right)^{\lambda} \varpi^{-\lambda} e^{\int \frac{\left[\frac{A}{A^{'}}\left(\mathcal{F}_0 + \gamma \frac{P_{\infty} M^{2'}}{M^2}\right) - \mathcal{F}_1\right]_{\infty}}{\mathcal{F}_3} d\varpi} \tag{4.61}$$

(iii) for $\varepsilon = f(\varpi)\, g(z)$,

$$\varepsilon = g(z)\, e^{\int \frac{\left[\frac{A}{A'}\left(\mathcal{F}_0 + \gamma \frac{P_\infty M^{2'}}{M^2}\right) - \mathcal{F}_1\right]_\infty}{\mathcal{F}_3} d\varpi} \,. \tag{4.62}$$

where g is an arbitrary function of z. In all cases Eq. (4.11) gives ε_1.

Case (b) with $\mathcal{F}_2 + \gamma P_\infty \neq 0$ on the other hand, turns out to be and the most interesting and will be analyzed in more detail in the following. Then Eq. (4.11) takes the form :

$$\mathcal{H}_1 \varepsilon + \mathcal{H}_2 \frac{\partial \varepsilon}{\partial \varpi} + \mathcal{H}_3 \frac{\partial^2 \varepsilon}{\partial \varpi^2} + \frac{\partial^2 \varepsilon}{\partial z^2} = 0 \,. \tag{4.63}$$

4.5.1 Perturbations separable in $\varpi\,, r$

Assume first that the variables of the cylindrical and axial distances, (ϖ, z) are separable in ε, $\varepsilon = f(\varpi)\, g(r)\,, \mid g \mid \ll 1$. Then Eq. (4.63) gives,

$$g^{''}\left[1 + \frac{\varpi^2 (\mathcal{H}_3 - 1)}{r^2}\right] + \frac{g^{'}}{r}\left[\varpi \mathcal{H}_2 + \mathcal{H}_3 + +2\varpi \mathcal{H}_3 \frac{f^{'}}{f} - \frac{\varpi^2 (\mathcal{H}_3 - 1)}{r^2}\right] +$$
$$+ g\left(\mathcal{H}_1 + \mathcal{H}_2 \frac{f^{'}}{f} + \mathcal{H}_3 \frac{f^{''}}{f}\right) = 0 \,. \tag{4.64}$$

Therefore (Appendix 4.B), there are constants (s, k, s_1, s_2) such that:

$$g^{''}\left(1 + \frac{s_1}{r^2}\right) + \frac{g^{'}}{r}\left(2s + \frac{s_2}{r^2}\right) + k^2 g = 0 \,. \tag{4.65}$$

The asymptotic solution of the previous equation is the solution of the section (4.3.1), although the relations between the functions of ϖ are different.

4.5.2 Perturbations separable in $\varpi\,, \theta$

Assume next that the variables of the cylindrical distance and meridional angle (ϖ, θ), are separable in ε, $\varepsilon = f(\varpi)\, g(\theta)\,, \mid g \mid \ll 1$. Then Eq. (4.63) gives,

$$\sin^2\theta g^{''} + \sin^2\theta \cos^2\theta g^{''} (\mathcal{H}_3 - 1) +$$
$$\sin\theta \cos\theta g^{'} \varpi \left(\mathcal{H}_2 + 2\frac{f^{'}}{f}\mathcal{H}_3\right) - 2\sin^3\theta \cos\theta g^{'} \times$$
$$(\mathcal{H}_3 - 1) + g\varpi^2 \left(\mathcal{H}_1 + \mathcal{H}_2 \frac{f^{'}}{f} + \mathcal{H}_3 \frac{f^{''}}{f}\right) = 0 \tag{4.66}$$

Therefore (Appendix 4.B), there are constants s_1, s_2, s_3 such that:

$$\sin^2\theta g^{''}\left(1+s_1-s_1\sin^2\theta\right)+\sin\theta\cos\theta g^{'}\left(s_3-2s_1\sin^2\theta\right)+s_2 g=0 \quad (4.67)$$

For $s_1=-1$ the solution goes asymptotically as $g=(tan\theta)^{-s_2/s_3}$, while for the most interesting case of $s_1\neq -1$ we may introduce the new constants μ,ν with $\mu\geq 0$ and $2\nu+1=s_3/(s_1+1)$, $\nu^2-\mu^2=s_2/(s_1+1)$, such that the differential equation for g becomes:

$$\sin^2\theta g^{''}\left(1-\frac{s_1}{s_1+1}\sin^2\theta\right)+\sin\theta\cos\theta g^{'}\times$$
$$\left(2\nu+1+\frac{s_3}{s_1+1}\sin^2\theta\right)+\left(\nu^2-\mu^2\right)g=0\,. \quad (4.68)$$

The asymptotic solution of the previous equation is similar to the solution of Eq. (4.36), i.e., it is given by Eq. (4.39), with of course different relations between the functions of ϖ. Oscillations like those predicted by the analysis of this section have been indeed found in the model of Contopoulos & Lovelace [CL94] where:

$$A\propto\left(\frac{\varpi}{G\left(\theta\right)}\right)^{x}\,,\qquad \Psi_A\propto A^{1-\frac{s}{2x}}\,,$$
$$L\propto A^{\frac{1}{2x}}\,,\qquad \Omega\propto A^{-\frac{s}{2x}}\,,\qquad Q\propto A^{2-\frac{4}{x}}\,, \quad (4.69)$$

and where (M_∞, f) are constants.

4.5.3 Perturbations separable in $\varpi\,, z$

Finally, assume that the variables of the cylindrical and axial distances, (ϖ, z) are separable in ε, $\varepsilon=f\left(\varpi\right)g\left(z\right),\mid g\mid\ll 1$. Then Eq. (4.63) gives,

$$g^{''}+g\left(\mathcal{H}_1+\mathcal{H}_2\frac{f^{'}}{f}+\mathcal{H}_3\frac{f^{''}}{f}\right)=0 \quad (4.70)$$

Therefore (Appendix 4.B), there is a constant k such that:

$$g^{''}+k^2 g=0\Leftrightarrow g=D\sin\left(kz+\phi_0\right)\,, \quad (4.71)$$

and the oscillations do not decay due to the lack of scale in the direction z, similarly to the case of Sec. (4.3.3). Examples of models with such oscillations have been analyzed by Chan & Henriksen [CH80], Bacciotti & Chiuderi [BC92] and Del Zanna & Chiuderi [DZC96].

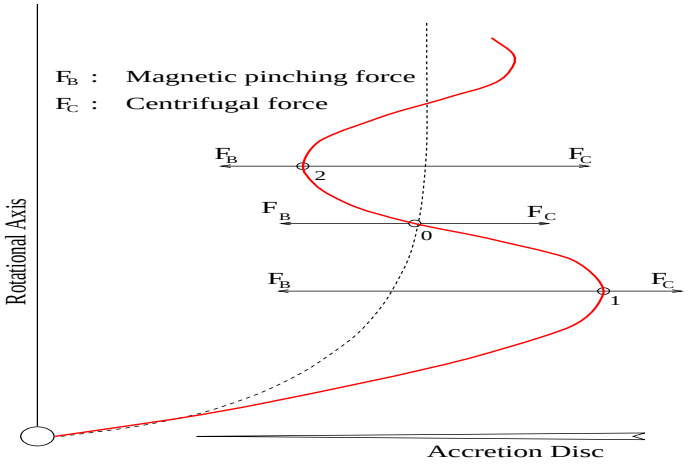

Figure 4.4: Sketch of an oscillating streamline on the poloidal plane (ϖ, z) of an MHD outflow from a central object. The inwards magnetic pinching force F_B equals the outward inertial centrifugal force F_C at position 0. At position 1 F_B is greater than F_C while at position 2 F_B is greater than F_C.

4.6 Discussion

Previous studies have shown that under fairly general conditions magnetized outflows may become asymptotically cylindrical [HN89]. And, this tendency for asymptotic collimation has been also demonstrated via quasi-analytic self-similar solutions [ST94, CL94, TST96, VT98]. A common feature in all such self-similar solutions is that before the final cylindrical collimation is achieved, the jet passes through a stage of oscillations in its radius, Alfvén number and other physical parameters. In the previous sections we have shown under rather general assumptions that this oscillatory behaviour of collimated outflows is not restricted to the few specific models studied so far, but instead it is a rather generic physical property of the MHD outflow as it reaches collimation.

A simple way to demonstrate physically this effect can be provided by the simplified construction shown in Fig. 4.4. A single streamline $A(\varpi, z) = const.$ of an initially *radial* magnetized and rotating outflow becomes asymptotically *cylindrical* (dotted line). Assume for simplicity that the jet carries an electric current $I_z \propto \varpi^2$ with a uniform surface density $J_z = const.$ In its asymptotic regime the jet is confined by the interplay of the magnetic pinching force, the gas pressure gradient and the centrifugal force of rotation [ST94, TST96]. Assume for simplicity that the gas pressure gradient and the magnetic pressure gradient associated with the poloidal magnetic field are negligible such that at equilibrium the magnetic pinching force exactly balances the centrifugal force. In the superAlfvénic regime, most of the conserved specific angular momentum is carried by the fluid, such that $L \approx \varpi V_\varphi$. The magnetic pinching force F_B which results from such a current I_z and the centrifugal force F_C for the assumed

angular momentum conservation are then,

$$F_B = \frac{B_\varphi^2}{4\pi\varpi} + \frac{\partial}{\partial\varpi}\frac{B_\varphi^2}{8\pi} \propto \varpi\,, \qquad F_C = \frac{\rho V_\varphi^2}{\varpi} \propto \frac{L^2}{\varpi^3}\,, \tag{4.72}$$

under uniform density conditions. If now at some equilibrium location 0, say at the cylindrical distance $\varpi = \varpi_0$ on the dotted line in Fig. 4.4, we have $F_B(\varpi_0) = F_C(\varpi_0)$, then at larger distances $\varpi_1 > \varpi_0$ (location 1 in Fig. 4.4) we have according to Eq. (4.72) that $F_B(\varpi_1) > F_C(\varpi_1)$. Conversely, at the smaller cylindrical distances $\varpi_2 < \varpi_0$ (location 2 in Fig. 4.4) we have again according to Eq. (4.72) $F_C(\varpi_2) > F_B(\varpi_2)$. The net result is that as the parcel of gas moves along the poloidal streamline from the central object to infinity, it feels an inward force at location 1 which brings it towards the rotation axis. On the other hand, due to inertia and its poloidal speed, it overpasses the equilibrium position 0 and arrives at location 2 where now feels an outward force bringing it again away from the rotation axis towards location 0, etc. The final result is the oscillatory shape of the streamline shown in Fig. 4.4 and derived in the previous sections. The oscillations start at the collimation distance R_c where the streamlines start to deviate significantly from radiality and by means of the magnetic pinching forces are brought to the cylindrical geometry. Obviously, at large distances from the collimation radius R_c the cause of the oscillations disappears and accordingly their amplitude decays to zero, i.e., the uniform cylindrical shape is finally reached.

At the asymptotic and collimated regime of the outflow, we expect that gravity should be negligible. For this reason and in order to simplify the mathematics, in the analysis presented in this Chapter gravity was not included. Indeed, this assumption is verified by the plot of Figs. 4.1,4.2 where with dotted line is given a full solution of the problem by including gravity while by solid line is the approximate solution which is calculated by neglecting gravity. These two curves almost coincide with some deviation starting as we approach the source of the flow where gravity becomes rather important.

In the example shown for illustrative purposes in Figs. 4.1,4.2, the oscillations in the magnitudes of the flow speed, temperature, density and pressure of the beam are rather weak at the few percent level. However, this is only due to the fact that the availability of exact super-fast solutions for model 2 is constrained by numerical problems associated with the crossing of the fast critical point. See for details the analysis of this model in Chapter 7 and in [VT98] (for sub-Alfvénic at infinity solutions the oscillations are strong enough). In [ST94] stronger oscillations of similar origin at the 10% level have been presented which also emerge from the present perturbation analysis. Then, such large amplitude oscillations in the beam may have notable effects, for example via enhanced radiation emission either in local compressions of the flow pattern or in shock transitions. For example, observed brightness enhancements (knots) along the jet of M87 in Virgo have been attributed to shocks [Bir96] with a similar situation for stellar jets [Ray96]. Such shocks may be caused by an oscillatory flow channel in which case the hydrodynamic equations allow multiple transonic solutions connected by shocks [FMBR96]. In the present study we have shown

that oscillations in the cross-section of the jet may be due, in addition to the familiar Kelvin-Helmholz instabilities, to the interplay of the magnetic and inertial forces in the acceleration region of the outflow. Although an examination of the detailed solution topologies of the present MHD case is far more complicated than the corresponding hydrodynamic solution topologies, it is naturally expected that similar shocks connecting various transonic solutions may exist in the present MHD case as well. However, a demonstration of their existence in self-similar MHD solutions is beyond the scope of this thesis and remains a challenge for future studies. It will also be interesting to check if fully numerical studies of collimated MHD outflows show an oscillatory behaviour in the shape of the streamlines. In the only available so far such study of a paraboloidally collimated disk wind [Sak87] such oscillations are not evident.

4.7 Appendix 4.A: functions of ϖ

$$\mathcal{F}_0(\varpi) = \frac{1}{4\pi\varpi^2}\left[A^{'}\left(\frac{A^{'}}{\varpi} - A^{''}\right) - A^{'}\frac{\frac{\partial}{\partial A}\left(L\Psi_A - \varpi^2\Omega\Psi_A\right)^2}{2\left(1-M^2\right)^2} - M^{2'}\frac{\left(L\Psi_A - \varpi^2\Omega\Psi_A\right)^2}{\left(1-M^2\right)^3} - \frac{\left(2M^2-1\right)\left(\varpi^2\Omega\Psi_A\right)^2 - \left(L\Psi_A\right)^2 M^4}{\varpi M^2\left(1-M^2\right)^2}\right]_\infty \tag{4.73}$$

$$\mathcal{F}_1(\varpi) = -\frac{1}{4\pi\varpi^2}\left[\left(1-M^2\right)A\left(A^{''} - \frac{A^{'}}{\varpi}\right) + M^2A^{'2} - M^{2'}AA^{'} + A\frac{\frac{\partial}{\partial A}\left(L\Psi_A - \varpi^2\Omega\Psi_A\right)^2}{2\left(1-M^2\right)^2}\right]_\infty \tag{4.74}$$

$$\mathcal{F}_2(\varpi) = -\frac{1}{4\pi\varpi^2}\left(M^2A^{'2} + M^2\frac{\left(L\Psi_A - \varpi^2\Omega\Psi_A\right)^2}{\left(1-M^2\right)^3}\right)_\infty \tag{4.75}$$

$$\mathcal{F}_3(\varpi) = -\frac{1}{4\pi\varpi^2}\left(M^2AA^{'}\right)_\infty \tag{4.76}$$

$$\mathcal{G}_0(\varpi) = -\frac{1}{4\pi\varpi^2}\left[AA^{'}\left(1-M^2\right)\right]_\infty \tag{4.77}$$

$$\mathcal{G}_1(\varpi) = \left[\frac{M^2 \frac{d}{dA}(L\Psi_A)^2 - \varpi^4 \frac{d}{dA}(\Omega\Psi_A)^2}{\varpi M^2 (1-M^2)^2 A'} - \right.$$
$$- \frac{A'''}{A'} + \frac{3A''}{\varpi A'} + \frac{A''}{A} - \frac{A'}{\varpi A} - \frac{3}{\varpi^2} +$$
$$\left. \frac{M^{2''}}{1-M^2} + \frac{M^{2'}}{1-M^2}\left(\frac{2A''}{A'} - \frac{3}{\varpi}\right) \right]_\infty \tag{4.78}$$

$$\mathcal{G}_2(\varpi) = \left[\frac{2M^2}{1-M^2}\left(\frac{A'}{\varpi A} - \frac{A''}{A}\right) - \frac{M^{2'}A'}{A(1-M^2)} + \right.$$
$$\left. \frac{M^4 (L\Psi_A)^2 - (2M^2-1)(\varpi^2\Omega\Psi_A)^2}{\varpi M^2 (1-M^2)^3 AA'} \right]_\infty \tag{4.79}$$

$$\mathcal{G}_3(\varpi) = -\frac{1}{4\pi\varpi^2}\left[2A'^2 - 2A\frac{A'}{\varpi} + AA'' + \right.$$
$$\left. A\frac{\frac{\partial}{\partial A}(L\Psi_A - \varpi^2\Omega\Psi_A)^2}{2(1-M^2)^2} \right]_\infty \tag{4.80}$$

$$\mathcal{G}_4(\varpi) = -\frac{1}{4\pi\varpi^2}\left[M^2 \frac{(L\Psi_A - \varpi^2\Omega\Psi_A)^2}{(1-M^2)^3} \right]_\infty \tag{4.81}$$

$$\mathcal{G}_5(\varpi) = -\frac{1}{4\pi\varpi^2}\left(AA'\right)_\infty \tag{4.82}$$

$$\mathcal{K}_1(\varpi) = \frac{\left[\frac{A}{A'}\left(\mathcal{F}_0 + \gamma \frac{P_\infty M^{2'}}{M^2} \right) - \mathcal{F}_1 \right]_\infty}{\mathcal{F}_2 + \gamma P_\infty} \tag{4.83}$$

$$\mathcal{K}_2(\varpi) = -\frac{\mathcal{F}_3}{\mathcal{F}_2 + \gamma P_\infty} \tag{4.84}$$

$$\mathcal{H}_1(\varpi) = \mathcal{G}_1 + \mathcal{K}_1\mathcal{G}_2 - \mathcal{K}_1'\left(\frac{M^2}{1-M^2}\frac{A'}{A}\right)_\infty \tag{4.85}$$

$$\mathcal{H}_2(\varpi) = 2\left(\frac{A'}{A}\right)_\infty - \frac{1}{\varpi} - (\mathcal{K}_1 +$$
$$\mathcal{K}_2'\left(\frac{M^2}{1-M^2}\frac{A'}{A}\right)_\infty + \mathcal{K}_2\mathcal{G}_2 \tag{4.86}$$

$$\mathcal{H}_3(\varpi) = 1 - \mathcal{K}_2 \left(\frac{M^2}{1-M^2} \frac{A'}{A} \right)_\infty \tag{4.87}$$

4.8 Appendix 4.B: theorem

Theorem: If $F(x)$, $f_i(x)$, $g_i(y)$, $i = 1, 2, \cdots, n$ are arbitrary functions of the independent variables x and y and

$$F(x) = f_1(x) g_1(y) + f_2(x) g_2(y) + \cdots + f_n(x) g_n(y), \tag{4.88}$$

then, there exist constants $c_1, c_2, \ldots, c_n$ such that,

$$F(x) = c_1 f_1(x) + c_2 f_2(x) + \cdots + c_n f_n(x). \tag{4.89}$$

Proof. We 'll use the method of mathematical induction:

(i) For $n = 1$, $F(x) = f_1(x) g_1(y)$.
If $f_1(x) = 0$ then $F(x) = 0 = c_1 f_1(x)$.
If $f_1(x) \neq 0$ then,

$$\frac{F(x)}{f_1(x)} = g_1(y) = c_1 \quad \Rightarrow \quad F(x) = c_1 f_1(x), \tag{4.90}$$

i.e. for $n = 1$ Eq. (2) holds.

(ii) Assume that for $n = k$ Eq. (2) holds, i.e., for given

$$F(x) = f_1(x) g_1(y) + f_2(x) g_2(y) + \cdots + f_k(x) g_k(y) \tag{4.91}$$

$\Rightarrow \exists\, c_1, c_2, \cdots, c_k$ such that, $F(x) = c_1 f_1(x) + c_2 f_2(x) + \cdots + c_k f_k(x)$ for every $F, f_i, g_i, i = 1, 2, \cdots, k$.

(iii) Then, for $n = k + 1$, let $F(x) = f_1(x) g_1(y) + \cdots + f_{k+1}(x) g_{k+1}(y)$. If $f_{k+1}(x) = 0$ then from the previous hypothesis:

$$\begin{aligned} &F(x) = c_1 f_1(x) + \ldots + c_k f_k(x) = c_1 f_1(x) + \ldots \\ &+ c_{k+1} f_{k+1}(x), \end{aligned} \tag{4.92}$$

i.e., Eq. (2) holds. If on the other hand, $f_{k+1}(x) \neq 0$ then,

$$\begin{aligned} \frac{F(x)}{f_{k+1}(x)} &= \frac{f_1(x)}{f_{k+1}(x)} g_1(y) + \cdots \\ &+ \frac{f_k(x)}{f_{k+1}(x)} g_k(y) + g_{k+1}(y) \quad \Rightarrow \end{aligned} \tag{4.93}$$

$$\frac{d}{dx}\left(\frac{F(x)}{f_{k+1}(x)}\right) = \frac{d}{dx}\left(\frac{f_1(x)}{f_{k+1}(x)}\right) g_1(y) + \cdots$$
$$+\frac{d}{dx}\left(\frac{f_k(x)}{f_{k+1}(x)}\right) g_k(y)\,. \tag{4.94}$$

So from the hypothesis that for n=k there are c_i such that,

$$\frac{d}{dx}\left(\frac{F(x)}{f_{k+1}(x)}\right) = c_1\frac{d}{dx}\left(\frac{f_1(x)}{f_{k+1}(x)}\right) + \cdots$$
$$+c_k\frac{d}{dx}\left(\frac{f_k(x)}{f_{k+1}(x)}\right) \Longrightarrow \tag{4.95}$$

$$\frac{F(x)}{f_{k+1}(x)} = c_1\frac{f_1(x)}{f_{k+1}(x)} + \cdots + c_k\frac{f_k(x)}{f_{k+1}(x)} + c_{k+1}$$
$$\Longleftrightarrow \quad F(x) = c_1 f_1(x) + \cdots + c_{k+1} f_{k+1}(x)\,, \tag{4.96}$$

and therefore Eq. (2) holds for every n.

Bibliography

[AC92] S. Appl and M. Camenzind, A&A **256** (1992), 354.

[App96] S. Appl, A&A **314** (1996), 995.

[AS72] M. Abramowitz and I. A. Stegun, *Handbook of Mathematical Functions*, Dover Publications, Inc., New York, 1972.

[BC92] F. Bacciotti and C. Chiuderi, Phys. Fluids **4(1)** (1992), 35.

[Bir96] T. Biretta, *in Solar and Astrophysical MHD Flows*, K. Tsinganos (ed.), Kluwer Academic Publishers, p. 357, 1996.

[BMFT94] G. Bodo, S. Massaglia, A. Ferrari, and E. Trussoni, A&A **283** (1994), 655.

[BMR+95] G. Bodo, S. Massaglia, P. Rossi, R. Rosner, A. Malagoli, and A. Ferrari, A&A **303** (1995), 281.

[BP82] R.D. Blandford and D.G. Payne, MNRAS **199** (1982), 883.

[CH80] K.L. Chan and R.N. Henriksen, ApJ **241** (1980), 534.

[CL94] J. Contopoulos and R.V.E. Lovelace, ApJ **429** (1994), 139.

[DZC96] L. Del Zanna and C. Chiuderi, A&A **310** (1996), 341.

[FH96] J.D. Fiege and R.N. Henriksen, MNRAS **281** (1996), 1038.

[FMBR96] A. Ferrari, S. Massaglia, G. Bodo, and P. Rossi, *in Solar and Astrophysical MHD Flows*, K. Tsinganos (ed.), Kluwer Academic Publishers, p. 607, 1996.

[FTZ78] A. Ferrari, E. Trussoni, and L. Zaninetti, A&A **64** (1978), 43.

[FTZ81] A. Ferrari, E. Trussoni, and L. Zaninetti, MNRAS **196** (1981), 1051.

[HN89] J. Heyvaerts and C.A. Norman, ApJ **347** (1989), 1055.

[Ray96] T.P. Ray, *in Solar and Astrophysical MHD Flows*, K. Tsinganos (ed.), Kluwer Academic Publishers, p. 539, 1996.

[Sak87] T. Sakurai, Publ. Astron. Soc. Japan **39** (1987), 821.

[ST94] C. Sauty and K. Tsinganos, A&A **287** (1994), 893.

[TSS+96] K. Tsinganos, C. Sauty, G. Surlantzis, E. Trussoni, and J. Contopoulos, *in Solar and Astrophysical MHD Flows*, K. Tsinganos (ed.), Kluwer Academic Publishers, p. 427, 1996.

[TST96] E. Trussoni, C. Sauty, and K. Tsinganos, *in Solar and Astrophysical MHD Flows*, K. Tsinganos (ed.), Kluwer Academic Publishers, p. 383, 1996.

[TT91] K. Tsinganos and E. Trussoni, A&A **249** (1991), 156.

[VT98] N. Vlahakis and K. Tsinganos, MNRAS **in press** (1998).

Chapter 5

Systematic Construction of Exact MHD models

By a systematic method we construct general classes of exact and selfconsistent axisymmetric MHD solutions describing flows which originate at the near environment of a central gravitating astrophysical object. The unifying scheme contains three large groups of exact MHD outflow models, (I) meridionally self-similar ones with *spherical* critical surfaces, (II) radially self-similar models with *conical* critical surfaces and (III) generalized self-similar models with arbitrary shape critical surfaces. This classification includes known polytropic models, such as the classical Parker description of a stellar wind and the Blandford and Payne (1982) model of a disk-wind; it also contains nonpolytropic models, such as those of winds/jets in Sauty and Tsinganos (1994), Lima et al (1996) and Trussoni et al (1997). Besides the unification of all known cases under a common scheme, several new classes emerge and some are briefly analyzed; they could be explored for a further understanding of the physical properties of MHD outflows from various magnetized and rotating astrophysical objects in stellar or galactic systems.

5.1 Introduction

A widespread phenomenon in astrophysics is the outflow of plasma from the environment of stellar or galactic objects, either in the form of a noncollimated wind [Par58, FPBH96], or, in the form of collimated jets [BR74, Bir96]. These outflows not only occur around typical stars and the nuclei of many radio galaxies and quasars, but they are also associated with young stars, older mass losing stars and planetary nebulae nuclei, symbiotic stars, black hole X-ray transients, low- and high-mass X-ray binaries and cataclysmic variables (for recent reviews see *e.g.*, respectively, [FMBR96, Ray96, Kaf96, MR96, Liv97]. Even for the two spectacular rings seen with the HST in SN1987A, it has been proposed that they may be inscribed by two processing jets from an object similar to SS433

on a hourglass-shaped cavity which is created by nonuniform winds of the progenitor star [BK95, Bea95]. Also recently, in the well known long jet of the distant radio galaxy NGC 6251 an about 10^3 light-year-wide warped dust disk perpendicular to the main jet's axis has been observed by HST to surround and reflect UV light from the bright core of the galaxy which probably hosts a black hole [CV97].

Nevertheless, despite their abundance the questions of the formation, acceleration and propagation of nonuniform winds and jets have not been fully resolved. One of the main difficulties in dealing with the theoretical problem posed by cosmical outflows is that their dynamics needs to be described - even to lowest order - by the highly intractable set of the MHD equations. As is well known, this is a nonlinear system of partial differential equations with several critical points, etc, and only very few classes of solutions are available for axisymmetric systems obtained by assuming a separation of variables in several key functions. This hypothesis allows an analysis in a 2-D geometry of the full MHD equations which reduce then to a system of ordinary differential equations. The basis of such self-similarity treatment is the prescription of a scaling law in the variables as a function of one of the coordinates. The choice of the scaling variable depends on the specific astrophysical problem.

In spherical coordinates $(r\,,\theta\,,\phi)$, a *first* broad class for describing outflows are the so-called meridionally self-similar MHD models. Parker's classical modeling of the spherically symmetric polytropic solar wind [Par58] is the simplest member of this class. A new class of such type of models for describing magnetized and rotating MHD outflows from a central gravitating object has also been examined [ST94, LTP96, TTS97]. For example, an energetic criterion for the transition of an asymptotically conical outflow originating at an inefficient magnetic rotator to an asymptotically cylindrical outflow from an efficient magnetic rotator was derived. In the present Chapter, it will be shown that this special class of meridionally self-similar solutions is one of the simplest possible meridionally self-similar models. Furthermore, a new interesting member of this class of radially self-similar MHD models will be briefly sketched.

A *second* broad class of solutions contains the radially self-similar MHD models. Bardeen & Berger [BB78] presented the first such models in the context of hydrodynamic and polytropic galactic winds. Nevertheless, their generalization to a cold magnetized plasma by Blandford & Payne [BP82], remains widely known because of their success in showing for the first time that astrophysical jets can be accelerated magnetocentrifugally from a Keplerian accretion disk, *if* the poloidal fieldlines are inclined by an angle of 60^o, or less, to the disk midplane (when the flow on the equatorial plane is cold and exactly Keplerian); see also, Cao [Cao97]. A further extension has been presented by Contopoulos & Lovelace [CL94] for a hot plasma with a more general parametrization of the magnetic flux on the disc, while these models form the basis of several investigations of accretion-ejection flows from stars and AGN [Kon89, FP95, Fer97, Li95, Li96]. In this Chapter it will be shown that this special class of radially self-similar solutions is one of the simplest possible such models. Furthermore, a new interesting member of the radially

self-similar MHD models will be sketched.

The Chapter is organized as follows. After a brief introduction of the basic MHD quantities, in subsection 5.2 we use a theorem in order to construct several classes of meridionally self-similar solutions and the resulting cases are then summarized in Tables 5.1 and 5.2. The general method is applied in subsection 5.2.2 to a step by step construction of a new model for collimated outflows which is also briefly sketched there. In section 5.3 the other remaining possibility in spherical coordinates, i.e., radial self similarity is taken up. The resulting cases are summarized in Table 5.3 while a new model is also briefly sketched which gives asymptotically cylindrical, paraboloidal and conical streamlines. In section 5.4 we present a new class of self similar solutions where the shape of the critical surfaces comes out from the solution. The results are summarized in Sec. 5.5. Finally, in Sec. 5.6 some other solutions are briefly presented.

5.2 Meridionally self-similar MHD outflows

Consider the steady ($\partial/\partial t = 0$) hydromagnetic equations. They consist of a set of eight coupled, nonlinear, partial differential equations expressing momentum, magnetic and mass flux conservation, together with Faraday's law of induction in the ideal MHD limit,

$$\rho\left(\vec{V}\cdot\vec{\nabla}\right)\vec{V} = \frac{\left(\vec{\nabla}\times\vec{B}\right)\times\vec{B}}{4\pi} - \vec{\nabla}P - \rho\vec{\nabla}\mathcal{V}\,, \tag{5.1}$$

$$\vec{\nabla}\cdot\vec{B} = 0\,, \quad \vec{\nabla}\cdot\left(\rho\vec{V}\right) = 0\,, \quad \vec{\nabla}\times\left(\vec{V}\times\vec{B}\right) = 0\,. \tag{5.2}$$

$\vec{B}$, $\vec{V}$, $-\vec{\nabla}\mathcal{V} = -\vec{\nabla}\left(-\mathcal{GM}/r\right)$ denote the magnetic, velocity and external gravity fields, respectively, while ρ and P the gas density and pressure.
With axisymmetry ($\partial/\partial\phi = 0$), we may introduce the magnetic flux function A, such that three free integrals exist for the total specific angular momentum carried by the flow and the magnetic field, $L(A)$, the corotation angular velocity of each streamline at the base of the flow, $\Omega(A)$ and the ratio of the mass and magnetic fluxes, $\Psi_A(A)$ (Chapter 2). In terms of these integrals and the square of the poloidal Alfvén Mach number (or simply Alfvén number),

$$M^2 = \frac{4\pi\rho V_p^2}{B_p^2} = \frac{\Psi_A^2}{4\pi\rho}\,, \tag{5.3}$$

the magnetic field and bulk flow speed are given in spherical coordinates (r,θ,ϕ) by,

$$\vec{B} = \vec{\nabla}\times\frac{A(r,\theta)\hat{\phi}}{r\sin\theta} - \frac{L\Psi_A - r^2\sin^2\theta\Omega\Psi_A}{r\sin\theta(1-M^2)}\hat{\phi}\,, \tag{5.4}$$

$$\vec{V} = \frac{\Psi_A}{4\pi\rho}\vec{\nabla}\times\frac{A(r,\theta)\hat{\phi}}{r\sin\theta} + \frac{r^2\sin^2\theta\Omega - LM^2}{r\sin\theta(1-M^2)}\hat{\phi}\,. \tag{5.5}$$

To construct classes of exact solutions, we shall make two crucial assumptions:

1. that the Alfvén number M is some function of the dimensionless radial distance $R = r/r_\star$,

$$\boxed{M = M(R)}, \tag{5.6}$$

and

2. that the poloidal velocity and magnetic fields have a dipolar angular dependence,

$$A = \frac{r_\star^2 B_\star}{2}\mathcal{A}(\alpha)\ , \qquad \alpha = \frac{R^2}{G^2}\sin^2\theta\ , \tag{5.7}$$

$$\text{with} \qquad \boxed{G = G(R)}. \tag{5.8}$$

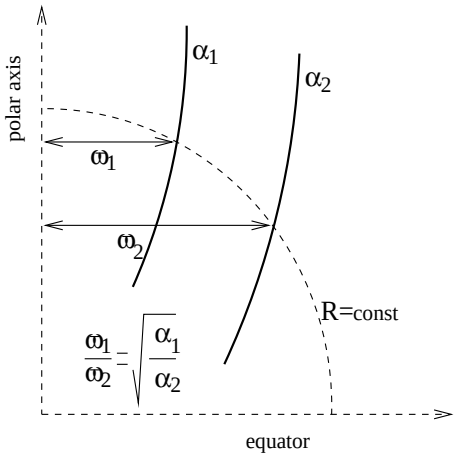

Figure 5.1: An illustration of the construction of the streamlines $\alpha = const.$ on the poloidal plane in meridionally selfsimilar outflows.

By choosing $G\,(R=1)=1$ at the Alfvén transition $R = 1$, $G(R)$ evidently measures the cylindrical distance ϖ to the polar axis of each fieldline labeled by α, normalized to its cylindrical distance ϖ_α at the Alfvén point, $G\,(R) = \varpi/\varpi_\alpha$. For a smooth crossing of the Alfvén sphere $R = 1$ $[r = r_\star, \theta = \theta_a(\alpha)]$, the free integrals L and Ω are related by

$$\frac{L}{\Omega} = \varpi_\alpha^2(A) = r_\star^2\sin^2\theta_a(\alpha) = r_\star^2\alpha\ . \tag{5.9}$$

Therefore, the second assumption is equivalent with the statement that at the Alfvén surface the cylindrical distance ϖ_α of each magnetic flux surface $\alpha = const$ is simply proportional to $\sqrt{\alpha}$.

Note also that the gravitational potential $\mathcal{V} = -\mathcal{GM}/r$ can be expressed in terms of the escape speed V_{esc} at the Alfvén radius $r_\star$,

$$\mathcal{V} = -\frac{\nu^2 V_\star^2}{2R}\ , \qquad \nu = \frac{V_{esc}}{V_\star}\ , \qquad V_{esc} = \sqrt{\frac{2\mathcal{GM}}{r_\star}}\ .$$

Instead of using the three free functions of α, $(\mathcal{A}\,,\Psi_A\,,\Omega)$, we found it more convenient to work instead with the three dimensionless functions of α, $(g_1\,,\,g_2\,,\,g_3)$,

$$g_1(\alpha) = \int \mathcal{A}'^2\,d\alpha\ ,\ g_2(\alpha) = \frac{r_\star^2}{B_\star^2}\int \Omega^2\Psi_A^2\,d\alpha\ ,\ g_3(\alpha) = \frac{\Psi_A^2}{4\pi\rho_\star}\ . \tag{5.10}$$

Also, we shall indicate by Π the total pressure in units of the magnetic pressure at the Alfvén surface on the polar axis, $B_\star^2/8\pi = \rho_\star V_\star^2/2$,

$$\Pi = \frac{8\pi}{B_\star^2}\left(P + \frac{B^2}{8\pi}\right) ,$$

such that,

$$P = \frac{B_\star^2}{8\pi}\left(\Pi + f_1 g_1^{'} + f_2 \alpha g_1^{'} + f_3 \alpha g_2^{'}\right) . \tag{5.11}$$

The functions $f_i(R)$, $i = 1,2,3$ are given in Appendix 5.A while all starred quantities refer to their respective values at the polar Alfvén point ($R = 1\,, \alpha = 0$). Hence,

$$\mathcal{A}^{'}(\alpha = 0) = 1\,,\ \Psi_A(\alpha = 0) = \sqrt{4\pi\rho_\star}\,,$$

or,

$$g_1^{'}(\alpha = 0) = 1\,,\ g_3(\alpha = 0) = 1\,. \tag{5.12}$$

With assumptions (i)-(ii) and in this notation, the $\hat{r}-$ and $\hat{\theta}-$components of the momentum equation become,

$$\frac{\partial \Pi(R,\theta)}{\partial R} = f_6 g_1^{'} + \left(f_7 + \frac{F}{R} f_4\right)\alpha g_1^{'} + \left(f_8 + \frac{F}{R} f_5\right)\alpha g_2^{'} + f_9 g_3\,, \tag{5.13}$$

$$\frac{\partial \Pi(R,\theta)}{\partial \theta} = 2\cot\theta\left(f_4 \alpha g_1^{'} + f_5 \alpha g_2^{'}\right) . \tag{5.14}$$

Next, by using α instead of θ as an independent variable, we may transform from the pair of the independent variables $(R\,,\theta)$ to the pair of the independent variables $(R\,,\alpha)$. With the following elementary relations valid for any differentiable function $\mathcal{G}$,

$$\frac{\partial \mathcal{G}(R,\theta)}{\partial R} = \frac{\partial \mathcal{G}(R,\alpha)}{\partial R} + \alpha\frac{F}{R}\frac{\partial \mathcal{G}(R,\alpha)}{\partial \alpha}\,, \tag{5.15}$$

$$\frac{\partial \mathcal{G}(R,\theta)}{\partial \theta} = 2\alpha\cot\theta\frac{\partial \mathcal{G}(R,\alpha)}{\partial \alpha}\,, \tag{5.16}$$

we may transform Eqs. (5.13), (5.14) into the following two equations:

$$\frac{\partial \Pi(\alpha,R)}{\partial \alpha} = f_4 g_1^{'} + f_5 g_2^{'}\,, \tag{5.17}$$

$$\frac{\partial \Pi(\alpha,R)}{\partial R} = f_6 g_1^{'} + f_7 \alpha g_1^{'} + f_8 \alpha g_2^{'} + f_9 g_3\,. \tag{5.18}$$

By integrating Eq. (5.17) we get $\Pi = f_4 g_1 + f_5 g_2 + f_0$ where f_0 is an arbitrary function of R. From Eq. (6.12) the pressure is

$$P = \frac{B_\star^2}{8\pi}\left(f_4 g_1 + f_5 g_2 + f_0 + f_1 g_1^{'} + f_2 \alpha g_1^{'} + f_3 \alpha g_2^{'}\right) , \tag{5.19}$$

Table 5.1: Meridionally Self-similar Models

Case	$g_1(\alpha)$	$g_2(\alpha)$	$g_3(\alpha)$	constraints on constants
(1) [a]	α	$\lambda^2\alpha$	$1+\delta\alpha$	
(2) [b]	α	$\xi\alpha+\mu\alpha^\epsilon/\epsilon$	$1+\delta\alpha+\mu\delta_0\alpha^\epsilon$	$\epsilon\neq 0,1, \mu\neq 0$
(3)	α	$\xi\alpha+\mu\alpha\ln\alpha$	$1+\delta\alpha+\mu\delta_0\alpha\ln\alpha$	$\mu\neq 0$
(4)	$\alpha_0 e^{\frac{\alpha}{\alpha_0}}$	$\lambda e^{\frac{\alpha}{\alpha_0}}$	$1+\delta\alpha e^{\frac{\alpha}{\alpha_0}}+\mu\left(e^{\frac{\alpha}{\alpha_0}}-1\right)$	
(5)	$\frac{\alpha_0}{\epsilon}\mid\frac{\alpha}{\alpha_0}-1\mid^{\epsilon-1}\left(\frac{\alpha}{\alpha_0}-1\right)$	$\xi\mid\frac{\alpha}{\alpha_0}-1\mid^\epsilon$	$1+\delta\mid\frac{\alpha}{\alpha_0}-1\mid^\epsilon+\mu\mid\frac{\alpha}{\alpha_0}-1\mid^{\epsilon-1}-\delta-\mu$	$\epsilon\neq 0,1$
(6)	$-\alpha_0\ln\mid\frac{\alpha}{\alpha_0}-1\mid$	$\xi\ln\mid\frac{\alpha}{\alpha_0}-1\mid$	$1+\delta\ln\mid\frac{\alpha}{\alpha_0}-1\mid+\mu\frac{\alpha}{\alpha_0(\alpha-\alpha_0)}$	
(7)	$\frac{\alpha}{1-\alpha_{ref}}$	$\mu\ln\frac{\alpha}{\alpha_{ref}}+\xi\alpha$	$1+\delta(\alpha-\alpha_{ref})+\mu\delta_0\ln\frac{\alpha}{\alpha_{ref}}$	$\mu\neq 0$
(8)	$\frac{\alpha_{ref}}{\epsilon\left(1-\alpha_{ref}\right)}\left(\frac{\alpha}{\alpha_{ref}}\right)^\epsilon$	$\lambda_1\alpha^\epsilon+\lambda_2\alpha^{\epsilon-1}$	$1+\delta_1\left(\alpha^\epsilon-\alpha_{ref}^\epsilon\right)+\delta_2\left(\alpha^{\epsilon-1}-\alpha_{ref}^{\epsilon-1}\right)$	$\epsilon\neq 0,1$
(9)	$\frac{\alpha_{ref}}{1-\alpha_{ref}}\ln\frac{\alpha}{\alpha_{ref}}$	$\lambda_1\ln\frac{\alpha}{\alpha_{ref}}+\frac{\lambda_2}{\alpha}$	$1+\delta_1\ln\frac{\alpha}{\alpha_{ref}}+\delta_2\left(\frac{1}{\alpha}-\frac{1}{\alpha_{ref}}\right)$	

[a] [TT91, ST94]
[b] see Chapter 7, or [VT98]

or,

$$P=\frac{B_\star^2}{8\pi}\mathbf{Y}\mathbf{P}^\dagger\,,$$

where $\mathbf{P}$ and $\mathbf{Y}$ are the (1×7) matrices,

$$\mathbf{P}=[\,f_0\;\;f_4\;\;f_1\;\;f_2\;\;f_5\;\;f_3\;\;0\,]\,, \tag{5.20}$$

and

$$\mathbf{Y}=[\,Y_1\;\;Y_2\;\;Y_3\;\;Y_4\;\;Y_5\;\;Y_6\;\;Y_7\,]=\left[\,1\;\;g_1\;\;g_1^{'}\;\;\alpha g_1^{'}\;\;g_2\;\;\alpha g_2^{'}\;\;g_3\right]\,. \tag{5.21}$$

Substituting for Π in Eq. (5.18) it follows,

$$-f_9g_3-f_8\alpha g_2^{'}+f_5^{'}g_2-f_7\alpha g_1^{'}-f_6g_1^{'}+f_4^{'}g_1+f_0^{'}=0\,, \tag{5.22}$$

an expression of the form

$$X_7(R)\,Y_7(\alpha)+X_6(R)\,Y_6(\alpha)+\cdots+X_1(R)\,Y_1(\alpha)=0\,,\;\text{or}\,,\;\mathbf{Y}\mathbf{X}^\dagger=\mathbf{0}\,, \tag{5.23}$$

with $\mathbf{X}$ the (1×7) matrix:

$$\mathbf{X}=[\,X_1\;\;X_2\;\;X_3\;\;X_4\;\;X_5\;\;X_6\;\;X_7\,]=\left[\,f_0^{'}\;\;f_4^{'}\;\;-f_6\;\;-f_7\;\;f_5^{'}\;\;-f_8\;\;-f_9\,\right] \tag{5.24}$$

5.2.1 Systematic construction of classes of meridionally self-similar MHD outflows

It is straightforward to prove the following useful theorem (see Appendix 4.B. or [VT97]):

Theorem: If $F_n(\alpha)$, $Y_i(\alpha)$, $X_i(R)$, $i = 1, 2, \cdots, n$ are arbitrary functions of the independent variables α and R and

$$F_n(\alpha) = Y_1(\alpha) X_1(R) + \cdots + Y_n(\alpha) X_n(R), \tag{5.25}$$

then, there exist constants $c_1, c_2, \ldots, c_n$ such that,

$$F_n(\alpha) = c_1 Y_1(\alpha) + c_2 Y_2(\alpha) + \cdots + c_n Y_n(\alpha). \tag{5.26}$$

Consider then a relation of the form,

$$X_n(R) Y_n(\alpha) + \cdots + X_1(R) Y_1(\alpha) = 0. \tag{5.27}$$

Regarding the first term of the sum there are evidently only two possibilities. Either,

1. $X_n(R) = 0$ for every R, in which case (indicated by the digit "0") we have

$$X_{n-1}(R) Y_{n-1}(\alpha) + \cdots + X_1(R) Y_1(\alpha) = 0,$$

or,

2. $X_n(R) \neq 0$, in which case (indicated by the digit "1") we have

$$Y_n(\alpha) = -\frac{X_1(R)}{X_n(R)} Y_1(\alpha) - \cdots - \frac{X_{n-1}(R)}{X_n(R)} Y_{n-1}(\alpha).$$

Then, according to the theorem stated in the beginning of this section, there are constants $\mu_i^{(n)}, i = 1, 2, \cdots, n-1$ such that $Y_n(\alpha) = \sum_{i=1}^{n-1} \mu_i^{(n)} Y_i(\alpha)$. This gives a condition between the functions of α. Substituting this condition in the initial sum we find:

$$\begin{aligned} &\left[X_{n-1}(R) + \mu_{n-1}^{(n)} X_n(R)\right] Y_{n-1}(\alpha) + \\ &\left[X_{n-2}(R) + \mu_{n-2}^{(n)} X_n(R)\right] Y_{n-2}(\alpha) + \cdots \\ &+ \left[X_1(R) + \mu_1^{(n)} X_n(R)\right] Y_1(\alpha) = 0. \end{aligned} \tag{5.28}$$

Hence, in both cases (i)-(ii) we find a sum with $n-1$ terms. Following this algorithm at the end we 'll have only one term. Since for each product we have the above two possibilities, totally we obtain 2^n cases. Each of them corresponds to a set "xx$\cdots$xx" with $x = 1, 0$ (n digits). The number of "1" digits is the number of conditions between functions of α while the number of "0" digits is the number of conditions between functions of R.

Following this method from Eq. (5.22) we get 2^7 solutions. Each of them corresponds to a set "xxxxxxx" with x either 1, or, 0. Of those numbers:

1. The first digit is always "1" (because $X_7 \neq 0$).

2. The last digit is always "0" (because $Y_1 \neq 0$).

3. Since $\mathcal{A}' \neq 0$, it follows that $g_1' \neq 0$ and thus g_1 cannot be a constant. Hence, the function $Y_2 = g_1$ cannot be proportional to Y_1 and therefore all numbers always have "00" at the end.

4. We have totally six unknown functions: the three functions of R, (G, M, f_0) and the three functions of α, (g_1, g_2, g_3). On the other hand, the number of conditions between the functions of R (their number is equal to the number of digits "0") and the functions of α (their number equals to the number of digits "1") in each one of the sets "xxxxxxx" is seven. It follows that the system of (G, M, f_0) and $(g_1,\ g_2,\ g_3)$ is overdetermined. Note however that since the forms of the functions $X_i(R)$ are more complicated than the forms of the functions $Y_i(\alpha)$, we choose sets "xxxxxxx" with at most three "0's" because in the case of 4 or more "0's" we have correspondingly 4 or more relations between the 3 functions of R, which in general overdetermines the system of (G, M, f_0). In this way we shift the difficulty of overdetermination of the problem to the set of the 3 functions of α, $(g_1,\ g_2,\ g_3)$ which need to satisfy 4 relations. In this system however, it is possible to choose the constants $\mu_i^{(j)}$ such that a consistent solution for the functions of α can be finally constructed.

Altogether, then and with these considerations in mind, from the $2^7 = 128$ possible cases we end up with only five: 1011100, 1101100, 1110100, 1111000, 1111100. For each of one of those sets we can solve the system for $g_1\,, g_2\,, g_3$, as it is shown in the example of the next section.
From a different perspective, $g_1(\alpha)$, $g_2(\alpha)$, $g_3(\alpha)$ are vectors in a 3D α-space with basis vectors $[u_1(\alpha)\,, u_2(\alpha)\,, u_3(\alpha)]$. This space contains all vectors $g_i(\alpha)$, $i = 1, 2, 3$ subject to the θ-self-similarity constraint manifested by Eq. (5.22), i.e., that for a given such set $g_i(\alpha)$, $i = 1, 2, 3$, the vectors $1, \alpha g_1^{'}(\alpha)\,, \alpha g_2^{'}(\alpha)$ and $g_1^{'}(\alpha)$ also belong to the same space. Each of the resulting functions $g_i(\alpha)$, $i = 1, 2, 3$ are then a linear combination of the basis vectors $u_1(\alpha), u_2(\alpha), u_3(\alpha)$. In the following, we choose $u_1 = 1$, $u_2 = g_1(\alpha)$. All such sets of basis vectors give all possible meridionally self-similar solutions. Therefore, collecting all possibilities, we end up with the classes of solutions shown in Table 5.1.
Note that in the last three cases $A^{'}\ (\alpha = 0) \neq 1$, but one can say that the starred quantities refer to values at the point $R = 1, \alpha = \alpha_{ref} < 1$. [1]

In all nine cases of Table 5.1, from Eqs. (5.10) we may easily find the forms of the free integrals from the relations,

[1] We have assumed that at point $r = r_\star, \alpha = 0$ we have $\rho = \rho_\star$. So we have excluded solutions with zero density on the axis. But we may easily extent the models of Table 5.1: Generally, if the starred quantities $B_\star, V_\star, \rho_\star$ refer to values of $B_r\,, V_r\,, \rho$ at the point $r = r_\star\,, \alpha = \alpha_{ref}$, then we may substitute $g_1 \rightarrow constant \times g_1$ and $g_3 \rightarrow constant + g_3$ in a way such at $\alpha = \alpha_{ref}\,, g_1^{'}\,(1 - \alpha) = 1$ and $g_3 = 1$.

$$A = \frac{B_\star r_\star^2}{2} \int_0^\alpha \sqrt{g_1'}\, d\alpha \,,\; \Psi_A = \sqrt{4\pi\rho_\star g_3}\,,$$

$$\Omega = \frac{V_\star}{r_\star}\sqrt{\frac{g_2'}{g_3}}\,,\quad L = r_\star V_\star \alpha \sqrt{\frac{g_2'}{g_3}}\,, \tag{5.29}$$

while by substituting g_1, g_2, g_3 in Eqs. (5.19), (5.22), the corresponding ordinary differential equations for the jet radius $G(R)$, Alfvén number $M(R)$ and pressure component $f_0(R)$ are found from the R-relations, as it is illustrated in the following section.
From the perspective of the α-space, in each one of the cases of Table 5.1 there exists a 3×7 matrix $\mathbf{K}$ such that

$$\mathbf{Y} = [\, u_1 \;\; u_2 \;\; u_3 \,]\, \mathbf{K}\,, \tag{5.30}$$

so that from Eq. (7.14),

$$[\, u_1 \;\; u_2 \;\; u_3 \,]\, \mathbf{K}\mathbf{X}^\dagger = \mathbf{0}\,.$$

If u_i are linearly independent then

$$\mathbf{K}\mathbf{X}^\dagger = \mathbf{0}\,.$$

These three equations are the ordinary differential equations for the functions of R in each model while the pressure is,

$$P = \frac{B_\star^2}{8\pi}[\, u_1 \;\; u_2 \;\; u_3 \,]\, \mathbf{K}\mathbf{P}^\dagger = \frac{B_\star^2}{8\pi}(P_0 + P_1 g_1 + P_2 u_3)\,,$$

where

$$\mathbf{K}\mathbf{P}^\dagger = [P_0 \; P_1 \; P_2]^\dagger\,.$$

The first two cases of Table 5.1 are of some interest. The first, is a degenerate one with $u_3 = 0$ and the following form of the free integrals:

$$A = \frac{B_\star r_\star^2}{2}\alpha\,,\; \Psi_A = \sqrt{4\pi\rho_\star\,(1+\delta\alpha)}\,, \Omega = \frac{\lambda V_\star}{r_\star}\frac{1}{\sqrt{1+\delta\alpha}}\,. \tag{5.31}$$

This is a special case of the more general following case (2) for $\mu = 0$ (and $\xi = \lambda^2$) and has been studied in detail in [ST94] and [TTS97]. It is the single case where we have only two conditions between the functions of R, so that the third relation between the unknown functions G, M, f_0 is freely chosen. In [TTS97] this corresponds to an *a priori* specification of the shape of the poloidal streamlines, while in ST94 in an *a priori* imposed relationship between the spherically and nonspherically symmetric components of the pressure. This

Table 5.2: Meridionally Self-similar Radial Models

Case	$g_1(\alpha)$	$g_2(\alpha)$	$g_3(\alpha)$
(1) [a]	$-\ln\mid 1-\alpha\mid$	0	1
(2) [b]	$\mu\int\frac{\alpha^\epsilon}{1-\alpha}d\alpha-\ln\mid 1-\alpha\mid$	$\lambda^2\frac{\alpha^\epsilon}{\epsilon}$	$1+\delta\alpha^\epsilon$
(3)	$\mu_1\ln\mid 1-\alpha\mid+\mu_2\int\frac{\ln\alpha}{1-\alpha}d\alpha$	$\lambda\ln\alpha$	$\delta_1+\delta_2\ln\alpha$
(4)	$g_1(\alpha)\neq\mu_1\ln\mid 1-\alpha\mid+\mu_2$	0	$\delta g_1^{'}(1-\alpha)+\lambda$
(5)	$\mu\ln\mid 1-\alpha\mid$	$g_2(\alpha)\neq(\mu,\mu_1\ln\alpha+\mu_2,\mu_1\alpha^{\mu_2}+\mu_3)$	δ

[a] Parker's solution [Par63]
[b] [LTP96]

last case leads to a generalized polytropic-type relation between pressure and density of the form,

$$\frac{P(\alpha,R)}{P(0,R)}=\text{ function of }\frac{\rho(\alpha,R)}{\rho(0,R)}\,. \tag{5.32}$$

As a result, a Bernoulli-type constant exists and, among others, this constant gives a quantitative criterion for the transition of an asymptotically conical wind from an inefficient magnetic rotator to an asymptotically cylindrical jet from an efficient magnetic rotator.
The second case with $\epsilon\neq 0,1,\mu\neq 0$ has $u_2=\alpha$, $u_3=\alpha^\epsilon$. The corresponding form of the free integrals is :

$$A=\frac{B_\star r_\star^2}{2}\alpha,\ \Psi_A=\sqrt{4\pi\rho_\star\left(1+\delta\alpha+\mu\delta_0\alpha^\epsilon\right)},\Omega=\frac{V_\star}{r_\star}\sqrt{\frac{\mu\alpha^{\epsilon-1}+\xi}{1+\delta\alpha+\mu\delta_0\alpha^\epsilon}}\,. \tag{5.33}$$

This is a new case which emerged from the present systematic construction. The corresponding differential equations are derived in detail in the example of the next section where the solution is briefly analysed.

In the special configuration with $G=R\Leftrightarrow\alpha=\sin^2\theta$, the field and stream lines on the poloidal plane are radial. The functions $f_i\,,i=1,\ldots 9$ are given in Appendix 5.A. Eqs. (5.19),(5.22) are simplified to

$$P=\frac{B_\star^2}{8\pi}\left(f_5g_2+f_0+f_1g_1^{'}(1-\alpha)+f_3\alpha g_2^{'}\right)\,, \tag{5.34}$$

$$-f_9g_3-f_8\alpha g_2^{'}+f_5^{'}g_2-f_6\,(1-\alpha)\,g_1^{'}+f_0^{'}=0\,. \tag{5.35}$$

If this is the case, following the algorithm of the previous sections, we find the five cases shown in Table 5.2.
The first case is a *degenerate* one, wherein there is only one condition between the unknown functions $M(R)\,,f_0(R)$. Thus, a second relation between $M(R)-f_0(R)$ can be imposed *a priori*, for example, a polytropic relation between pressure and density. This last possibility leads precisely to Parker's

[Par63] classical solar wind solution with a radial and nonrotating outflow (see Chapter 6). All other cases (2)-(5) are *non-degenerate*, i.e., there are two relations between $M(R) - f_0(R)$.
The second case has been analyzed in detail in Lima et al [LTP96] and corresponds to a radial but heliolatitudinally depended outflow. If in addition $\mu = -1, \epsilon = 1$ this case coincides with (1) in Table 5.1 for radial poloidal streamlines. Note that a common feature of all rotating cases with radial stream lines on the poloidal plane is that they cannot be extended in all the poloidal plane, for sufficiently fast magnetic rotators. For example, in the model of Lima et al. (1996) the pressure becomes negative at some colatitude θ_{max}, for large values of rotation. This is basically due to the fact that with the poloidal magnetic field dropping like $1/R^2$ and the azimuthal field dropping like $1/R$, the magnetic pressure drops like $1/R^4$ and by itself alone cannot balance the magnetic tension which drops like $1/R^3$; a strong pressure gradient is then needed from the pole towards the equator to balance the magnetic pinching. In fast magnetic rotators this pressure gradient is so strong that it leads to negative values of the pressure at angles $\theta > \theta_{max}$. A collimated outflow with uniform asymptotic conditions is the only way left for an everywhere valid outflow from an efficient magnetic rotator [HN89, ST94].

5.2.2 Example of a new model for a meridionally self-similar MHD outflow

Let us illustrate the previous construction with the example 1101100 obtained from the present case with $n = 7$. This number means the following:
Since the first digit is 1, there are six constants $\mu_i^{(7)}, i = 1, 2, \cdots, 6$ such that the following relation holds between the functions $Y_i(\alpha)$, i=1,2, ..7,

$$Y_7 = \sum_{i=1}^{6} \mu_i^{(7)} Y_i \,, \qquad (\alpha\text{-relation-1}) \,. \tag{5.36}$$

Substituting this expression of Y_7 in the initial relation Eq. (7.14) between the functions (X_i, Y_i), i=1,..7, we obtain

$$\left(X_6 + \mu_6^{(7)} X_7\right) Y_6 + \left(X_5 + \mu_5^{(7)} X_7\right) Y_5 + \cdots + \left(X_1 + \mu_1^{(7)} X_7\right) Y_1 = 0 \,. \tag{5.37}$$

Now the second digit is again 1 and thus there are five constants $\mu_i^{(6)}, i = 1, 2, \cdots, 5$ such that

$$Y_6 = \sum_{i=1}^{5} \mu_i^{(6)} Y_i \,, \qquad (\alpha\text{-relation-2}) \,, \tag{5.38}$$

while substituting this relation in Eq. (5.37) we obtain,

$$\begin{aligned} &\left[\left(X_5 + \mu_5^{(7)} X_7\right) + \mu_5^{(6)} \left(X_6 + \mu_6^{(7)} X_7\right)\right] Y_5 + \cdots \\ &+ \left[\left(X_1 + \mu_5^{(7)} X_7\right) + \mu_1^{(6)} \left(X_6 + \mu_6^{(7)} X_7\right)\right] Y_1 = 0 \,. \end{aligned} \tag{5.39}$$

The third digit is 0 and hence

$$\left(X_5 + \mu_5^{(7)} X_7\right) + \mu_5^{(6)} \left(X_6 + \mu_6^{(7)} X_7\right) = 0 \qquad (R\text{-relation-1}) \tag{5.40}$$

a relation between the functions of R. With the help of Eq. (5.40), Eq. (5.39) now reduces to,

$$\sum_{i=1}^{4} \left[\left(X_i + \mu_i^{(7)} X_7\right) + \mu_i^{(6)} \left(X_6 + \mu_6^{(7)} X_7\right)\right] Y_i = 0 \,. \tag{5.41}$$

The fourth digit is 1 and thus there are three constants $\mu_i^{(4)}, i = 1, 2, 3$ such that

$$Y_4 = \sum_{i=1}^{3} \mu_i^{(4)} Y_i \,, \qquad (\alpha\text{-relation-3}) \,. \tag{5.42}$$

Substituting this relation in Eq. (5.41) we obtain

$$\begin{aligned} &\textstyle\sum_{i=1}^{3} \Big\{ \left[\left(X_i + \mu_i^{(7)} X_7\right) + \mu_i^{(6)} \left(X_6 + \mu_6^{(7)} X_7\right)\right] + \\ &\mu_i^{(4)} \left[\left(X_4 + \mu_4^{(7)} X_7\right) + \mu_4^{(6)} \left(X_6 + \mu_6^{(7)} X_7\right)\right] \Big\} Y_i = 0 \,. \end{aligned} \tag{5.43}$$

The fifth digit is 1 and there are two constants $\mu_i^{(3)}, i = 1, 2$ such that

$$Y_3 = \mu_1^{(3)} Y_1 + \mu_2^{(3)} Y_2 \,, \qquad (\alpha\text{-relation-4}) \,. \tag{5.44}$$

Substituting this in Eq. (5.43) we find a relation involving Y_1 and Y_2. Finally, we must put equal to zero the multipliers of Y_1, Y_2 in this relation because the two remaining digits are 0. So we have:

$$\begin{aligned} &\left[\left(X_i + \mu_i^{(7)} X_7\right) + \mu_i^{(6)} \left(X_6 + \mu_6^{(7)} X_7\right)\right] + \\ &\mu_i^{(4)} \left[\left(X_4 + \mu_4^{(7)} X_7\right) + \mu_4^{(6)} \left(X_6 + \mu_6^{(7)} X_7\right)\right] + \\ &\mu_i^{(3)} \left(\left[\left(X_3 + \mu_3^{(7)} X_7\right) + \mu_3^{(6)} \left(X_6 + \mu_6^{(7)} X_7\right)\right] + \right. \\ &\left. \mu_3^{(4)} \left[\left(X_4 + \mu_4^{(7)} X_7\right) + \mu_4^{(6)} \left(X_6 + \mu_6^{(7)} X_7\right)\right]\right) = 0 \,, \\ &\text{for } i = 1, 2 \qquad (R\text{-relations-2,3}) \,. \end{aligned} \tag{5.45}$$

These last two equations together with Eq. (5.40) are the three equations for the functions of R. On the other hand, Eq. (5.36), Eq. (5.38), Eq. (5.42) and

Eq. (5.44) are four relations among the three functions of α. These relations of the functions of α [Eqs. (5.44), (5.42), (5.38), (5.36)] are equivalent to the system:

$$\left.\begin{array}{l} Y_3 = c_1 Y_1 + c_2 Y_2 \\ Y_4 = c_3 Y_1 + c_4 Y_2 \\ Y_6 = c_5 Y_1 + c_6 Y_2 + c_7 Y_5 \\ Y_7 = c_8 Y_1 + c_9 Y_2 + c_{10} Y_5 \end{array}\right\} \Leftrightarrow \left\{\begin{array}{l} g_1^{'} = c_1 + c_2 g_1 \\ \alpha g_1^{'} = c_3 + c_4 g_1 \\ \alpha g_2^{'} = c_5 + c_6 g_1 + c_7 g_2 \\ g_3 = c_8 + c_9 g_1 + c_{10} g_2 \end{array}\right.$$

Note that we have renamed the constants and also used Eq. (7.11). From the first, if $c_2 \neq 0$ it follows that $g_1 = -c_1/c_2 + ce^{c_2\alpha}$. Then, from the second $c = 0$ and hence $g_1 = -c_1/c_2$. But g_1 cannot be a constant. Thus, $c_2 = 0$ while the first two equations combined with Eq. (5.12) give $g_1 = \alpha + c_{11}$ while the third has the solutions:

$$g_2 = \left\{\begin{array}{l} \frac{c_6}{1-c_7}\alpha + c_{12} + c_{13}\alpha^{c_7}\,, \text{ if } c_7 \neq 0, 1 \\ c_6\alpha \ln\alpha + c_{14} + c_{15}\alpha\,, \text{ if } c_7 = 1 \\ c_6\alpha + c_{16}\ln\alpha + c_{17}\,, \text{ if } c_7 = 0\,. \end{array}\right.$$

For the first possibility, we have finally the second case of Table 5.1 :

$$\begin{array}{l} g_1 = \alpha \\ g_2 = \xi\alpha + \mu\alpha^{\epsilon}/\epsilon\,, \qquad \epsilon \neq 0, 1 \\ g_3 = 1 + \delta\alpha + \mu\delta_0\alpha^{\epsilon} \end{array}$$

where we have absorbed the constants c_{11}, c_{12} in the unknown function f_0, $c_{11}f_4 + c_{12}f_5 + f_0 \rightarrow f_0$, Eqs. (5.19), (5.22).

After substituting these values of g_1, g_2, g_3 in Eqs. (5.19) - (5.22), we find that

$$[f_0^{'} - f_6 - f_9] + \left[f_4^{'} + \xi f_5^{'} - f_7 - \xi f_8 - \delta f_9\right]\alpha + \mu\left[f_5^{'}/\epsilon - f_8 - \delta_0 f_9\right]\alpha^{\epsilon} = 0 \quad (5.46)$$

and

$$\begin{aligned} P &= \frac{B_\star^2}{8\pi}\left(P_0 + P_1\alpha + P_2\alpha^{\epsilon}\right) \\ &= \frac{B_\star^2}{8\pi}\left[f_0 + f_1 + \left(f_4 + \xi f_5 + f_2 + \xi f_3\right)\alpha + \mu\left(\frac{f_5}{\epsilon} + f_3\right)\alpha^{\epsilon}\right]\,. \end{aligned} \quad (5.47)$$

By setting equal to zero the three expressions in the square brackets of Eq. (5.46) (since $\mu \neq 0$ and $1\,, \alpha\,, \alpha^{\epsilon}$ are linearly independent vectors in the α-space for $\epsilon \neq 0, 1$) we find the three R-relations for the functions $G(R)$, $M(R)$, $f_0(R)$ (which are the same with Eqs. (5.40),(5.45)). Using the functions f_4, F and the definitions of P_0 and P_1 we obtain five, first order, ordinary differential equations for $G(R)$, $F(R)$, $M(R)$ and the two pressure components $P_1(R)$ and $P_0(R)$,

$$\frac{dG^2}{dR} = -\frac{F-2}{R}G^2\,, \quad (5.48)$$

$$\frac{dF}{dR} = \frac{F}{1-M^2}\frac{dM^2}{dR} - \frac{F\left(F-2\right)}{2R} - \frac{F^2-4}{2R\left(1-M^2\right)} - \frac{2G^2RP_1}{1-M^2} - \frac{2\xi R}{M^2\left(1-M^2\right)^3}\left[\left(2M^2-1\right)G^4 - M^4 + 2M^2\left(1-G^2\right)\right] \tag{5.49}$$

$$\frac{dM^2}{dR} = \frac{M^2\left(1-M^2\right)}{\left(2M^2-1\right)G^4 - M^4}\left\{-\epsilon\delta_0\nu^2\,\frac{G^2\left(1-M^2\right)}{R^2} + \frac{F-2}{R}\left[\left(\epsilon+1\right)M^2 - \left(\epsilon-1\right)G^4\right]\right\} \tag{5.50}$$

$$\frac{dP_1}{dR} = -\left[\frac{F^2-4}{2R^2G^2} + 2\xi\frac{\left(1-G^2\right)^2}{G^2\left(1-M^2\right)^3}\right]\frac{dM^2}{dR} - \frac{M^2F}{2R^2G^2}\frac{dF}{dR} - \frac{\delta\nu^2}{R^2M^2} - \frac{M^2\left(F^2-4\right)\left(F-4\right)}{4R^3G^2} + \xi\frac{\left(F-2\right)\left[\left(2M^2-1\right)G^4 - M^4\right]}{RG^2M^2\left(1-M^2\right)^2} \tag{5.51}$$

$$\frac{dP_0}{dR} = -\frac{2}{G^4}\frac{dM^2}{dR} - \frac{\nu^2}{R^2M^2} - \frac{2M^2\left(F-2\right)}{RG^4} \tag{5.52}$$

Note that the third pressure component $P_2(R)$ is given explicitly in terms of M and G (f_3 and f_5). An integration of the above set of equations will give the complete solution. However, this exercise is rather complicated since any physically accepted solution should pass through the various MHD critical points [TSS$^+$96]. This undertaking, together with a discussion of the solution and application to collimated outflows is the subject of Chapter 7.

It is worth mentioning at this point that our analysis of model (2) of Table 5.1 shows that mainly cylindrically collimated solutions are obtained. The set of Figures 5.2,5.3 illustrates such a typical solution for a representative set of the constants describing the particular model. This solution crosses the Alfvén surface for appropriate values of the slope of the square of the Alfvén number $p_\star = \left(dM^2/dR\right)_\star$, the expansion function $F_\star$ and $P_{1\star}$ which satisfy the Alfvén regularity condition [HN89, ST94] which is easily obtained from Eq. (5.83) of Appendix 5.A at $(R = G = M = 1)$, i.e.,

$$F_\star p_\star = 2f_{4\star}\,. \tag{5.53}$$

The nonspherically symmetric part of the pressure $P_{1\star}$ is obtained from its definition while the functions $f_{3\star}$, $f_{5\star}$ are calculated for $R = 1$ using the L'Hospital

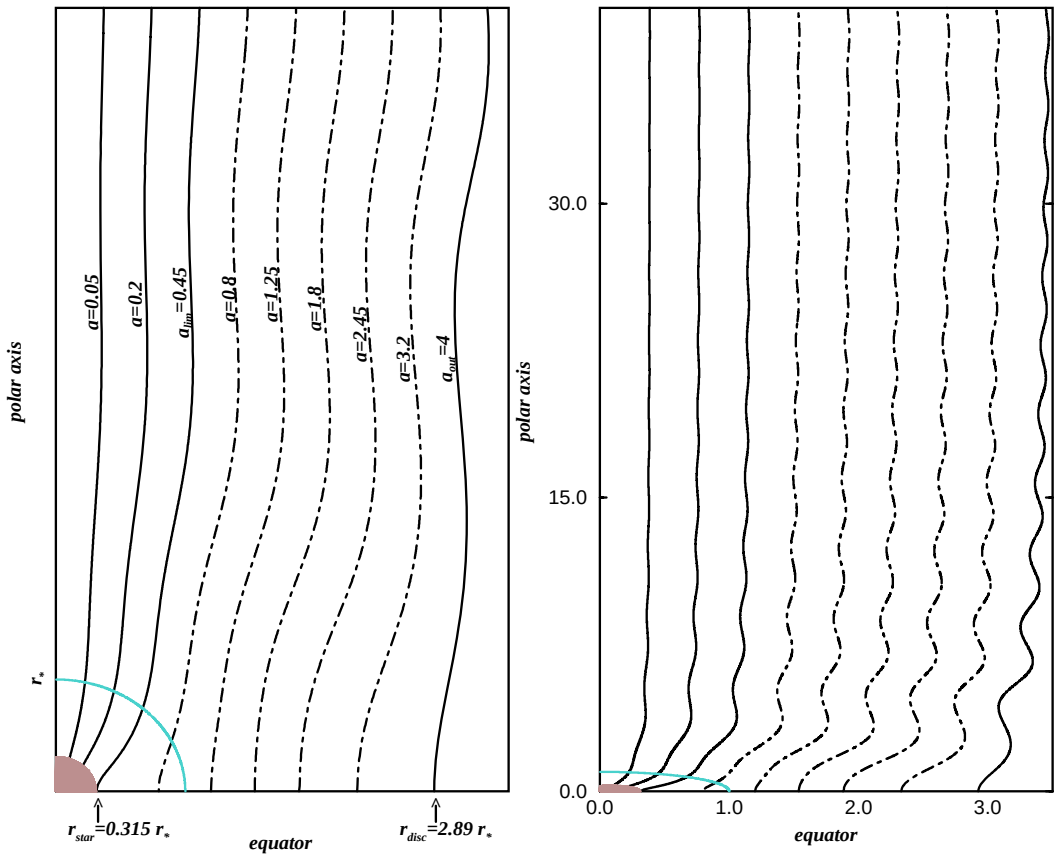

Figure 5.2: Poloidal field and streamlines close to the stellar base (left panel) and in an enlarged scale to show the asymptotical collimation reached after the oscillations have decayed (right panel) for the θ-self similar model of case (2) from Table 5.1, for the following set of parameters: $\epsilon = 0.5$, $\nu^2 = 2\mathcal{G}\mathcal{M}/r_\star V_\star^2 = 10$, $\delta\nu^2 = 3.5$, $\delta_0\nu^2 = 0.1$, $\xi = -10$, $\mu = 20$, $p_\star = \left(dM^2/dR\right)_\star = 1.6$,$F_\star = 1.1$.

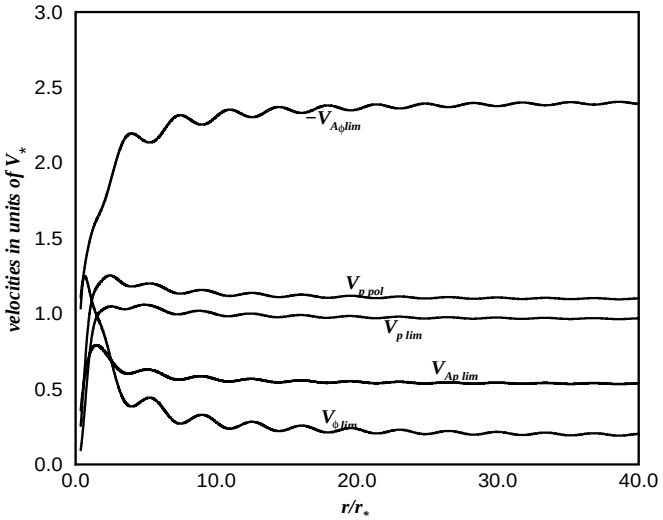

Figure 5.3: Outflow velocities in units of $V_\star$, the radial speed at the Alfvén point ($\alpha = 0, R = 1$), for the parameters given in the caption of Fig. 5.2 of model (2) of Table 5.1.

rule. Figs. 5.2,5.3 correspond to the set $F_\star = 1.1$ and $p_\star = 1.6$. Note that after the Alfvén star-type critical point is crossed, the modified by self-similarity X-type fast critical point [TSS$^+$96] may be crossed by further adjusting appropriately the triplet of the variables ($F_\star$, $p_\star$, $P_{1\star}$). It suffices to note that solutions crossing only the Alfvén surface do not differ qualitatively from those which in addition cross the modified by the present meridional self-similarity fast critical surface.

The left panel fig. 5.2 shows the shape of the streamlines on the poloidal plane and close to the Alfvén surface. The cylindrical asymptotical shape of the poloidal streamlines may be better seen in the enlarged scale of the right panel of the same figure. Note also the constant wavelength but the decaying with distance amplitude of the oscillations, in full agreement with the analysis in [VT97].At the last shown fieldline $\alpha_{out} = 4$, the toroidal fields vanish, $B_\phi = 0$, $V_\phi = 0$. For $\alpha > \alpha_{out}$, Ω^2 becomes negative, so there is no solution there. The same oscillatory behaviour can be seen in the fieldlines which are not rooted on the star but they are perpendicular to a thin disk around it (dotted curves in Figs. 5.2,5.3.) The oscillatory structure of all flow speeds before the flow reaches full cylindrical collimation is also shown in Fig. 5.3 where we have plotted the characteristic velocities in units of the Alfvén speed at the polar axis and Alfvén sphere ($\alpha = 0$, $R = 1$), $V_\star$.

The poloidal speed along the polar axis $V_{p,pol}$ increases to a uniform super-

Alfvénic value and is higher than the same speed along the limiting streamline $V_{p,lim}$ (i.e., the last fieldline rooted on the stellar base r_{star} taken to be at $0.315 r_\star$). Both reach asymptotically uniform values after $V_{p,lim}$ intersects the curve of the poloidal Alfvén speed $V_{Ap,lim}$ at $R = 1$. Note that corotation may be seen up to the Alfvén distance $R = 1$: the azimuthal speed $V_{\phi,lim}$ at the 'limiting fieldline' increases until the Alfvén surface is reached and drops from angular momentum conservation as the outflow expands almost conically. Further away however, this speed too levels off to a constant value when full collimation is achieved, as expected. Finally, the fact that the jet has a large component of toroidal field is reflected by the large values of the Alfvén speed associated with the toroidal magnetic field, $V_{A\phi,lim}$, as compared to the rotational speed $V_{\phi,lim}$.

5.3 Systematic construction of classes of radially self-similar MHD outflows

To construct general classes of radially self-similar solutions, we make the following two key assumptions:
(i) the Alfvén Mach number M is solely a function of θ,

$$\boxed{M = M(\theta)}\,, \tag{5.54}$$

with $M(\theta_\star) = 1$ and
(ii) that the poloidal velocity and magnetic fields have a dipolar angular dependence,

$$A = \frac{B_o \varpi_o^2}{2}\mathcal{A}(\alpha)\ , \qquad \alpha = \frac{R^2}{G^2}\sin^2\theta\,, \quad R = \frac{r}{\varpi_o}\ , \text{ with} \tag{5.55}$$

$$\boxed{G = G(\theta)}\,. \tag{5.56}$$

where B_o, ϖ_o are constants.

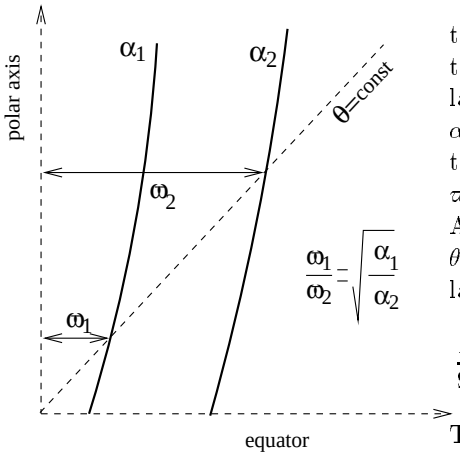

Figure 5.4: An illustration of the construction of the streamlines $\alpha = const.$ on the poloidal plane in radial selfsimilar outflows.

By choosing $G(\theta_\star) = 1$ at the Alfvén transition $\theta_\star$, $G(\theta)$ evidently measures the cylindrical distance ϖ to the polar axis of each fieldline labeled by α, normalized to its cylindrical distance ϖ_α at the Alfvén point, $G(\theta) = \varpi/\varpi_\alpha$. For a smooth crossing of the Alfvén cone $\theta = \theta_\star$ [$r = r_\alpha(\alpha)\,, \theta = \theta_\star$], the free integrals L and Ω are related by

$$\frac{L}{\Omega} = \varpi_\alpha^2(A) = r_\alpha^2(\alpha)\sin^2\theta_\star = \varpi_o^2\alpha\,. \tag{5.57}$$

Therefore, the second assumption is equivalent with the statement that at the Alfvén conical surface, the cylindrical distance ϖ_a of each magnetic flux surface $\alpha = const$ is simply proportional to $\sqrt{\alpha}$, exactly as in the previous meridionally self-similar case.

Instead of using the three functions of α, $(\mathcal{A}\,, \Psi_A, \Omega)$ we found it more convenient to work with the three dimensionless functions of α, $(q_1\,, q_2\,, q_3)$,

$$q_1(\alpha) = \int \frac{\mathcal{A}'^2}{\alpha}d\alpha\,, q_2(\alpha) = \frac{\varpi_o^2}{B_o^2}\int \Omega^2\Psi_A^2 d\alpha\,, q_3(\alpha) = \frac{\mathcal{GM}}{B_o^2\varpi_o}\int \frac{\Psi_A^2}{\alpha^{\frac{3}{2}}}d\alpha\,. \tag{5.58}$$

Table 5.3: Radially Self-similar Models

Case	$q_1(\alpha)$	$q_2(\alpha)$	$q_3(\alpha)$	constants
(1) [a]	$\frac{E_1}{x-2}\alpha^{x-2}$	$\frac{D_1}{x-2}\alpha^{x-2}$	$\frac{C_1}{x-2}\alpha^{x-2}$	$E_1, x-2\neq 0$
(2) [b]	$E_1\ln\alpha$	$D_1\ln\alpha$	$C_1\ln\alpha$	$E_1\neq 0$
(3)	$E_1\alpha^{x_1}+E_2\alpha^{x_2}$	$D_1\alpha^{x_1}+D_2\alpha^{x_2}$	$C_1\alpha^{x_1}+C_2\alpha^{x_2}$	$E_1^2+D_1^2+C_1^2, E_2, x_1, x_2, x_1-x_2\neq 0$
(4)	$E_1\ln\alpha+E_2\alpha^x$	$D_1\ln\alpha+D_2\alpha^x$	$C_1\ln\alpha+C_2\alpha^x$	$E_i^2+D_i^2+C_i^2, x\neq 0, i=1,2$
(5)	$E_1(\ln\alpha)^2+E_2\ln\alpha$	$D_1(\ln\alpha)^2+D_2\ln\alpha$	$C_1(\ln\alpha)^2+C_2\ln\alpha$	$E_1^2+D_1^2+C_1^2\neq 0$
(6)	$E_1\alpha^x\ln\alpha+E_2\alpha^x$	$D_1\alpha^x\ln\alpha+D_2\alpha^x$	$C_1\alpha^x\ln\alpha+C_2\alpha^x$	$E_1^2+D_1^2+C_1^2\neq 0$

[a] [CL94, BP82]
[b] [CL94] for $x=2$

Following the same algorithm as in the previous case, we shall use $(\alpha\,,\theta)$ as the independent variables and transform the derivatives with respect to r and θ to derivatives with respect to α and θ in the $\hat{r}$- and $\hat{\theta}$-components of the momentum equation. Integrating the resulting $\hat{r}$–component of the momentum equation we get

$$P=\frac{B_o^2}{8\pi}\left(h_1\alpha q_1^{'}+h_2\alpha q_2^{'}+h_3q_2+h_4q_3+h_5q_1+h_0\right)\,, \tag{5.59}$$

or

$$P=\frac{B_o^2}{8\pi}\mathbf{Y}\mathbf{P}^{\dagger}$$

with

$$\mathbf{P}=[\,h_0\;h_5\;h_1\;h_3\;h_2\;h_4\;0\,]\,, \tag{5.60}$$

and

$$\mathbf{Y}=[\,Y_1\;Y_2\;Y_3\;Y_4\;Y_5\;Y_6\;Y_7\,]=\left[\,1\;q_1\;\alpha q_1^{'}\;q_2\;\alpha q_2^{'}\;q_3\;\alpha q_3^{'}\,\right]\,, \tag{5.61}$$

and after substituting the pressure in the other component of the momentum equation we obtain

$$\begin{aligned}&Fh_4\alpha q_3^{'}+h_4^{'}q_3+h_3(F-2)\alpha q_2^{'}+h_3^{'}q_2+\\&\frac{\left(h_1\left[1-M^2\right]^2\right)^{'}\alpha q_1^{'}}{(1-M^2)}+h_5^{'}q_1+h_0^{'}=0\,,\end{aligned} \tag{5.62}$$

where a prime in the functions of $q_i(\alpha)$, i=1,2,3 and h_i indicates a derivative with respect to their variables α and $\ln\sin\theta$, respectively, while the functions $h_j\,(\theta)\,, j=1,2,3,4,5$ and F are given in Appendix 5.B.
This expression is again of the form

$$X_7\,(\theta)\,Y_7\,(\alpha)+X_6\,(\theta)\,Y_6\,(\alpha)+\cdots+X_1\,(\theta)\,Y_1\,(\alpha)=0\,,\text{or}\,,\mathbf{Y}\mathbf{X}^{\dagger}=\mathbf{0} \tag{5.63}$$

with $\mathbf{X}$ the (1×7) matrix

$$\mathbf{X} = [\, X_1 \; X_2 \; X_3 \; X_4 \; X_5 \; X_6 \; X_7 \,] =$$

$$\left[h_0^{'} \; h_5^{'} \; \frac{\left(h_1 \left[1-M^2\right]^2\right)^{'}}{(1-M^2)} \; h_3^{'} \; h_3 \left(F-2\right) \; h_4^{'} \; F h_4 \right] . \tag{5.64}$$

As in the previous case of meridionally self-similar solutions, we classify the various possibilities by the sets "xxxxxxx". And, these sets always have "00" at the end, their first digit is "1", they have at most three "0's", while from the 2^7 possibilities we end up again with the cases 1011100, 1101100, 1110100, 1111000, 1111100. Now the vectors $q_1(\alpha)$, $q_2(\alpha)$, $q_3(\alpha)$ belong to a 3D α-space with basis vectors $[e_1(\alpha)\,, e_2(\alpha)\,, e_3(\alpha)]$. This space contains all vectors $q_i(\alpha)$, $i = 1,2,3$ subject to the r-self-similarity constraint manifested by Eq. (5.62), i.e., that for a given such set $q_i(\alpha)$, $i = 1,2,3$, the vectors $1, \alpha q_i^{'}(\alpha)$, $i = 1,2,3$ also belong to the same space. Each of the functions $q_i(\alpha)$, $i = 1,2,3$ which satisfy this constraint are then a linear combination of the basis vectors $e_1(\alpha), e_2(\alpha), e_3(\alpha)$. In the following, we choose $e_1 = 1$, $e_2 = q_1(\alpha)$. All such sets of basis vectors give all possible radially self-similar solutions. Therefore, collecting all possibilities, we end up with the 6 classes of solutions shown in Table 5.3.

In all of the cases of Table 5.3, from Eqs. (5.58) we find the form of the functions of α,

$$A = \frac{B_o \varpi_o^2}{2} \int_0^\alpha \sqrt{\alpha q_1^{'}} d\alpha \,, \qquad \Psi_A^2 = \frac{B_o^2 \varpi_o}{\mathcal{GM}} \alpha^{\frac{3}{2}} q_3^{'} \,,$$

$$\Omega^2 = \frac{\mathcal{GM}}{\varpi_o^3} \frac{q_2^{'}}{q_3^{'}} \alpha^{-\frac{3}{2}} \,, \qquad L^2 = \mathcal{GM} \varpi_o \frac{q_2^{'}}{q_3^{'}} \alpha^{\frac{1}{2}} \,. \tag{5.65}$$

Finally, by substituting $q_1\,, q_2\,, q_3$ in Eqs. (5.59), (5.62), we find the ordinary differential equations which the functions $G(\theta)\,, M(\theta)\,, h_0(\theta)$ obey.
In α-space, for each of the cases of Table 5.3 there exists a (3×7) matrix $\mathbf{K}$ such that

$$\mathbf{Y} = [\, e_1 \; e_2 \; e_3 \,] \;\; \mathbf{K} \,, \tag{5.66}$$

and from Eq. (5.63)

$$[\, e_1 \; e_2 \; e_3 \,] \; \mathbf{K}\mathbf{X}^\dagger = \mathbf{0} \,.$$

If the basis vectors e_i are linearly independent, then,

$$\mathbf{K}\mathbf{X}^\dagger = \mathbf{0} \,.$$

These three equations are the ordinary differential equations for the functions of θ in each model of Table 5.3, while for the pressure,

$$P = \frac{B_o^2}{8\pi} [\, e_1 \; e_2 \; e_3 \,] \, \mathbf{K}\mathbf{P}^\dagger = \frac{B_*^2}{8\pi} \left(P_0 + P_1 q_1 + P_2 e_3\right) \,,$$

where

$$\mathbf{K}\mathbf{P}^{\dagger} = [P_0 \; P_1 \; P_2]^{\dagger} \; .$$

As with the previous meridionally self-similar solutions, the first three classes are of particular interest. The first corresponds to the following form of the free integrals:

$$A = \frac{B_o \varpi_o^2 \sqrt{E_1}}{x} \alpha^{\frac{x}{2}} \; , \; \Psi_A^2 = \frac{C_1 B_o^2 \varpi_o}{\mathcal{G}\mathcal{M}} \alpha^{(x-3/2)} \; , \; \Omega^2 = \frac{D_1 \mathcal{G}\mathcal{M}}{\varpi_o^3 C_1} \alpha^{-\frac{3}{2}} \; . \qquad (5.67)$$

This is a degenerate case, i.e., $e_3 = 0$ and we have only two conditions between the functions of θ. It follows that we are free to impose a third relation between the unknown functions $[G(\theta) \, , M(\theta) \, , h_0(\theta)]$. One possibility is that such a third imposed relation is of the polytropic type, $P \propto \rho^{\gamma}$ (in this case $h_0 = 0$). In such a polytropic case which has been analyzed in detail in Contopoulos & Lovelace [CL94], the magnetic flux is of the form $A = f_f(\theta) R^x$ with $f_f(\theta) \propto [\sin\theta / G(\theta)]^x$ (for notation see also [TSS+96]). The magnetic field at the equatorial plane $\theta = 90^o$ is $B \propto R^{x-2}$, the density $\rho \propto R^{2x-3}$, while the sound, Alfvén and rotational speeds scale as their Keplerian counterparts, i.e., as $R^{-1/2}$. Note that if $[D_1 G \, (\pi/2)/C_1] \left[(G^2 - M^2)/G \left(1 - M^2\right)\right]^2_{\theta=\frac{\pi}{2}} = 1$, the rotational velocity at the equatorial plane is exactly Keplerian. The classical and simplest subcase analyzed in [BP82] corresponds to the subclass with $x = 3/4$, wherein $B \propto R^{-5/4}$. The two relations among the functions of θ are the two resulting first order differential equations for the Alfvén number $M(\theta)$ and dimensionless radius $G(\theta)$ ($m(\chi) = M^2(\theta)$ and $\xi(\chi) = G(\theta)/G(\frac{\pi}{2})$ in the notation of [BP82]).

The second case is also degenerate since $e_3 = 0$ with again only two conditions between the functions of θ. As before, we are free to impose a third relation between the unknown functions $[G(\theta) \, , M(\theta) \, , h_0(\theta)]$, for example, a polytropic relationship. Then one can prove that this case is a subcase of the first one (if it is polytropic), for $x = 2$.

All other cases shown in Table 5.3 are nondegenerate. The third class, is characterized *first* by a set of parameters describing the particular model and the dependence of the free integrals on the magnetic flux function $A \, (\alpha)$, $(x_1 \, , x_2 \, , E_1 \, , E_2 \, , C_1 \, , C_2 \, , D_1 \, , D_2)$, *second* by the Alfvén angle $\theta_\star$, and *third*, by the set of the critical point parameters $p_\star = \left(dM^2/d\theta\right)_\star$ and $\varphi_\star$ which denote the slope of the Alfvén number and the expansion angle, respectively, at the Alfvén angle $\theta_\star$, together with the pressure component $P_{1\star}$ through $h_{5\star}$. This triplet of 'dynamical' parameters fixes the physical solution and they are related through the Alfvén regularity condition which is now obtained from Eq. (5.98) of Appendix 5.B at the Alfvén angle $\theta_\star$ where $M = G = 1$ and $h_5 = h_{5\star}$, i.e., .

$$h_{5\star} = -\sin^2 \theta_\star \tan(\theta_\star + \varphi_\star) p_\star \; . \qquad (5.68)$$

As with the previous case of meridional self-similarity, this condition relates the slope of the square of the Alfvén number $p_\star = \left(dM^2/d\theta\right)_\star$ and the expansion angle $\varphi_\star$ with the pressure component $P_{1\star}$ through $h_{5\star}$. Finally, the requirement

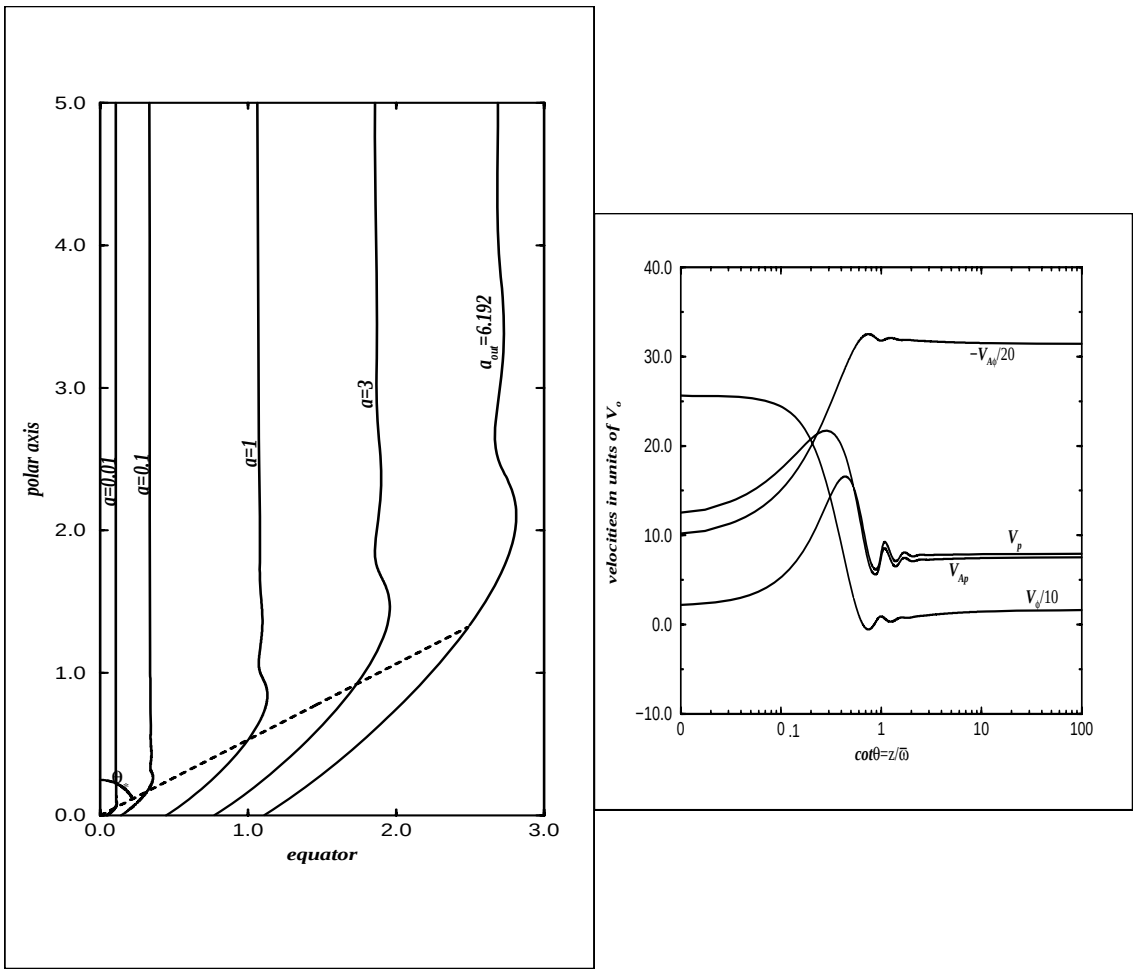

Figure 5.5: Left panel: Field and streamlines for the cylindrical r-self similar model of case (3) from Table 5.3 and the following set of parameters: $x_1 = -0.6$, $x_2 = -0.5$, $E_1 = -0.03$, $E_2 = 0.03$, $C_1 = -1.5$, $C_2 = -0.6$, $D_1 = -25$, $D_2 = -10$, $\theta_\star = 62^o$, $\varphi_\star = 55^o$, $p_\star = -3$. At the disk level, $V_\phi \propto R^{-1/2}$ while on the poloidal field/streamline $\alpha_{out} = 6.191736$, $B_p = V_p = 0$. Right panel: The characteristic velocities in units of the z-component of the flow speed at the point $(\alpha = 1, \theta = \pi/2)$, V_o.

that the solution crosses the two slow and fast X-type critical points (modified by the radial self-similarity assumption, [TSS+96] determines all these three 'dynamical' parameters $[\varphi_\star\,, p_\star\,, P_{1\star}]$.

It is interesting to note that contrary to classes (1)-(2) in Table 5.3, this model (3) may be characterized by a scale, for example the radial distance on the plane of the disk where the magnitudes of the poloidal speed and magnetic field or the toroidal speed and magnetic field become zero. Hence, it occurred to us that this is an interesting generalization of the [BP82] model and therefore worthy of further investigation.

Fig. 5.5 are a typical illustration of model (3) for describing collimated jet-type outflows with an oscillatory behaviour. In the left panel the poloidal field and streamlines reach a cylindrical shape after undergoing oscillations in their radius. As we move downstream, the amplitude of these oscillations decays while their wavelength increases. In fact, the exact behaviour of the oscillations is analytically described in [VT97] (see also Chapter 4) where it is shown that they can be regarded as perturbations on an asymptotically cylindrical shape which can be expressed in terms of the Legendre functions $P_\nu^\mu(\cos\theta)$ and $Q_\nu^\mu(\cos\theta)$. According to this analysis, when $\mu^2 < 0$, the asymptotically cylindrical shape is finally obtained through those oscillations. Then the perturbation (for $\theta \to 0$) is proportional to $\theta^{\pm\mu-\nu}$, or since $\mu^2 < 0$, proportional to $\left(\frac{\varpi}{z}\right)^{-\nu} \cos\left(\mid \mu \mid \ln\frac{\varpi}{z} + D_o\right)$. In the example shown in Fig. 5.5 the amplitude of the oscillations is rather weak. Note however, that cases also exist with an extremely strong oscillation amplitude and such examples will be analyzed in another Chapter. On the other hand, when $\mu^2 \geq 0$ the asymptotically cylindrical shape is reached without such oscillations. Exactly this last possibility is shown in the following case of Figs. 5.6.

To further illustrate the various possibilities for the asymptotic behaviour of outflows starting from a Keplerian disk, we examine briefly the group of three models in Figs. 5.6,5.8,5.8 where depending on the values of the model constants, we get one with cylindrical, parabolical, or conical terminal geometry:

(1) In Fig. 5.6 a *cylindrically* collimated outflow $\lim_{\theta\to 0}(M^2\,, G^2) = \; constants$, is obtained for a set of the model parameters: $(x_i,\, E_i,\, C_i,\, D_i)$, i=1,2. The Alfvén conical surface is taken at $\theta_\star = 60^o$ where the slope of the square of the Alfvén number is fixed as $p_\star = -1.1$ while the expansion angle $\varphi_\star \approx 75^o$ (the angle of the poloidal streamline with the cylindrical radius). The characteristic scale of the model is taken to indicate approximately the radius of the jet, or more precisely, the distance along the disk where for $\alpha_{out} = 2$ we have $B_p = V_p = 0$. In the right panel of Fig. 5.6 the velocities on the reference line $\alpha = 1$ are plotted in units of V_o, the z-component of the flow speed at the point $(\alpha = 1, \theta = \pi/2)$.

(2) In Fig. 5.7 an r-self similar model belonging to case (3) in Table 5.3 with *parabolic* asymptotical geometry $\lim_{\theta\to 0}(M^2\,, G^2) = \infty$, is examined for another set of parameters $(x_i,\, E_i,\, C_i,\, D_i)$, i=1,2. The Alfvén conical surface is taken now at $\theta_\star = 45^o$ where the slope of the square of the Alfvén number is chosen as $p_\star = -1.7$ and the expansion angle $\varphi_\star \approx 75^o$.

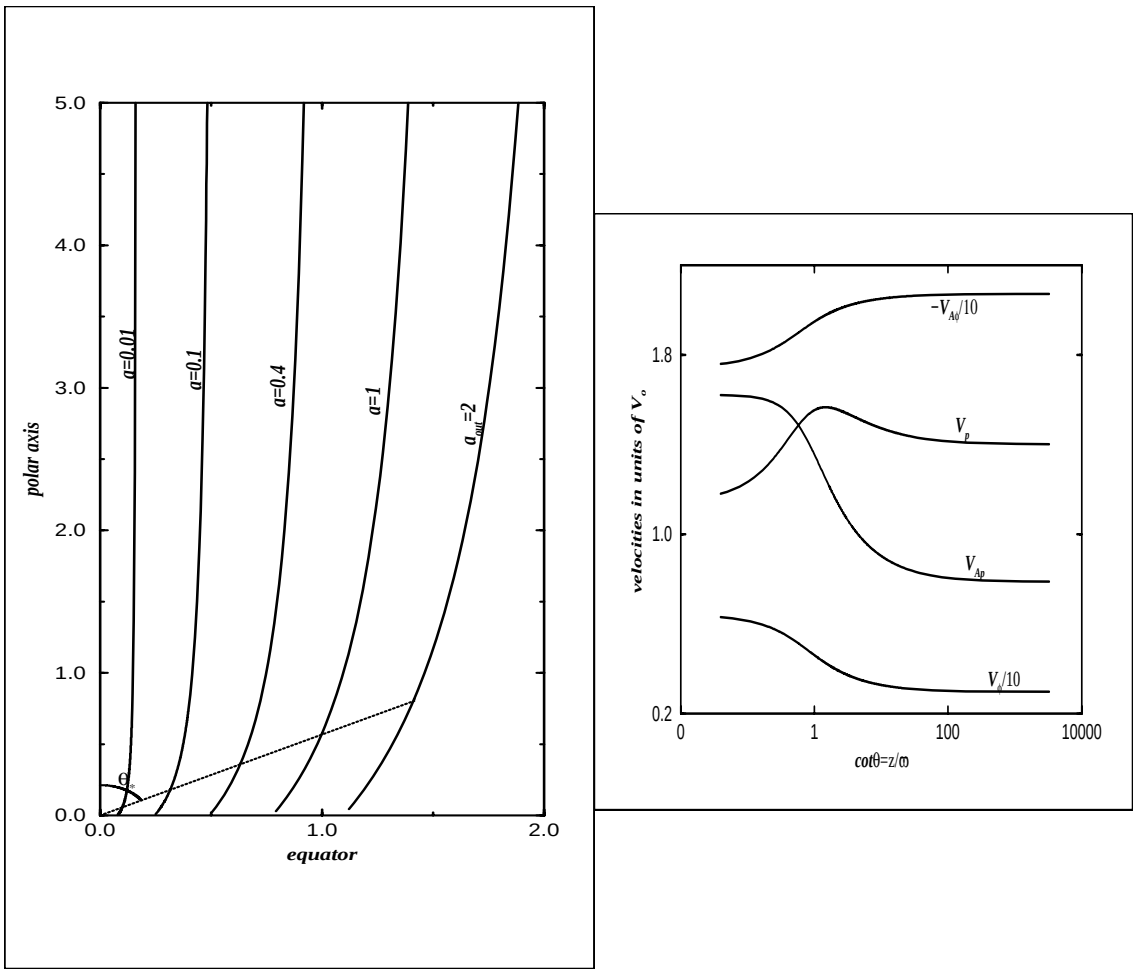

Figure 5.6: Left panel: Field and streamlines for the cylindrical r-self similar model of case (3) from Table 5.3 and the following set of parameters: $x_1 = -0.9$, $x_2 = -0.6$, $E_1 = -2.1421466$, $E_2 = 2.60994552$, $C_1 = -3.2132198$, $C_2 = D_2 = 0$, $D_1 = -160.66099$, $\theta_\star = 60^o$, $\varphi_\star = 74.704656^o$, $p_\star = -1.1$. At the disk level, $V_\phi \propto R^{-1/2}$ while on the poloidal field/streamline $\alpha_{out} = 2$, $B_p = V_p = 0$. Right panel: The characteristic velocities in units of the z-component of the flow speed at the point $(\alpha = 1, \theta = \pi/2)$, V_o.

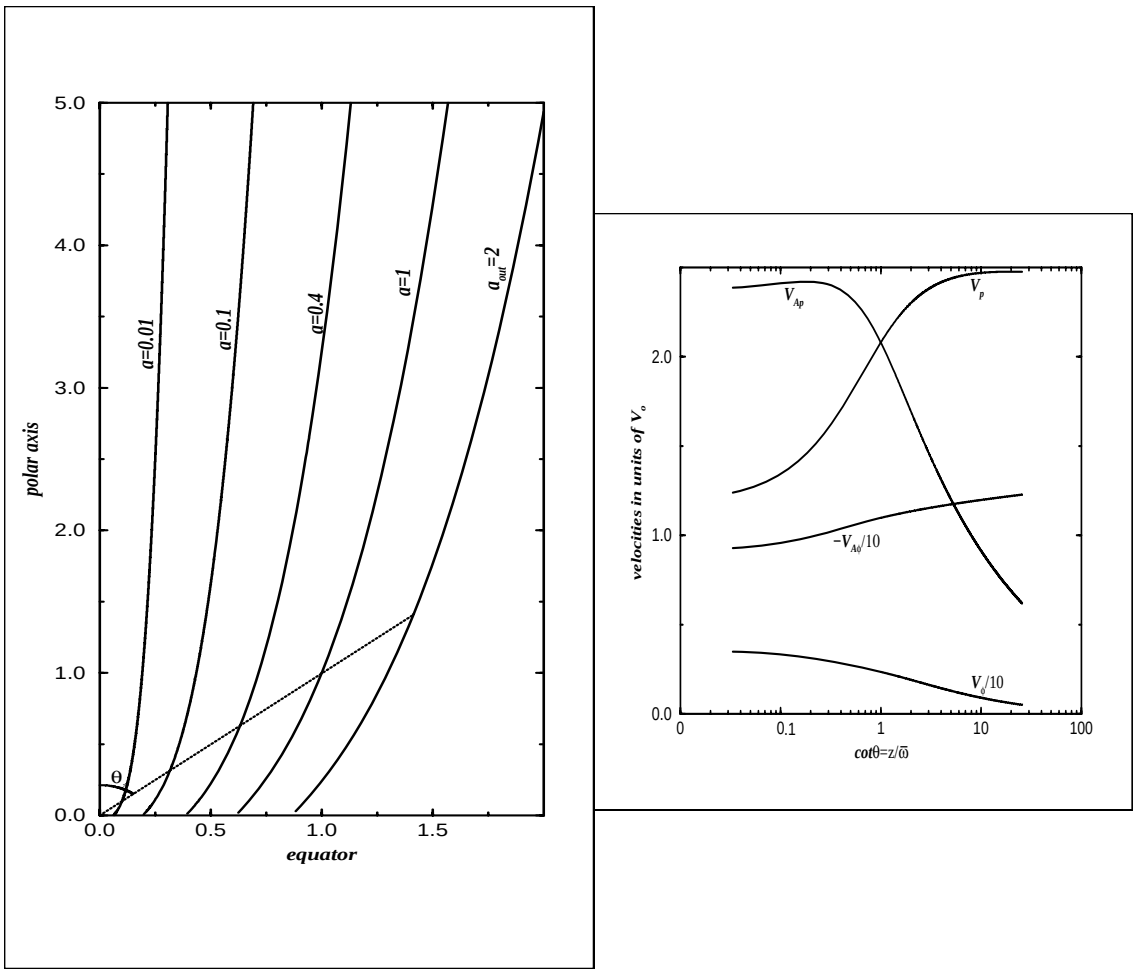

Figure 5.7: Left panel: Poloidal field and streamlines for the parabolic r-self similar model of case (3), Table 5.3 and the following set of parameters: $x_1 = -0.9$, $x_2 = -0.6$, $E_1 = -0.8252542$, $E_2 = 1.00547$, $C_1 = -1.23788$, $C_2 = D_2 = 0$, $D_1 = -12.378813$, $\theta_\star = 45^o$, $\varphi_\star = 75.465545^o$, $p_\star = -1.7$. In this case $V_\phi \propto R^{-1/2}$ on the equatorial plane while on the streamline $\alpha_{out} = 2$, $B_p = V_p = 0$. Right panel: The characteristic velocities in units of the z-component of the flow speed at the point $(\alpha = 1, \theta = \pi/2)$, V_o.

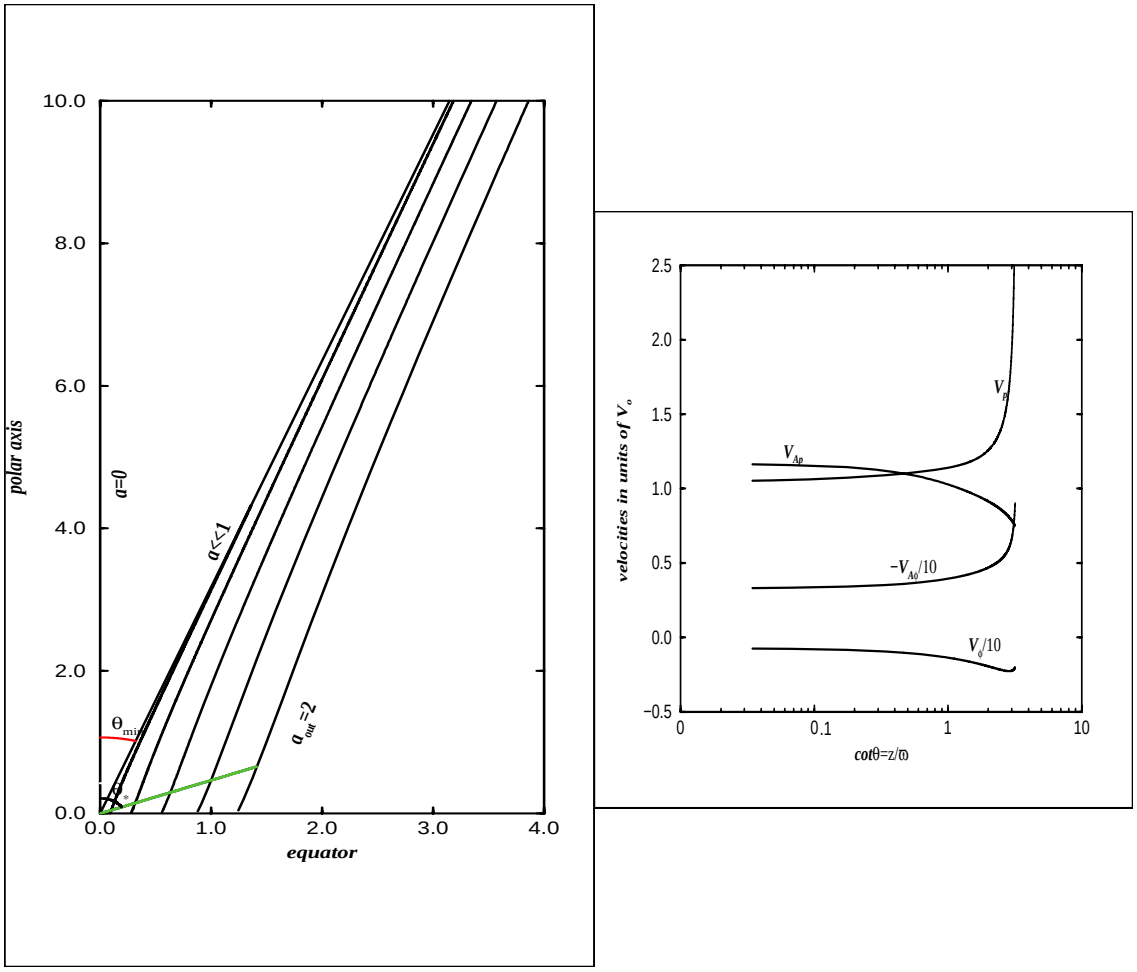

Figure 5.8: Left panel: Field and streamlines for the conical r-self similar model of case (3), Table 5.3 and the following set of parameters: $x_1 = -0.1, x_2 = 0.01$ and $E_1 = -78.601635$, $E_2 = -728.31337$, $C_1 = -4.3231$, $C_2 = D_2 = 0$, $D_1 = -43.231$, $\theta_\star = 65^o$, $\varphi_\star = 75.784234^o$, $p_\star = -0.5$. In this case $V_\phi \propto R^{-1/2}$ on the equatorial plane while on the poloidal field/streamline $\alpha_{out} = 2$, $B_p = V_p = 0$. For large distances from the disk all lines with $\alpha > 0$ go asymptotically to the line $\theta = \theta_{min}$. Right panel: The characteristic velocities in units of the z-component of the flow speed at the point $(\alpha = 1, \theta = \pi/2)\,, V_o$.

(3) Finally, in Fig. 5.8 the r-self similar model of case (3) in Table 5.3 gives a *conical* asymptotical geometry for a third set of the parameters (x_i, E_i, C_i, D_i), i=1,2 and $\theta_\star = 65^o$, $\varphi_\star = 75^o$, $p_\star = -0.5$. Note that now the solution exists only for $\theta > \theta_{min}$ where $\theta_{min} \approx 17.5^o$. When this value of θ is approached, $\lim_{\theta \to \theta_{min}} (M^2, G^2) = \infty$.

In all these four possibilities and along a given field/streamline, the outflow starts from the equator where $V_\phi \propto R^{-1/2}$ with a low subAlfvénic poloidal speed. This poloidal speed V_p crosses the Alfvén conical surface at $\theta_\star$ in all cases. In the cylindrical case of Fig. 5.6, V_p increases rapidly to a uniform value when collimation is achieved. The azimuthal speed V_ϕ on the other hand, drops with height in all cases, as rotational energy is transformed to poloidal kinetic energy. Finally, the azimuthal Alfvén speed is the strongest in the cylindrical case where the toroidal magnetic field is responsible for the ensuing final collimation.

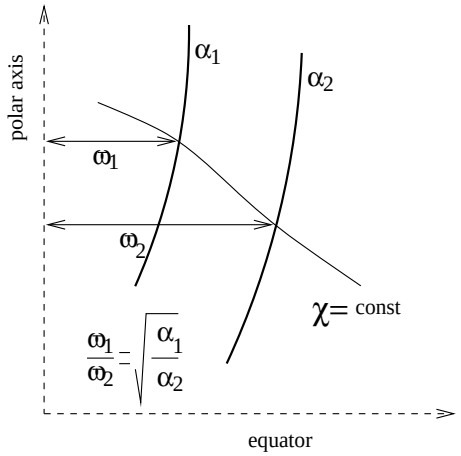

Figure 5.9: An illustration of the construction of the streamlines $\alpha = const.$ on the poloidal plane in general selfsimilarity.

5.4 Construction of general self similar models

5.4.1 General equations

In this section we 'll examine general self similar solutions of the MHD equations. In general, M^2 is a function of some variable χ (with χ a function of r and θ, which in some cases is not known *a-priori*).

Thus, $M^2 = M^2(\chi) \Leftrightarrow \dfrac{\rho_\alpha(\alpha)}{\rho(\alpha,\chi)} = M^2(\chi)$, where ρ_α is the density at the Alfvén surface.

First let's define the function α as the ratio between the free integrals L, Ω: $\alpha = \dfrac{L}{\varpi_o^2 \Omega}$ where ϖ_o is some reference scale (for adimensionalization). We are interested for transAlfvénic flows, where $L = \Omega \varpi_\alpha^2$, and ϖ_α is the cylindrical radius at the Alfvén surface. Thus $\alpha = \dfrac{\varpi_\alpha^2}{\varpi_o^2}$. Without loss of generality, we define the adimensional cylindrical distance from the polar axis

$$G(\alpha,\chi) = \frac{\varpi(\alpha,\chi)}{\varpi_\alpha(\alpha)} = \frac{\varpi(\alpha,\chi)}{\varpi_o\sqrt{\alpha}}\,.$$

At the Alfvén point $M(\chi = \chi_\star) = 1$ it's obvious that $G(\alpha, \chi = \chi_\star) = 1$, for each line α =constant. So $\alpha = \dfrac{\varpi^2}{\varpi_o^2 G^2}$. As in the previous self similar solutions, our first assumption is that G is a function of χ only:

$$G = G(\chi)\,, \text{ or } \boxed{G = G(M)}\,. \tag{5.69}$$

This is then a general "definition" of self similarity: G and M are functions of the same variable, or in other words M is a function of G and vice-versa. Self

similarity means that if we know one fieldline then we can find all the others as follows: Moving along a single line M =constant (or χ =constant), $\sqrt{\frac{\alpha_1}{\alpha_2}} = \frac{\varpi_1}{\varpi_2}$ (because at this curve G =constant).
The second crucial assumption is

$$\boxed{r = \varpi_o f(\chi)\, g(\alpha)}\,. \tag{5.70}$$

Note that this assumption is made because in the momentum equation we have the gravitational force which is a function of r.
So we may transform from the familiar spherical coordinates $(r\,,\theta)$ to the new coordinates $(\chi\,,\alpha)$ via the relations

$$\sin\theta = \frac{G(\chi)\sqrt{\alpha}}{f(\chi)\, g(\alpha)} \text{ and } r = \varpi_o f(\chi)\, g(\alpha)\ . \tag{5.71}$$

We can use these two relations in order to move from the $(r\,,\theta)$ to the $(\chi\,,\alpha)$ coordinates on the poloidal plane.
Note that, the assumption Eq. (5.70), for $g = 1$ takes the form $r = \varpi_o f(\chi)$, or $\chi = \chi(r)$. Thus Eqs. (5.69)-(5.70) are equivalent to $M = M(r)\,, G = G(r)$.
On the other hand, for $g = \sqrt{\alpha}$, using $\varpi = \varpi_o G\sqrt{\alpha}$, it takes the form $\sin\theta = G(\chi)/f(\chi)$, or $\chi = \chi(\theta)$. Thus Eqs. (5.69)-(5.70) are equivalent to $M = M(\chi)\,, G = G(\chi)$.
Introduce the functions

$$Y(\alpha) = \frac{d\ln\mid g\mid}{d\ln\alpha}\,, Z(\chi) = -\frac{d\ln\mid f\mid}{d\ln G^2} = \frac{1}{F-2}\frac{d\ln\mid f\mid}{d\ln\mid\chi\mid}\,,$$

if the expansion factor is defined by $F = 2 - \dfrac{d\ln G^2}{d\ln\mid\chi\mid}$.
Then,

$$\frac{\partial\ln G^2}{\partial\ln r} = \frac{2Y-1}{Y+Z}\,,\quad \frac{\partial\ln G^2}{\partial\ln\mid\sin\theta\mid} = \frac{2Y}{Y+Z} \text{ and}$$
$$\frac{\partial\ln\alpha}{\partial\ln r} = \frac{2Z+1}{Y+Z}\,,\quad \frac{\partial\ln\alpha}{\partial\ln\mid\sin\theta\mid} = \frac{2Z}{Y+Z}$$

.
At this point we note the following two inportand facts:

- If we were to choose the coordinates χ and α to be orthogonal, then we would have $\vec{\nabla}\alpha\cdot\vec{\nabla}G = 0$, or after solving the resulting differential equation it follows that: $G = r/\varpi_o\,, g$ =constant, f/G =constant and $\alpha = \sin^2\theta$. Thus the only case is the radial θ- self similar model.

- We can take the previous r- or θ- self similar solutions as special cases. First, by choosing $Y = \dfrac{1}{2}$, in which case $\chi = \chi(\theta)$; if in addition $\chi \propto \sin\theta\,, Z = -\dfrac{1}{2} - \dfrac{1}{F-2}$. Second, by choosing $Y = 0$, in which case $\chi = \chi(r)$; if in addition $\chi \propto r\,, Z = \dfrac{1}{F-2}$.

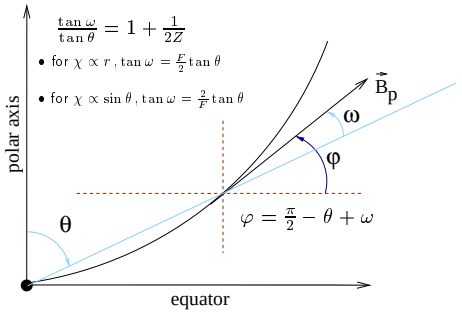

Figure 5.10: Expansion factor and angle.

In the general self similar case we have

$$A = \frac{B_o \varpi_o^2}{2} \mathcal{A}(\alpha) \ , \quad \alpha = \frac{R^2}{G^2(\theta)} \sin^2\theta \ , \quad R = \frac{r}{\varpi_o} \ ,$$

$$\Omega^2 \Psi_A^2 = \frac{B_o^2}{\varpi_o^2} g_2^{'}(\alpha) \ , \quad L = \varpi_o^2 \alpha \Omega \ ,$$

$$B_r = B_o \frac{Z\cos\theta}{G^2(Y+Z)} \frac{d\mathcal{A}}{d\alpha} \ , B_\theta = -B_o \frac{\left(Z+\frac{1}{2}\right)\sin\theta}{G^2(Y+Z)} \frac{d\mathcal{A}}{d\alpha} \ , B_\phi = -B_o \sqrt{\alpha g_2^{'}} \frac{1}{G} \frac{1-G^2}{1-M^2} \ ,$$

$$V_r = \frac{M^2}{\Psi_A^2} B_r \ , \quad V_\theta = \frac{M^2}{\Psi_A^2} B_\theta \ , \quad V_\phi = \frac{B_o \sqrt{\alpha g_2^{'}}}{\Psi_A} \frac{1}{G} \frac{G^2 - M^2}{1-M^2} \ .$$

If we substitute χ and α instead of r and θ in the momentum equation we get for the component in the direction of $\vec{\nabla} A$: $\mathcal{M}_\alpha = 0$ or

$$\begin{aligned}
&\frac{\partial}{\partial\alpha}\left(\frac{8\pi}{B_o^2}P\right) + \frac{1+4Z}{2G^2 f^2 (Z+Y)^2} \frac{\alpha \mathcal{A}^{'} \mathcal{A}^{''}}{g^2} + \frac{2Z^2}{G^4 (Z+Y)^2} \mathcal{A}^{'} \mathcal{A}^{''} - \frac{2}{G^4} \frac{Z^2}{(Z+Y)^3} Y^{'} \mathcal{A}^{'2} + \\
&+ \frac{2Z}{G^4} \frac{M^2 - 1 - \frac{dM^2}{d\ln G^2}}{(Z+Y)^2} \frac{Y \mathcal{A}^{'2}}{\alpha} + 2\frac{1-M^2}{G^4} \frac{\frac{dZ}{d\ln G^2}}{(Z+Y)^3} \frac{Y^2 \mathcal{A}^{'2}}{\alpha} - \frac{1}{2f^2 G^2} \frac{1+4Z}{(Z+Y)^3} \frac{\alpha \mathcal{A}^{'2}}{g^2} Y^{'} + \\
&+ \frac{q_3^{'}}{M^2 f} + \frac{1}{G^2}\left(\frac{1-G^2}{1-M^2}\right)^2 \alpha g_2^{''} + \frac{\left(2M^2-1\right)G^4 - M^4 + 2M^2\left(1-G^2\right)}{G^2 M^2 \left(1-M^2\right)^2} g_2^{'} + \\
&+ \frac{\left(1-M^2\right)\frac{dZ}{d\ln G^2}}{2G^2 f^2} \frac{1+4Z}{(Z+Y)^3} \frac{\mathcal{A}^{'2}}{g^2} - \frac{\frac{dM^2}{d\ln G^2} + 1 + 4ZM^2}{2G^2 f^2} \frac{1}{(Z+Y)^2} \frac{Y \mathcal{A}^{'2}}{g^2} + \\
&+ \frac{1 + 3Z - \frac{M^2}{2} - ZM^2 + (2Z+1)\frac{dM^2}{d\ln G^2} - 4\left(1-M^2\right)\frac{dZ}{d\ln G^2}}{2G^2 f^2 (Z+Y)^2} \frac{\mathcal{A}^{'2}}{g^2} = 0
\end{aligned} \tag{5.72}$$

and for the component of the momentum equation in the direction of $\vec{\nabla}\chi$: $\mathcal{M}_\chi = 0$, or

$$\frac{M^2}{\Psi_A^2}\frac{\partial}{\partial\chi}\left(\frac{8\pi}{B_o^2}P\right) - \frac{\partial}{\partial\chi}\left(\frac{2\mathcal{G}\mathcal{M}}{B_o^2\varpi_o fg}\right) + \\ + \frac{\partial}{\partial\chi}\left(\frac{\dfrac{M^4Z^2}{G^4} + \dfrac{\alpha}{g^2}\dfrac{M^4(1+4Z)}{4f^2G^2}}{(Z+Y)^2}\frac{\mathcal{A}'^2}{\Psi_A^2} + \left[\frac{1-G^2}{1-M^2} + \frac{1}{2G^2}\left(\frac{M^2-G^2}{1-M^2}\right)^2\right]\frac{2\alpha g_2'}{\Psi_A^2}\right) = 0\,, \tag{5.73}$$

where $Y' \equiv \dfrac{dY}{d\alpha}\,, \mathcal{A}' \equiv \dfrac{d\mathcal{A}}{d\alpha}, \mathcal{A}'' \equiv \dfrac{d^2\mathcal{A}}{d\alpha^2}$ and $q_3' \equiv \dfrac{dq_3}{d\alpha} = \dfrac{2\mathcal{G}\mathcal{M}}{B_o^2\varpi_o}\dfrac{\Psi_A^2 Y}{g\alpha}$. Note that this last equation can be written in the form

$$\frac{1}{\rho}\frac{\partial P}{\partial\chi} + \frac{\partial}{\partial\chi}\left(\frac{V^2}{2} + \mathcal{V} - \frac{\varpi B_\phi \Omega}{\Psi_A}\right) = 0\,,$$

which gives the familiar Bernoulli integral if we have a polytropic relation $P = Q(A)\rho^\gamma$, or in general if $P = \mathcal{P}_1(A)\mathcal{P}_2(\rho)$.
It is worth to mention that if $P = \mathcal{P}_1(A)\mathcal{P}_2(\chi)$ then we can again integrate this equation as in the θ- self similar model [ST94] where $\mathcal{P}_1(A) = 1 + \delta\alpha$ and $\mathcal{P}_2(\chi) = \Pi(R)$.

5.4.2 Solutions with constant Y

In order to find solutions of Eqs. (5.72)-(5.73) the simplest way to proceed is to assume that

$$Y = (\alpha) \text{ constant, or equivalently } g = (\alpha)\,\alpha^Y\,.$$

If this is the case, Eq. (5.72) is a sum of products between functions of α and functions of χ, so we may proceed as in the previous self similar cases.
For that goal we introduce the functions of $\alpha\,, q_1\,, q_2\,, q_3\,, g_1\,, g_2$ and $g_{3,o}$ such that

$$q_1' = 2Y\frac{\mathcal{A}'^2}{\alpha}\,,\quad q_2' = \frac{\varpi_o^2}{B_o^2}\Omega^2\Psi_A^2\,,\quad q_3' = \frac{2Y\mathcal{G}\mathcal{M}}{B_o^2\varpi_o}\frac{\Psi_A^2}{\alpha^{Y+1}}\,,$$
$$g_1' \equiv \frac{\alpha^{1-2Y}}{2Y}q_1' = \frac{\mathcal{A}'^2}{\alpha^{2Y}}\,,\quad g_2 = q_2\,, g_{3,o} \equiv \frac{\alpha}{Y}q_3' = \frac{2\mathcal{G}\mathcal{M}\Psi_A^2}{\varpi_o B_o^2\alpha^Y}\,, \tag{5.74}$$

where primes indicate derivative with respect to α.
Then, Eq. (5.72) can be integrated at once with respect to α to yield

$$P = \frac{B_o^2}{8\pi}\left(\mathcal{S}_0 + \mathcal{S}_1 g_1 + \mathcal{S}_2\alpha g_1' + \mathcal{S}_3\alpha^{2Y}g_1' + \mathcal{S}_4 q_1 + \mathcal{S}_5 q_2 + \mathcal{S}_6\alpha q_2' + \mathcal{S}_7 q_3\right)\,, \tag{5.75}$$

where $\mathcal{S}_0 = \mathcal{S}_0(\chi)$ is the constant of the integration, while the functions $\mathcal{S}_i(\chi)$, $i = 1, \ldots, 7$ are given in Appendix 5.C.
If we substitute this form of the pressure in Eq. (5.73) we find

$$\mathcal{S}_0^{'} + \mathcal{S}_1^{'} g_1 + \mathcal{Q}_1 \alpha g_1^{'} + \mathcal{Q}_2 \alpha^{2Y} g_1^{'} + \mathcal{S}_5^{'} g_2 + \mathcal{Q}_3 \alpha g_2^{'} + \frac{(F-2)\,Z}{f \chi M^2} g_{3,o} + \mathcal{S}_7^{'} q_3 + \mathcal{S}_4^{'} q_1 = 0 \,, \tag{5.76}$$

where the functions $\mathcal{Q}_i(\chi)$, $i = 1, 2, 3$ are given in Appendix 5.C. Primes in the functions of χ indicate derivatives with respect to χ.
This case where $Y =$constant, includes the cases of r- and θ- self similarities as special cases:

- For $Y = \frac{1}{2}$ we have $\chi = \chi(\theta)$. If we choose $\chi \propto \sin\theta$, say, $\chi = \dfrac{\sin\theta}{\sin\theta_\star}$, then Eqs. (5.74) give Eqs. (5.58), while Eq. (5.75) and Eq. (5.76) are equivalent to Eq. (5.59) and Eq. (5.62) respectively.
- For $Y = 0$ we have $\chi = \chi(r)$. If we choose $\chi \propto r$, say, $\chi = \dfrac{r}{\varpi_o}$ with $\varpi_o \equiv r_\star$, then Eq. (5.74) gives Eqs. (5.10), while Eq. (5.75) and Eq. (5.76) are equivalent with Eq. (5.19) and Eq. (5.22) respectively.

Now we may proceed looking for solutions with $Y \neq 0\,, \frac{1}{2}$.
Eq. (5.76) can be written in the form

$$\sum_{i=1}^{9} X_i(\chi)\, Y_i(\alpha) = 0 \text{ or } \mathbf{Y}\mathbf{X}^{\dagger} = \mathbf{0}\,,$$

with $\mathbf{X}\,, \mathbf{Y}$ the (1×9) matrices

$$\begin{aligned} \mathbf{Y} &= \left[\, 1 \;\; g_1 \;\; \alpha g_1^{'} \;\; \alpha^{2Y} g_1^{'} \;\; q_1 \;\; g_2 \;\; \alpha g_2^{'} \;\; q_3 \;\; \alpha q_3^{'} \,\right] \\ \mathbf{X} &= \left[\, \mathcal{S}_0^{'} \;\; \mathcal{S}_1^{'} \;\; \mathcal{Q}_1 \;\; \mathcal{Q}_2 \;\; \mathcal{S}_4^{'} \;\; \mathcal{S}_5^{'} \;\; \mathcal{Q}_3 \;\; \mathcal{S}_7^{'} \;\; \frac{(F-2)\,Z}{f\chi M^2 Y} \,\right] . \end{aligned} \tag{5.77}$$

As in the previous self similar cases (previous sections of this Chapter) the solutions correspond to sets "$\underbrace{xx\cdots xxx}_{9\,digits}$" where $x = 0, 1$.
We have four unknown functions of χ: $\mathcal{S}_0\,, M^2\,, f\,, Z$ and three unknown functions of α: $g_1\,, g_2\,, q_3$ (we remind that the functions $g_3\,, q_1\,, q_2$ depend on $g_1\,, g_2\,, q_3$; see Eq. (5.74)). So following the method of the previous sections (choosing numbers with at most four "0's", which corresponds to at most four relations between functions of χ and examining the overdetermination of the system for the functions of α), from the 2^9 cases we end up with only seven:
111110100,111010100,110110100,101110100,011110100,111101000 and 111110000.
Only the first set corresponds to degenerate cases, because in this set we have only three relations between the four functions of χ.
One can solve in each set the system for the functions $g_1\,, g_2\,, q_3$ and $M^2\,, G^2\,, f\,, \mathcal{S}_0$ in order to construct new models.

Examination of the degenerate set 111110100

If we solve the system for g_1 , g_2 , q_3 in the frame of this set we end up with three cases:

1. $g_1 = E_1\alpha^{\beta}$, $g_2 = D_1\alpha^{\beta} + D_2\alpha^{2Y-1+\beta}$, $q_3 = C_1\alpha^{\beta} + C_2\alpha^{2Y-1+\beta}$, where $\beta \neq 0$, $1-2Y$. In this case we have for the functions of χ
   $\mathcal{S}_0^{'} = 0$
   $E_1\mathcal{S}_1^{'} + E_1\beta\mathcal{Q}_1 + D_1\mathcal{S}_5^{'} + D_1\beta\mathcal{Q}_3 + C_1\beta\dfrac{(F-2)Z}{f\chi M^2 Y} + C_1\mathcal{S}_7^{'} = 0$
   $E_1\beta\mathcal{Q}_2 + D_2\mathcal{S}_5^{'} + D_2(2Y-1+\beta)\mathcal{Q}_3 + C_2(2Y-1+\beta)\dfrac{(F-2)Z}{f\chi M^2 Y} + C_2\mathcal{S}_7^{'} + \dfrac{2YE_1\beta}{2Y-1+\beta}\mathcal{S}_4^{'} = 0$
   We may close the system by choosing a form for the pressure $P = \dfrac{B_o^2}{8\pi}Q(\alpha)\mathcal{S}(\chi)$. Under this assumption we have one more unknown (the function $\mathcal{S}(\chi)$) and the following relations
   $\mathcal{S}_0 = 0$
   $Q = \lambda_1\alpha^{\beta} + \lambda_2\alpha^{2Y-1+\beta}$
   $E_1\mathcal{S}_1 + E_1\beta\mathcal{S}_2 + D_1\mathcal{S}_5 + D_1\beta\mathcal{S}_6 + C_1\mathcal{S}_7 = \lambda_1\mathcal{S}$
   $E_1\beta\mathcal{S}_3 + \dfrac{2YE_1\beta}{2Y-1+\beta}\mathcal{S}_4 + D_2\mathcal{S}_5 + D_2(2Y-1+\beta)\mathcal{S}_6 + C_2\mathcal{S}_7 = \lambda_2\mathcal{S}$

2. $g_1 = E_1\alpha^{1-2Y}$, $g_2 = D_1\alpha^{1-2Y} + D_2\ln\alpha$, $q_3 = C_1\alpha^{1-2Y} + C_2\ln\alpha$.
   In this case we have for the functions of χ
   $\mathcal{S}_0^{'} + E_1(1-2Y)\mathcal{Q}_2 + D_2\mathcal{Q}_3 + C_2\dfrac{(F-2)Z}{f\chi M^2 Y} = 0$
   $E_1\mathcal{S}_1^{'} + E_1(1-2Y)\mathcal{Q}_1 + D_1\mathcal{S}_5^{'} + D_1(1-2Y)\mathcal{Q}_3 + C_1(1-2Y)\dfrac{(F-2)Z}{f\chi M^2 Y} + C_1\mathcal{S}_7^{'} = 0$
   $(D_2\mathcal{S}_5 + C_2\mathcal{S}_7 + 2Y(1-2Y)E_1\mathcal{S}_4)^{'} = 0$
   We may close the system by choosing a form for the pressure $P = \dfrac{B_o^2}{8\pi}Q(\alpha)\mathcal{S}(\chi)$. Under this assumption we have one more unknown (the function $\mathcal{S}(\chi)$) and the following relations
   $Q = \lambda_1 + \lambda_2\alpha^{1-2Y}$
   $D_2\mathcal{S}_5 + C_2\mathcal{S}_7 + 2Y(1-2Y)E_1\mathcal{S}_4 = 0$
   $\mathcal{S}_0 + E_1(1-2Y)\mathcal{S}_3 + D_2\mathcal{S}_6 = \lambda_1\mathcal{S}$
   $E_1\mathcal{S}_1 + E_1(1-2Y)\mathcal{S}_2 + D_1\mathcal{S}_5 + D_1(1-2Y)\mathcal{S}_6 + C_1\mathcal{S}_7 = \lambda_2\mathcal{S}$

3. $g_1 = E_1\ln\alpha$, $g_2 = D_1\ln\alpha + D_2\alpha^{2Y-1}$, $q_3 = C_1\ln\alpha + C_2\alpha^{2Y-1}$.
   In this case we have for the functions of χ
   $\mathcal{S}_0^{'} + E_1\mathcal{Q}_1 + D_1\mathcal{Q}_3 + C_1\dfrac{(F-2)Z}{f\chi M^2 Y} = 0$
   $(E_1\mathcal{S}_1 + D_1\mathcal{S}_5 + C_1\mathcal{S}_7)^{'} = 0$

$$E_1\mathcal{Q}_2+D_2\mathcal{S}_5^{'}+D_2\left(2Y-1\right)\mathcal{Q}_3+C_2\left(2Y-1\right)\frac{\left(F-2\right)Z}{f\chi M^2Y}+C_2\mathcal{S}_7^{'}+\frac{2YE_1}{2Y-1}\mathcal{S}_4^{'}=0$$

We may close the system by choosing a form for the pressure $P=\frac{B_o^2}{8\pi}Q\left(\alpha\right)\mathcal{S}\left(\chi\right)$. Under this assumption we have one more unknown (the function $\mathcal{S}\left(\chi\right)$) and the following relations

$Q=\lambda_1+\lambda_2\alpha^{2Y-1}$

$\mathcal{S}_0+E_1\mathcal{S}_2+D_1\mathcal{S}_6=\lambda_1\mathcal{S}$

$E_1\mathcal{S}_1+D_1\mathcal{S}_5+C_1\mathcal{S}_7=0$

$E_1\mathcal{S}_3+\frac{2YE_1}{2Y-1}\mathcal{S}_4+D_2\mathcal{S}_5+D_2\left(2Y-1\right)\mathcal{S}_6+C_2\mathcal{S}_7=\lambda_2\mathcal{S}$

5.4.3 Solutions with constant Z

Another way to separate the variables $(\chi\,,\alpha)$ in Eq. (5.76) is to assume

$$Z=\text{ constant, or } f=G^{-2Z}\,.$$

If this is the case, from Eq. (5.71), α is a function of $r\varpi^{2Z}$. Equivalently, the equation of the lines is

$$\frac{z}{\varpi}=\sqrt{\left(\frac{\varpi}{\varpi\left(z=0\right)}\right)^{-4Z-2}-1}\,.$$

So if we find solutions of Eq. (5.76) they will correspond to cases with prescribed fieldlines.

If $Z=-\frac{1}{2}$ we have radial fieldlines on the poloidal plane while for other values of Z fig. 5.11 shows the shape of the lines.

5.5 Summary

In this Chapter we have examined a systematic way for constructing exact MHD solutions for plasma flows. The *first* assumption was to consider the ideal plasmas MHD equations for time-independent conditions, Eq. (5.1)-(5.2), *without* imposing the extra constraint of the frequently used polytropic assumption. *Second*, we confined our attention to axisymmetric situations, without an electric field in the ignorable direction [Con94], in which case the poloidal magnetic and velocity fields can be expressed in terms of the magnetic flux function A while several integrals exist, Eq. (5.4)-(5.5). In that case, besides A, a second natural variable is the Alfvén Mach number M, Eq. (5.3). We denoted by G the cylindrical distance ϖ of a poloidal streamline from the system's symmetry axis, in units of the cylindrical distance of the Alfvén surface from the same axis, ϖ_α. *Third*, we further confined our attention to transAlfvénic outflows in which case the regularization of the azimuthal components in Eq. (5.4-5.5) requires that the ratio of the two integrals of the total specific angular momentum in

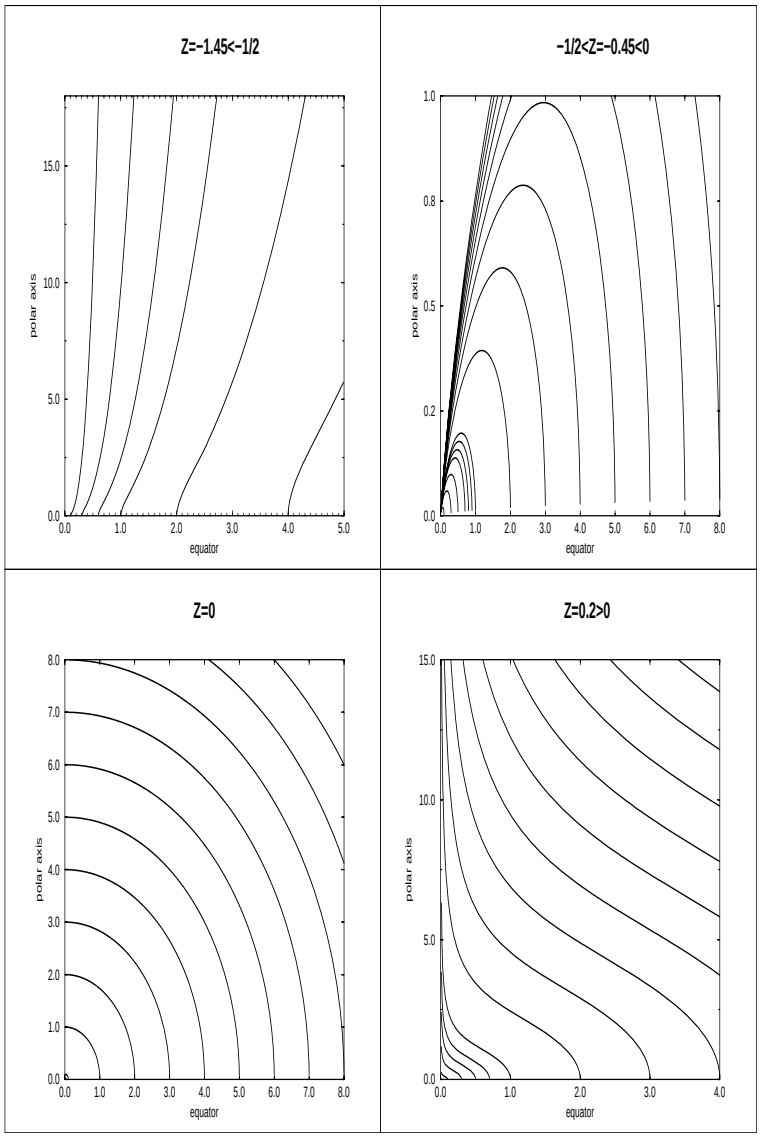

Figure 5.11: Lines on the poloidal plane when Z =constant

the flow $L(A)$ and corotation frequency $\Omega(A)$ is some function $\alpha(A)$ [as in Eq. (5.9)]. By introducing some reference scale ϖ_o this function α is dimensionless, [as in Eq. (5.7) where $\varpi_o \equiv r_\star$]. Apparently (M, α) is a rather convenient set of dimensionless variables for describing all physical quantities in the poloidal plane. For any set of orthogonal curvilinear coordinates suitable for describing axisymmetric problems, we may then convert their poloidal coordinates to (M, α). Examples are spherical coordinates $[r(M,\alpha), \theta(M,\alpha), \phi]$, cylindrical coordinates $[z(M,\alpha), \varpi(M,\alpha), \phi]$, toroidal coordinates $[u(M,\alpha), v(M,\alpha), \phi]$, oblate/prolate spheroidal coordinates $[\xi(M,\alpha), \eta(M,\alpha), \phi]$, paraboloidal coordinates, etc. Then, the distance from the symmetry axis of the outflow in units of the corresponding Alfvén distance, is $G(M,\alpha)$. In the present first study we made the simplifying *fourth* assumption that G is independent of α, $G = G(M)$ only. Finally, to re-establish the connection with the geometry of the problem and the particular set of the coordinates used, we made our *fifth* and final assumption that $M = M(\chi)$ (and $G = G(\chi)$), where $\chi = r$, or, $\chi = \theta$, or generally, $r = \varpi_o f(\chi)\, g(\alpha)$. This leads then to the three broad classes of meridionally (with spherical critical surfaces, $M = M(R)$), radially (with conical critical surfaces, $M = M(\theta)$), and generalized self-similar outflows (with χ =constant critical surfaces, $M = M(\chi)$). Needless to say that additional symmetries may in principle be considered, something which may be taken up in another connection (equilibria in tokamak geometries, etc).

After these five assumptions are well posed and with the help of a simple theorem, it is possible to (i) unify all existing exact solutions for astrophysical outflows (Tables 5.1, 5.2 and 5.3) and (ii), to qualitatively sketch a few of them. With this method, the system of the coupled MHD equations for r- or θ- self similar outflows, reduces to a set of five ordinary differential equations for the dimensionless jet radius (G), the flow's expansion factor or angle (F, or φ), the Alfvén Mach number (M) and the two pressure components (P_1 and P_0). The requirement that the solutions pass through the Alfvén critical point gives a condition relating the values of the expansion function or angle, Alfvén number slope and pressure component at this critical point. The Alfvén regularity conditions, Eqs. (5.68), (5.53) are similar to that discussed in [HN89, ST94].

As a byproduct of this construction, two representative models for radially and meridionally self-similar outflows, [BP82] and [ST94], respectively, have been generalized. In the former case of [BP82], it is well known that the cold plasma solution is terminated at a finite height above the disk while the general case (3) in Table 5.3 extends all the way to infinity. Also, it is shown that the expressions of the MHD integrals which correspond to the [ST94] model are only a special case of case (2) in Table 5.1.

Having in mind the ubiquitously observed collimated outflows from astrophysical objects, we paid more attention to the selfconsistently derived asymptotical shape of the streamlines. Of the various such asymptotic geometries derived, a prominent member seem to be the cylindrically collimated jet-type solutions, in accordance also with the conclusions of observations [Liv97], general theoretical arguments (Heyvaerts & Norman [HN89]) and recent numerical

simulations [GWB97]. Another feature that appeared in the solutions is that cylindrical collimation may or may not be achieved with oscillations in the width of the jet [VT97]. Although in the examples analyzed here the amplitude of the oscillations is rather weak and the flow collimates rather smoothly, preliminary results show that cases also exist where it can become rather large and the final radius of the jet can be much smaller than the initial large cylindrical radius and corresponding opening angle. Finally, we should note that the pressure P denotes the total pressure (including gas pressure, Alfvén waves pressure, radiative forces, etc). For example, the same formalism may be used also in radiation driven winds.

5.6 Some other solutions

In the previous sections, we have described a method to construct axisymmetric MHD models. However, this is a general method and can be applied in other similar situations. Next we apply it in two such cases.

5.6.1 Translational symmetry in uniform gravity

Suppose that we want to study flows near the surface of a star or galaxy (for example solar arcades). Then we assume uniform gravitational field $\mathcal{V} = gz$, with g =constant. $\hat{z}$ is the direction normal to the surface. We choose a system of coordinates $(x\,,y)$ on this surface, such that the y is ignorable. We search polytropic flows, $P = Q(A)\rho^{\gamma}$, (for $\gamma = 1$ isothermal flows), with $V_y = 0$ and $B_y = 0$. Assume now that the flow is self similar in a way such that

1. for the Alfvén Mach number, $M = M(\chi)\,, \chi = x/z_o$ and z_o some reference length

2. for the flux function $A = B_o z_o \mathcal{A}(\alpha)\,, \alpha = e^{G(\chi) - z/z_o}$ and B_o is a constant. Choosing $G(\chi = 0) = 0$ and $\left(\alpha \dfrac{d\mathcal{A}}{d\alpha}\right)_{\alpha=1} = 1$, B_o is the $\hat{x}$- component of the magnetic field at $x = z = 0$.

Then in the cartesian coordinate system $Ox_1x_2x_3$, with $x_1 = z\,, x_2 = x\,, x_3 = y$ and the Eqs. (2.15)-(2.18) with $\Omega = 0\,, L = 0$ we get finally that the only possible case in order to be separable the coordinates $x\,, z$, is the following

$$\mathcal{A} = \alpha\ ,\ \Psi_A^2 = 4\pi\rho_o M^2(\chi = 0)\alpha^2\ ,\ Q = Q_o\alpha^{-2(\gamma-1)}\ ,$$
$$E = \begin{cases} V^2/2 + \mathcal{V} + Q_o \ln\frac{\rho}{\rho_o} = E_o + (2Q_o - gz_o)\ln\alpha\ \ , & \text{if } \gamma = 1 \\ V^2/2 + \mathcal{V} + \frac{\gamma}{\gamma-1}\frac{P}{\rho} = E_o - gz_o\ln\alpha\ \ , & \text{if } \gamma \neq 1 \end{cases} . \quad (5.78)$$

The case $\gamma = 1\,, E_o = 0$ have been analyzed in [TSP93] (in this paper, $1/z_o = \xi/2H\,, Q_o/g = H$).

5.6.2 HD θ- self similar axisymmetric flows

In general, in steady axisymmetric hydrodynamical (HD) case, we have

$$V_r = \frac{1}{4\pi\rho r^2 \sin\theta}\frac{d\Psi}{d\alpha}\frac{\partial\alpha}{\partial\theta}\,,\; V_\theta = -\frac{1}{4\pi\rho r \sin\theta}\frac{d\Psi}{d\alpha}\frac{\partial\alpha}{\partial r}\,,\; V_\phi = \frac{L(\alpha)}{r\sin\theta}\,,$$

where $\alpha = R^2\sin^2\theta/G^2$, $R = r/r_o$.
We search for self similar solutions with

1. $G = G(R)$, and
2. $\rho = \rho_o\, g_3(\alpha)/N^2$, with $N = N(R)$.

Then, after introducing the functions

$$g_1 = \frac{1}{4\pi^2\rho_o^2 r_o^4 V_o^2}\int\frac{1}{g_3}\left(\frac{d\Psi}{d\alpha}\right)^2 d\alpha\,,\; g_2 = \frac{1}{r_o^2 V_o^2}\int\frac{L^2 g_3}{\alpha^2}\,d\alpha$$

instead of $\Psi(\alpha)\,, L(\alpha)$, we find that in order to separate the variables $\alpha\,, R$ the set of the functions $g_1\,, g_2\,, g_3$ must be one of the nine cases of Table 5.1.

5.7 Appendix 5.A: Functions of R in meridional self similarity

$$F(R) = 2 - R\frac{G^{2'}}{G^2} \equiv \frac{\partial\ln\alpha(R,\theta)}{\partial\ln R}\,, \tag{5.79}$$

$$f_1(R) = -\frac{1}{G^4}\,, \tag{5.80}$$

$$f_2(R) = -\frac{F^2-4}{4G^2R^2}\,, \tag{5.81}$$

$$f_3(R) = -\frac{1}{G^2}\left(\frac{1-G^2}{1-M^2}\right)^2\,, \tag{5.82}$$

$$f_4(R) = \frac{F}{2RG^2}M^{2'} - \frac{1-M^2}{2RG^2}F' - \frac{\left(1-M^2\right)F(F-2)}{4R^2G^2}\,. \tag{5.83}$$

Then,

$$F' = \frac{F}{1-M^2}M^{2'} - \frac{F(F-2)}{2R} - \frac{2RG^2}{1-M^2}f_4\,, \tag{5.84}$$

$$f_5(R) = \frac{G^4-M^2}{G^2M^2\left(1-M^2\right)}\,, \tag{5.85}$$

$$f_6(R) = -f_1^{'} - \frac{1}{M^2}\left(\frac{M^4}{G^4}\right)^{'} = -\frac{2}{G^4}M^{2'} + \frac{2\left(1-M^2\right)(F-2)}{RG^4}\,, \tag{5.86}$$

$$f_7(R) = \frac{2}{R^2G^2}M^{2'} - \frac{\left(1-M^2\right)(F-2)(F+4)}{2R^3G^2} - \frac{F}{R}f_4\,, \tag{5.87}$$

$$f_8(R) = -\frac{F-2}{R} f_5 \,, \tag{5.88}$$

$$f_9(R) = -\frac{\nu^2}{R^2 M^2} \,. \tag{5.89}$$

In the special case of meridional self similarity with $G = R$ we have:

$$G = R\,, F = 0\,,\ \ f_1 = -\frac{1}{R^4}\,,\ \ f_2 = -f_1\,,$$
$$f_3 = -\frac{1}{R^2}\left(\frac{1-R^2}{1-M^2}\right)^2\,,\ \ f_4 = 0\,,\ \ f_5 = \frac{R^4 - M^2}{R^2 M^2 \left(1-M^2\right)}\,,$$
$$f_6 = -\frac{2}{R^4} M^{2'} - \frac{4}{R^5}\left(1-M^2\right)\,,\ \ f_7 = -f_6\,,\ \ f_8 = \frac{2}{R} f_5\,,\ \ f_9 = -\frac{\nu^2}{R^2 M^2}\,.$$

5.8 Appendix 5.B: Functions of θ in radial self similarity

$$F(\theta) = 2 - \frac{G^{2'}}{G^2} \equiv \frac{\partial \ln \alpha(R,\theta)}{\partial \ln \sin\theta}\,, \tag{5.90}$$

$$F = -2\frac{\sin\theta \sin(\varphi+\theta)}{\cos\theta\cos(\varphi+\theta)} = 2 - 2\frac{\cos\varphi}{\cos\theta\cos(\varphi+\theta)}\,, \tag{5.91}$$

where the expansion angle $\varphi(\theta)$ is the angle between the line and the equatorial plane.

Note that, for constant α, $\dfrac{dz}{d\varpi} = \dfrac{d\left(\varpi_o\sqrt{\alpha}G/\tan\theta\right)}{d\left(\varpi_o\sqrt{\alpha}G\right)} = \tan\varphi$.

$$\frac{dG^2}{d\theta} = \frac{2G^2\cos\varphi}{\sin\theta\cos(\varphi+\theta)}\,, \tag{5.92}$$

$$h_1(\theta) = -\frac{\left(\sin^2\theta + \cos^2\theta\frac{F^2}{4}\right)}{G^4} = -\frac{\sin^2\theta}{G^4\cos^2(\varphi+\theta)}\,, \tag{5.93}$$

$$h_2(\theta) = -\frac{1}{G^2}\left(\frac{1-G^2}{1-M^2}\right)^2\,, \tag{5.94}$$

$$h_3(\theta) = \frac{G^4 - M^2}{M^2 G^2\left(1-M^2\right)}\,, \tag{5.95}$$

$$h_4(\theta) = -\frac{\sin\theta}{GM^2}\,, \tag{5.96}$$

$$h_5(\theta) = -\frac{\cos^2\theta}{2G^4}\left\{\left[F\left(1-M^2\right)\right]' + \left(F-2\right)\left(1-M^2\right)\left(F-\tan^2\theta\right)\right\}\,, \tag{5.97}$$

or,

$$h_5(\theta) = \frac{1-M^2}{G^4}\frac{\sin^2\theta}{\cos^2(\varphi+\theta)}\frac{d\varphi}{d\theta} - \frac{\sin^2\theta\sin(\varphi+\theta)}{G^4\cos(\varphi+\theta)}\frac{dM^2}{d\theta} - \frac{1-M^2}{G^4}\frac{\sin\theta\cos\varphi\sin(\varphi+\theta)}{\cos^2(\varphi+\theta)}. \quad (5.98)$$

Then,

$$\frac{d\varphi}{d\theta} = \frac{\sin(\varphi+\theta)\cos(\varphi+\theta)}{1-M^2}\frac{dM^2}{d\theta} + \frac{\sin(\varphi+\theta)\cos\varphi}{\sin\theta} + \frac{\cos^2(\varphi+\theta)}{\sin^2\theta}\frac{G^4}{1-M^2}h_5\,. \quad (5.99)$$

5.9 Appendix 5.C: Functions of χ in generalized self similarity

$$F(\chi) = 2 - \frac{d\ln G^2}{d\ln|\chi|}\,. \quad (5.100)$$

Note that χ and F are intermediate variables. If we change χ, F changes too but the derivative $\frac{\chi}{(F-2)}\frac{d}{d\chi}$ remains the same:

$$\frac{\chi d\mathcal{G}}{(F-2)\,d\chi} = -\frac{d\mathcal{G}}{d\ln G^2}\,,\ \text{for any function } \mathcal{G}(\chi)\,. \quad (5.101)$$

$$\mathcal{S}_1(\chi) = -\frac{1-M^2}{2G^2f^2(Z+Y)^2}\times \times\left[Z+\frac{1}{2}+4ZY-\frac{4Y-1}{Z+Y}\frac{dZ}{d\ln G^2}-(2Y-2Z-1)\frac{dM^2}{(1-M^2)\,d\ln G^2}\right] \quad (5.102)$$

$$\mathcal{S}_2(\chi) = -\frac{4Z+1}{4G^2f^2(Z+Y)^2}\,, \quad (5.103)$$

$$\mathcal{S}_3(\chi) = -\frac{Z^2}{G^4(Z+Y)^2}\,, \quad (5.104)$$

$$\mathcal{S}_4(\chi) = \frac{1-M^2}{G^4(Z+Y)^2}\left[Z+Z\frac{dM^2}{(1-M^2)\,d\ln G^2}-\frac{Y}{Z+Y}\frac{dZ}{d\ln G^2}\right]\,, \quad (5.105)$$

$$\mathcal{S}_5(\chi) = \frac{G^4-M^2}{G^2M^2(1-M^2)}\,, \quad (5.106)$$

$$\mathcal{S}_6(\chi) = -\frac{1}{G^2}\left(\frac{1-G^2}{1-M^2}\right)^2 , \tag{5.107}$$

$$\mathcal{S}_7(\chi) = -\frac{1}{M^2 f} , \tag{5.108}$$

$$\mathcal{Q}_1(\chi) = \mathcal{S}_2^{'} + \frac{M^2}{4(Z+Y)^2}\frac{d}{d\chi}\left(\frac{4Z+1}{f^2G^2}\right) + \frac{M^2}{2(Z+Y)^3}\frac{dZ}{d\chi}\frac{4Z+1}{f^2G^2} + \frac{1}{2(Z+Y)^2}\frac{dM^2}{d\chi}\frac{4Z+1}{f^2G^2} , \tag{5.109}$$

$$\mathcal{Q}_2(\chi) = \mathcal{S}_3^{'} + \frac{M^2}{(Z+Y)^2}\frac{d}{d\chi}\left(\frac{Z^2}{G^4}\right) - \frac{2M^2Z^2}{G^4(Z+Y)^3}\frac{dZ}{d\chi} + \frac{2Z^2}{G^4(Z+Y)^2}\frac{dM^2}{d\chi} , \tag{5.110}$$

$$\mathcal{Q}_3(\chi) = \mathcal{S}_6^{'} + \frac{2}{G^2}\frac{1-G^2}{1-M^2}\frac{d}{d\chi}\left(\frac{1-G^2}{1-M^2}\right) + \frac{F-2}{\chi G^2 M^2}\left(\frac{G^2-M^2}{1-M^2}\right)^2 . \tag{5.111}$$

Bibliography

[BB78] J.M. Bardeen and B.K. Berger, ApJ **221** (1978), 105.

[Bea95] C.J. Burrows et al, ApJ **452** (1995), 680.

[Bir96] T. Biretta, *in Solar and Astrophysical MHD Flows*, K. Tsinganos (ed.), Kluwer Academic Publishers, p. 357, 1996.

[BK95] L. Burderi and A.R. King, MNRAS **276** (1995), 1141.

[BP82] R.D. Blandford and D.G. Payne, MNRAS **199** (1982), 883.

[BR74] R.D. Blandford and M.J. Rees, MNRAS **169** (1974), 395.

[Cao97] X. Cao, MNRAS **291** (1997), 145.

[CL94] J. Contopoulos and R.V.E. Lovelace, ApJ **429** (1994), 139.

[Con94] J. Contopoulos, ApJ **432** (1994), 508.

[CV97] P. Crane and J. Vernet, ApJ **486** (1997), L91.

[Fer97] J. Ferreira, A&A **319** (1997), 340.

[FMBR96] A. Ferrari, S. Massaglia, G. Bodo, and P. Rossi, *in Solar and Astrophysical MHD Flows*, K. Tsinganos (ed.), Kluwer Academic Publishers, p. 607, 1996.

[FP95] J. Ferreira and G. Pelletier, A&A **295** (1995), 807.

[FPBH96] W.C. Feldman, J.L. Phillips, B.L. Barraclough, and C.M. Hammond, *in Solar and Astrophysical MHD Flows*, K. Tsinganos (ed.), Kluwer Academic Publishers, p. 265, 1996.

[GWB97] A.P. Goodson, R.M. Winglee, and K.H. Bohm, ApJ **489** (1997), 199.

[HN89] J. Heyvaerts and C.A. Norman, ApJ **347** (1989), 1055.

[Kaf96] M. Kafatos, *in Solar and Astrophysical MHD Flows*, K. Tsinganos (ed.), Kluwer Academic Publishers, p. 585, 1996.

[Kon89] A. Konigl, ApJ **342** (1989), 208.

[Li95] Z.-Y Li, ApJ **444** (1995), 848.

[Li96] Z.-Y Li, ApJ **465** (1996), 855.

[Liv97] M. Livio, *in IAU Colloq. 163, Accretion Phenomena and Related Outflows*, D.T. Wickramasinghe, L. Ferrario, & G.V. Bicknel (eds.), ASP: San Francisco, 1997.

[LTP96] J. Lima, K. Tsinganos, and E. Priest, Astrophys. Letts. and Comms. **34** (1996), 281.

[MR96] I.F. Mirabel and L.F. Rodriguez, *in Solar and Astrophysical MHD Flows*, K. Tsinganos (ed.), Kluwer Academic Publishers, p. 683, 1996.

[Par58] E.N. Parker, ApJ **128** (1958), 664.

[Par63] E.N. Parker, *in: Interplanetary Dynamical Processes*, Interscience Publishers, New York, 1963.

[Ray96] T.P. Ray, *in Solar and Astrophysical MHD Flows*, K. Tsinganos (ed.), Kluwer Academic Publishers, p. 539, 1996.

[ST94] C. Sauty and K. Tsinganos, A&A **287** (1994), 893.

[TSP93] K. Tsinganos, G. Surlantzis, and E. R. Priest, aa **275** (1993), 613.

[TSS+96] K. Tsinganos, C. Sauty, G. Surlantzis, E. Trussoni, and J. Contopoulos, MNRAS **283** (1996), 811.

[TT91] K. Tsinganos and E. Trussoni, A&A **249** (1991), 156.

[TTS97] E. Trussoni, K. Tsinganos, and C. Sauty, A&A **325** (1997), 1099.

[VT97] N. Vlahakis and K. Tsinganos, MNRAS **292** (1997), 591.

[VT98] N. Vlahakis and K. Tsinganos, MNRAS **in press** (1998).

Chapter 6

Some known self similar models

In this Chapter we briefly review several exact MHD models for cosmic outflows which belong in our net of the meridionally and radially self similar models. For completeness of the review of all existing models we also discuss the classical Weber-Davis model for a magnetized equatorial wind. At the end we also briefly present a novel and unique polytropic radially self similar model in which the solution passes from all critical points.

6.1 Parker's classical solution

We shall begin our analytical examination of meridionally self similar models with the first case of Table 5.2. In this case we have $g_1 = -\ln|\,1-\alpha\,|\,, g_2 = 0$ and $g_3 = 1$, with $\alpha = \sin^2\theta$, so from Eq. (5.29) we have

$$A = B_\star r_\star^2\,(1-\cos\theta) = 2B_\star r_\star^2 \sin^2\frac{\theta}{2}\,, \Psi_A = \sqrt{4\pi\rho_\star}\,, \Omega = 0 \text{ and } L = 0\,.$$

Thus, we have a non-rotating, radial outflow. The magnetic field is from Eq. (5.4) $\vec{B} = \dfrac{B_\star}{R^2}\hat{r}$, i.e., a monopole-like field. The density is spherically symmetric, since $\rho = \dfrac{\Psi_A^2}{4\pi M^2} = \dfrac{\rho_\star}{M^2}$. From Eq. (5.5) we have $\vec{V} = V_\star \dfrac{M^2}{R^2}\hat{r}$ (equivalently $4\pi r^2 \rho V =$constant) where $V_\star$ is the velocity at the Alfvén point $r = r_\star \Leftrightarrow R = r/r_\star = 1$. At this point $B_\star^2/8\pi = \rho_\star V_\star^2/2$.
Substituting the functions $g_1\,, g_2$ and g_3 in Eqs. (5.34) and (5.35) we get (we remind that in all radial models, we have $G = R$ and $F = 0$),

$$P = \frac{B_\star^2}{8\pi}\,(f_0 + f_1) = \frac{B_\star^2}{8\pi}\left(f_0 - \frac{1}{R^4}\right) \text{ and} \tag{6.1}$$

$$f_0^{'} - f_6 - f_9 = 0 \Leftrightarrow \frac{\nu^2}{R^2M^2} + \frac{2}{R^4}M^{2'} + 4\frac{1-M^2}{R^5} + f_0^{'} = 0\,. \tag{6.2}$$

Eliminating f_0 from the two previous equations we have

$$\frac{d}{dR}\left(\frac{8\pi P}{B_\star^2}\right) = -\frac{\nu^2}{R^2M^2} + 4\frac{M^2}{R^5} - \frac{2}{R^4}M^{2\prime} \,. \tag{6.3}$$

This equation has two unknowns $P\,, M^2$ (or the pressure and density). Thus this case is degenerate. If we assume a polytropic relation between P and ρ of the form $P = \frac{P_\star}{\rho_\star^\gamma}\rho^\gamma$ then we have only one unknown, say M^2:

$$\frac{R}{M^2}\frac{dM^2}{dR} = \frac{4\frac{M^{2(\gamma+1)}}{R^4} - \nu^2\frac{M^{2(\gamma-1)}}{R}}{2\frac{M^{2(\gamma+1)}}{R^4} - 2\gamma\frac{P_\star}{\rho_\star V_\star^2}} \text{ or } \frac{r}{\rho}\frac{d\rho}{dr} = \frac{\mathcal{GM}/r - 2V^2}{V^2 - \gamma P/\rho} \,, \tag{6.4}$$

where $r^2\rho V$ =constant= $r_\star^2\rho_\star V_\star$ and P/ρ^γ =constant= $P_\star/\rho_\star^\gamma$.
This is exactly Parker's solution for the solar wind [Par63]. Defining the sound speed $C_s = \sqrt{\gamma P/\rho}$ we have after some manipulation,

$$\frac{r}{V}\frac{dV}{dr} = \frac{2C_{s\star}^2V_\star^{\gamma-1}r_\star^{2(\gamma-1)} - \mathcal{GM}V^{\gamma-1}r^{2\gamma-3}}{V^{\gamma+1}r^{2(\gamma-1)} - C_{s\star}^2V_\star^{\gamma-1}r_\star^{2(\gamma-1)}} \text{ or } \frac{r}{V}\frac{dV}{dr} = \frac{2\gamma P/\rho - \mathcal{GM}/r}{V^2 - \gamma P/\rho} \,, \,. \tag{6.5}$$

This equation after integration gives the Bernoulli integral

$$\frac{V^2}{2} + \mathcal{V} + \frac{\gamma}{\gamma-1}\frac{P}{\rho} = E = \text{ constant.} \tag{6.6}$$

Note that for the isothermal case $\gamma = 1$ the term $\frac{\gamma}{\gamma-1}\frac{P}{\rho}$ must be replaced with the term $C_{s\star}^2\ln\rho$.
The solution has a critical point when the numerator and denominator of Eq. (6.5) simultaneously vanish. This happens at the point r_x where (for $\gamma \neq 5/3$)

$$\frac{r_x}{r_\star} = \left(\frac{V_\star}{C_{s\star}}\right)^{-\frac{2(\gamma-1)}{3(5/3-\gamma)}}\left(\frac{2r_\star C_{s\star}^2}{\mathcal{GM}}\right)^{-\frac{\gamma+1}{3(5/3-\gamma)}} \text{ and}$$

$$\frac{V_x}{V_\star} = \left(\frac{V_\star}{C_{s\star}}\right)^{-\frac{4(3/2-\gamma)}{3(5/3-\gamma)}}\left(\frac{2r_\star C_{s\star}^2}{\mathcal{GM}}\right)^{\frac{2(\gamma-1)}{3(5/3-\gamma)}} \,.$$

For $\gamma = 5/3$ we have a critical line $V_x^2 = \frac{\mathcal{GM}}{2r_x}$ if $C_{s\star}^3V_\star = \left(\frac{\mathcal{GM}}{2r_\star}\right)^2$.
At this point $V_x = C_{sx}$, so the fluid velocity is equal with the local sound speed (sonic point). For $E = E_x = \frac{3}{2}V_x^2\frac{5/3-\gamma}{\gamma-1}$ we have the only acceptable solution, the critical solution.
Eq. (6.6) with $x = r/r_x\,, y = V/V_x\,, C = (E - E_x)/V_x^2$ is equivalent with

$$C = \frac{y^2-1}{2} - 2\left(\frac{1}{x} - 1\right) + \frac{1}{\gamma-1}\left(x^{-2(\gamma-1)}y^{-(\gamma-1)} - 1\right) \,, \tag{6.7}$$

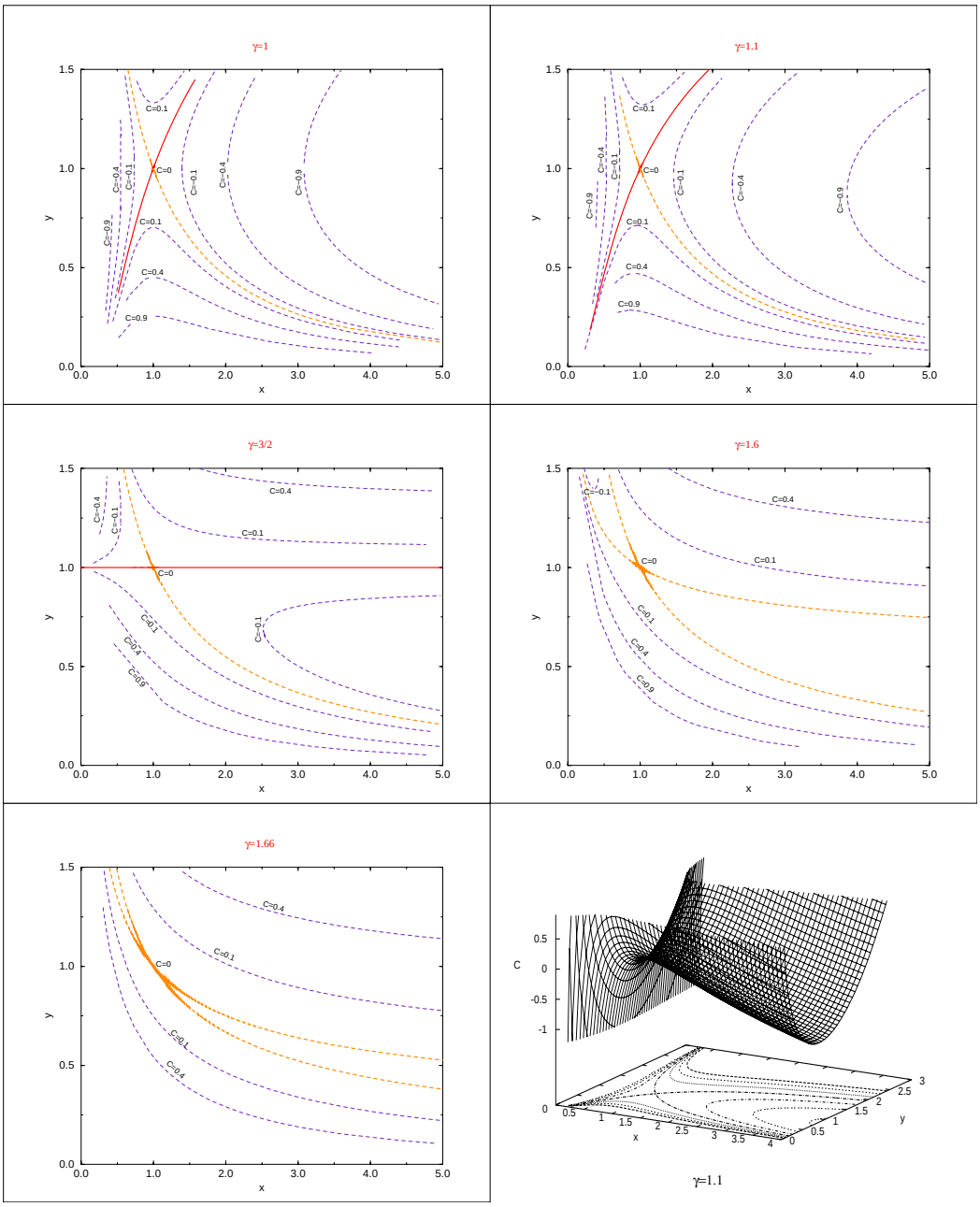

Figure 6.1: Topologies of Parker's solution for various values of γ.

which is the integral of the differential equation (equivalent with Eq. (6.5))

$$\frac{x}{y}\frac{dy}{dx} = 2\frac{1 - x^{2\gamma-3}y^{\gamma-1}}{x^{2(\gamma-1)}y^{\gamma+1} - 1} .$$

Fig. 6.1 shows various solutions in the plane $x - y$ (isocontoures of Eq. (6.6) for various values of C). We see that for $\gamma \geq 3/2$ we get unphysical solutions, in the sense that $\lim_{x\to 0} y = \infty$. For $\gamma < 3/2$ the solution begins with subsonic velocity near the stellar surface and becomes supersonic at larger distances. Note however, that since the density decreases monotonically, in this case we must have heat reservoir, extending all the way to infinity, since the heating function is always positive: $q = \frac{\gamma - \Gamma}{\Gamma - 1}\frac{P}{\rho}\vec{V}\cdot\vec{\nabla}\rho = \frac{\Gamma - \gamma}{\Gamma - 1}\frac{P}{\rho}V\left(-\frac{d\rho}{dr}\right)$.
Nevertheless, the thermal speed is finite and the total Bernoulli energy is $E = V_\infty^2/2$.

6.2 The Weber-Davis equatorial model

In this section we sketch briefly the model of Weber and Davis [WD67], for an equatorial wind. A monopole like field is assumed near the equator, $A = B_\star r_\star^2 (1-\cos\theta)$, or, $B_r = B_\star / R^2$, with $R = r/r_\star$, and the starred quantities referring to their values at the point $r = r_\star$ on the equatorial plane. In this case, on the equator A =constant. If we want to solve the MHD equations only near the equator, we regard A and all free functions $L\,,\Omega\,,\Psi_A$ as constants, with $L = r_\star^2 \Omega$ for transAlfvénic solutions. The transfield equation is ignored since the poloidal fieldlines are prescribed [1], and only the Bernoulli equation is examined. This last equation, for polytropic flows, $P = Q\rho^\gamma$, and after introducing the constants

$$\omega = \frac{r_\star \Omega}{V_\star}\,,\ \beta = \frac{2\gamma Q}{(\gamma-1)\,\rho_\star V_\star^2}\,,\ \nu^2 = \frac{2\mathcal{G}\mathcal{M}}{r_\star V_\star^2}\,,\ \epsilon = \frac{2E}{V_\star^2}\,,$$

gives $\mathcal{B}_0\left(R\,,M^2\right) = \epsilon$, with

$$\mathcal{B}_0\left(R\,,M^2\right) \equiv \frac{M^4}{R^4} + \frac{\beta}{M^{2(\gamma-1)}} - \frac{\nu^2}{R} + \omega^2\left[\frac{\left(R^2-M^2\right)^2}{R^2\left(1-M^2\right)^2} + 2\frac{1-R^2}{1-M^2}\right]\,.$$

Obviously, the parameter ω measures rotation [2], such that for $\omega \gg 1$ a star is characterized as a fast rotator, while for $\omega \ll 1$, a slow rotator. The parameter β measures pressure gradient and ν^2 gravity.
The various isocontours of the Bernoulli equation, give the solutions
$M^2 = M^2(R\,;\omega\,,\beta\,,\nu^2\,,\gamma\,,\epsilon)$ on the equatorial plane.
As we discuss in Chapter 3, this equation has two critical points. They appear when the poloidal velocity of the flow is equal to the phase speed of an MHD wave. This can be seen in this case also, if we differentiate the Bernoulli equation, to get

$$\frac{dM^2}{dR} = -\frac{\partial\mathcal{B}_0}{\partial R}\Big/\frac{\partial\mathcal{B}_0}{\partial M^2}\,,\ \text{with}$$

$$\left(1-M^2\right)\frac{\partial\mathcal{B}_0}{\partial M^2} = \left(1-M^2\right)\left[\frac{2M^2}{R^4} - \beta\left(\gamma-1\right)M^{-2\gamma}\right] + 2\omega^2\frac{M^2}{R^2}\left(\frac{1-R^2}{1-M^2}\right)^2 =$$

$$-\frac{2}{V_\star^2 V_p^2}\left[V_p^4 - V_p^2\left(C_s^2+V_A^2\right) + C_s^2 V_{A\,,p}^2\right],\ \text{and}$$

$$\left(1-M^2\right)\frac{\partial\mathcal{B}_0}{\partial R} = \left(1-M^2\right)\left(-4\frac{M^4}{R^5} + \frac{\nu^2}{R^2}\right) + 2\omega^2\frac{\left(2M^2-1\right)R^4 - M^4}{R^3\left(1-M^2\right)}\,.$$

Note that the Alfvén point is not critical for the Bernoulli equation (all the contours $\mathcal{B}_0 = \epsilon$ pass through this star-type point). The slow point $(R_s\,,M_s)$ and the fast $(R_f\,,M_f)$ are critical points. If we give the values $R_s\,,M_s\,,R_f\,,M_f$ then from the equations $(\partial\mathcal{B}_0/\partial R)_{R_s\,,M_s} = \left(\partial\mathcal{B}_0/\partial M^2\right)_{R_s\,,M_s} = (\partial\mathcal{B}_0/\partial R)_{R_f\,,M_f} =$

[1] For $\theta = \pi/2$, the transfield equation is an identity if $\left[\frac{\partial}{\partial\theta}\left(P + \frac{B_\phi^2}{8\pi}\right)\right]_{\theta=\pi/2} = 0$

[2] For $\omega = 0$ we have the Parker's solution

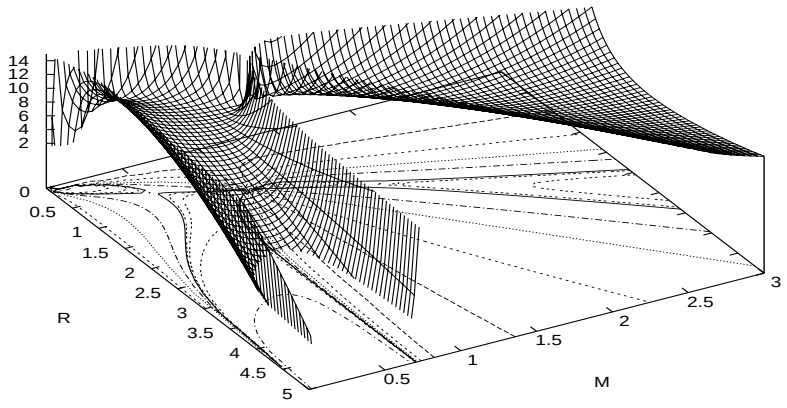

Figure 6.2: A solution of the Weber-Davis model, for $R_s = 0.6\,, M_s = 0.5\,, R_f = 1.46\,, M_f = 1.62$, when $\omega = 1.034\,, \nu^2 = 1.96352\,, \beta = 8.2712\,, \gamma = 1.13316\,, \epsilon = 9$. We show the Bernoulli function on the $R - M$ plane. The critical solution pass through the two saddle critical points (slow, fast) and the Alfvén point.

$\left(\partial \mathcal{B}_0/\partial M^2\right)_{R_f\,,M_f} = 0$ we find a one to one correspondence with the constants $\omega\,, \beta\,, \nu^2\,, \gamma$. If in addition $(\mathcal{B}_0)_{R_s\,,M_s} = (\mathcal{B}_0)_{R_f\,,M_f}$ [3] then we have a solution which pass through all critical points. In Figs. 6.2,6.3,6.4,6.5, we show various solutions of this equation.

Note that only for $\gamma < 3/2$ we get physically acceptable solutions, in the sence that $\lim_{R\to 0} V = 0$ [Hey96].

As $R \to \infty$ the Bernoulli energy along the critical solution becomes

$$\epsilon = \frac{M^4}{R^4} + 2\omega^2 \frac{R^2}{M^2} = \left(\frac{V_\infty}{V_\star}\right)^2 + 2\omega^2 \frac{V_\star}{V_\infty}\,.$$

For $\epsilon = 3\omega^{4/3}$ we get the minimum energy solution [Mic69, Hey96, BM76], when the fast ctitical point is at infinity, where $V_\infty = \omega^{2/3} V_\star$.

If at the base the Poynting energy dominates (neglecting at the base the thermal and gravitational terms) we have $\epsilon = 2\omega^2$. In this case, the minimum energy solution has $\omega = (3/2)^{3/2}$. This characteristic solution has $V_\infty = 3V_\star/2$ and it is called Michel's solution. For all other $\omega > (3/2)^{3/2}$ we have one superfast and one subfast solutions at infinity. For $\omega < (3/2)^{3/2}$ no superAlfvénic solution exist at infinity.

[3] This is the regularity condition in order to pass the solution for both critical points; the slow and the fast. The other one is simply the choice of ϵ.

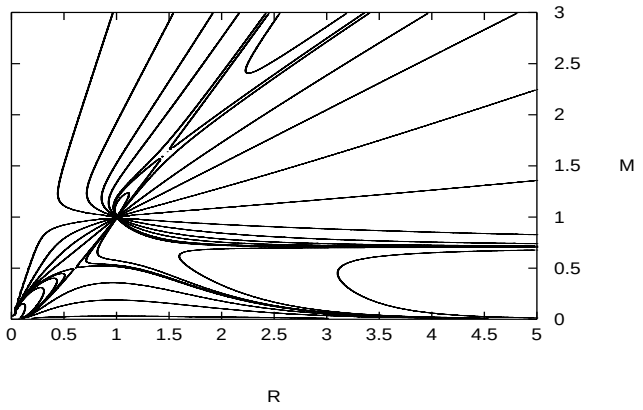

Figure 6.3: Isocontours of the Bernoulli function for the Weber-Davis model. The parameters are the same as in the previous figure.

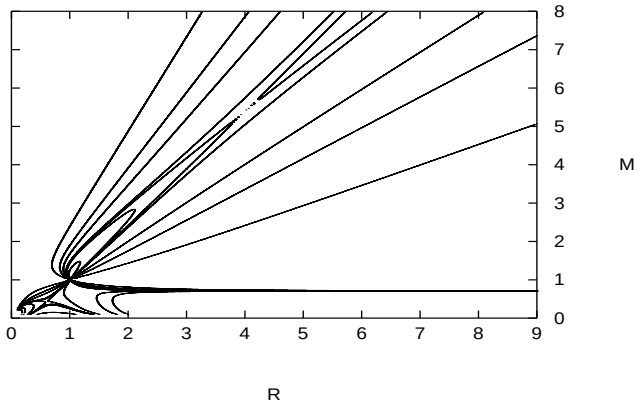

Figure 6.4: Fast magnetic rotator with parameters $R_s = 0.6$, $M_s = 0.44$, $R_f = 4$, $M_f = 5.4$, when $\omega = 2.37$, $\nu^2 = 4.068$, $\beta = 6.283$, $\gamma = 1.178$, $\epsilon = 11.6$.

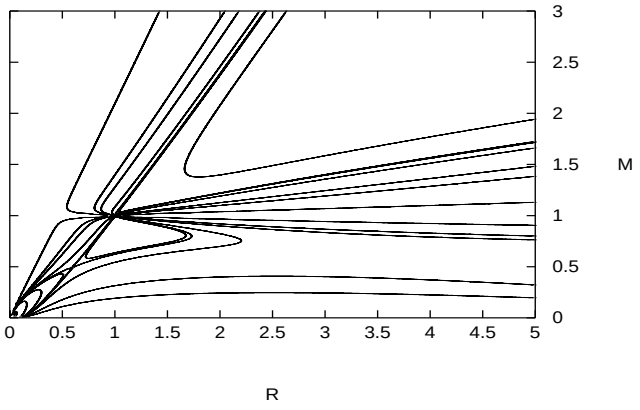

Figure 6.5: Slow magnetic rotator with parameters $R_s = 0.6\,, M_s = 0.5\,, R_f = 1.015\,, M_f = 1.02$, when $\omega = 0.195\,, \nu^2 = 1.186\,, \beta = 32.9\,, \gamma = 1.028\,, \epsilon = 32.8$. We see that the fast point is close to the Alfvén, as in the solution presented by [WD67] and appropriate for the solar wind.

6.3 The models [LTP96] and [TT91]

In the second meridionally, radial self similar solution of Table 5.2 we have $g_1 = \mu \int \frac{\alpha^\epsilon}{1-\alpha} d\alpha - \ln |\, 1-\alpha \,|$, $g_2 = \lambda^2 \alpha^\epsilon / \epsilon$ and $g_3 = 1 + \delta \alpha^\epsilon$, with $\alpha = \sin^2\theta$, so that from Eq. (5.29) we have

$$A = B_\star r_\star^2 \int_0^\theta \sin\theta \sqrt{1 + \mu \sin^{2\epsilon}\theta}\, d\theta \,, \Psi_A = \sqrt{4\pi\rho_\star \left(1 + \delta \sin^{2\epsilon}\theta\right)} \,,$$

$$\Omega = \lambda \frac{V_\star}{r_\star} \frac{\sin^{\epsilon-1}\theta}{\sqrt{1 + \delta \sin^{2\epsilon}\theta}} \,, L = \lambda r_\star V_\star \frac{\sin^{\epsilon+1}\theta}{\sqrt{1 + \delta \sin^{2\epsilon}\theta}} \,.$$

Substituting the functions g_1 , g_2 and g_3 in Eqs. (5.34) and (5.35) we have

$$P = \frac{B_\star^2}{8\pi} \left[f_0 + f_1 + \left(\lambda^2 f_5/\epsilon + \mu f_1 + \lambda^2 f_3 \right) \sin^{2\epsilon}\theta \right] \,,$$

and

$$f_0^{'} - f_6 - f_9 + \left(\lambda^2 f_5^{'}/\epsilon - \mu f_6 - \lambda^2 f_8 - \delta f_9 \right) \sin^{2\epsilon}\theta = 0 \,,$$

or, (since $\epsilon \neq 0$)

$$f_0^{'} - f_6 - f_9 = 0 \,, \text{ and } \lambda^2 f_5^{'}/\epsilon - \mu f_6 - \lambda^2 f_8 - \delta f_9 = 0 \,.$$

These last two equations are the ODE for this model. The first of these two is exactly the same with that for Parker's Eq. (6.2). But now the rotation term $\sin^{2\epsilon}\theta$ does not allow us to impose polytropic relation between P , ρ. Instead, we have a case with nonconstant γ. This model has been examined in [LTP96] and succeeded to fit the Ulysses observations for the solar wind out of the ecliptic plane.
The subcase $\mu = -1$, $\epsilon = 1$ has been examined in [TT91].

6.4 The solution of Sauty, Trussoni and Tsinganos

Let's start the examination of meridionally self similar non-radial models with the first case of Table 5.1. In this case we have
$g_1 = \alpha$, $g_2 = \lambda^2 \alpha$ and $g_3 = 1 + \delta\alpha$ [4].
So substituting the functions g_1 , g_2 and g_3 in Eq. (5.29) we have

$$A = \frac{B_\star r_\star^2}{2} \alpha \,, \Psi_A = \sqrt{4\pi\rho_\star \left(1 + \delta\alpha\right)} \,,$$

$$\Omega = \frac{\lambda V_\star}{r_\star} \frac{1}{\sqrt{1 + \delta\alpha}} \,, L = \lambda r_\star V_\star \frac{\alpha}{\sqrt{1 + \delta\alpha}} \,,$$

[4] Note that the density on the polar axis cannot be taken equal to zero. But if we choose $g_1 = \frac{\alpha}{1 - \alpha_{ref}}$, $g_2 = \lambda^2\alpha$ and $g_3 = 1 + \delta\left(\alpha - \alpha_{ref}\right)$ then for $\delta\alpha_{ref} = 1$ we have zero density on the axis (the ODE are almost the same; only the constants must be changed).

while from Eqs. (5.19) and (5.22) $P = \frac{B_\star^2}{8\pi}(P_0 + P_1\alpha)$ with

$$P_0 = f_0 + f_1 \text{ and } P_1 = f_4 + f_2 + \lambda^2 (f_3 + f_5) \text{ and}$$
$$f_0^{'} - f_6 - f_9 = 0\,,\ f_4^{'} - f_7 + \lambda^2 \left(f_5^{'} - f_8\right) - \delta f_9 = 0\,.$$

We have two ODE with three unknowns $M^2\,, G^2$ and f_0. So the system is degenerate and we are free to impose a third relation. Up to now, this is done in two different ways [LT86, TL89, HL89, TT91, TS92, TT93, ST94].

6.4.1 The prescribed field-streamline subcase

Trussoni and Tsinganos in [TT91] give explicitly the function $G(R)$, or equivalently their $f(R) \equiv \frac{R^2}{G^2}$. They choose $f(R) \propto 1 + R^2/R_c^2$ in order to have an asymptotically cylindrically collimated outflow.
Note that the denominator in the resulting differential equation for M^2 contains simply the derivative of the function f. A comparison of this equation with Eq. (3.18) shows that the modified by the self similarity slow and fast singular points may appear when the lines are radial, or equivalently when the expansion factor $F \equiv Rf^{'}/f$ vanishes (note that in this case the modified singular points coincides with the points $V_p = V_{s\,,f}$ since at these points the poloidal velocity is radial, normal to the surfaces of constant R). So if one chooses an appropriate function $f(R)$ such that its derivative have two zeros, he will found a solution with three singular points (the Alfvén together with the modified by the self similarity slow and fast magnetosonic points). This can be done, for example, via a function

$$f(R) = 2R_s + 4R_f - 2R_f^2 R_s + R^2 - 2\,(R_s + 2R_f)\,R + 2R_f\,(R_f + 2R_s)\ln R + 2R_f^2 R_s/R$$

with $R_s < 1\,, R_f > 1$. For this function, $f^{'}(R) = 2\frac{(R - R_f)^2\,(R - R_s)}{R^2}$ so the modified slow point is at $R = R_s$ while the fast is at $R = R_f$. The fieldlines are cylindrical at infinity, since $\lim_{R\to\infty} R\frac{f^{'}}{f} = 2 \Leftrightarrow f(R) \overset{R\gg 1}{\propto} R^2 \Leftrightarrow A \overset{R\gg 1}{\propto} \varpi^2$.
There is a closed regime near the stellar surface which ends at $R = R_s$ (in this regime $F < 0$). Note that we can put the stellar surface in a desired position in the domain $0 < R < R_s$. For example in the root of $Rf^{'}/f = -1$ (which corresponds to a dipole like magnetic field $A \propto \sin^2\theta/R$). Fig. 6.6 shows these fieldlines for $R_s = 0.7$ and $R_f = 1.5$.

6.4.2 The free field-streamline subcase

Sauty and Tsinganos in [ST94] imposed a third relation between $P_0\,, P_1$ of the form $P_0 = \Pi$ [5] and $P_1 = \kappa\Pi$. In this case, $P = \frac{B_\star^2}{8\pi}\Pi\,(R)\,(1 + \kappa\alpha)$, so the

[5] A more general form is $P_0 = \Pi + P_{00}$ with constant P_{00}.

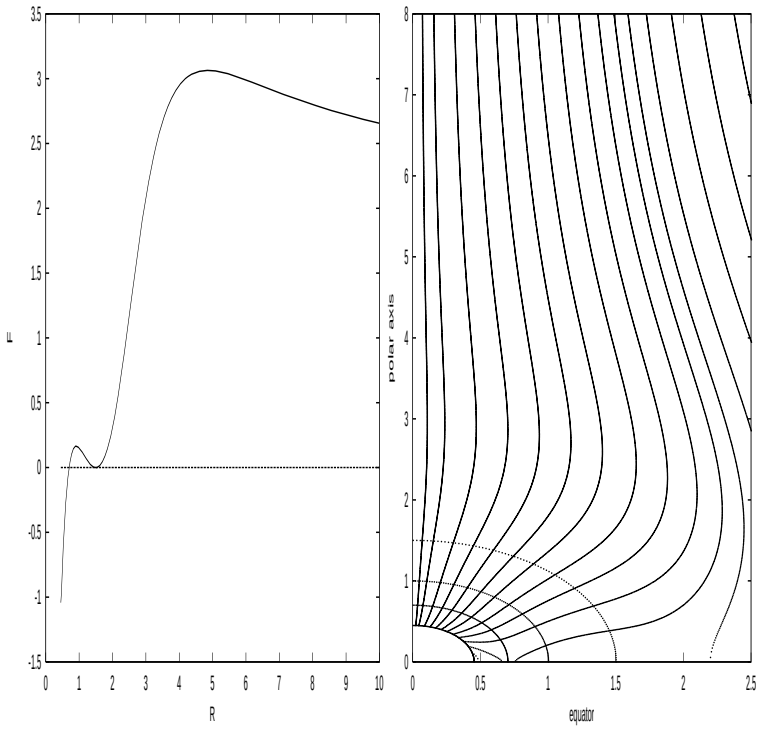

Figure 6.6: The expansion factor and the poloidal streamlines for $R_s = 0.7$ and $R_f = 1.5$.

pressure is a product of function of R times a function of α. If this is the case, there exist a Bernoulli-type integral. The function $\mathcal{S} = V^2/2 + \mathcal{V} - \varpi\Omega B_\phi/\Psi_A$ is written as

$$\mathcal{S} = \frac{V_\star^2}{2}\frac{\mathcal{S}_0(R) + \mathcal{S}_1(R)\,\alpha}{1+\delta\alpha}\ , \text{ while } \frac{\partial P}{\partial R} = \frac{\rho_\star V_\star^2}{2}\left(P_0^{'} + P_1^{'}\alpha\right)\ .$$

Then, the general Bernoulli equation $\partial\mathcal{S}/\partial R + \partial P/\rho\partial R = 0$ gives two equations $\mathcal{S}_i^{'} + M^2 P_i^{'} = 0\ , i = 1,2$. Using $P_0 = \Pi\ , P_1 = \kappa\Pi$ and eliminating Π we get $\mathcal{S}_1^{'} - \kappa\mathcal{S}_0^{'} = 0$, or $\mathcal{S}_1 - \kappa\mathcal{S}_0 =$constant.
After the integration of the ODE, Sauty and Tsinganos found two types of solutions: cylindrically collimated ones with oscillations (jet type solutions) and wind-type solutions (with asymptotically radial lines). They succeed in passing through the modified slow and Alfvén singular points.

6.5 Polytropic radially self similar models

6.5.1 Derivation of the ODEs

In this section we examine the first two cases of Table 5.3. In the first one we have $q_1 = \frac{E_1}{x-2}\alpha^{x-2}\,, q_2 = \frac{D_1}{x-2}\alpha^{x-2}\,, q_3 = \frac{C_1}{x-2}\alpha^{x-2}$. So the free integrals are

$$A = \frac{B_o \varpi_o^2 \sqrt{E_1}}{x}\alpha^{\frac{x}{2}}\,,\ \Psi_A^2 = \frac{C_1 B_o^2 \varpi_o}{\mathcal{GM}}\alpha^{x-3/2}\,,$$
$$\Omega^2 = \frac{D_1 \mathcal{GM}}{\varpi_o^3 C_1}\alpha^{-\frac{3}{2}}\,, L^2 = \frac{D_1 \mathcal{GM}\varpi_o}{C_1}\alpha^{\frac{1}{2}}\,, \tag{6.8}$$

where $\alpha = \frac{R^2}{G^2(\theta)}\sin^2\theta\,, R = r/\varpi_o$ and $B_o\,, \varpi_o$ are constants. As we discuss in Chapter 5, the function $G(\theta)$ measures the cylindrical distance ϖ to the polar axis of each fieldline labeled by α, normalized to its cylindrical distance ϖ_α at the Alfvén point, $G(\theta) = \varpi/\varpi_\alpha$.
The density is $\rho = \frac{\Psi_A^2}{4\pi M^2} = \frac{C_1 B_o^2 \varpi_o}{4\pi \mathcal{GM}}\frac{\alpha^{x-3/2}}{M^2}$ and $M(\theta)$ is the poloidal Alfvén Mach number.
In this case the form of the magnetic field is

$$\vec{B} = B_o\sqrt{E_1}\alpha^{\frac{x}{2}-1}\left\{\frac{1}{G^2}\frac{\sin\theta}{\cos(\pi-\varphi-\theta)}(\cos\varphi\hat{\varpi}+\sin\varphi\hat{z}) + \sqrt{\frac{D_1}{E_1}}\frac{1}{G}\frac{1-G^2}{1-M^2}\hat{\phi}\right\}\,, \tag{6.9}$$

while for the velocity

$$\vec{V} = \sqrt{\frac{E_1\mathcal{GM}}{C_1\varpi_o}}\alpha^{-1/4}\left\{\frac{M^2}{G^2}\frac{\sin\theta}{\cos(\pi-\varphi-\theta)}(\cos\varphi\hat{\varpi}+\sin\varphi\hat{z}) + \sqrt{\frac{D_1}{E_1}}\frac{1}{G}\frac{G^2-M^2}{1-M^2}\hat{\phi}\right\} \tag{6.10}$$

We remind that φ is the angle between the poloidal field-streamline and the equatorial plane. From Eq. (5.62) (see also [VT98]) we have

$h_0^{'} = 0$, and

$$C_1 F h_4 + \frac{C_1}{x-2}h_4^{'} + D_1 h_3 (F-2) + \frac{D_1}{x-2}h_3^{'} + E_1\frac{\left(h_1\left[1-M^2\right]^2\right)^{'}}{1-M^2} + \frac{E_1}{x-2}h_5^{'} = 0 \tag{6.11}$$

where primes indicate derivatives with respect to $\ln(\sin\theta)$. So in this degenerate case we have two equations for the three unknown functions $G\,, M$ and h_0. Choosing $h_0 = 0$ we impose the polytropic relationship, $P \propto \rho^\gamma$ in each fieldline, as the third relationship, or using Eq. (5.59)

$$P = \frac{B_o^2}{8\pi}D_0 E_1 M^{-2\gamma}\alpha^{x-2} \text{ with constant } D_0 \text{ and} \tag{6.12}$$

$$h_5 = D_0\,(x-2)\,M^{-2\gamma} - (x-2)\,h_1 - \frac{D_1}{E_1}\,(x-2)\,h_2 - \frac{D_1}{E_1}h_3 - \frac{C_1}{E_1}h_4\,. \quad (6.13)$$

If we substitute Eq. (6.13) in Eqs. (5.99,6.11) we have two differential equations for the functions G and M. The functions F and φ are related with the derivative of G via Eqs. (5.90),(5.91),(5.92) , so we have three first order differential equations for the functions G,φ and M.
In this polytropic case, there exist the Bernoulli integral

$$\frac{1}{2}V^2 + \frac{\gamma}{\gamma-1}\frac{P}{\rho} + \mathcal{V} - \frac{\Omega r\sin\theta}{\Psi_A}B_\phi = E(A)\,,$$

$$\text{where } \mathcal{V} = -\frac{\mathcal{G}\mathcal{M}}{\varpi_o R} \text{ and } E(A) = \frac{\mathcal{G}\mathcal{M}E_1E_0}{\varpi_o C_1}\alpha^{-1/2}\,, \text{ with constant } E_0\,,$$

or, solving for φ

$$\varphi = \pi - \theta \mp \arctan\left\{\frac{G^4}{M^4\sin^2\theta}\left[2E_0 - \frac{\gamma D_0}{(\gamma-1)\,M^{2(\gamma-1)}} + \right.\right.$$
$$\left.\left.\frac{2C_1\sin\theta}{E_1G} - \frac{D_1}{E_1}\left(\frac{\left(G^2-M^2\right)^2}{G^2\left(1-M^2\right)^2} + 2\frac{1-G^2}{1-M^2}\right)\right] - 1\right\}^{1/2}. \quad (6.14)$$

The upper sign corresponds to the outflow case $V_r > 0$.
The two remaining equations are

$$\frac{dG^2}{d\theta} = \frac{2G^2\cos\varphi}{\sin\theta\cos(\varphi+\theta)}\,, \quad (6.15)$$

$$\frac{dM^2}{d\theta} = -2\frac{\sin(\varphi+\theta)}{\cos(\varphi+\theta)}\left\{-\frac{C_1\sin\theta}{E_1G} - D_0\,(x-2)\,M^{4-2\gamma} + \right.$$
$$\frac{M^4}{G^4}\left(1-M^2\right)\frac{\cos\varphi\sin\theta}{\sin(\varphi+\theta)} - \frac{M^4}{G^4}(x-2)\frac{\sin^2\theta}{\cos^2(\varphi+\theta)} -$$
$$\frac{D_1}{E_1}\frac{M^4}{G^2}(x-2)\left(\frac{1-G^2}{1-M^2}\right)^2 + \frac{D_1}{E_1}\frac{M^2}{G^2}\frac{G^4-M^2}{1-M^2} - \quad (6.16)$$
$$\left.\frac{D_1}{E_1}\frac{\cos\varphi}{\sin\theta\sin(\varphi+\theta)}\frac{\left(2M^2-1\right)G^4 - M^4}{G^2\left(1-M^2\right)}\right\} /$$
$$\left\{\gamma D_0\left(1-M^2\right)M^{-2\gamma} - 2\frac{D_1}{E_1}\frac{M^2}{G^2}\left(\frac{1-G^2}{1-M^2}\right)^2 + 2\frac{M^4\sin^2\theta}{G^4}\left(1 - \frac{1}{M^2\cos^2(\varphi+\theta)}\right)\right\}.$$

The denominator of the last equation equals to,

$$2\frac{M^4\sin^2\theta}{G^4}\frac{V_\theta^4 - V_\theta^2\left(C_s^2+V_A^2\right) + C_s^2V_{A,\theta}^2}{V_\theta^4}\,.$$

Thus we see that at the singular points $V_\theta = V_{s\,,f\,,\theta}$ in agreement with the analysis in Chapter 3.
If we introduce new constants:
$E_1 = \frac{G^4\left(\frac{\pi}{2}\right)}{\alpha_o^{x-2}}, D_1 = \frac{\lambda^2}{\alpha_o^{x-2}}, C_1 = \frac{\mathcal{GM}M^4\left(\frac{\pi}{2}\right)}{\varpi_o V_o^2 \alpha_o^{x-3/2}}, D_0 = \frac{8\pi P_o M^{2\gamma}\left(\frac{\pi}{2}\right)}{B_o^2 G^4\left(\frac{\pi}{2}\right)}$, and
$M^2\left(\frac{\pi}{2}\right) = \frac{4\pi\rho_o V_o^2}{B_o^2}$, we have

$$\rho = \rho_o \left(\frac{\alpha}{\alpha_o}\right)^{x-3/2} \frac{M^2\left(\frac{\pi}{2}\right)}{M^2},\ P = P_o \left(\frac{\alpha}{\alpha_o}\right)^{x-2-\gamma(x-3/2)} \left(\frac{\rho}{\rho_o}\right)^{\gamma},$$

$$\vec{B_p} = B_o \left(\frac{\alpha}{\alpha_o}\right)^{\frac{x}{2}-1} \frac{G^2\left(\frac{\pi}{2}\right)}{G^2} \frac{\sin\theta}{\cos(\pi-\varphi-\theta)} (\sin\varphi\hat{z} + \cos\varphi\hat{\varpi}) =$$

$$= B_o \left(\frac{\alpha}{\alpha_o}\right)^{\frac{x}{2}-1} \frac{G^2\left(\frac{\pi}{2}\right)}{G^2} \sin\theta \left[\tan(\pi-\varphi-\theta)\,\hat{r} - \hat{\theta}\right],$$

$$\vec{V_p} = V_o \left(\frac{\alpha}{\alpha_o}\right)^{-1/4} \frac{G^2\left(\frac{\pi}{2}\right)}{G^2} \frac{M^2}{M^2\left(\frac{\pi}{2}\right)} \frac{\sin\theta}{\cos(\pi-\varphi-\theta)} (\sin\varphi\hat{z} + \cos\varphi\hat{\varpi}) =$$

$$= V_o \left(\frac{\alpha}{\alpha_o}\right)^{-1/4} \frac{G^2\left(\frac{\pi}{2}\right)}{G^2} \frac{M^2}{M^2\left(\frac{\pi}{2}\right)} \sin\theta \left[\tan(\pi-\varphi-\theta)\,\hat{r} - \hat{\theta}\right],$$

$$B_\phi = -\lambda B_o \left(\frac{\alpha}{\alpha_o}\right)^{\frac{x}{2}-1} \frac{1-G^2}{G(1-M^2)},\ V_\phi = \lambda V_o \left(\frac{\alpha}{\alpha_o}\right)^{-1/4} \frac{1}{M^2\left(\frac{\pi}{2}\right)} \frac{G^2-M^2}{G(1-M^2)}.$$

Then $\rho_o\,, P_o\,, B_o\,, V_o$ are the values of $\rho\,, P\,, B_z\,, V_z$ respectively at the point $\alpha = \alpha_o\,, \theta = \frac{\pi}{2}$.
The footpoint of the line α_o on the equator lies at distance $\varpi_o G\left(\frac{\pi}{2}\right)\sqrt{\alpha_o}$ from the axis while the Alfvén point in the same line is at radius $\varpi_o\sqrt{\alpha_o}$. So if we choose $\alpha_o = 1$, then ϖ_o is the radius of the jet at the Alfvén point on the line α_o. If we choose $\alpha_o = \frac{1}{G^2\left(\frac{\pi}{2}\right)}$ then ϖ_o is the radius of the footpoint of the line α_o on the equator.
If the flow begins from the equator with zero poloidal velocity (as in [BP82]), then $V_o = 0\,, M\left(\frac{\pi}{2}\right) = 0$ but the ratio between them is constant. Note that the polytropic second case of Table 5.3 corresponds to the previous equations with $x = 2$.

6.5.2 Other ways of deriving the ODEs

Generally in this radially self similar case we have two relations for the functions of θ:

1. the Bernoulli integral, $f_1\left(\theta\,, M\,, G\,, G'\right) = 0$ and
2. the GSE, $f_2\left(\theta\,, M\,, G\,, G'\,, G''\right) = 0$.

Note that, since the model is self similar, the flux function A does not appear in these two equations.
In order to find the ordinary differential equations (ODEs), one way is to solve

Table 6.1: The notation of [BP82].

[BP82]	our notation
cold	$D_0 = 0$
$V_p\,(z=0)=0$	$M\,(\pi/2)=0$
exactly Keplerian	$\dfrac{C_1}{D_1} = G^3\,(\pi/2)$
3/4	x
r_o	$\varpi_o G\,(\pi/2)\sqrt{\alpha}$
χ	$\dfrac{G\,(\theta)}{G\,(\pi/2)\tan\theta} = z\,(\alpha\,,\theta)\,/\varpi\,(\alpha\,,\pi/2)$
$\xi\,(\chi)$	$\dfrac{G\,(\theta)}{G\,(\pi/2)} = \varpi\,(\alpha\,,\theta)\,/\varpi\,(\alpha\,,\pi/2)$
$\xi^{'}\,(\chi)$	$\dfrac{1}{\tan\varphi}$
λ	$\dfrac{1}{G^2\,(\pi/2)} = \sqrt{\dfrac{D_1}{C_1 G\,(\pi/2)}}$
J	$-\dfrac{G\,(\theta)}{G\,(\pi/2)}\dfrac{\cos\,(\varphi+\theta)}{\sin\theta\sin\varphi}$
$m\,(\chi)$	$M^2\,(\theta)$
$f\,(\chi)$	$-\sqrt{\dfrac{E_1 G\,(\pi/2)}{C_1}}\dfrac{M^2}{G^2}\dfrac{\sin\theta\sin\varphi}{\cos\,(\varphi+\theta)} = V_z\alpha^{1/4}\sqrt{\dfrac{\varpi_o G\,(\pi/2)}{\mathcal{GM}}}$
k	$\Psi_A(A)$
l	$L(A)$
ω	$\Omega(A)$
e	$E(A)$
B_o	$B_o\sqrt{E_1}\dfrac{\alpha^{x/2-1}}{G^2\,(\pi/2)\sin\left[\varphi\,(\theta=\pi/2)\right]}$
κ	$\sqrt{\dfrac{C_1}{E_1}G^3\,(\pi/2)}$
ϵ	$\dfrac{E_1 E_0}{C_1}G\,(\pi/2)$
$\dfrac{B_o^2 r_o}{4\pi\rho\mathcal{GM}}$	$\dfrac{E_1 M^2}{C_1 G^3\,(\pi/2)\sin^2\left[\varphi\,(\theta=\pi/2)\right]}$
μ	$D_0\dfrac{G^4\,(\pi/2)\sin^2\left[\varphi\,(\theta=\pi/2)\right]}{2}\left(\dfrac{E_1}{C_1 G^3\,(\pi/2)\sin^2\left[\varphi\,(\theta=\pi/2)\right]}\right)^{\gamma}$
U	$\dfrac{1}{\sin^2\varphi}$
S	$\dfrac{G\,(\pi/2)}{G\,(\theta)}\sin\theta$
$-3/2$	$\dfrac{E_1 E_0}{C_1}G\,(\pi/2) - \dfrac{1}{G^2\,(\pi/2)}$
g$=\dfrac{\xi-\lambda m/\xi}{1-m}$	$\dfrac{G^2-M^2}{G\,(\pi/2)\,G\,(1-M^2)}$
$n=\dfrac{m}{1+(B_\phi/B_p)^2}$	$\dfrac{M^2}{1+\dfrac{D_1}{E_1}G^2\dfrac{\cos^2\,(\varphi+\theta)}{\sin^2\theta}\left(\dfrac{1-G^2}{1-M^2}\right)^2}$

Table 6.2: The notation of [CL94].

[CL94]	our notation
Ψ	A
F	Ψ_A
H	$-L\Psi_A$
$J-\dfrac{\Omega H}{F}$	E
$J_o-\dfrac{\Omega_o H_o}{F_o}$	$E_0\left[\dfrac{G^6}{\lambda^2}\left(\dfrac{1-M^2}{1-G^2}\right)^2\right]_{\theta=\pi/2}$
a_i	$\varpi_o G(\pi/2)\sqrt{\alpha_o}$
r_Ψ	$\sqrt{\dfrac{\alpha}{\alpha_o}}$
Ψ_o	$\dfrac{B_o\varpi_o^2}{x}\alpha_o G^2(\pi/2)$
B_o	B_o
v_o	$\left(\dfrac{\lambda V_o}{M^2 G}\dfrac{G^2-M^2}{1-M^2}\right)_{\theta=\pi/2}$
F_o	$\lambda\left(\dfrac{G^2-M^2}{G(1-M^2)}\right)_{\theta=\pi/2}$
Γ	γ
x	x
H_o	$-\dfrac{\lambda}{G(\pi/2)}$
Ω_o	$\left(G^2\dfrac{1-M^2}{G^2-M^2}\right)_{\theta=\pi/2}$
J_o	$\left[\dfrac{G^2}{\lambda^2}\left(\dfrac{1-M^2}{G^2-M^2}\right)^2\left(E_0G^4-\lambda^2\right)\right]_{\theta=\pi/2}$
$\delta_o=\dfrac{\mathcal{GM}}{a_i v_o^2}$	$\dfrac{\mathcal{GM}}{\varpi_o V_o^2\sqrt{\alpha_o}}\left[\dfrac{M^4G}{\lambda^2}\left(\dfrac{1-M^2}{G^2-M^2}\right)^2\right]_{\theta=\pi/2}=\dfrac{C_1}{E_1}\left[\dfrac{G^5}{\lambda^2}\left(\dfrac{1-M^2}{G^2-M^2}\right)^2\right]_{\theta=\pi/2}$
$v_o\dfrac{1-\Omega_o}{H_o+F_o}$	V_o
$\mathcal{K}$	$\dfrac{P_o}{B_o^2}\left[\dfrac{4\pi M^2G^2}{\lambda^2}\left(\dfrac{1-M^2}{G^2-M^2}\right)^2\right]^\gamma_{\theta=\pi/2}=\dfrac{D_0G^4(\pi/2)}{8\pi}\left[\dfrac{4\pi G^2}{\lambda^2}\left(\dfrac{1-M^2}{G^2-M^2}\right)^2\right]^\gamma_{\theta=\pi/2}$
$V_z\,(Z=0)$	$\left[\dfrac{M^2G}{\lambda}\dfrac{1-M^2}{G^2-M^2}\right]_{\theta=\pi/2}$

Table 6.3: The notation of [Ost97].

[Ost97]	our notation
cold	$D_0 = 0$
$V_p(z=0) = 0$	$M(\pi/2) = 0$
exactly Keplerian, $\mathcal{GM}/\Omega_1 R_0^3 = 1$	$\frac{C_1}{D_1} = G^3(\pi/2)$
$\mathbf{\Phi}$	A
β	$4\pi/\Psi_A$
J	L
$\mathcal{E}$	$E - L\Omega$
$\frac{3-q}{2}$	x
R_0/R_A	$G(\pi/2)$
R_1/R_A	$G(0)$
$j = (R_A/R_1)^2$	$1/G^2(0)$
$e = \frac{3}{2}(R_0/R_1)^2$	$\frac{3}{2}[G(\pi/2)/G(0)]^2$
$R/R_A = (\phi(\theta)/\phi(\theta_\star))^{\frac{2}{q-3}}$	$G(\theta) = \varpi/\varpi_\alpha$
$R = (\phi(\theta)\mathbf{\Phi}_1/\mathbf{\Phi})^{\frac{2}{q-3}} R_1$	ϖ
$2 - \frac{4}{q-3}\frac{\phi'}{\phi}\tan\theta$	F
R_A	ϖ_α
M_A	M

the Bernoulli integral for $G^{'}$ and substituting this in the GSE to yield $M^{'}$. Then we have a system of two first order ODE. We have followed this method in the previous analysis (see also [BP82, CL94]).
Another way is to use the Bernoulli integral in order to find at each point of the solution the value of M (knowing $G\,,G^{'}$ at this point), while substituting M on the GSE we get a second order ODE for G. This method followed in [Ost97].

6.5.3 Alfvén singularity

At the Alfvén angle $\theta_\star$, using the L'Hospital's rule,

$$\left(\frac{1-G^2}{1-M^2}\right)_\star \overset{0/0}{=} \frac{2\cos\varphi_\star}{p_\star \sin\theta_\star \cos\left(\varphi_\star+\theta_\star\right)}\,,$$

where $p_\star$ is the slope of the square of the Alfvén number $p_\star = \left(dM^2/d\theta\right)_\star$. So from Eq. (5.68), (or from Eq. (6.16) at $\theta=\theta_\star$) we find the Alfvén regularity condition

$$\begin{aligned}
&(x-2)\left(\frac{4D_1}{E_1}+p_\star^2\sin^2\theta_\star\right)\tan^2\left(\varphi_\star+\theta_\star\right)+\\
&\left(p_\star^3\sin^2\theta_\star+\tfrac{4D_1}{E_1}p_\star+\frac{8D_1\left(x-2\right)}{E_1\tan\theta_\star}\right)\tan\left(\varphi_\star+\theta_\star\right)+\\
&(x-2)\left(D_0p_\star^2+p_\star^2\sin^2\theta_\star+\frac{4D_1}{E_1\tan^2\theta_\star}\right)+\frac{C_1}{E_1}p_\star^2\sin\theta_\star-\frac{D_1}{E_1}p_\star\left(p_\star-\frac{4}{\tan\theta_\star}\right)=0
\end{aligned} \tag{6.17}$$

6.5.4 About the criterion $\varphi\left(\theta=\pi/2\right)<60^o$

The Bernoulli integral can be written as

$$E-L\Omega=\frac{V_p^2}{2}+\frac{\left(V_\phi-\varpi\Omega\right)^2}{2}+\frac{\gamma}{\gamma-1}\frac{P}{\rho}+\mathcal{V}-\frac{1}{2}\varpi^2\Omega^2$$

or, after substituting all the quantities (when the flux function disappears)

$$E_1E_0-D_1=\frac{E_1M^4\sin^2\theta}{2G^4\cos^2\left(\pi-\varphi-\theta\right)}+\frac{D_1M^4}{2G^2}\left(\frac{1-G^2}{1-M^2}\right)^2+\frac{\gamma}{\gamma-1}\frac{D_0E_1}{2M^{2(\gamma-1)}}-\frac{C_1\sin\theta}{G}-\frac{D_1G^2}{2}\,.$$

Assume cold plasma ($D_0=0$) and $V_p\left(\theta=\pi/2\right)=0$, or $M\left(\pi/2\right)=0$. Then the constant $E_1E_0-D_1$ can be determined at $\theta=\pi/2$:

$$E_1E_0-D_1=-\frac{C_1}{G\left(\pi/2\right)}-\frac{D_1G^2\left(\pi/2\right)}{2}\,.$$

So at each θ we have

$$f\left(\theta\right)\equiv C_1\left[\frac{\sin\theta}{G}-\frac{1}{G\left(\pi/2\right)}\right]+\frac{D_1}{2}\left[G^2-G^2\left(\pi/2\right)\right]=$$

$$\frac{E_1 M^4 \sin^2\theta}{2G^4\cos^2(\pi-\varphi-\theta)}+\frac{D_1 M^4}{2G^2}\left(\frac{1-G^2}{1-M^2}\right)^2 .$$

The RHS of this last equation is positive, for any $\theta\in(0\,,\pi/2)$. So the function $f(\theta)$ must be positive too, $f(\theta)>0$.
For values of θ close to $\pi/2$ we have (using Eq. (6.15) we find the Taylor expansion up to the first order) $f(\theta)\approx f^{'}(\pi/2)(\theta-\pi/2)$, with $f^{'}(\pi/2)=\left[C_1-D_1G^3(\pi/2)\right]/G(\pi/2)\tan\left[\varphi(\pi/2)\right]$. Since $\theta-\pi/2<0$, this derivative must be negative (if it is nonzero). Equivalently $\left(V_\phi^2/\frac{\mathcal{GM}}{r}\right)_{\theta=\pi/2}>1$. The rotation (if it is not Keplerian) must be superKeplerian on the equatorial plane. This happens if $f^{'}(\pi/2)\neq 0$.
If on the other hand the rotation is exactly Keplerian, when $C_1=D_1G^3(\pi/2)$, we must expand $f(\theta)$ up to the second order. We have

$$f^{'}(\theta)=\frac{C_1\cos\theta}{G}+\frac{\cos\varphi\left[D_1G^3-C_1\sin\theta\right]}{G\sin\theta\cos(\varphi+\theta)}\ \text{and}\ f^{''}(\pi/2)=-\frac{C_1}{G(\pi/2)}+\frac{3D_1G^2(\pi/2)}{\tan^2\left[\varphi(\pi/2)\right]}.$$

Since $f(\theta)\approx f^{''}(\pi/2)(\theta-\pi/2)^2$ must be positive, $f^{''}(\pi/2)>0$, or using $C_1=D_1G^3(\pi/2)$, $\varphi(\pi/2)<60^o$. [6]
This criterion is valid only if the plasma is cold and begin with Keplerian velocity from the equatorial plane. If the velocity is not Keplerian, then we found that the only possible case for the acceleration of a cold plasma is to have superKeplerian rotation.
Of course, if the pressure is not negligible, we can find a smallest value for the pressure gradient in order to have acceleration in any case. However, thermal effects are important near the disk surface [7].

6.5.5 [BP82]

Blandford and Payne in [BP82] examined the acceleration of a cold plasma, [7] rotating on the equatorial plane with a Keplerian speed. Their equations correspond to the previous analysis with $x=3/4$. As a consequence, there exist only two singular points: the Alfvén and the modified fast point (for $C_s=0$, the slow point disappears while on the fast $V_\theta^2=V_A^2$, since the roots of $V_{s,f\,,\,\theta}^4-V_{s,f\,,\,\theta}^2\left(C_s^2+V_A^2\right)+C_s^2V_{A\,,\theta}^2=0$, when $C_s=0$, are simply $V_{s,\,\,\theta}^2=0\,,V_{f,\,\,\theta}^2=V_A^2$).
In this case the flow begins from the equatorial plane (i.e., the disk) with zero poloidal velocity (while for the toroidal component $V_\phi^2=\mathcal{GM}/r$). Equivalently, $M(\pi/2)=0$ and $\lim_{\theta\to\pi/2}\rho=\infty$.
They found two types of solutions:

[6] For relativistic flows there exist again an upper bound for the angle φ, at each point of the disk, i.e., $\varphi<\varphi_{max}(\alpha)$ [Cao97].

[7] Blandford and Payne appreciated that their model of a "cold" wind does not properly describe the flow in the neighborhood of the surface of the disk, where thermal effects must become impotrtant. See also [OL98].

1. Solutions which are elliptic everywhere and the conical surface $V_p = V_f$ is reached by the plasma at infinite heights above the disk (at $\theta = 0$).

2. Solutions which have the surface $V_p = V_f$ at a finite angle. They analyzed this case numerically. A limiting characteristic then exist at some angle above the line $V_p = V_f$, (at a smaller angle), but they did not succeeded to pass the solution through this. Note that if a solution passes through this point, it must pass it again, because from the construction of the model $\lim_{\theta \to 0} V_\theta / V_A = 0$).
   They found a turning point in these solutions (wich we will discuss later) and stopped the solution before reaching it.

The procedure for constructing a solution is to solve the Bernoulli integral for f (or equivalently for V_z) and then substitute it in the GSE to yield $dm/d\chi$ (or $dM^2/d\theta$). Among their main results is to explicitly show that the real singular points are not the points where the poloidal flow speed is equal with the poloidal phase velocity of MHD waves but the points where the components of the previous velocities normal to the direction of symmetries are equal. In the r- self similar models this means for the Alfvén that: $V_\theta = V_{A,\theta}$ (which however is the same with $V_p = V_{A,p}$) and for the slow-fast that $V_\theta = V_{s,f,\theta}$.

6.5.6 [CL94]

Contopoulos and Lovelace in [CL94] examined the generalization of the Blandford and Payne model introducing the exponent x which is not always equal to 3/4 including the pressure in the solution. They found three kinds of solutions (see Fig. 2 in [CL94]) [8]

- $x_{crit} < x < 1$: with parabolic asymptotical geometry
- $x < x_{crit}$: recollimated solutions
- $x > 1$: the magnetic tension is always inward (the jet carries a nonzero axial current) and the flow recollimates. They found oscillating solutions with cylindrical asymptotical geometry.

Nevertheless we found that if we continue the integration at larger heights (small enough values of θ), the solution always has one of the following problems:

1. reaches again the Alfvén point $M = 1, G = 1$
2. hits the modified fast singular point and it is needed to change the initial conditions until it is passed
3. reach a point where $V_r = 0$ (a turning point). Note that the exact position of this point depends on how we use the Bernoulli integral. If we solve for V_r, the turning point occurs when $V_r = 0$. Above this point we must

[8] See also [RP94]. In this paper, the parameter β is used instead of our exponent x.

change sign in V_r and continue the integration (see Eq. (6.14). If we solve for V_z, it occurs when $V_z = 0$. One can overpass this technical problem using the differential form of the Bernoulli equation, but the solution is anyway unphysical.

6.5.7 Asymptotic analysis for the oscillating solution $x > 1$

Assume that we have a cylindrically collimated solution at infinity. Then $\lim_{\theta \to 0} G = G_\infty$, so $\lim_{\theta \to 0} A = A_\infty(\varpi) \propto (\varpi/G_\infty)^x$. Before the solution reaches this exactly cylindrical stage, we have

$$A \propto (\varpi/G(\theta))^x \approx (\varpi/G_\infty)^x (1 + g(\theta))$$

where $g = x(1 - G/G_\infty)$, with $\mid g \mid \ll 1$.
Following the analysis of Chapter 4 (see also [VT97]) we see that Eq. (4.73) with f =constant holds. As explained there, the solution is of the form

$$g = D\theta^{-\nu} \cos(\mid \mu \mid \ln\theta + D_0) \Leftrightarrow g = D(\varpi/z)^{-\nu} \cos\left(\mid \mu \mid \ln\frac{\varpi}{z} + D_0\right). \tag{6.18}$$

After substituting this in Eq. (4.73), we find the relation of the free functions A, Ψ_A, L, Ω with the constants ν, μ. Long calculations find that

$$\nu = x - 1. \tag{6.19}$$

But in this case, $x > 1 \Leftrightarrow \nu > 0$, and the amplitude of the oscillations grows as a power of $1/\theta$. Then the function g and consequently the functions G, M together with their derivatives have no limit as $\theta \to 0$. The analysis of [HN89] has no relation with these solutions, since the limits which are discussed there do not appear here. We can see that as this function grows, the functions G, M will reach the values $G = 1, M = 1$, thus the solution hits again an Alfvén point. It is remarkable that this may happens at very small values of θ, so one can argue that the solution is not self similar there, or it has already connected to the interstellar medium (ISM). We remind however that without passing the limiting characteristic it will be unstable to perturbations at infinity. Note that numerical results verifies the previous analysis although (as we have prove) the function g is not small at all.

6.5.8 [Ostr97]

Ostriker [Ost97] examined the cold case with $x > 1$, i.e., with cylindrical asymptotics. The integration began upstream from infinity ($\theta = 0$) and found non oscillating solutions which pass only from the Alfvén critical point and reach the equator (the disk) with zero poloidal velocity and exactly Keplerian toroidal velocity. (The Bernoulli integral was used in order to find the value of M and then solve a second order ODE for G).
After the previous asymptotic analysis we can understand why these solutions

were obtained. As we have said, when $x > 1$, the form of the perturbations is given by Eq. (6.18). But then the function g and its derivative has no limit at $\theta = 0$ unless $D = 0$. Assuming that at $\theta = 0$ the function g has a real value as it was assumed in order to begin the integration from infinity, it is equivalent with choosing $D = 0$. So, the first deviation for the cylinder is of order $\sin\theta \approx \theta$, or of the order of the gravitational potential (this is effectively what happens when the integration starts from infinity, see the paragraph A2 in Appendix of [Ost97]).

6.5.9 A solution which pass from all singular points

The main difficulty in finding exact MHD solutions is the appearance of singular points. Although we have assumed self similarity (so we have to solve ODEs) the problem is still highly intractable. The right solution should pass through the SMSS (if the outflow starts from the stellar surface or the disk with subslow velocity), the AS and finally the FMSS (for details see Chapter 3). The last two singular points are very important and the solution must pass through them because

- at infinity we want the solution to carry small magnetic fields and has large velocities (so $M_\infty > 1$), while on the disk or stellar surface the opposite holds ($M(\pi/2) \ll 1$). Thus at some $\theta = \theta_\star$, $M(\theta_\star) = 1$.
- as we discuss in Chapter 3 in order to connect the solution to the ISM with a fast shock (only then a small disturbance at infinity does not affect the solution upstream from this shock), the solution must be superfast at some distance beyond the Alfvén surface.

In the AS we know the regularity condition, Eq. (6.17). Also at the modified by the self similarity slow and fast singular points we know that the numerator of $dM^2/d\theta$ vanishes (simultaneously with the denominator). But the position of these singular points is not known a-priori. So we know only some relations between functions at some points. That can not help us much. It remains the shooting method. We start the integration from a point $\theta = \theta_i$ and continue until the solution hits a singular point (for example the modified fast, or FMSS). That is to say, we see that the numerator (or denominator) in $dM^2/d\theta$ vanishes, but not the denominator (or numerator). We go back in $\theta = \theta_i$, change one parameter and integrate again. We use this algorithm until it converges, i.e., the numerator and the denominator simultaneously vanish. We do the same for passing through the other singular points.
Until now all researchers who have tried to integrate the equations of this model, start their integration from the equator [BP82, CL94], or, from infinity [Ost97], and they have not succeed in passing through all singular points.
We propose that it is easier to start the integration from one of these critical points. For example, let us start from the Alfvén surface (AS). This surface is the cone $\theta = \theta_\star$. We give the parameters $\theta_\star$, x, γ, C_1/E_1, $\varphi_\star$, D_1/E_1, $p_\star$. As we see later, we use the last two parameters for passing through the SMSS and FMSS

singular surfaces (points in self similar models). From the Alfvén regularity condition Eq. (6.17) we calculate the constant D_0 (it must be positive). From the Bernoulli integral Eq. (6.14) we calculate E_0 (the ratio $\left(1-G^2\right)/\left(1-M^2\right)$ can be found using L' Hospital's rule). We start the integration upstream from the Alfvén point. We encounter the SMSS but we can't pass through it. For example the numerator of $dM^2/d\theta$ vanishes but not the denominator. We go back on the Alfvén point, change the parameter $p_\star$ and integrate again, until we find the opposite behaviour on the SMSS (the denominator vanishes but not the numerator). With fine tuning in the value of $p_\star$ we find the solution which pass the SMSS.
Now we integrate downstream from the Alfvén point. We encounter the FMSS but we can't cross it. We go back at the AS, change the parameter D_1/E_1 and integrate upstream. After some iterations we find the right value of $p_\star$ for passing through the SMSS. Then we integrate downstream from the AS. We do the same until we find the right value for the pair $p_\star\,, D_1/E_1$. Then we have the solution which begins subslow from the disk, cross the SMSS, the AS and the FMSS. After crossing the FMSS we stop the solution at some angle θ, because if we continue the integration, the solution will find another modified fast point, in order to be subfast at $\theta = 0$ (from the construction of this model, $\lim\limits_{\theta\to 0}\dfrac{V_\theta}{V_{f\,,\theta}} = 0$).

Such a solution is shown in Figs. 6.7,6.8.
With this method of integration (i.e. begining from the AS) the solution itself finds the correct values of all quantities at $\theta = 0$ and $\theta = \pi/2$. These values are functions of the parameters $\theta_\star\,, x\,, \gamma\,, C_1/E_1\,, \varphi_\star$.
Note that, such a solution can be found without the self similar ansatz. We can integrate the system of the MHD, PDE, beginning from a cone $\theta = \theta_i$. On this boundary we 'll give the conditions $A \propto r^x$, the normal derivative $dA/d\theta \propto r^x$ and the free functions $\Psi_A\,, L\,, \Omega\,, Q\,, E$ as functions of A. These boundary conditions together with $E_\phi = 0$ determine the unique solution of the problem (as we discuss it in Chapter 3). Thus, one may test any numerical code which solves the steady state axisymmetric MHD equations with the previous, self similar solution.
After finding this solution, one should connect it with the ISM through a fast MHD shock, but we have not done this yet.

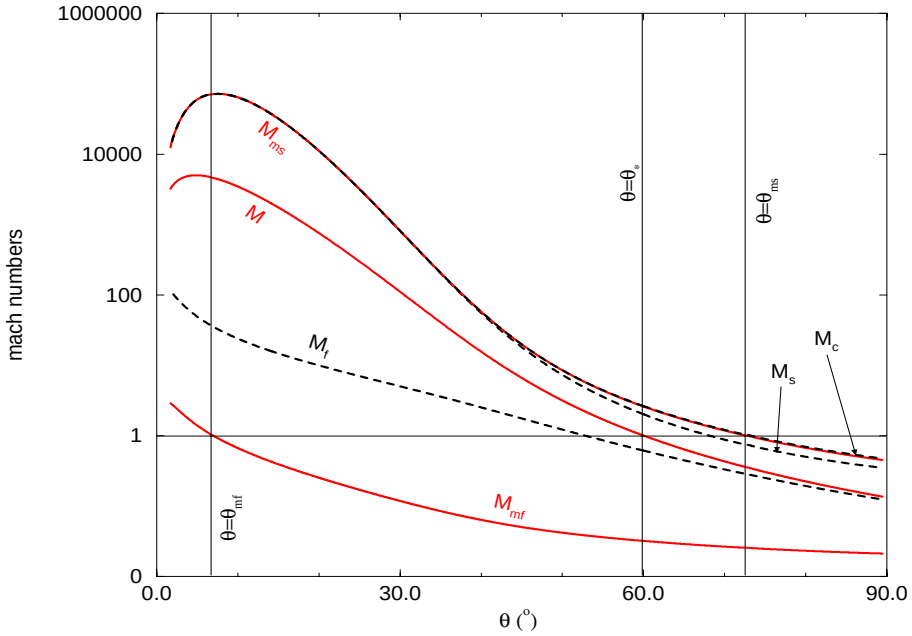

Figure 6.7: The various Mach numbers for the polytropic radially self similar model and parameters $x = 3/4\,, \theta_\star = 60^o\,, \gamma = 5/3\,, C_1/E_1 = 15\,, \varphi_\star = 45^o$. From the Bernoulli integral at the Alfvén point we find $E_0 = 9.44868687$, from the Alfvén regularity condition $D_0 = 10.923935115$ while the parameters which are determined such that the solution passes through the SMSS and FMSS are $D_1/E_1 = 2.793464953\,, p_\star = -5.57440185546875$.

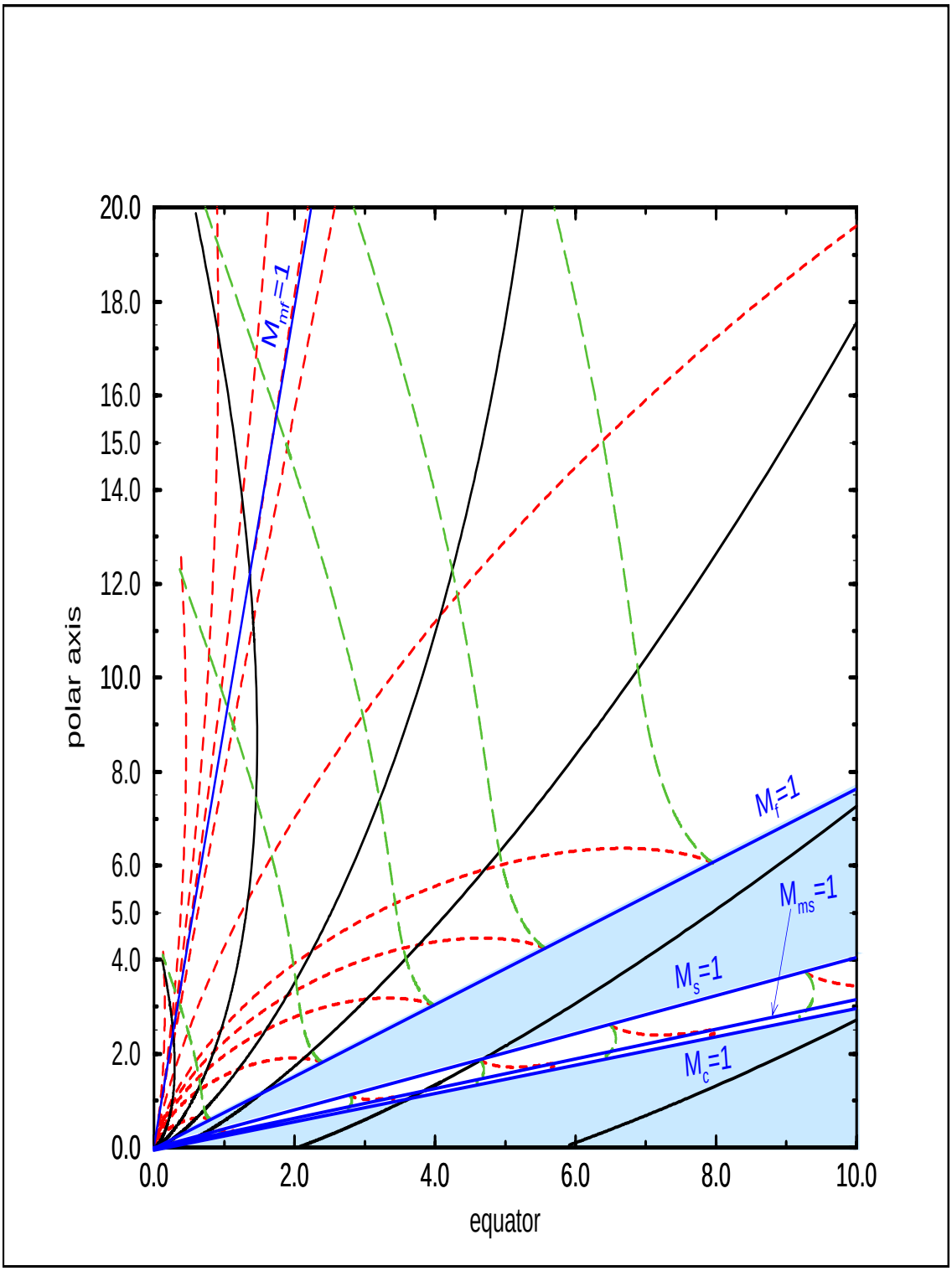

Figure 6.8: The fieldlines (solid lines) and the characteristics (dashed and long dashed lines). We see the limiting characteristics $M_{ms} \equiv V_\theta / V_{s\ \theta} = 1$, $M_{mf} \equiv V_\theta / V_{f\ \theta} = 1$ and the surfaces where the solution changes character from elliptic to hyperbolic and vice-versa $M_c \equiv V_p / V_c = 1$, $M_s \equiv V_p / V_s = 1$, $M_f \equiv V_p / V_f = 1$. In the shadowed region the governing partial differential equations are of elliptic type and no characteristics exist.

Bibliography

[BM76] J. W. Belcher and K. B. MacGregor, apj **210** (1976), 498.

[BP82] R.D. Blandford and D.G. Payne, MNRAS **199** (1982), 883.

[Cao97] X. Cao, MNRAS **291** (1997), 145.

[CL94] J. Contopoulos and R.V.E. Lovelace, ApJ **429** (1994), 139.

[Hey96] J. Heyvaerts, *in Plasma Astrophysics, (EADN Astrophysics School VII, San Miniato, Italy 1994)*, C. Ghiuderi & G. Einaudi (Eds.), Springer, p. 31, 1996.

[HL89] Y.Q. Hu and B.C. Low, ApJ **342** (1989), 1049.

[HN89] J. Heyvaerts and C.A. Norman, ApJ **347** (1989), 1055.

[LT86] B.C. Low and K. Tsinganos, ApJ **302** (1986), 163.

[LTP96] J. Lima, K. Tsinganos, and E. Priest, Astrophys. Letts. and Comms. **34** (1996), 281.

[Mic69] F. C. Michel, ApJ **158** (1969), 727.

[OL98] G. I. Ogilvie and M. Livio, ApJ **499** (1998), 329.

[Ost97] E. C. Ostriker, ApJ **486** (1997), 306.

[Par63] E.N. Parker, *in: Interplanetary Dynamical Processes*, Interscience Publishers, New York, 1963.

[RP94] F. Rosso and G. Pelletier, A&A **287** (1994), 325.

[ST94] C. Sauty and K. Tsinganos, A&A **287** (1994), 893.

[TL89] K. Tsinganos and B.C. Low, ApJ **342** (1989), 1028.

[TS92] K. Tsinganos and C. Sauty, A&A **257** (1992), 790.

[TT91] K. Tsinganos and E. Trussoni, A&A **249** (1991), 156.

[TT93] E. Trussoni and K. Tsinganos, A&A **269** (1993), 589.

[VT97] N. Vlahakis and K. Tsinganos, MNRAS **292** (1997), 591.

[VT98] N. Vlahakis and K. Tsinganos, MNRAS **298** (1998), 777.

[WD67] E.J. Weber and L.J. Davis, ApJ **148** (1967), 217.

Chapter 7

A class of exact MHD models for astrophysical jets

This Chapter examines a new class of exact and self-consistent MHD solutions which describe steady and axisymmetric hydromagnetic outflows from the magnetized atmosphere of a rotating gravitating central object with possibly an orbiting accretion disk. [1] The plasma is driven by a thermal pressure gradient, as well as by magnetic rotator and radiative forces. At the Alfvénic and fast critical points the appropriate criticality conditions are applied. The outflows start almost radially but after the Alfvén transition and before the fast critical surface is encountered the magnetic pinching force bends the poloidal streamlines into a cylindrical jet-type shape. The terminal speed, Alfvén number, cross-sectional area of the jet, as well as its final pressure and density obtain uniform values at large distances from the source. The goal of the study is to give an analytical discussion of the two-dimensional interplay of the thermal pressure gradient, gravitational, Lorentz and inertial forces in accelerating and collimating an MHD flow. A parametric study of the model is given, as well as a brief sketch of its applicability to a self-consistent modeling of collimated outflows from various astrophysical objects. For example, the obtained characteristics of the collimated outflow in agreement with those in jets associated with YSO's.

7.1 Introduction

Collimated outflows are ubiquitous in astrophysics and cosmic jets are observed in the radio, infrared, optical, UV and X-ray parts of the spectrum, from the

[1] This class of models is similar with the case (2) of Table 5.1, with the exception of including here a radiative force.

ground and space, most recently via the Hubble Space Telescope. Classes of objects in association with which jets are observed include young stellar objects [Ray96], old mass losing stars and planetary nebulae [Liv97], black hole X-ray transients [MR96], supersoft X-ray sources [KT96], high-mass X-ray binaries and cataclysmic variables [SLSC97] and many AGN and quasars [Bir96, FMBR96]. Despite their observed abundance however, several key questions on their acceleration and collimation among others, have not been resolved yet.

The theoretical MHD modeling of jets is not a simple undertaking, basically due to the fact that the set of the MHD equations is highly nonlinear with singular (or critical) points appearing in their domain of solutions; these singularities - through which a physical solution inevitably will have to pass - are not known a *priori* but they are determined only simultaneously with the complete solution. The purpose of the present study is to construct systematically a self-consistent MHD model for astrophysical jets where the interplay of the various forces acting on the plasma and which are able to accelerate and collimates the outflow, is analytically examined. This modeling is an improvement over the very few existing models developed so far to the same goal. For example, it is fully 2-dimensional (*c.f.* Parker 1958 [Par58], Weber & Davis 1967 [WD67]), it does not contain singularities along the symmetry axis and the outflow is not overfocused but extends to large distances (*e.g.* [BP82, Ost97], the equation of state is not constrained by the artificial polytropic assumption (as *e.g.* in [CL94, HN89]), the thermal pressure is meridionally anisotropic (*e.g.* [ST94]), the shape of the jet is self-consistently determined (*e.g.* [TTS97]), there is a steady asymptotic state (*c.f.* [US85, OP97a, OP97b, GWB97], etc).

In the following Sec. 7.2 the basic steps for the systematic construction of this class of models are described. Then in Sec. 7.3 we discuss the critical surfaces in the solution domain and in Sec, 7.4 the asymptotic behaviour of the solution. In Sec. 7.5 we discuss about the integration of the resulting equations (in relation with the boundaries and the singular points). A detailed parametric study of the model is given in Sec. 7.6 while in the last Sec. 7.7 the connection of the dimensionless parameters characterizing the present model to the observable physical quantities of collimated outflows is sketched.

7.2 Construction of the model

In this section we describe in some detail how our model can be systematically obtained from the closed set of the governing MHD equations.

7.2.1 Governing equations

The *kinematics* of astrophysical outflows may be described to zeroth order by the well known set of the steady ($\partial/\partial t = 0$) ideal hydromagnetic equations:

$$\rho\left(\vec{V}\cdot\vec{\nabla}\right)\vec{V}=\frac{\left(\vec{\nabla}\times\vec{B}\right)\times\vec{B}}{4\pi}-\vec{\nabla}P-\rho\vec{\nabla}\mathcal{V}+\vec{F}_{rad}\,, \tag{7.1}$$

$$\vec{\nabla}\cdot\vec{B}=0\,,\quad \vec{\nabla}\cdot\left(\rho\vec{V}\right)=0\,,\quad \vec{\nabla}\times\left(\vec{V}\times\vec{B}\right)=0\,, \tag{7.2}$$

where $\vec{B}$, $\vec{V}$, $-\vec{\nabla}\mathcal{V}=-\vec{\nabla}\left(-\mathcal{GM}/r\right)$ denote the magnetic, velocity and external gravity fields, respectively, $\vec{F}_{rad}$ the volumetric force of radiation while ρ and P the gas density and pressure.
The *energetics* of the outflow on the other hand is governed by the first law of thermodynamics :

$$q=\rho\vec{V}\cdot\left[\vec{\nabla}\left(\frac{1}{\Gamma-1}\frac{P}{\rho}\right)+P\vec{\nabla}\frac{1}{\rho}\right]\,,\ \text{or} \tag{7.3}$$

$$q=\rho\vec{V}\cdot\left[\vec{\nabla}\left(\frac{\Gamma}{\Gamma-1}\frac{P}{\rho}\right)-\frac{1}{\rho}\vec{\nabla}P\right]=\frac{\rho^{\Gamma}}{\Gamma-1}\vec{V}\cdot\vec{\nabla}\left(\frac{P}{\rho^{\Gamma}}\right)\,,$$

where q is the volumetric rate of net energy input/output [LT86], while $\Gamma=c_p/c_v$ with c_p and c_v the specific heats for an ideal gas.
With axisymmetry in spherical coordinates (r,θ,ϕ), the azimuthal angle ϕ is ignorable ($\partial/\partial\phi=0$) and we may introduce the poloidal magnetic flux function $A(r,\theta)$, such that three free integrals of A exist. They are the total specific angular momentum carried by the flow and magnetic field, $L(A)$, the corotation angular velocity of each streamline at the base of the flow, $\Omega(A)$ and the ratio of the mass and magnetic fluxes, $\Psi_A(A)$ [Tsi82].
From Stoke's theorem wee have,

$$F_{mag}=\iint\limits_S\vec{B}_p\cdot d\vec{S}=\iint\limits_S\vec{\nabla}\times\left(A\frac{\hat{\phi}}{\varpi}\right)\cdot d\vec{S}=\oint\limits_c A\frac{\hat{\phi}}{\varpi}\cdot\left(\varpi d\phi\hat{\phi}\right)=2\pi A_{out}\,.$$

The mass loss rate from both hemispheres is

$$\dot{\mathcal{M}}=2\iint\limits_S\rho\vec{V}_p\cdot d\vec{S}=\int\limits_0^{A_{out}}\Psi_A\,dA=\Psi\left(A_{out}\right)$$

(although we have a steady state, $\partial\mathcal{M}/\partial t\neq 0$ since the comoving derivative is zero

$$\frac{d\mathcal{M}}{dt}=0\Leftrightarrow\frac{\partial\mathcal{M}}{\partial t}+\vec{V}\cdot\vec{\nabla}\mathcal{M}=0\ \text{with}\ \frac{\partial\mathcal{M}}{\partial t}=-\dot{\mathcal{M}})\,.$$

The total angular momentum loss rate from each hemisphere is

$$\dot{\mathcal{J}}=\iint\limits_S L\rho\vec{V}_p\cdot d\vec{S}=\frac{1}{2}\int\limits_0^A L\Psi_A\,dA\,.$$

The system of Eqs. (7.1) - (7.2) reduces now to a set of two partial and nonlinear differential equations, i.e., the r- and θ- components of the momentum equation on the poloidal plane. Note that by using the projection of the momentum equation along a stream-field line $A = const$ on the poloidal plane (r, θ), Eq. (7.3) becomes,

$$\rho \vec{V} \cdot \vec{\nabla} \left(\frac{1}{2} V^2 + \frac{\Gamma}{\Gamma - 1} \frac{P}{\rho} + \mathcal{V} - \frac{\Omega r \sin\theta}{\Psi_A} B_\phi \right) - \vec{V} \cdot \vec{F}_{rad} = q \, . \qquad (7.4)$$

For a given set of the integrals $L(A)$, $\Omega(A)$ and $\Psi(A)$, equations (7.1) - (7.2) - (7.3) could be solved to give $\rho(r, \theta)$, $P(r, \theta)$ and $A(r, \theta)$, if the heating function $q(r, \theta)$ and the radiation force $\vec{F}_{rad}$ are known. Similarly, one may close the system of Eqs. (7.1) - (7.2) - (7.3), if a functional relation of q with the unknowns ρ, P and A exists. As an example, consider the following special functional relation of q with the unknowns ρ, P and A [TTS92],

$$q = \frac{\gamma - \Gamma}{\Gamma - 1} \frac{P}{\rho} \vec{V} \cdot \vec{\nabla} \rho \, , \qquad (7.5)$$

where $\gamma \leq \Gamma$. Then, Eq. (7.3) can be integrated at once to give the familiar polytropic relation between P and ρ,

$$P = Q\,(A)\, \rho^\gamma \, , \qquad (7.6)$$

for some function $Q(A)$ corresponding to the enthalpy along a poloidal surface $A = const$. In this special case we can integrate the projection of the momentum equation along a stream-field line $A = const$ on the poloidal plane, Eq. (7.4) by further assuming that $\vec{V} \cdot \vec{F}_{rad} = 0$, to get the well known Bernoulli integral [2] which subsequently can be combined with the component of the momentum equation across the poloidal fieldlines (the transfield equation) to yield ρ and A. After finding a solution, one may go back to Eq. (7.3) and fully determine the function $q(r, \theta)$. It is evident that even in this special polytropic case with $\gamma \neq \Gamma$ the heating function q (not its functional form but the function $q(r, \theta)$ itself) can be found only *a posteriori*. Note that for $\gamma = \Gamma$ and only then the flow is isentropic.

Evidently, it is not possible to integrate Eq. (7.3) for *any* functional form of the heating function q, such as it was possible with the special form of the heating function given in Eq. (7.5). To proceed further then and find other more general solutions effectively having a variable value for γ, one may choose some other functional form for the heating function q and from the first law, Eq. (7.3) derive a functional form for the pressure. Equivalently, one may choose a functional form for the pressure P and determine the volumetric rate of thermal energy *a posteriori* from Eq. (7.3), after finding the expressions of ρ, P and A which satisfy the two remaining components of the momentum equation. Hence, in such a treatment the heating sources which produce some specific solution are

[2] in general, if there is a function $\mathcal{V}'$ such that $\vec{V} \cdot \vec{F}_{rad} = -\rho \vec{V} \cdot \vec{\nabla} \mathcal{V}'$, the Bernoulli integral exist,

not known *a priori*; instead, they can be determined only *a posteriori*. However, it is worth to keep in mind that as explained above, this situation is analogous to the more familiar constant γ polytropic case, with $\gamma \neq \Gamma$. In this Chapter we shall follow this approach, which is further illustrated in the following section.

However, even with this approach, the integration of the system of mixed elliptic/hyperbolic partial differential equations (7.1) - (7.2) is not a trivial undertaking. This is largely due to the fact that a physically interesting solution is bound to cross some critical surfaces which are not known *a priori* but they are determined simultaneously with the solution. For this reason only a very few such self-consistent solutions are available. Further assumptions on the shape of the critical surfaces are needed, as discussed in the following.

7.2.2 Assumptions

In order to construct analytically a new class of exact solutions, we shall proceed by making the following two key assumptions:

1. that the Alfvén number M is some function of the dimensionless radial distance $R = r/r_\star$, i.e., $M = M(R)$
   and

2. that the poloidal velocity and magnetic fields have a dipolar angular dependence,
$$A = \frac{r_\star^2 B_\star}{2}\mathcal{A}(\alpha) , \qquad \alpha = \frac{R^2}{G^2(R)}\sin^2\theta . \tag{7.7}$$
   for some function $G(R)$.

3. for the radiative acceleration we have assumed that it has two components. The first component is due to continuum absorption and is set proportional to the radiative flux. It drops with distance as r^{-2}, similarly to gravity. If L_ε is the Eddington luminocity, we may use the ratio $\Gamma_\varepsilon = L/L_\varepsilon$ such that this part of the radiative acceleration is $\Gamma_\varepsilon \rho \mathcal{GM}/r^2$. We have also assumed a second component of the radiative acceleration due to line contribution. By adopting the optically thin atmosphere approximation [Lam86, CM94, KM97, KM98], this part of the acceleration is simply a function of r since in general the total number of weak lines is a function of r. Then, the corresponding expression of the radiative acceleration is $V_\star^2/r_\star \rho Q(R)$.
   The combination of gravitational and radiative acceleration is thus
$$-\rho\vec{\nabla}\mathcal{V} + \vec{F}_{rad} = \frac{V_\star^2}{r_\star}\rho\left(Q(R) - \frac{\nu^2}{2R^2}\right)\hat{r} ,$$
   where
$$\nu^2 = \frac{V_{esc}^2}{V_\star^2}(1-\Gamma_\varepsilon) = \frac{2\mathcal{GM}}{r_\star V_\star^2}(1-\Gamma_\varepsilon) .$$

The ratio between the radiative and gravitational forces is then

$$\frac{F_{rad}}{-F_{gravity}} = \Gamma_\varepsilon + \frac{2R^2 Q\,(1-\Gamma_\varepsilon)}{\nu^2}\,.$$

Furthermore, we use for Q the approximation of a power law, $Q\,(R) = \mu_0/R^x$ with μ_0, and x constants. The constant x measures the loss ($x > 2$) or gain ($x < 2$) in radiative energy as a function of radial distance.

We are interested in transAlfvénic flows and denote by a $\star$ the respective value of all quantities at the Alfvén surface. By choosing the function $G(R)$ such that $G\,(R=1) = 1$ at the Alfvén transition $R = 1$, it is evident that $G(R)$ measures the cylindrical distance ϖ to the polar axis of each fieldline labeled by α, normalized to its cylindrical distance ϖ_α at the Alfvén point, $G\,(R) = \varpi/\varpi_\alpha$. For a smooth crossing of the Alfvén sphere $R = 1$ [$r = r_\star, \theta = \theta_a(\alpha)$], the free integrals L and Ω are related by

$$\frac{L}{\Omega} = \varpi_\alpha^2(A) = r_\star^2 \sin^2\theta_a(\alpha) = r_\star^2\alpha\,. \tag{7.8}$$

Therefore, the second assumption is equivalent with the statement that at the Alfvén surface the cylindrical distance ϖ_α of each magnetic flux surface $\alpha = const$ is simply proportional to $\sqrt{\alpha}$.
Instead of using the three remaining free functions of α, ($\mathcal{A}$, Ψ_A , Ω), we found it more convenient to work instead with the three dimensionless functions of α, (g_1 , g_2 , g_3),

$$g_1(\alpha) = \int \mathcal{A}'^2 d\alpha\,,\quad g_2(\alpha) = \frac{r_\star^2}{B_\star^2}\int \Omega^2\Psi_A^2 d\alpha\,,\quad g_3(\alpha) = \frac{\Psi_A^2}{4\pi\rho_\star}\,. \tag{7.9}$$

These functions $g_1(\alpha)$, $g_2(\alpha)$, $g_3(\alpha)$ are vectors in a 3D α-space with some basis vectors $u_1(\alpha)$, $u_2(\alpha)$, $u_3(\alpha)$ [VT98]. Note that the forms of $g_1\,, g_2\,, g_3$ or equivalently the forms of A, Ψ_A, Ω, $L = r_\star^2\alpha\Omega$ and P should be such that the two remaining components of the momentum equation are separable in the α and R coordinates.

7.2.3 The method

The main steps of the general method for getting exact solutions under the previous two assumptions are briefly the following.

First, by using α instead of θ as the independent variable, we transform from the pair of the independent variables $(R\,,\theta)$ to the pair of the independent variables $(R\,,\alpha)$. The resulting form of the α- component of the momentum equation can be integrated at once to yield for the gas pressure,

$$P(R,\alpha) = \frac{B_\star^2}{8\pi}\left(f_0 + f_4 g_1 + f_1 g_1^{'} + f_2\alpha g_1^{'} + f_5 g_2 + f_3\alpha g_2^{'}\right) = \frac{B_\star^2}{8\pi}\mathbf{Y}\mathbf{P}^\dagger\,, \tag{7.10}$$

where $f_0(R)$ is a free function emerging from this integration, $f_i(R)$, $i = 1, 2, \ldots, 8$ are functions of the spherical radius R given in the Appendix 5.A while $f_9 = \dfrac{2}{M^2}\left(Q - \dfrac{\nu^2}{2R^2}\right)$ and $\mathbf{P}$, $\mathbf{Y}$ are the (1×7) matrices,

$$\mathbf{Y} = [\, Y_1 \;\; Y_2 \;\; Y_3 \;\; Y_4 \;\; Y_5 \;\; Y_6 \;\; Y_7 \,] = \left[\, 1 \;\; g_1 \;\; g_1^{'} \;\; \alpha g_1^{'} \;\; g_2 \;\; \alpha g_2^{'} \;\; g_3 \right] , \tag{7.11}$$

$$\mathbf{P} = [\, f_0 \;\; f_4 \;\; f_1 \;\; f_2 \;\; f_5 \;\; f_3 \;\; 0 \,] . \tag{7.12}$$

Second, by substituting Eq. (7.10) in the r-component of the momentum equation we obtain in terms of the (1×7) matrix $\mathbf{X}$

$$\mathbf{X} = [\, X_1 \;\; X_2 \;\; X_3 \;\; X_4 \;\; X_5 \;\; X_6 \;\; X_7 \,] = \left[\, f_0^{'} \;\; f_4^{'} \;\; -f_6 \;\; -f_7 \;\; f_5^{'} \;\; -f_8 \;\; -f_9 \right] , \tag{7.13}$$

the following equation:

$$\mathbf{Y}\mathbf{X}^{\dagger} = \mathbf{0} . \tag{7.14}$$

A key step in the method is to find a possible set of vectors $u_1(\alpha)$, $u_2(\alpha)$, $u_3(\alpha)$ such that all components of the matrix $\mathbf{Y}$ belong to the same α-space. So we choose $u_1(\alpha) = 1$ and $u_2(\alpha) = g_1(\alpha)$. If this is the case, then our *third* step is to construct a 3×7 matrix $\mathbf{K}$ such that

$$\mathbf{Y} = [\, u_1 \;\; u_2 \;\; u_3 \,]\mathbf{K} . \tag{7.15}$$

Then, from Eq. (7.14),

$$[\, u_1 \;\; u_2 \;\; u_3 \,]\; \mathbf{K}\mathbf{X}^{\dagger} = \mathbf{0} ,$$

and since u_i are linearly independent it follows

$$\mathbf{K}\mathbf{X}^{\dagger} = \mathbf{0} . \tag{7.16}$$

Finally, it follows from Eq. (7.10) , (7.12) and (7.15) that,

$$P = \frac{B_*^2}{8\pi}\left(P_0 + g_1 P_1 + u_3 P_2\right) ,$$

where the three components of the pressure P_0, P_1 and P_2 are

$$[P_0 \; P_1 \; P_2]^{\dagger} = \mathbf{K}\mathbf{P}^{\dagger} . \tag{7.17}$$

7.2.4 The Model

Let us know apply this method in the construction of a specific model. We may recall that in [VT98] (see also Chapter 5), it was found that only nine distinct general families of such vectors exist. One of them is,

$$u_1(\alpha) = 1 , \quad u_2(\alpha) = \alpha , \quad u_3(\alpha) = \alpha^{\epsilon} , \tag{7.18}$$

while the corresponding free functions are,

$$g_1(\alpha) = a\,, \quad g_2(\alpha) = \xi\alpha + \mu\alpha^{\epsilon}/\epsilon\,, \quad g_3(\alpha) = 1 + \delta\alpha + \mu\delta_0\alpha^{\epsilon}\,, \tag{7.19}$$

(see the case (2) in Table 5.1).
For this particular choice of $u_1(\alpha) = 1\,, u_2(\alpha) = \alpha\,, u_3(\alpha) = \alpha^{\epsilon}$ we find the following form of the matrix $\mathbf{K}$,

$$\mathbf{K} = \begin{bmatrix} 1 & 0 & 1 & 0 & 0 & 0 & 1 \\ 0 & 1 & 0 & 1 & \xi & \xi & \delta \\ 0 & 0 & 0 & 0 & \mu/\epsilon & \mu & \mu\delta_0 \end{bmatrix}\,. \tag{7.20}$$

Then, from Eqs. (7.12) and (7.17) we get,

$$\begin{bmatrix} P_0 \\ P_1 \\ P_2 \end{bmatrix} = \begin{bmatrix} f_0 + f_1 \\ f_4 + f_2 + \xi\,(f_3 + f_5) \\ \mu\,(f_5/\epsilon + f_3) \end{bmatrix}\,. \tag{7.21}$$

Finally, from Eq. (7.16) using the definitions of Eqs. (7.13), (7.20) we obtain, three ordinary differential equations for the functions of R in the model for $\epsilon \neq 0, 1$ and $\mu \neq 0$ (only then we have a 3D α-space with $1\,, \alpha\,, \alpha^{\epsilon}$ linearly independent)

$$\left.\begin{aligned} f_0^{'} - f_6 - f_9 &= 0 \\ f_4^{'} - f_7 + \xi\left(f_5^{'} - f_8\right) - \delta f_9 &= 0 \\ \mu\left(f_5^{'}/\epsilon - f_8 - \delta_0 f_9\right) &= 0 \end{aligned}\right\} \tag{7.22}$$

with the functions $f_i\,(R)$, $i = 1, 2, \ldots, 8$ given in the Appendix 5.A and $f_9 = \dfrac{2}{M^2}\left(Q - \dfrac{\nu^2}{2R^2}\right)$.
Eqs. (7.22) can be found by setting equal to zero the three expressions in the square brackets of Eq. (5.46), but in this Chapter we have proposed a simpler way of finding them. This method could easily be applied in all the other models of Table 5.1.

7.2.5 Physical quantities and final differential equations of model

Altogether, let us summarize the characteristics of our model. The MHD integrals have the following forms,

$$\Psi_A = \sqrt{4\pi\rho_{\star}\,(1 + \delta\alpha + \mu\delta_0\alpha^{\epsilon})}\,, \tag{7.23}$$

$$\Omega = \frac{V_{\star}}{r_{\star}}\sqrt{\frac{\mu\alpha^{\epsilon-1} + \xi}{1 + \delta\alpha + \mu\delta_0\alpha^{\epsilon}}}\,, \tag{7.24}$$

$$L = V_{\star}r_{\star}\sqrt{\frac{\mu\alpha^{\epsilon+1} + \xi\alpha^2}{1 + \delta\alpha + \mu\delta_0\alpha^{\epsilon}}}\,. \tag{7.25}$$

The physical quantities of the outflow have the following exact expressions:

$$\rho = \frac{\rho_\star}{M^2}\left(1+\delta\alpha+\mu\delta_0\alpha^\epsilon\right) \tag{7.26}$$

$$P = \frac{\rho_\star V_\star^2}{2}\left(P_0+P_1\alpha+P_2\alpha^\epsilon\right), \tag{7.27}$$

$$\vec{V} = V_\star \frac{\dfrac{M^2\cos\theta}{G^2}\hat{r} - \dfrac{M^2 F\sin\theta}{2G^2}\hat{\theta} + \sqrt{\xi\alpha+\mu\alpha^\epsilon}\,\dfrac{G^2-M^2}{G\left(1-M^2\right)}\hat{\phi}}{\sqrt{1+\delta\alpha+\mu\delta_0\alpha^\epsilon}} \tag{7.28}$$

$$\vec{B} = B_\star\left(\frac{\cos\theta}{G^2}\hat{r} - \frac{F\sin\theta}{2G^2}\hat{\theta} - \sqrt{\xi\alpha+\mu\alpha^\epsilon}\,\frac{1-G^2}{G\left(1-M^2\right)}\hat{\phi}\right), \tag{7.29}$$

where the five unknown functions $G^2(R)$, $F(R)$, $M^2(R)$, $P_0(R)$ and $P_1(R)$ entering in the above expressions are obtained from the integration of the following five first order ordinary differential equations:

$$\frac{dG^2}{dR} = -\frac{F-2}{R}G^2, \tag{7.30}$$

$$\frac{dF}{dR} = \frac{F}{1-M^2}\frac{dM^2}{dR} - \frac{F\left(F-2\right)}{2R} - \frac{F^2-4}{2R\left(1-M^2\right)} - \frac{2G^2RP_1}{1-M^2} - \frac{2\xi R}{M^2\left(1-M^2\right)^3}\left[\left(2M^2-1\right)G^4 - M^4 + 2M^2\left(1-G^2\right)\right] \tag{7.31}$$

$$\frac{dM^2}{dR} = \frac{M^2\left(1-M^2\right)}{\left(2M^2-1\right)G^4-M^4}\left\{2\epsilon\delta_0 G^2\left(1-M^2\right)\left(Q-\frac{\nu^2}{2R^2}\right) + \frac{F-2}{R}\left[\left(\epsilon+1\right)M^2 - \left(\epsilon-1\right)G^4\right]\right\} \tag{7.32}$$

$$\frac{dP_1}{dR} = -\left[\frac{F^2-4}{2R^2G^2} + 2\xi\frac{\left(1-G^2\right)^2}{G^2\left(1-M^2\right)^3}\right]\frac{dM^2}{dR} - \frac{M^2F}{2R^2G^2}\frac{dF}{dR} + \frac{2\delta}{M^2}\left(Q-\frac{\nu^2}{2R^2}\right) - \frac{M^2\left(F^2-4\right)\left(F-4\right)}{4R^3G^2} + \xi\frac{\left(F-2\right)\left[\left(2M^2-1\right)G^4-M^4\right]}{RG^2M^2\left(1-M^2\right)^2} \tag{7.33}$$

$$\frac{dP_0}{dR} = -\frac{2}{G^4}\frac{dM^2}{dR} + \frac{2}{M^2}\left(Q-\frac{\nu^2}{2R^2}\right) - \frac{2M^2\left(F-2\right)}{RG^4} \tag{7.34}$$

while the pressure component $P_2(R)$ is given explicitly in terms of the other variables,

$$P_2 = \frac{\mu}{G^2}\left[\frac{G^4 - M^2}{\epsilon M^2\left(1-M^2\right)} - \left(\frac{1-G^2}{1-M^2}\right)^2\right] . \tag{7.35}$$

The functional form of the pressure, Eq. (7.27), corresponds to the following functional form for the heating function

$$\frac{q}{\rho V_r} = \frac{V_\star^2}{2r_\star}\frac{\mathcal{Q}_0 + \mathcal{Q}_1\alpha + \mathcal{Q}_2\alpha^\epsilon}{1+\delta\alpha+\mu\delta_0\alpha^\epsilon}$$

with $\mathcal{Q}_i = \dfrac{M^{-2(\Gamma-1)}}{\Gamma-1}\dfrac{d\left(P_i M^{2\Gamma}\right)}{dR}$, $i = 0,1,2$. As discussed in subsection 7.2.1, one could proceed in the reverse way, i.e., to start with the functional form of the heating function and deduce the functional form of the pressure Eq. (7.27).

The current density $\vec{J} = \dfrac{c}{4\pi}\vec{\nabla}\times\vec{B}$ has a poloidal component

$$\vec{J_p} = \frac{c}{4\pi}\vec{\nabla}\times\vec{B_\phi} = \vec{\nabla}\times\left(\frac{c\varpi B_\phi}{4\pi}\vec{\nabla}\phi\right) = \vec{\nabla}\left(\frac{c\varpi B_\phi}{4\pi}\right)\times\vec{\nabla}\phi ,$$

so the current lines on the poloidal plane are the lines $\dfrac{c\varpi B_\phi}{4\pi} =$ constant, or

$$\sqrt{\mu\alpha^{\epsilon+1}+\xi\alpha^2}\frac{1-G^2}{1-M^2} = -\frac{2I_p}{cr_\star B_\star} = \text{ constant} . \tag{7.36}$$

Note that from the structure of the model (basically from the forms of the integrals), we conclude that we could have solved the problem similarly, with a more general form for the radiative force

$$\vec{F}_{rad} = \frac{\rho_\star V_\star^2}{r_\star}\left(\left[\mathcal{L}_0(R)+\mathcal{L}_1(R)\,\alpha+\mathcal{L}_2(R)\,\mu\alpha^\epsilon\right]\hat{r}+\frac{\cos\theta}{\sin\theta}\left[\mathcal{L}_3(R)\,\alpha+\mathcal{L}_4(R)\,\mu\alpha^\epsilon\right]\hat{\theta}\right) ,$$

with given functions $\mathcal{L}_i$, $i = 0,1,2,3,4$.

7.2.6 Some properties of the model

Our model is meridionally self-similar, i.e., if we know the shape of one fieldline $\alpha = \alpha_1$ we may derive the shape of any other streamline $\alpha = \alpha_2$ by moving in the meridional direction along each cycle $R = const$ on the poloidal plane as illustrated in Fig. 7.1.

Note that the flux function A is simply proportional to α which means that for cylindrical solutions at $R \gg 1$, the magnetic field on the poloidal plane is uniform and its strength is independent of α, $\mid \vec{B_p} \mid_\infty = B_\star/G_\infty^2$.

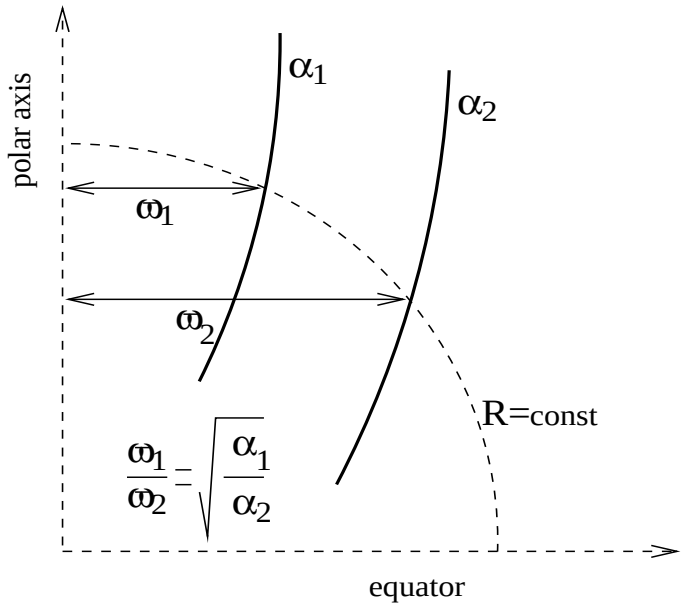

Figure 7.1: An illustration of the construction of the streamlines $\alpha = const.$ on the poloidal plane in meridionally selfsimilar outflows.

The density at the Alfvén surface is

$$\rho_\alpha = \frac{\Psi_A^2}{4\pi} = \rho_\star \left(1 + \delta\alpha + \mu\delta_0 \alpha^\epsilon\right) ,$$

i.e., it is similar to a Taylor expansion in the cylindrical distance ϖ_α from the rotation and magnetic axis $\alpha = 0$. For example, for $\epsilon = 0.5$ we have,

$$\frac{\rho_\alpha}{\rho_\star} = 1 + \mu\delta_0 \frac{\varpi_\alpha}{r_\star} + \delta \left(\frac{\varpi_\alpha}{r_\star}\right)^2 .$$

Also the parameters $\delta\,, \mu\delta_0\,, \epsilon$ help us to fit a desired profile for the density on a given spherical distance (on the stellar surface, or at infinity etc). For example we can choose low density on the polar axis and increased density with increased α (hollow jets), or we can choose an outer line α_{out} such that $\rho = 0$ in this line, etc.

We've also introduced the expansion factor

$$F \equiv \frac{\partial \ln \alpha(R,\theta)}{\partial \ln R} = 2 - R\frac{G^{2'}}{G^2} ,$$

which measures the flaring of the fieldlines on the poloidal plane, as illustrated in Fig. 7.2. If locally, the function F is constant, then $G^2 \propto R^{2-F}$, or $A \propto$

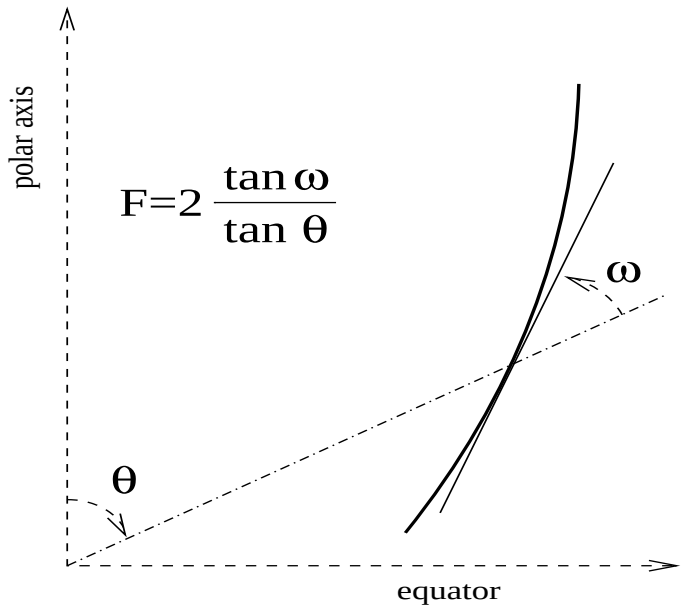

Figure 7.2: A geometrical illustration of the expansion factor $F(R)$ which determines the shape of the poloidal streamlines in a meridionally selfsimilar outflow.

$R^F \sin^2\theta$. Thus, if $F > 2$ the fieldlines turn towards the axis, if $F = 2$ they expand cylindrically, if $F = 0$ they are purely radial while if $F < 0$ the fieldlines turn toward the equator (in that case, there is a closed region near the equator). If we eliminate F in Eq. (7.31) [using Eq. (7.30)] we have the second derivative of G (which corresponds to the term $\dfrac{\partial^2 A}{\partial r^2}$ in the transfield equation). So, using F us an intermediate function we have only first order differential equations.

Looking at the form of Ω, we see that we can choose the parameters $\mu\,,\xi\,,\delta\,,\delta_0\,,\epsilon$, in order to fit the differential rotation of a star (we remind that Ω is the angular velocity of the star, since near the stellar surface, if $M^2 \ll 1$, $V_\phi = M^2/\Psi_A + \Omega\varpi \approx \Omega\varpi$).

In the following we shall discuss the results of the integration of the previous system of differential equations (7.30), (7.31), (7.32), (7.33), (7.34), (7.35). Finally, we shall calculate all the other remaining physical quantities. A parametric study will be made only for $\epsilon > 0$, since for $\epsilon < 0$ we have $\lim_{\alpha \to 0} \rho = \infty$.

For $\epsilon = 0$ or 1 (or equivalently for $\mu = 0$), we get a degenerate case which needs an extra condition between the functions of R. This case has been studied in [ST94] (where the components of the pressure $P_0\,,P_1$ are set proportional to each other) and [TTS97] (where the function $G(R)$ is given *a priori*). Here, in the case $\mu = 0$ we 've chosen this extra condition to be $f_5'/\epsilon - f_8 - \delta_0 f_9 = 0$ (*c.f.*, the last equation of the system (7.22)).

7.3 Critical Surfaces

In the domain of the solutions there exist several critical surfaces. In the following we briefly discuss the physical context of these critical surfaces.

7.3.1 Alfvén critical surface

We recall that one of our goals is to investigate transAlfvénic solutions wherein $L = \varpi_\alpha^2 \Omega$. By multiplying Eq. (7.31) with $1 - M^2$ and evaluating the resulting expression at the Alfvén point we get

$$F_\star p_\star - \frac{F_\star^2 - 4}{2} - 2P_{1\star} = 0\,, \tag{7.37}$$

with $F_\star$, $P_{1\star}$ and $p_\star = \left(dM^2/dR\right)_\star$ the respective values of these quantities at the Alfvén transition $R = 1$. Eq. (7.37) is the so-called Alfvén regularity condition in the present model. Note that if we also multiply Eq. (7.33) with $1 - M^2$ and evaluate the resulting expression at the Alfvén point we get an identical expression while Eq. (7.32) after using L'Hospital's rule gives an identity (corresponds to a star-type critical point). At the Alfvén point, the parameters $F_\star\,, p_\star$ are related with $V_{\phi\star}\,, B_{\phi\star}$ since (using the L'Hospital rule $\left(\frac{1-G^2}{1-M^2}\right)_\star = \frac{2-F_\star}{p_\star}$)

$$V_{\phi\star} = V_\star \sqrt{\frac{\mu\alpha^\epsilon + \xi\alpha}{1 + \delta\alpha + \mu\delta_0\alpha^\epsilon}} \left(1 - \frac{2 - F_\star}{p_\star}\right)\,, \quad B_{\phi\star} = -B_\star \sqrt{\mu\alpha^\epsilon + \xi\alpha}\frac{2 - F_\star}{p_\star}\,.$$

7.3.2 Slow/fast critical surfaces.

In order to locate the critical surfaces where the radial component of the flow speed equals to the corresponding slow/fast MHD wave speeds [TSS+96], we need to calculate first the sound speed C_s; to this goal we may proceed as follows.

Consider that at some fixed distance R of a given streamline labeled by α we make a small change in the density ρ and the pressure P. We may define the square of the sound speed as the ratio of such an infinitesimal change of P and ρ, (see subsection 3.2.1)

$$C_s^2 = \left(\frac{\partial P}{\partial \rho}\right)_{\alpha, R} = \frac{\dfrac{\partial P\left(\alpha, R, M^2\right)}{\partial M^2}}{\dfrac{\partial \rho\left(\alpha, R, M^2\right)}{\partial M^2}}\,, \tag{7.38}$$

or, from Eqs. (7.26) - (7.27)

$$C_s^2 = -\frac{V_\star^2}{2} M^4 \frac{\dfrac{\partial P_0\left(R, M^2\right)}{\partial M^2} + \dfrac{\partial P_1\left(R, M^2\right)}{\partial M^2}\alpha + \dfrac{\partial P_2\left(R, M^2\right)}{\partial M^2}\alpha^\epsilon}{1 + \delta\alpha + \mu\delta_0\alpha^\epsilon}. \qquad (7.39)$$

Substituting

$$\frac{dP_0}{dR} = \frac{\partial P_0\left(R, M^2\right)}{\partial R} + \frac{\partial P_0\left(R, M^2\right)}{\partial M^2}\frac{dM^2}{dR}$$

in Eq. (7.34) we get

$$\left(\frac{\partial P_0\left(R, M^2\right)}{\partial M^2} + \frac{2}{G^4}\right)\frac{dM^2}{dR} = \frac{2}{M^2}\left(Q - \frac{\nu^2}{2R^2}\right) - \frac{2M^2\left(F-2\right)}{RG^4} - \frac{\partial P_0\left(R, M^2\right)}{\partial R}.$$

At the critical point where $\dfrac{dM^2}{dR} = \dfrac{0}{0}$ we have

$$\left[\frac{\partial P_0\left(R, M^2\right)}{\partial M^2}\right]_{R=R_x} = \left[-\frac{2}{G^4}\right]_{R=R_x}. \qquad (7.40)$$

From Eq. (7.33) after substituting dF/dR from Eq. (7.31) we can calculate in the same way $\partial P_1\left(R, M^2\right)/\partial M^2$:

$$\left[\frac{\partial P_1\left(R, M^2\right)}{\partial M^2}\right]_{R=R_x} = \left[-\frac{F^2-4}{2R^2G^2} - 2\xi\frac{\left(1-G^2\right)^2}{G^2\left(1-M^2\right)^3} - \frac{M^2F^2}{2R^2G^2\left(1-M^2\right)}\right]_{R=R_x}. \qquad (7.41)$$

Finally, from Eq. (7.35) by taking the derivative of $P_2(G, M^2)$ for constant $G(R)$ we get similarly,

$$\frac{\partial P_2\left(R, M^2\right)}{\partial M^2} = \frac{\mu}{G^2}\left[\frac{\left(2M^2-1\right)G^4 - M^4}{\epsilon M^4\left(1-M^2\right)^2} - 2\frac{\left(1-G^2\right)^2}{\left(1-M^2\right)^3}\right]. \qquad (7.42)$$

Substituting Eqs. (7.40), (7.41) and (7.42) in Eq. (7.39) we obtain the expression of the sound speed. The general formula for the sound speed may have an additional term, which vanishes at the critical point. So in general

$$C_s^2 = V_\star^2\frac{M^6}{G^4\left(1-M^2\right)\left(1+\delta\alpha+\mu\delta_0\alpha^\epsilon\right)}\left(\frac{1-M^2}{M^2} + \right.$$
$$\alpha\left[-\frac{G^2\left(1-M^2\right)}{R^2M^2} + \frac{F^2G^2}{4R^2M^2} + \xi\frac{G^2\left(1-G^2\right)^2}{M^2\left(1-M^2\right)^2}\right] +$$
$$\mu\alpha^\epsilon\left[\frac{G^2\left(1-G^2\right)^2}{M^2\left(1-M^2\right)^2} - G^2\frac{\left(2M^2-1\right)G^4 - M^4}{2\epsilon M^6\left(1-M^2\right)}\right] -$$
$$\left.G^2\frac{\left(2M^2-1\right)G^4 - M^4}{2M^6\left(1-M^2\right)}\mathcal{L}\left(R, \alpha\right)\right). \qquad (7.43)$$

where we have introduced some unknown function $\mathcal{L}(R,\alpha)$.
An inspection of Eq. (7.32) for the Alfvén number $M(R)$ reveals that besides the Alfvén transition where $M = G = R = 1$, there may be other distances $R_x \neq 1$ where the denominator of this equation becomes zero, $\mathcal{D} \equiv \left[\left(2M^2-1\right)G^4 - M^4\right]_{R=R_x} = 0$ [3]. In such a case, the numerator of Eq. (7.32) should be also set equal to zero and we have conditions typical of a critical point (using L'Hospital's rule we find two solutions for the slope of M^2 in this point, i.e., this singularity corresponds to an x-type critical point). To clarify the physical identity of such a critical point, we may manipulate the denominator $\mathcal{D}$ and write it in the form

$$\mathcal{D} = 2G^2 \frac{1+\delta\alpha+\mu\delta_0\alpha^{\epsilon}}{V_\star^2 V_{A,r}^4\left(\mu\alpha^{\epsilon}/\epsilon+\mathcal{L}\right)}\left(V_r^2-V_{A,r}^2\right)\left[V_r^4 - V_r^2\left(C_s^2+V_A^2\right)+C_s^2V_{A,r}^2\right], \tag{7.44}$$

where V_A, $V_{A,r}$ are the total and radial Alfvén speeds, respectively. So the zeros of $\mathcal{D}$ correspond to surfaces $R = R_x$ where the component of the flow perpendicular to them, is equal with the same component of the phase velocity of fast or slow MHD waves (see also subsection 3.2.1). Evidently, a critical point at R_x corresponds to the modified by the meridional self-similarity fast/slow critical points [TSS+96]. In other words, the sphere $R = R_x$ is the corresponding spherical separatrix in the hyperbolic domain of the system of the MHD differential equations [Bog96]. The sound speed is well defined at the critical points where $\mathcal{D} = 0$, but it is an open question if this definition can be extended everywhere.
Suppose we know the sound speed everywhere. Then the characteristics are

$$\left(\frac{rd\theta}{dr}\right)_{\pm} = \frac{b \pm \sqrt{b^2-ac}}{a}$$

where

$$a = V_p^2\left[V_r^2 - C_s^2 - V_A^2 + C_s^2/M^2\right], \quad b = V_p^2 V_r V_\theta \quad \text{and}$$
$$c = V_p^2\left[V_\theta^2 - C_s^2 - V_A^2 + C_s^2/M^2\right].$$

We see that there is a closed characteristic when $a = 0$ (only then the characteristic is r = constant). This is the limiting characteristic. Looking at Eq. (7.44) we see that when $a = 0$, $\mathcal{D} = 0$ too. In $\theta-$ self similar models, we start the integration from a surface $r = r_i$ and continue always on spherical surfaces. When we reach the position of a spherical (limiting-closed) characteristic (the one where $a = 0$) as we have studied in Chapter 3, we can not continue the integration without imposing some regularity condition (the numerator of $\dfrac{dM^2}{dR}$ also vanishes there).

[3] From this equality, $G_x^4 = \dfrac{M_x^4}{2M_x^2-1} \Rightarrow G_x > 1$, so the point is in the superAlfvénic regime (corresponds to a modified fast magnetosonic singular point).

On the polar axis ($\alpha = 0$), where $V_A = V_{A,r}$, the zeros of a, ($a = 0$) correspond to points where $V_r = V_A$ (Alfvén point) or $V_r = C_s$ (sonic point). So the second equality must hold in any possible critical point ($R = R_x \neq 1$) on the axis. Eq. (7.43) verifies this result, because for $\alpha = 0$ and $\mathcal{D} = 0$ gives $C_s = V_r$.
Generally speaking, there may be more than two critical points on the axis (in all these points with $R = R_x \neq 1$, $V_r = C_s$, since C_s changes as we move downstream). But from the integration of the equations (as we see in Sec. 7.6) we found at most two singular points: the Alfvén and the modified by the self similarity fast magnetosound critical point. On the basis of causality arguments, we should choose the superfast solution because only then, conditions at infinity will not influence the solution at the base, since no signal can be propagated from infinity upstream in a flow which is superfast (see Chapter 3). Note that there is no necessity for passing the solution through the other limiting characteristic which correspond to the modified slow magnetosound singular point. As we discuss in Chapter 3 there are not causality problems in this surface. The flow, simply starts from the stellar surface with superslow velocity.

7.4 Asymptotic analysis

According to the asymptotical behaviour of the poloidal streamlines we may distinguish two different types of solutions.

7.4.1 Cylindrical asymptotics achieved through oscillations (Type I solutions)

In this case the poloidal streamlines undergo oscillations of decaying amplitude and finally they become cylindrical. A similar oscillatory behaviour is found in all physical quantities, a situation which has been already analyzed in detail [VT97] (see also Chapter 4). According to this analysis, as $R \gg 1$ we have

$$M^2 = M_\infty^2 \left(1 + \lambda_0 \varepsilon\right), \quad G^2 = G_\infty^2 \left(1 - \varepsilon\right), \quad \varepsilon(r) \approx \frac{D}{r^s} \sin\left(kr + \phi_0\right), \tag{7.45}$$

$$k^2 = \frac{2\xi \left(1 - \epsilon\right) \left(M_\infty^2 - G_\infty^4\right)}{r_\star^2 M_\infty^2 \left(1 - M_\infty^2\right)^2}, \tag{7.46}$$

$$\lambda_0 = \left[\left(\epsilon + 1\right) M_\infty^2 - \left(\epsilon - 1\right) G_\infty^4\right] \frac{1 - M_\infty^2}{\left(2M_\infty^2 - 1\right) G_\infty^4 - M_\infty^4}, \tag{7.47}$$

$$s = 2 + \frac{\lambda_0 M_\infty^2}{M_\infty^2 - 1}. \tag{7.48}$$

Note that for $s > 1$ the gravitational term is dominant, but the analysis is still correct because the oscillatory perturbation is independent of the "background" term $1/r$ [VT97].

7.4.2 Converging to the axis asymptotics (Type II solutions)

An analysis of the system of the differential equations (7.31) - (7.35) for $\lim_{R\to\infty} G = 0$, $\lim_{R\to\infty} M = \infty$ and $\lim_{R\to\infty} F = F_\infty$ shows that in this case the value of the expansion factor F_∞ at $R \gg 1$ approaches a constant value, the positive root of the equation

$$(\epsilon+3)\left(\epsilon+\frac{3}{2}\right)F_\infty^2 - 2(\epsilon+2)\left(\epsilon+\frac{5}{2}\right)F_\infty - 4(\epsilon+2) = 0\,.$$

As we shall see later, interesting solutions are obtained mainly for $\epsilon > 0$, in which case this root is greater than 2, $F_\infty > 2$, i.e., the cross-sectional area of flow tube drops to zero at large radii, $G^2 \propto R^{2-F_\infty}$. The poloidal velocity goes to infinity as $V_r \propto R^{(\epsilon+2)(F_\infty-2)}$ to conserve mass , while the toroidal velocity grows like $V_\phi(R\to\infty) \propto R^{F_\infty-2}$ from angular momentum conservation.

7.5 Method of integration

Suppose that we start from a spherical surface $r = r_i$ and integrate in the downstream direction. First of all, we see that Eqs. (7.30)-(7.35) takes the forms:

$$\frac{dG^2}{d(r/r_i)} = -\frac{F-2}{(r/r_i)}G^2\,, \tag{7.49}$$

$$\frac{dF}{d(r/r_i)} = \frac{F}{1-M^2}\frac{dM^2}{d(r/r_i)} - \frac{F(F-2)}{2(r/r_i)} - \frac{F^2-4}{2(r/r_i)(1-M^2)} - \frac{2G^2(r/r_i)P_1(r_i/r_\star)^2}{1-M^2} - \frac{2\xi(r_i/r_\star)^2(r/r_i)}{M^2(1-M^2)^3}\left[(2M^2-1)G^4 - M^4 + 2M^2(1-G^2)\right] \tag{7.50}$$

$$\frac{dM^2}{d(r/r_i)} = \frac{M^2(1-M^2)}{(2M^2-1)G^4 - M^4}\left\{2\epsilon\delta_0 G^2(1-M^2)\left(\frac{r_i}{r_\star}Q - \frac{\nu^2 r_\star/r_i}{2(r/r_i)^2}\right) + \frac{F-2}{(r/r_i)}\left[(\epsilon+1)M^2 - (\epsilon-1)G^4\right]\right\} \tag{7.51}$$

$$\frac{dP_1\left(r_i/r_\star\right)^2}{d\left(r/r_i\right)}=-\left[\frac{F^2-4}{2\left(r/r_i\right)^2G^2}+2\xi\left(r_i/r_\star\right)^2\frac{\left(1-G^2\right)^2}{G^2\left(1-M^2\right)^3}\right]\frac{dM^2}{d\left(r/r_i\right)}-$$

$$\frac{M^2F}{2\left(r/r_i\right)^2G^2}\frac{dF}{d\left(r/r_i\right)}+\frac{2\delta\left(r_i/r_\star\right)^2}{M^2}\left(\frac{r_i}{r_\star}Q-\frac{\nu^2r_\star/r_i}{2\left(r/r_i\right)^2}\right)-\frac{M^2\left(F^2-4\right)\left(F-4\right)}{4\left(r/r_i\right)^3G^2}+ \quad (7.52)$$

$$\xi\left(r_i/r_\star\right)^2\frac{\left(F-2\right)\left[\left(2M^2-1\right)G^4-M^4\right]}{\left(r/r_i\right)G^2M^2\left(1-M^2\right)^2}$$

$$\frac{dP_0}{d\left(r/r_i\right)}=-\frac{2}{G^4}\frac{dM^2}{d\left(r/r_i\right)}+\frac{2}{M^2}\left(\frac{r_i}{r_\star}Q-\frac{\nu^2r_\star/r_i}{2\left(r/r_i\right)^2}\right)-\frac{2M^2\left(F-2\right)}{RG^4} \quad (7.53)$$

$$P_2\alpha^\epsilon=\mu\left(r_i/r_\star\right)^{2\epsilon}\frac{1}{G^2}\left[\frac{G^4-M^2}{\epsilon M^2\left(1-M^2\right)}-\left(\frac{1-G^2}{1-M^2}\right)^2\right]\left(\frac{r\sin\theta}{r_iG}\right)^{2\epsilon}. \quad (7.54)$$

We see that if we introduce new constants
$\mu_i=\mu\left(r_i/r_\star\right)^{2\epsilon}$, $\xi_i=\xi\left(r_i/r_\star\right)^2$, $\delta_i=\delta\left(r_i/r_\star\right)^2$, $\nu_i^2=\nu^2r_\star/r_i$, $\mu_{0i}=\mu_0\left(r_\star/r_i\right)^{x-1}$
and the new functions $P_{1i}=P_1\left(r_i/r_\star\right)^2$, $\alpha_i=\alpha\left(r_\star/r_i\right)^2$ then the parameter $r_\star$ disappears from the differential equations and from the integrals.
According to the analysis in Chapter 3 (see also [Bog97]) the steady solution is fully determined if we give on this boundary surface eight free functions. One of them ($E_\phi=0$) corresponds to the history of the flow, while the remaining seven corresponds to boundary conditions and regularity conditions at singular points. If we give on the spherical surface $r=r_i$ (with known r_i) the functions of θ:
B_r (or A), B_θ (or the normal derivative of A , $\partial A/\partial r$), V_r (or M^2), P , ρ , Ω , L and $E_\phi=0$, then we can find
$M^2=4\pi\rho V_r^2/B_r^2$, $G^2=r_i^2\sin^2\theta\Omega/L$, $F=-2B_\theta\cos\theta/B_r\sin\theta$, $P_0=\left(2P/\rho_\star V_\star^2\right)_{\theta=0}$, $P_{1i}=\left(2P/\rho_\star V_\star^2-P_0-P_2\alpha^\epsilon\right)/\left(\sin\theta/G\right)^2$ with $\rho_\star=\left(\rho\right)_{\theta=0}M^2$ and $V_\star=\left(V_r\right)_{\theta=0}G^2/M^2$ and we begin the integration. Note that the parameters ξ_i , δ_i , δ_0 , ϵ , μ_i are known from the expressions of the integrals on the surface $r=r_i$, while ν_i^2 , x , μ_{0i} are known from the expressions of the external forces.

7.6 Parametric study of solutions

The two crucial parameters which affect the qualitative behaviour of the model are ξ and ϵ.
First for ϵ, from the expression of the density ρ in Eq. (7.26) it is required that $\epsilon>0$ in order that the density at the axis, $\rho(\alpha=0,R)$ and the pressure are finite. In the case $\epsilon=1$ the electric current $I_p(\alpha,R)$ enclosed by a poloidal magnetic

flux tube $\alpha = const.$ and the corresponding confining azimuthal magnetic field $B_\phi(\alpha, R)$ are proportional to α; this case has been already studied in [ST94] and it was found that cylindrical asymptotics is obtained through oscillations. If $\epsilon > 1$, $I_p(\alpha, R)$ and $B_\phi(\alpha, R)$ are increasing faster with α which results in a stronger magnetic pinching force which eventually reduces the cross-sectional area of the flow tube to zero. Therefore we expect that when $0 < \epsilon < 1$ we obtain asymptotically cylindrical solutions while for larger values ($\epsilon > 1$), solutions where asymptotically $\lim_{R\to\infty} G = 0$, as it may be seen in Figure 7.11. For the larger values of $\epsilon > 1$ the pinching is so strong that oscillations do not exist. This may also be seen from Eq. (7.46) where $k^2 < 0$ for $\epsilon > 1$ (for $\xi(M_\infty^2 - G_\infty^4) > 0$). Note that if $\epsilon > 1$, it is needed to have $\xi > 0$ such that the square roots in Eqs. (7.24), (7.25) are positively defined near the axis $\alpha \approx 0$.

Altogether then, we shall divide accordingly our parametric study to the intervals $0 < \epsilon < 1$, for cylindrical asymptotics with oscillations [cases (a)-(b)] and $\epsilon > 1$, for converging to the axis fieldlines without oscillations [case (c)] .
Second, the parameter ξ is related to the asymptotic value of the pressure component P_1. For cylindrical solutions at $R \gg 1$ we get from the asymptotic analysis

$$P_{1,\infty} = -\xi \left(\frac{\left(M^2-1\right)\left(G^4-M^2\right) + M^2\left(1-G^2\right)^2}{G^2 M^2 \left(1-M^2\right)^2} \right)_\infty .$$

For example when $\xi > 0$, in which case from the integration we find $G_\infty < 1 \ll M_\infty$, we obtain $P_{1,\infty} > 0$ and the pressure gradient assists the magnetic pressure in collimating the outflow. In that respect solutions with $\xi > 0$ correspond to an underpressured jet [TTS97]. On the other hand when $\xi < 0$ in which case from the integration $G_\infty^4 > M_\infty^2 > 1$ and we find $P_{1,\infty} > 0$, $P_{2,\infty} < 0$. In all solutions with cylindrical asymptotics (i.e., for $\epsilon < 1$), one finds that for $\xi > 0$ the total pressure force in the $\hat{\varpi}$ direction $-\hat{\varpi}\vec{\nabla}\left(P + B^2/8\pi\right)$ is towards the axis while for $\xi < 0$ it is in the opposite direction. In all these cases we have $\xi(M_\infty^2 - G_\infty^4) > 0$, or, $\xi\left(\left(\rho V_r^2/2\right)_{\alpha=0,R\gg 1} - \left(\rho V_r^2/2\right)_{\alpha=0,R=1}\right) > 0$. In other words the sign of ξ determines if the poloidal kinetic energy on the axis is larger at the Alfvén point or at infinity. Thus, according to the range of values of ξ and ϵ we distinguish the following cases:

7.6.1 Case (a): $0 < \epsilon < 1$, $\xi > 0$

In this case cylindrical asymptotics is achieved through small amplitude oscillations of decaying amplitude (Type I solutions). In the left panel of Fig. 7.3 the shape of the field/streamlines on the poloidal plane is shown in the inner region between the stellar base, the Alfvén (dashed, $R = 1$) and fast (dot-dashed, $R = 2$) critical surfaces. The poloidal lines are almost radial up to the Alfvén surface while after the fast critical surface they have attained a cylindrical shape. However, the final cylindrical shape of the poloidal field/stream lines is reached further out, i.e., at about $R = 20$, as it is shown in the larger scale of Fig. 7.3

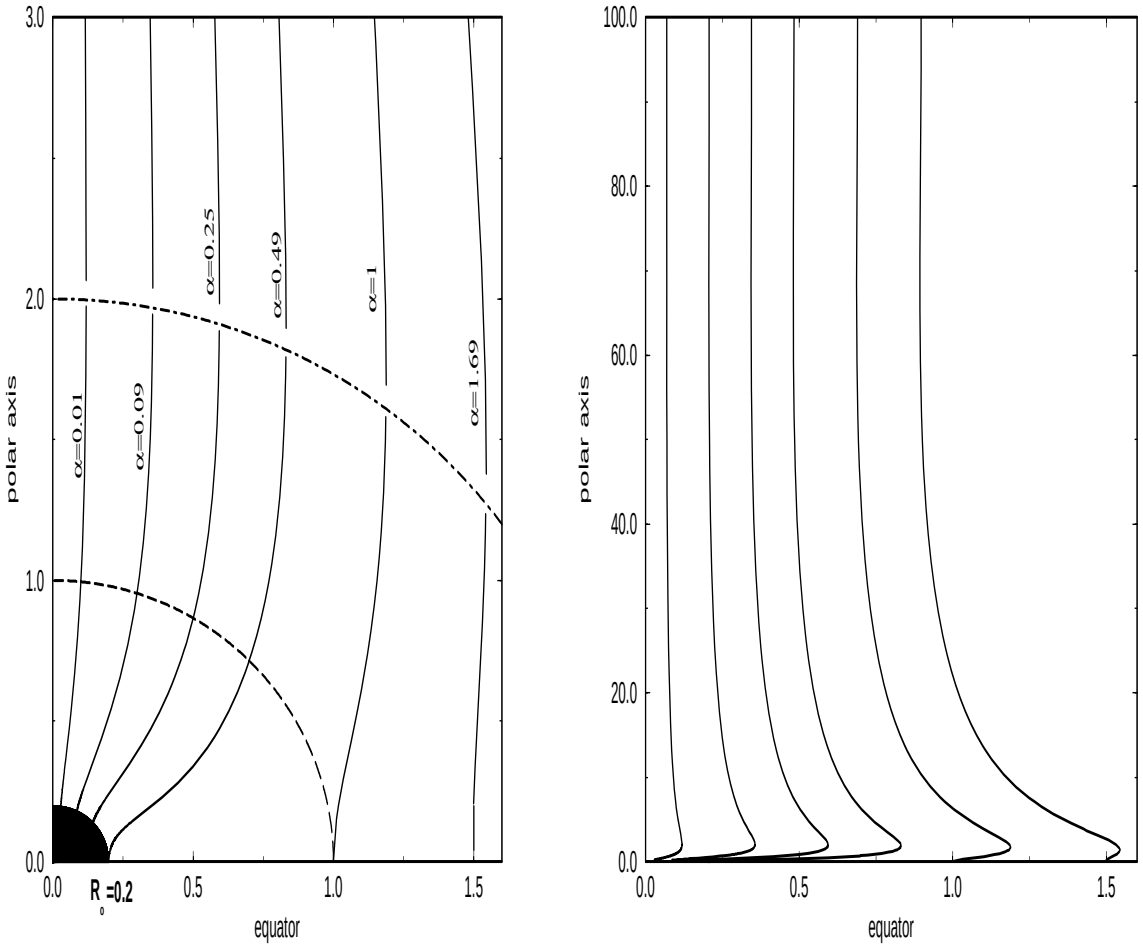

Figure 7.3: Poloidal streamlines for **case (a)** with parameters: $\epsilon = 0.5$, $\xi = 10$, $\delta\nu^2 = 3.5$, $\delta_0\nu^2 = 0.1$, $\mu_0 = 0$, $F_\star = 1$ and $p_\star \approx 2.2655$. For the value of $\epsilon = 0.5$, the magnetic pinching force just collimates the outflow to a jet of finite asymptotic radius.

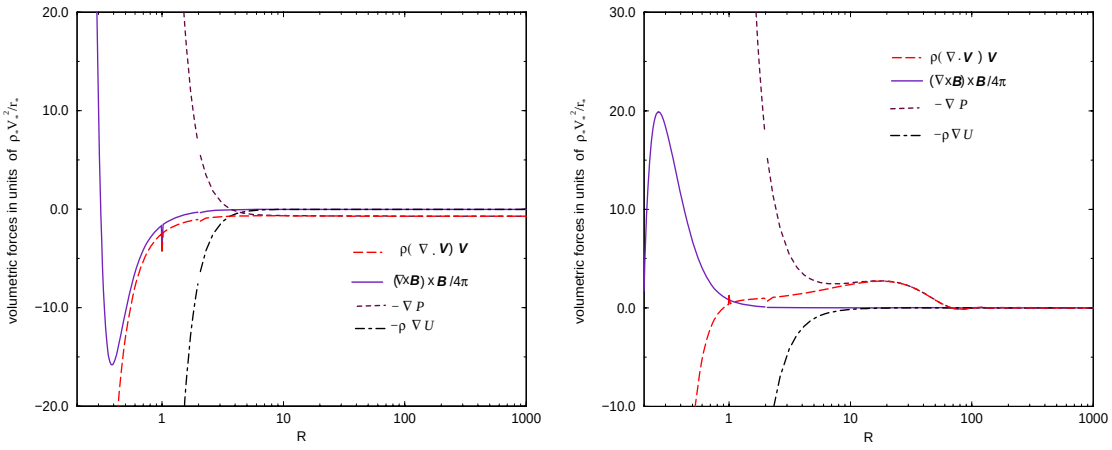

Figure 7.4: In the left panel are plotted the components of the magnetic (solid), pressure gradient (small dashes), gravitational (dot-dashed) and total acceleration (long dashes) perpendicular to the poloidal streamlines on line $\alpha = \alpha_{lim}$ for the parameters of the previous figure. In the right panel the corresponding components parallel to the poloidal lines are plotted also for **case (a)** and the same parameters: $\epsilon = 0.5$, $\xi = 10$, $\delta\nu^2 = 3.5$, $\delta_0\nu^2 = 0.1$, $\mu_0 = 0$, $F_\star = 1$ and $p_\star \approx 2.2655$

(right panel) where their asymptotically cylindrical shape can be better seen. The bending of the poloidal field/stream lines towards the magnetic/rotational axis is caused by the magnetic pinching force as it can be seen in the left panel of Fig. 7.4 where the various components of the forces acting on the plasma perpendicular to the poloidal fieldlines are plotted. In the inner region of the outflow, the total inertial force perpendicular to the lines (centripetal force) is almost exclusively provided by the inwards magnetic force, with the outward pressure gradient balancing the inward component of gravity. Asymptotically however, the magnetic pinching force and gravity are negligible and the pressure gradient of the underpressured jet balances the centrifugal force. The acceleration of the plasma along the poloidal lines can be seen in the right panel of Fig. 7.4. Evidently, in the inner region gravity is balanced by the pressure gradient force and the plasma is accelerated only by the remaining magnetic force while in the outer region where gravity and the magnetic force are negligible, it is accelerated by the dominant pressure gradient force. As it may also seen in the left panel of Fig. 7.6 most of the acceleration occurs on the far region at $R \geq 10$ by the thermal pressure gradient force.

The solution discussed in this representative example crosses the modified by self-similarity fast critical point and a note is in order here on how such a solution may be obtained. First, we integrated Eqs. (7.31) - (7.35) downstream

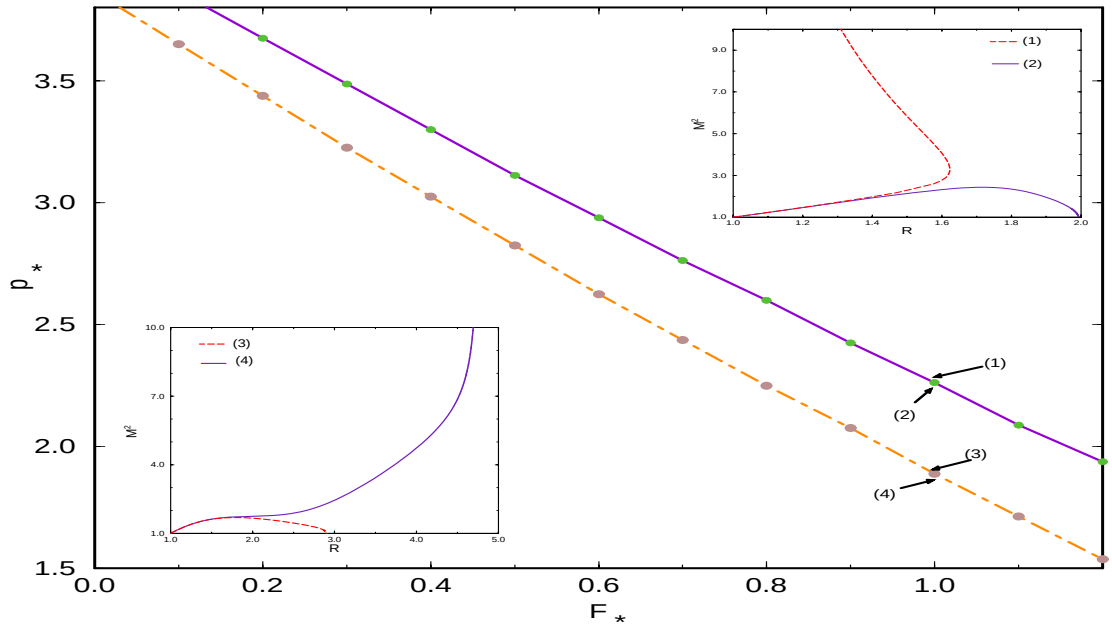

Figure 7.5: The solid line gives the relation between the expansion factor $F_\star$ and the slope $p_\star$ of $M^2(R)$ at the Alfvén point for a solution through all critical points, for **case (a)** with parameters: $\epsilon = 0.5$, $\xi = 10$, $\delta\nu^2 = 3.5$, $\delta_0\nu^2 = 0.1$, $\mu_0 = 0$. The topologies of $M^2(R)$ at the neighboring points (1), (2), (3) and (4) are also shown.

of the Alfvén critical point at which $R = G = M = 1$, $F = F_\star$, $P_1 = P_{1\star}$ and $P_0 = P_{0\star}$, a free parameter which determines the pressure at infinity. At $R = 1$ the Alfvén regularity condition relates $F_\star$, $p_\star$ and $P_{1\star}$, Eq. (7.37). Also there is a relation between $F_\star$, $p_\star$ such that the solution passes through the fast critical point; this is the solid line in Fig. 7.5. Assume for example that we choose $F_\star = 1$ and we vary $p_\star$, Fig. 7.5. There is only one value of $p_\star \approx 2.26$ which satisfies the Alfvén regularity condition and the solution crosses the fast critical point. For other values of $p_\star$ above and below $p_\star \approx 2.26$ we have three different types of unphysical solutions shown in Fig. 7.5:

- from point (1) of Fig. 7.5 corresponding to $p_\star$ higher than 2.26 we get solutions in which the denominator of the differential equation for M^2 becomes zero and the curve $M^2(R)$ turns back to smaller distances,
- from point (2) of Fig. 7.5 corresponding to $p_\star$ lower than 2.26 till point (3) we get solutions in which the numerator of the differential equation

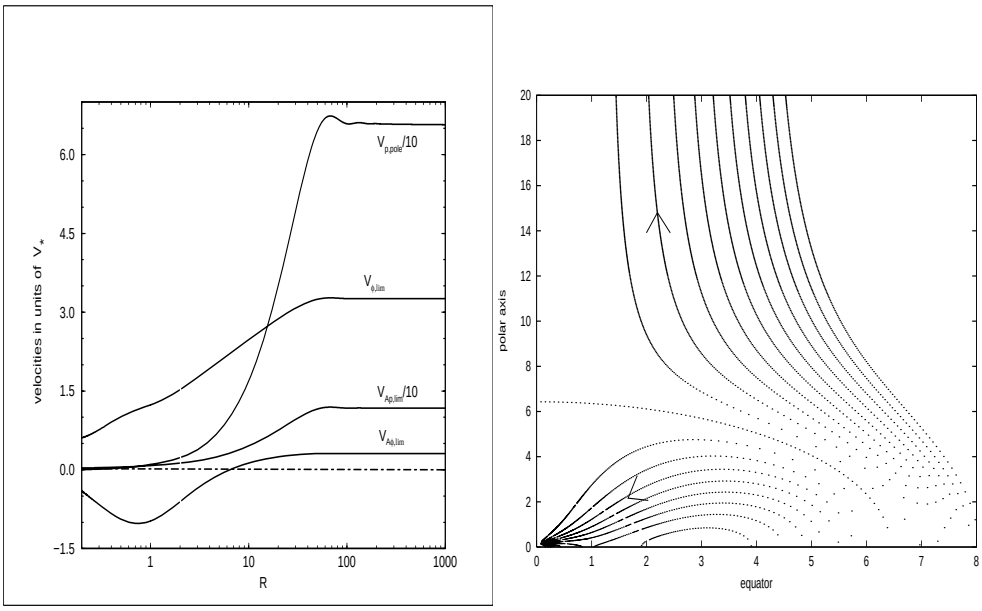

Figure 7.6: Dimensionless velocities (left panel) and current lines (right panel) for **case (a)** with parameters: $\epsilon = 0.5$, $\xi = 10$, $\delta\nu^2 = 3.5$, $\delta_0\nu^2 = 0.1$, $\mu_0 = 0$, $F_\star = 1$ and $p_\star \approx 2.2655$

for M^2 becomes zero and then the solutions become again subAlfvénic,

- finally, from point (4) of Fig. 7.5 we get solutions in which there is a distance R wherein $M \to \infty$ and the solutions terminate there.

A fine tuning between points (1) and (2) gives the unique solution which goes to infinity with superAlfvénic and superfast radial velocity, satisfying also the causality principle for the propagation of MHD perturbations. After finding such a critical value for $p_\star$ we also integrate Eqs. (7.31) - (7.35) upstream of the Alfvén point.
We found from the integration a spherical surface $R = R_I$ in the superAlfvénic regime, where $G = 1$ (but $M \neq 1$), or $B_\phi = 0$. This corresponds to a vanishing poloidal current I_p there (see Eq. (7.36)). For $R < R_I$, as we see in the right panel of Fig. 7.6, the current lines are closed, while for $R > R_I$ they are open.

7.6.2 Case (b): $0 < \epsilon < 1$, $\xi < 0$

In this case we may have two possibilities. In one the solution crosses the fast critical point and the situation is similar to the previous case (a). At the same time however asymptotically cylindrical solutions exist which do not cross the modified fast critical point, being simply superAlfvénic. An example of this type of behaviour is shown in Figures 7.7- 7.10. As in case (a), cylindrical asymptotics

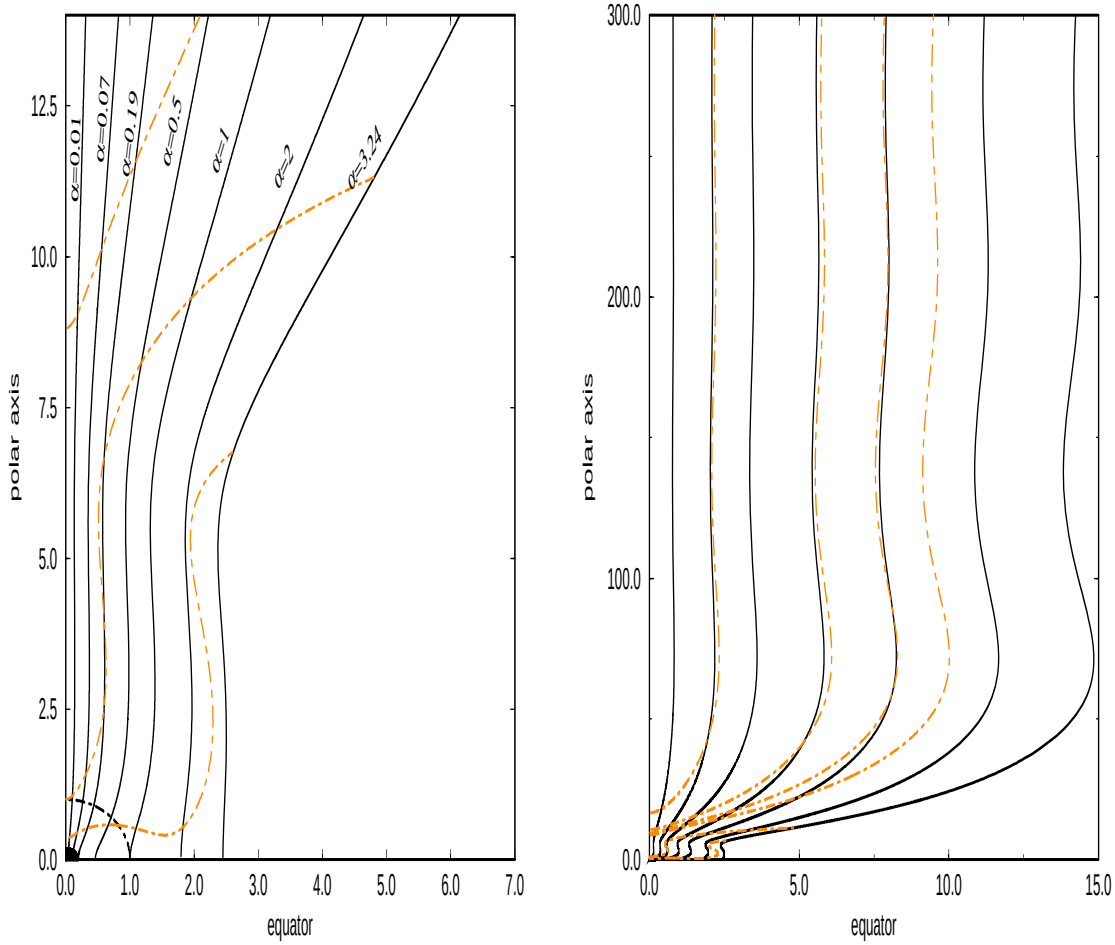

Figure 7.7: Poloidal streamlines for **case (b)** with parameters: $\epsilon = 0.5$, $\xi = -5$, $\delta\nu^2 = 4$, $\delta_0\nu^2 = 0.001$, $\mu_0 = 0$, $F_\star = 1$ and $p_\star = 2$. With dotted lines the density isocontoures are indicated with $\rho/\rho_\star = 0.1, 1, 10$ from top to bottom in the left panel and $\rho/\rho_\star = 0.01, 0.04, 0.07, 1, 10$ from left to right in the right panel. The jet has a finite asymptotic cylindrical radius.

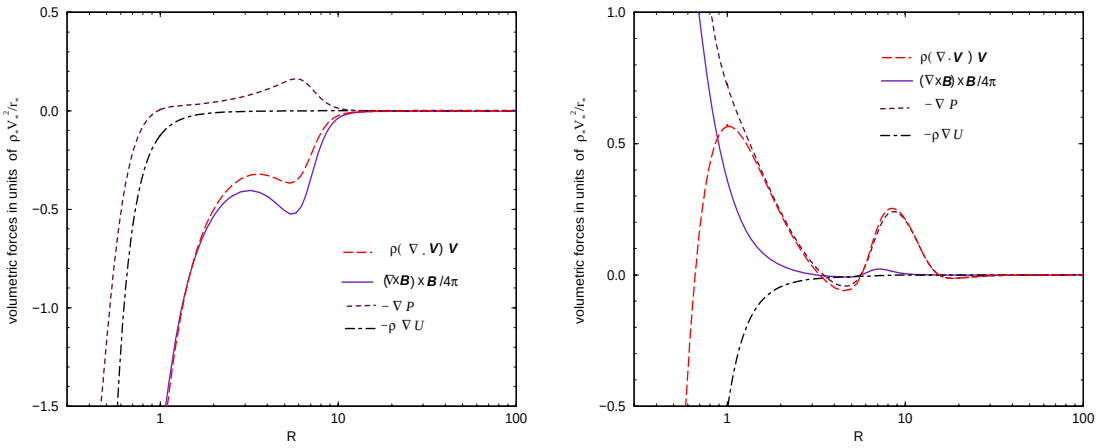

Figure 7.8: In the left panel are plotted the components of the magnetic (solid), pressure gradient (small dashes), gravitational (dot-dashed) and total acceleration (long dashes) perpendicular to the poloidal streamlines on line $\alpha = \alpha_{lim}$. In the right panel the corresponding components parallel to the poloidal lines are plotted also for **case (b)** and the same set of parameters: $\epsilon = 0.5$, $\xi = -5$, $\delta\nu^2 = 4$, $\delta_0\nu^2 = 0.001$, $\mu_0 = 0$, $F_\star = 1$ and $p_\star = 2$

is achieved through oscillations of decaying amplitude (Type I solutions). In the left panel of Fig. 7.7 the shape of the field/streamlines on the poloidal plane is shown in the inner region between the stellar base and the Alfvén (dashed, $R = 1$) critical surface. The poloidal lines are almost radial up to this Alfvén surface while outside $R = 1$ they attain a cylindrical shape. However, the final cylindrical shape of the poloidal field/stream lines is reached further out, i.e., at about $R = 20$, as it is shown in the larger scale of the right panel of Fig. 7.7 where their asymptotically cylindrical shape obtained through the decaying amplitude oscillations can be better seen.

As in case (a), the focusing of the poloidal field/stream lines towards the magnetic and rotation axis is caused predominantly by the magnetic pinching force; this may be seen in the left panel of Fig. 7.8 where the various components of the forces acting on the plasma *perpendicular* to the poloidal fieldlines are plotted. In the inner region of the outflow $R \lesssim 1$, the total inertial force perpendicular to the lines (centripetal force) is almost exclusively provided by the inwards magnetic force. In the far zone where gravity is negligible, $R \gtrsim 1$, the inwards magnetic pinching force is balanced by the pressure gradient of the overpressured jet and the centrifugal force. The acceleration of the plasma *along* the poloidal lines can be seen in the right panel of Fig. 7.8. In the inner region $R \lesssim 1$ the magnetic and pressure gradient forces accelerate the plasma; in the outer region where gravity and the magnetic forces are negligible, the pressure

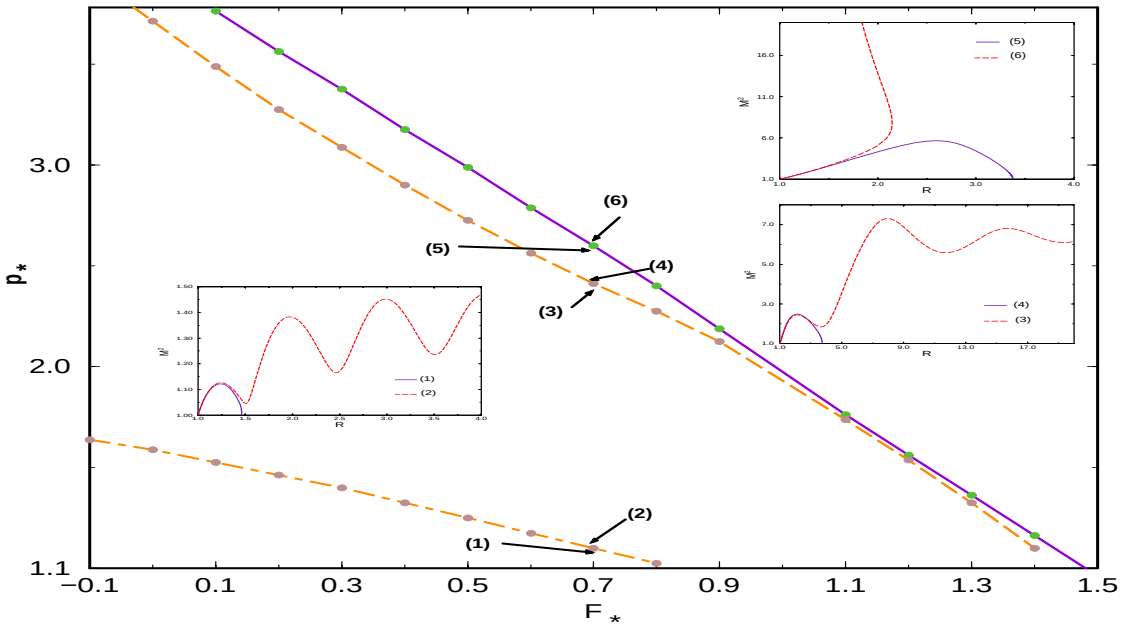

Figure 7.9: The solid line gives the relation between the expansion factor $F_\star$ and the slope $p_\star$ of $M^2(R)$ at the Alfvén point for a solution through all critical points, for **case (b)** with parameters: $\epsilon = 0.5$, $\xi = -5$, $\delta\nu^2 = 4$, $\delta_0\nu^2 = 0.001$, $\mu_0 = 0$. The topologies of $M^2(R)$ at the neighboring points (1) to (6) are also shown.

gradient force is left alone to accelerate the plasma. As in case (a), it may also be seen in the right panel of Fig. 7.8 that most of the acceleration occurs in the far region at $R \approx 10$ by the thermal pressure gradient force.

Figure 7.9 is a plot of the values of $p_\star$ and $F_\star$ for which the fast point is crossed. As in case (a), we integrated Eqs. (7.31) - (7.35) downstream of the Alfvén critical point at which $R = G = M = 1$, $F = F_\star$, $P_1 = P_{1\star}$ and $P_0 = P_{0\star}$. At $R = 1$ the Alfvén regularity condition relates $F_\star$, $p_\star$ and $P_{1\star}$, Eq. (7.37). Also there is a relation between $F_\star$,$p_\star$ such that the solution passes through the fast critical point; this is the solid line in Fig. 7.9. Assume for example that we choose $F_\star = 0.7$ and we vary $p_\star$, Fig. 7.9. There is only one value of $p_\star \approx 2.6$ which satisfies the Alfvén regularity condition and the solution crosses the fast critical point. For other values of $p_\star$ above and below $p_\star \approx 2.6$ we have different types of solutions shown in Fig. 7.9:

- at point (6) of Fig. 7.9 corresponding to $p_\star$ higher than $p_\star \approx 2.6$ we get solutions in which the denominator of the differential equation for M^2 becomes zero and the curve $M^2(R)$ turns back to smaller distances,

- at points (5), (4) and (1) of Fig. 7.9 we get solutions in which the numerator of the differential equation for M^2 becomes zero and then the solutions become again subAlfvénic,

- at points (2) and (3) of Fig. 7.9 we get oscillatory solutions which do not cross the fast critical point. These solutions were shown in the previous Figures 7.7,7.8,7.10.

A fine tuning between points (6) and (5) gives the unique solution which goes to infinity with superAlfvénic and superfast radial velocity.

Note that in this case there exists a value α_{out} where $V_\phi = 0$ and $B_\phi = 0$. In this streamline the poloidal current is zero. For $\mu = 9$ and the parameters as in Fig. 7.7, $\alpha_{out} = 3.24$.
If we examine Eq. (7.36) we see that in the case where $\xi < 0\,, 0 < \epsilon < 1$, there is a line $\alpha_I = \left(\frac{\mu\,(\epsilon+1)}{2\mid \xi \mid}\right)^{\frac{1}{1-\epsilon}}$ where the absolute poloidal current $\mid I_p \mid$ has a maximum. For $\alpha < \alpha_I$ the current density flows upstream, while for $\alpha > \alpha_I$ it flows downstream (see the right panel in Fig. 7.10). On the line $\alpha_{out} = \left(\frac{\mu}{\mid \xi \mid}\right)^{\frac{1}{1-\epsilon}}$ we have $I_p = 0$ and $B_\phi = 0$.

7.6.3 Case (c): $\epsilon > 1$, $\xi > 0$

As discussed in the beginning of Sec. 7.6, when $\epsilon > 1$ the strong magnetic pinching force results in a jet of zero asymptotic radius; in addition, this asymptotics is achieved without oscillations, i.e., we obtain type II solutions, Fig. 7.11 - 7.13. The values of $p_\star$ and $F_\star$ for which the solution crosses the fast critical point are shown in Fig. 7.12.

As with the previous cases, for each value of $F_\star$ there is only one value of the Alfvén number slope $p_\star$ such that the solution passes through the fast critical point; this is the solid line in Fig. 7.12. Assume for example that we choose $F_\star = 0.8$ and we vary $p_\star$, Fig. 7.12. There is only one value of $p_\star \approx 2.53$ which satisfies the Alfvén regularity condition and the solution crosses the fast critical point. For other values of $p_\star$ above and below $p_\star \approx 2.53$ we have two different types of unphysical solutions shown in Fig. 7.12:

- at point (1) of Fig. 7.12 corresponding to $p_\star$ higher than 2.53 we get solutions in which the denominator of the differential equation for M^2 becomes zero and the curve $M^2(R)$ turns back to smaller distances,

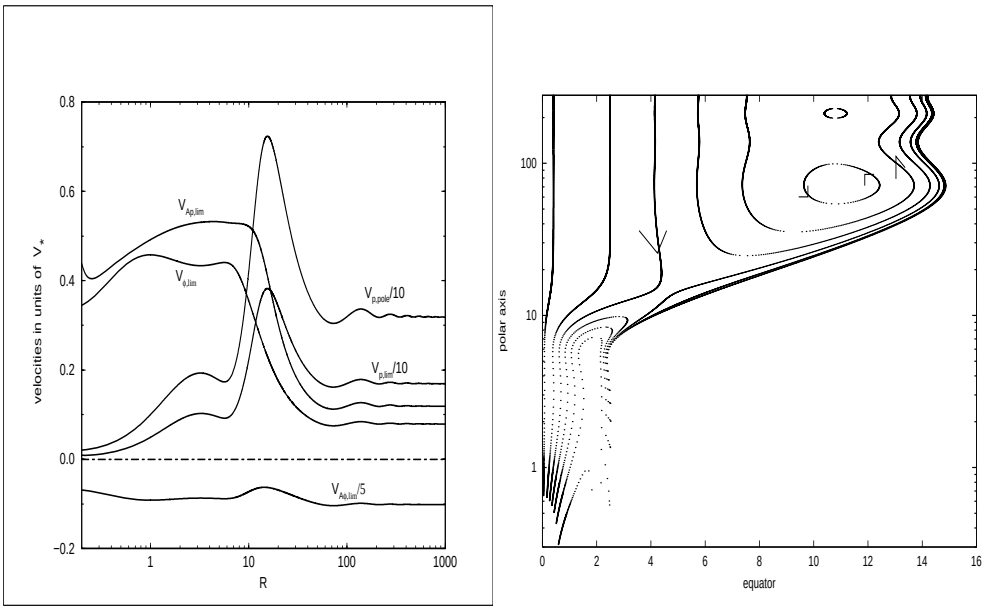

Figure 7.10: Dimensionless velocities (left panel) and current lines (right panel) for **case (a)** with parameters: $\epsilon = 0.5$, $\xi = -5$, $\delta\nu^2 = 4$, $\delta_0\nu^2 = 0.001$, $\mu_0 = 0$, $F_\star = 1$ and $p_\star = 2$

- at point (2) of Fig. 7.12 corresponding to $p_\star$ lower than 2.53 we get solutions in which the numerator of the differential equation for M^2 becomes zero and then the solutions become again subAlfvénic,

A fine tuning between points (1) and (2) gives the unique solution which goes to infinity with superAlfvénic and superfast radial velocity. Nevertheless, the jet radius goes to zero in this case.

7.6.4 The case where $\delta_0 = 0$

We examine this special case only because for $\delta_0 = 0$, Eq. (7.32) can be integrated at once to give

$$\frac{G^4 - M^2}{G^{2(\epsilon+1)} M^2 \left(1 - M^2\right)} = constant\,.$$

This constant is equal with $1 + 2\left(F_\star - 2\right)/p_\star$ (at the Alfvén point) or $\left(G_\infty^4 - M_\infty^2\right)/G_\infty^{2(\epsilon+1)} M_\infty^2 \left(1 - M_\infty^2\right)$ (at infinity).
The derivative dM^2/dG^2 is of the form 0/0 if $M_x^2 = (\epsilon+1)/(\epsilon+3)$, $G_x^4 = (\epsilon+1)^2/(\epsilon+3)(\epsilon-1)$, so there is a critical point if $\epsilon > 1$ (when $M_x < 1\,, G_x > 1$) or $\epsilon < -3$ (when $M_x > 1\,, G_x > 1$). The solution pass from this point when $p_\star = (2 - F_\star)/C_x$ with $C_x = \frac{1}{2} - \frac{\epsilon+3}{2(\epsilon-1)} \left[\frac{(\epsilon+3)(\epsilon-1)}{(\epsilon+1)^2}\right]^{\frac{\epsilon+1}{2}}$. Both solutions are

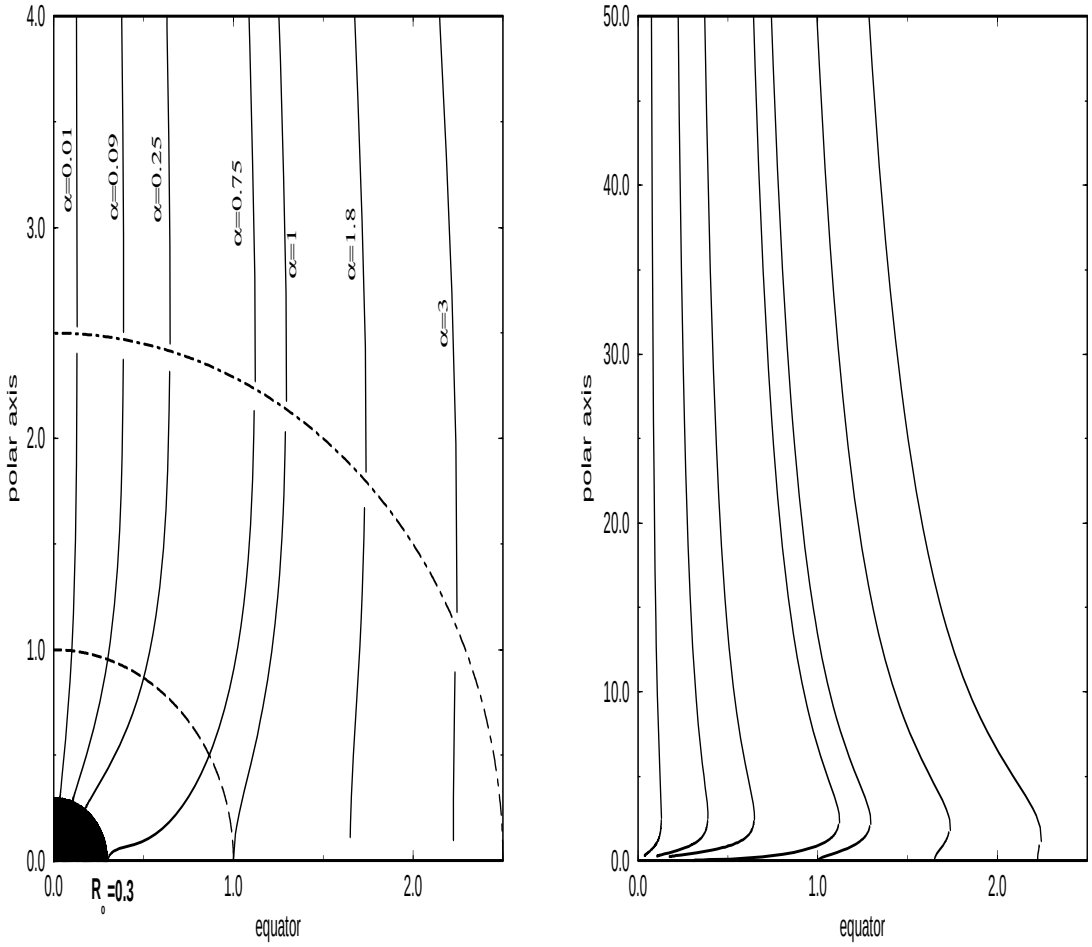

Figure 7.11: Poloidal streamlines for **case (c)** with parameters: $\epsilon = 2$, $\xi = 10$, $\delta\nu^2 = 4$, $\delta_0\nu^2 = 0.1$, $\mu_0 = 0$, $F_\star = 0.8$ and $p_\star \approx 2.5636$. The strong magnetic pinching force results in a jet of zero asymptotic cylindrical radius in this case.

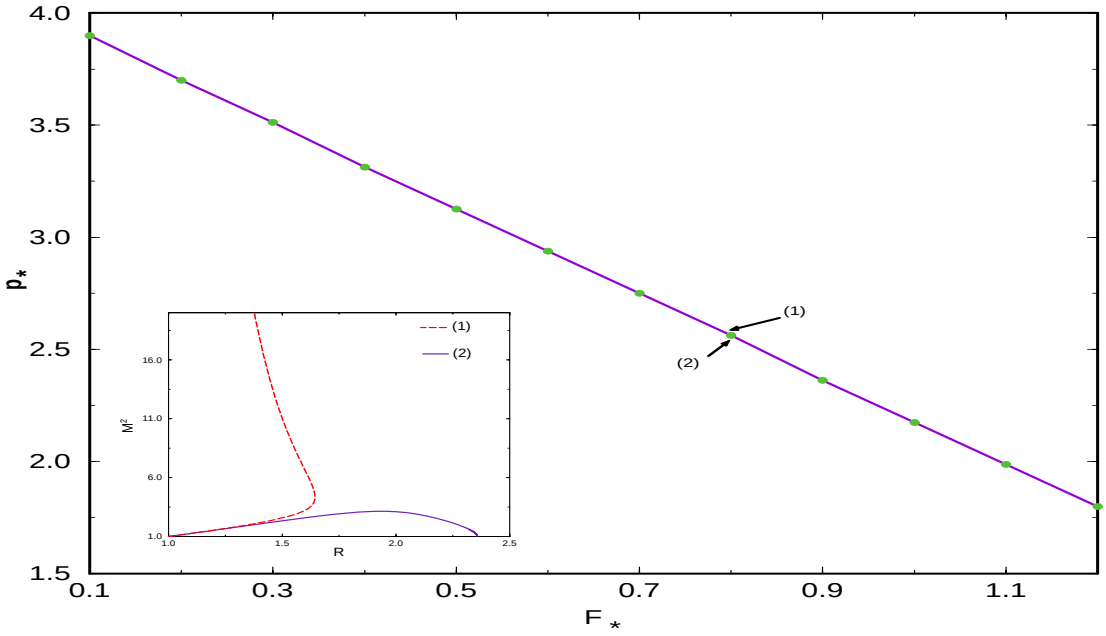

Figure 7.12: The solid line gives the relation between the expansion factor $F_\star$ and the slope $p_\star$ of $M^2(R)$ at the Alfvén point for a solution through all critical points, for **case (c)** with parameters: $\epsilon = 2$, $\xi = 10$, $\delta\nu^2 = 4$, $\delta_0\nu^2 = 0.1$, $\mu_0 = 0$.

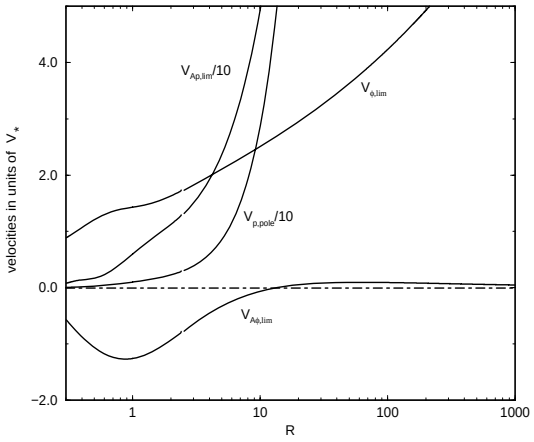

Figure 7.13: Dimensionless velocities for case (**c**) with parameters: $\epsilon = 2, \xi = 10$, $\delta\nu^2 = 4$, $\delta_0\nu^2 = 0.1$, $\mu_0 = 0$, $F_\star = 0.8$ and $p_\star \approx 2.5636$.

unphysical, since for $\epsilon < 0$ we have infinite density on the polar axis, and for $\epsilon > 1$ we are in the subAlfvén regime but we have cross section bigger than the Alfvén cross section.

7.7 Astrophysical Applications

It should be noted that the purpose of this study has not been to construct a specific model for a given collimated outflow; instead, our goal has been to outline via a specific class of exact and self-consistent models, the interplay of the various MHD processes contributing into the acceleration and collimation of jets. Nevertheless, the illustrative examples analyzed in this Chapter can be compared with the observable characteristics of outflows from stellar or galactic objects, say, those associated with young stellar objects. For this purpose, in the following we establish the connection between the nondimensional models and the observable parameters of the outflow.

Suppose that at the polar direction of the stellar surface ($r = r_0\,, \alpha = 0$) we know the values of $V_r\,, B_r$ and ρ, say, V_0, B_0 and ρ_0, respectively. Then we may calculate $M_0 = V_0\sqrt{4\pi\rho_0}/B_0$. From the integration we can find the distance R_0 where $M(R_0) = M_0$. Thus we may calculate the Alfvén distance $r_\star = r_0/R_0$. Each line which has its footpoint on the stellar surface at angle θ_i is labeled by $\alpha = \left(r_0 \sin\theta_i / r_\star G\left(r_0/r_\star\right)\right)^2$. The last line originating from the star is α_{lim}. Each line which has its footpoint on the disk at distance $r_i > r_0$ from the axis of rotation is labeled by $\alpha = \left(r_i/r_\star G\left(r_i/r_\star\right)\right)^2 > \alpha_{lim}$.

If at the stellar surface $G(R_0) = G_0$ we find the Alfvén values, $V_\star = V_0 G_0^2/M_0^2$, $B_\star = B_0 G_0^2$, $\rho_\star = \rho_0 M_0^2$ and from Eqs. (7.26) to (7.29) we can find all physical quantities at any point. For example at $R \gg 1$, $\alpha = 0$ we have the following asymptotic values: $V_\infty = V_0 G_0^2 M_\infty^2/M_0^2 G_\infty^2$, $B_\infty = B_0 G_0^2/G_\infty^2$, $\rho_\infty = \rho_0 M_0^2/M_\infty^2$.

7.7.1 Model of case (a)

For a typical solution with parameters as those plotted in Fig. 7.3 and $r_0 = 2 \times 10^{11} cm$, $V_0 = 3 \times 10^4 cm/sec$, $B_0 = 7 \times 10^{-3} G$, $\rho_0 = 1.6 \times 10^{-17} gr/cm^3$ we find $R_0 = 0.2$, $M_0^2 = 3,2 \times 10^{-3}$, $G_0^2 = 8.2 \times 10^{-2}$ and $M_\infty^2 = 31.3$, $G_\infty^2 = 0.477$ so we have $\alpha_{lim} = 0.49$, $r_\star = 10^{12} cm$ and $V_\infty = 5 \times 10^7 cm/sec$, $B_\infty = 10^{-3} G$, $\rho_\infty = 1.66 \times 10^{-21} gr/cm^3$ (or $n_\infty = 10^3/cm^3$). Choosing $\nu^2 = 462$ we have a stellar mass $2 \times 10^{33} gr$ while for $\mu = 0.01$ the angular velocity at the equatorial point of the stellar surface is $2 \times 10^{-6}/sec$.
Note that in this case (a) the toroidal component of the magnetic field changes sign at some spherical surface (*c.f.* the velocity $V_{A\phi,lim}$ in the left panel of Fig. 7.6). This means that the poloidal current enclosed by this surface is zero (see the right panel of Fig. 7.6). All fieldlines which pass through this surface have the same cylindrical distance from the axis with the Alfvén point ($G = 1$ at this spherical surface) while for larger distances $G < 1$. After crossing this surface the Poynting flux changes its sign and thus the toroidal component of the velocity becomes large enough (in general $V_\phi/\varpi\Omega = \left(M^2 - G^2\right)/G^2\left(M^2 - 1\right)$).

7.7.2 Model of case (b)

If the star has radius $r_0 = 2 \times 10^{11} cm$ and at the pole on the stellar surface $V_0 = 6.5 \times 10^6 cm/sec\,, B_0 = 0.3\ G\,, \rho_0 = 8 \times 10^{-18} gr/cm^3$ we find $r_\star = 10^{12} cm\,, M_0^2 = 4.22 \times 10^{-2}\,, G_0^2 = 0.206$ and $M_\infty^2 = 203\,, G_\infty^2 = 64\,, V_\infty = 10^8 cm/sec\,, \rho_\infty = 1.66 \times 10^{-21} gr/cm^3\,, B_\infty = 10^{-3} G$. The last line connected with the star has $\alpha_{lim} = 0.19$ while the disk has a radius $2.45 \times 10^{12} cm$. If we choose $\nu^2 = 0.3$ then the mass of the star is one solar mass. The equator of the star rotates with a speed $2.7 \times 10^4 cm/sec$ so the angular velocity is $1.3 \times 10^{-7}/sec$.

The asymptotic radius of the jet (which is bounded with the line α_{out}) is 1 *A.U.* while the part of the flow starting from the stellar surface has a radius 0.23 *A.U.*.This part of the jet is collimated at a distance about 4 *A.U.* from the equatorial plane, while the whole solution collimates at the height of 3.3 *A.U.* These results are consistent with recent observations of YSO's [Ray96].

7.7.3 Model of case (b) including radiation

There are two parameters $(\mu_0\,, x)$ related to the radiative force (the third is included into ν^2).

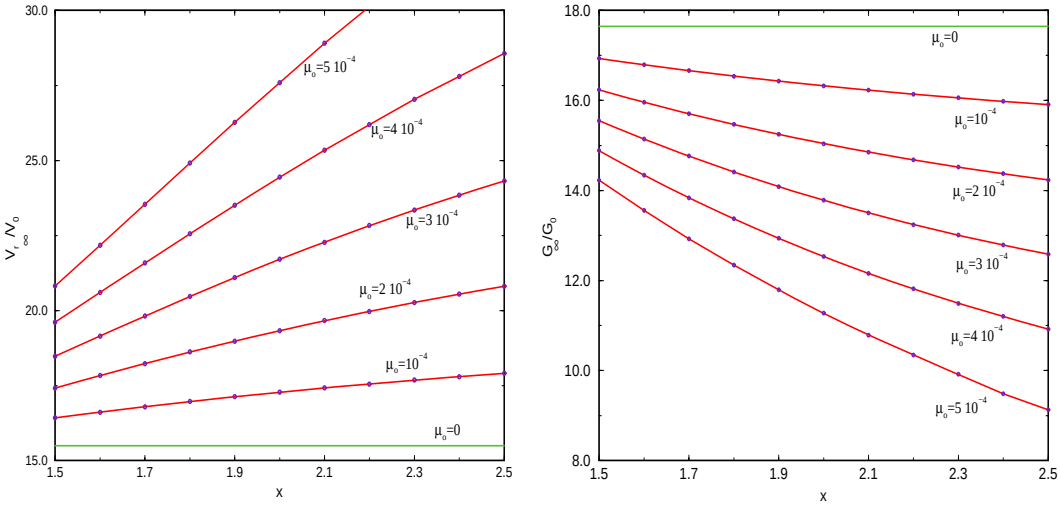

Figure 7.14: Dimensionless asymptotic values of the radial velocity (left panel) and dimensionless asymptotic values of the radius of the jet (right panel) as a function of the radiative force parameters x and μ_0 **for case (b)** with parameters: $\epsilon = 0.5$, $\xi = -5$, $\delta\nu^2 = 4$, $\delta_0\nu^2 = 0.001$, $\nu^2 = 0.3$, $F_\star = 1$ and $p_\star = 2$. In all these cases in the surface of the star $M_0^2 = 4.22 \times 10^{-2}$.

For the parameters of case (b) but for $\mu_0 \neq 0$ we examine the effect of the radiative force on the velocity and the asymptotic radius of the outflow. As we expect, as the radiative force increases, the terminal velocity becomes larger (Fig. 7.14) while the Alfvén surface moves closer to the stellar base. From mass conservation we expect that the cross sectional area of the jet decreases as x increases, as it is shown in Fig. 7.14.

7.8 Summary and Conclusions

In this study we have examined a class of exact solutions of the full set of the MHD equations (7.1) - (7.2) governing the kinematics of a magnetized outflow from a rotating gravitating object. For this system to be closed, an additional equation is needed to describe the energetics of the outflow, i.e., some form of the energy conservation principle, Eq. (7.3). The often used simplifying polytropic relationship between pressure and density which corresponds to a specific functional form of the net heating/cooling in the plasma, was not used. This led to the inconvenient result that the sound speed is ill defined and it can be calculated only at the modified by self-similarity fast MHD critical point. Besides this inconvenience we did not suffer any loss of generality in adopting a more

general functional form of the total heating, than the polytropic assumption implies. As it was explained in subsection 7.2.1, in both, the familiar polytropic case of constant γ and the present nonconstant γ approach, the detailed spatial distribution of the required heating can be calculated only a *posteriori*.

The analyzed class of solutions in this Chapter belongs to the group of nine classes of meridionally selfsimilar MHD solutions which have been shown to exist in [VT98] under the two assumptions that the Alfvén Mach number is a function of the radial distance and the poloidal magnetic field has a dipolar angular dependence, Eq. (7.7) (the only difference is the appearing of F_{rad}). No assumption was made about the asymptotics of the outflows. It is interesting that the self-consistently deduced shape of the streamlines and magnetic field lines was found to be helices wrapped on surfaces which asymptotically are cylindrical. In other words, the streamlines extended to infinite heights above the central object and its disk obtaining the form of a jet. This result may be contrasted to the quite often referred Blandford & Payne [BP82] solutions which by overfocusing towards the axis terminate at finite heights above the disk. The cylindrical asymptotics of the present nonpolytropic solutions agrees with the polytropic analysis of Heyvaerts & Norman [HN89] and also with the class of exact solutions of Sauty & Tsinganos [ST94] for efficient magnetic rotators. However, no radial asymptotics was found in this class of models, contrary to the other class of meridionally selfsimilar solutions examined in [ST94] where for inefficient magnetic rotators radial asymptotics was found; it may be that the present model belongs to the group of efficient magnetic rotators.

The topologies of the solutions are rather rich as it was shown in the plane defined by the slope of the Alfvén number $p_\star$ and the streamline expansion factor $F_\star$ at the Alfvén transition. For example, for a given streamline expansion factor $F_\star$ we obtained terminated solutions for $p > p_\star$, similarly to the corresponding terminated solutions in Parker's [Par58] HD wind, or, the Weber & Davis [WD67] magnetized wind. For a given pressure at the Alfvén point, the requirement that a solution crosses the Alfvén and fast critical points eliminates the freedom in choosing $p_\star$ and $F_\star$ through the corresponding regularity and criticality conditions.

A plotting of the various forces acting along and perpendicular to the poloidal streamlines reveals that the wrapping of the field lines around the symmetry axis is caused predominantly by the hoop stress of the magnetic field which it is already strong at the Alfvén (and fast) critical surfaces. Asymptotically the cylindrical column is confined by the interplay of the inwards magnetic pinching force, the outward centrifugal force and the pressure gradient, as in [TTS97]. On the other hand, the acceleration of the plasma along the poloidal magnetic lines, in the near zone close to the Alfvén distance it is due to the combination of thermal pressure and magnetic forces while at the intermediate zone beyond the Alfvén point it is basically the pressure gradient that is responsible for the acceleration.

Bibliography

[Bir96] T. Biretta, *in Solar and Astrophysical MHD Flows*, K. Tsinganos (ed.), Kluwer Academic Publishers, p. 357, 1996.

[Bog96] S.V. Bogovalov, MNRAS **280** (1996), 39.

[Bog97] S.V. Bogovalov, A&A **323** (1997), 634.

[BP82] R.D. Blandford and D.G. Payne, MNRAS **199** (1982), 883.

[CL94] J. Contopoulos and R.V.E. Lovelace, ApJ **429** (1994), 139.

[CM94] H. Chen and J.M. Marlborough, ApJ **427** (1994), 1005.

[FMBR96] A. Ferrari, S. Massaglia, G. Bodo, and P. Rossi, *in Solar and Astrophysical MHD Flows*, K. Tsinganos (ed.), Kluwer Academic Publishers, p. 607, 1996.

[GWB97] A.P. Goodson, R.M. Winglee, and K.H. Bohm, ApJ **489** (1997), 199.

[HN89] J. Heyvaerts and C.A. Norman, ApJ **347** (1989), 1055.

[KM97] A. Kakouris and X. Moussas, A&A **324** (1997), 1071.

[KM98] A. Kakouris and X. Moussas, A&A **333** (1998), 678.

[KT96] P. Kahabka and J. Trumper, *in Compact Stars in inaries*, E.P.J. Van den Heuvel & J. van Paradijs (eds.), (Dordrecht: Kluwer), p. 425, 1996.

[Lam86] H.J.G.L.M. Lamers, A&A **159** (1986), 90.

[Liv97] M. Livio, *in IAU Colloq. 163, Accretion Phenomena and Related Outflows*, D.T. Wickramasinghe, L. Ferrario, & G.V. Bicknel (eds.), ASP: San Francisco, 1997.

[LT86] B.C. Low and K. Tsinganos, ApJ **302** (1986), 163.

[MR96] I.F. Mirabel and L.F. Rodriguez, *in Solar and Astrophysical MHD Flows*, K. Tsinganos (ed.), Kluwer Academic Publishers, p. 683, 1996.

[OP97a] R. Ouyed and R.E. Pudritz, ApJ **482** (1997), 712.

[OP97b] R. Ouyed and R.E. Pudritz, ApJ **484** (1997), 794.

[Ost97] E. C. Ostriker, ApJ **486** (1997), 306.

[Par58] E.N. Parker, ApJ **128** (1958), 664.

[Ray96] T.P. Ray, *in Solar and Astrophysical MHD Flows*, K. Tsinganos (ed.), Kluwer Academic Publishers, p. 539, 1996.

[SLSC97] T. Shahbaz, M. Livio, K.A. Southwell, and P.A. Charles, ApJ **484** (1997), L59.

[ST94] C. Sauty and K. Tsinganos, A&A **287** (1994), 893.

[Tsi82] K.C. Tsinganos, ApJ **252** (1982), 775.

[TSS+96] K. Tsinganos, C. Sauty, G. Surlantzis, E. Trussoni, and J. Contopoulos, MNRAS **283** (1996), 811.

[TTS92] K. Tsinganos, E. Trussoni, and C. Sauty, *in The Sun: A Laboratory for Astrophysics*, J.T. Schmelz and J. Brown (eds.), Kluwer Academic Publishers, p. 349, 1992.

[TTS97] E. Trussoni, K. Tsinganos, and C. Sauty, A&A **325** (1997), 1099.

[US85] Y. Uchida and K. Shibata, Publ. Astron. Soc. Japan **37** (1985), 515.

[VT97] N. Vlahakis and K. Tsinganos, MNRAS **292** (1997), 591.

[VT98] N. Vlahakis and K. Tsinganos, MNRAS **298** (1998), 777.

[WD67] E.J. Weber and L.J. Davis, ApJ **148** (1967), 217.

Chapter 8

Accretion on dilatonic black hole

A detailed analysis of spherical steady state adiabatic hydrodynamical accretion onto a four dimensional dilatonic black hole is presented. Because the event horizon of a dilatonic black hole possess an area much smaller than a Schwarzschild one of the same mass, and at the same time its accretion radius is indistinguishable from that of an accreting Schwarzschild black hole, accretion flows on the dilatonic background exhibits novel effects particularly as the extreme limit is approached. By a combination of numerical and analytical techniques, it is shown that for any equation of state obeying the causality constraint and any subsonic at infinity flow, there always exist a transonic, regular over the event horizon flow. For background corresponding to a dilatonic black hole approaching the extreme limit, the asymptotic behavior of the transonic flow near the horizon, differs considerably from flows occurring near the horizon of a Schwarzschild black hole. For the former case the accreting plasma even though crosses the horizon supersonicaly, it is not any longer in the state of free fall. Furthermore it is heated enormously, so that the proton component becomes relativistic. As a consequence we have found that the adiabatic assumption is not any longer justified, the need for incorporating radiative transport effects is pointed out. It is argued that if such black holes exist in the universe, they should have a distinct observational signature associated with them.

8.1 Introduction

The discovery of a new class of asymptotically flat spherical black hole solutions of the Einstein non vacuum field equations [Gib82, GM88, GHS91] caught many researchers by surprise. The new class establishes beyond any doubts that in general non-linearities in field configurations may resist the pull of gravity and thus peacefully coexist with a regular event horizon. Furthermore the new class constitutes a counterexample to the popular believe that isolated black

holes have always their exterior empty apart from an electromagnetic field. The "hair" consists of a dilaton coupled to a U(1) field. In the domain of outer communication the geometry of a dilatonic black hole (nick name for the new class) can be written in the following manner:

$$ds^2 = -(1-\frac{2M}{r})dt^2 + (1-\frac{2M}{r})^{-1}dr^2 + g(r)d\Omega^2\,, \tag{8.1}$$

where $g(r) = r^2(1-\frac{Q}{Mr})$, $M > 0$ is the mass of the hole while Q stands for a combination of the electric or magnetic charge q and the value of the dilatonic field at infinity namely $Q = q^2e^{2\phi_o}$. We shall denote here after by $\overline{a} = \frac{Q}{M^2}$. The black hole sector characterized by positive M and values of $\overline{a}$ in the interval [0,2]. More specifically $\overline{a} = 2$ characterize the extreme dilatonic solution, $\overline{a} > 2$ covers the space of naked singularities while for $\overline{a} = 0$ the Schwarzschild black is recovered. Introducing a new dimensionless parameter $\chi = \frac{r}{2M}$ and computing the scalar curvature R and proper area A_o of r =constant spheres one finds

$$R = \frac{\overline{a}}{32}(\frac{M}{m_{pl}}l_{pl})^{-2}\frac{4(\chi-1)}{(2\chi-\overline{a})^2}\chi^{-3}\,, \tag{8.2}$$

$$\frac{A_o(\chi)}{4\pi} = \frac{1}{2}(\frac{M}{m_{pl}}l_{pl})^2[\chi(2\chi-\overline{a})]\,, \tag{8.3}$$

where m_{pl} and l_{pl} are respectively the Planck mass and length. Expression (8.3) implies for $\overline{a} > 2$ the spacetime singularity "lies outside the event horizon". Furthermore Eqs. (8.1)-(8.3) show that the dilatonic black hole possesses a few distinct properties worth mentioning. At first the extreme case and in sharp contrast to the extreme Reissner-Nordstrom solution, is characterized by a pointlike singular event horizon. Furthermore thermodynamically it possesses non zero Hawking temperature and vanishing entropy, in contradistinction to the thermodynamical properties of an extreme Reissner-Nordstrom solution (zero Hawking temperature, non vanishing entropy). Away from the extreme limit, a first look at the line elements in Eq. (8.1) suggests, that the geometry of a dilatonic black hole should not differ very much from the well known Schwarzschild one.The two metrics "differ at one point". The dilatonic metric endows the proper area of the SO(3) orbits with less area than the corresponding Schwarzschild. In fact Eq. (8.3) shows that a dilatonic state close to the extreme limit could possess an event horizon whose proper area lies many orders of magnitude bellow the corresponding area for a Schwarzschild black hole. In addition Eq. (8.3) shows that as one approaches the extreme limit, for instance even assuming an extremely fined-tuned value $\overline{a} - 2 = 10^{-5}$ then for a solar mass black hole the area radius, lies many orders of magnitude below the Planckian values. Therefore quantum gravitational effects on the black hole exterior can be ignored. In fact such nearly extreme states are rather bizzare. Extremely compact in size, but at the same time exerting the same gravitational influence as a solar mass Schwarzschild black hole does. Besides this purely geometrical difference, as already stated earlier,the dilatonic states are accompanied by classical hair. From

the observational point of view, the background dilaton field is not expected to play any significant role, at least for the range of energy scales where various astrophysical process take place. On the other hand the background monopole electric or magnetic field may be of importance. An electrically charged dilatonic black hole, residing somewhere in the universe, likely to get neutralized via preferential accretion of charge of the opposite sign. Such process presumably will drive $\overline{a}$ towards zero. It would be then of some independent interest to find out what will happen to the dilaton field. For the magnetically charged hole, the background monopole field cannot be transformed away. Depending on its strength it is expected to play significant role in astrophysical process involving angular momentum and charged particles. Note however for purely radial infall the exerted Lorentz force is vanishing and thus its role is insignificant.

In view of the above differences one wonders whether the new class interacts with the rest of the universe in an entirely different fashion than the corresponding Schwarzschild one. Since accretion of ambient matter is the dominant interaction mode of black holes with the external world, it is natural to examine accretion phenomena on a magnetically charged dilatonic background. As a preliminary step, in the present Chapter a detailed examination of Bondi adiabatic accretion [Bon52], will be discussed. Recall, such accretion is radial, therefore the background monopole magnetic field is unimportant. So the main focus of the present Chapter, is to probe possible effects upon hydrodynamical flows, due to the the rapid reduction in the area of the $SO(3)$ spheres as the event horizon is approached. A priori it is not clear whether smooth accretion flows exist for all values of $\overline{a}$ in [0,2]. For instance, development of standing shocks is a possibility. In addition presence of multiple critical points is not excluded. In particularly the second possibility is enhanced in view of the close connection between multiple critical points and the rapid convergence-divergence in the cross sectional area of the "tube" where the flow takes place [Hol77, HT83]. For comparison purposes we may recall that Bondi accretion on a Schwarzschild background is rather well behaved. It has been established that as long as adiabaticity is maintained and the flow is subsonic at infinity, there always exist a unique transonic flow regular over the event horizon. Because of the way $\overline{a}$ enters the metric, it is expected that Bondi accretion on a dilatonic background to share the same properties as well provided $\overline{a}$ remains close to zero. However things become unclear as $\overline{a}$ deviates away from the zero value and in particularly for the nearly extreme dilatonic backgrounds.

Primarily motivated by the above questions, we begin the Chapter by first reminding the reader of the relevant equations governing spherical, steady state flows on a dilatonic background. In section (8.4) we discuss the delicate issue of the critical points admitted by the flow equations. It is shown that for any dilatonic black hole, the relevant hydrodynamical equations, always admit a critical point of the sadle type, which is located outside the event horizon. The extreme one, admits an additional critical point residing on the pointlike singular event horizon. It is found that the accretion rate is insensitive to all values of $\overline{a}$, even for the extremal ones. In the same section an equivalent formulation of the flow equations are presented which shows that the critical point is actually

a sonic horizon. With the help of numerical integration the existence of a unique transonic solution subsonic at infinity, passing through the critical point and reaching supersonicaly the event horizon is established. Its asymptotic behavior as well as its regular nature near the horizon is discussed in details. We found that the transonic flow near the horizon may differ significantly from that occurring on a Schwarzschild background. Specifically while for the latter the flow is in a free fall state, for a nearly extreme dilatonic background that is any longer so. Because the even horizons cross section is reduced considerably the flow is retarded significantly, resulting into extreme dense plasma. Consequences of this retardation is discussed. In particularly the adiabaticity assumption is put under scrutiny. We present arguments indicating adiabaticity is not any longer compatible with flows taking place on holes approaching the extreme limit. The physical reasons leading to this behavior is presented in details. We finish the Chapter by commenting on some open problems and discussing possible observational signatures associated with dilatonic black holes.

8.2 Bondi accretion on a dilatonic black hole

We begin by considering a perfect fluid moving on the background of Eq. (8.1). The fluid is considered to be a test one, thus causing negligible distortion on the background geometry. It is described by a conserved stress tensor

$$T_{\alpha\beta} = (\rho + P)u_\alpha u_\beta + P g_{\alpha\beta} \tag{8.4}$$

and a conserved baryon current $J_\alpha = n u_\alpha$ i.e.:

$$\nabla_\alpha T^{\alpha\beta} = 0 \text{ and} \tag{8.5}$$

$$\nabla_\alpha (n u^\alpha) = 0 \,. \tag{8.6}$$

In above $\rho, n, P,$ are the total mass-energy density, baryon number density and pressure respectively as measured by an observer comoving with the fluid. As long as there is no external supply of energy and irrespectively of the equation of state, the first law of thermodynamics combined with the conservation Eqs. (8.5), (8.6) implies that the fluid evolves without its constituents exchanging any heat i.e. the motion is adiabatic. Thus if S, T are the entropy per baryon and temperature respectively as measured in the local rest frame of the fluid then,

$$u^\mu \nabla_\mu (\frac{\rho}{n}) + P u^\mu \nabla_\mu (\frac{1}{n}) = T u^\mu \nabla_\mu S = 0 \,. \tag{8.7}$$

The covariant conservation of the stress tensor is equivalent to:

$$u^\alpha \nabla_\alpha \rho + (\rho + P)\nabla_\alpha u^\alpha = 0 \,, \tag{8.8}$$

$$(\rho + P) u^\beta \nabla_\beta u_\alpha = -\nabla_\alpha P - u_\alpha u^\beta \nabla_\beta P \,. \tag{8.9}$$

Making use of Eq. (8.1), spherical symmetry and the steady state character of the flow, the continuity Eq. (8.6) and Euler Eq. (8.9) yield:

$$\frac{d}{dr}(nug) = 0\,, \tag{8.10}$$

$$(\rho + P)(\frac{du_o}{dr}) + u_o \frac{dP}{dr} = 0\,, \tag{8.11}$$

$$u\frac{du}{dr} = -\frac{1}{(\rho + P)}\frac{dP}{dr}(1 - \frac{2M}{r} + u^2) - \frac{M}{r^2}\,. \tag{8.12}$$

Eq. (8.8) is automatically satisfied, provided Eqs. (8.9)-(8.12) hold. In above u stands for the radial component of the flow i.e. u^r and $u_o = g_{tt}u^o$. Taking into account the adiabaticity assumption the following conservation laws can obtained from Eqs. (8.10)-(8.12):

$$4\pi mnug = \dot{M}\,, \tag{8.13}$$

$$(\frac{\rho + P}{n})^2(1 - \frac{2M}{r} + u^2) = (\frac{\rho + P}{n})^2|_\infty\,, \tag{8.14}$$

$$\frac{\rho + P}{n}u_o = -\frac{\rho + P}{n}|_\infty\,. \tag{8.15}$$

The parameter m stands for a mass scale associated with the baryons. $\dot{M}$ is a spacetime independent constant representing the accretion rate of rest mass energy down to the horizon while the right hand side of Eqs. (8.14), (8.15) are computed at infinity. Conservation laws Eqs. (8.14), (8.15) are actually not independent of each other. They are different ways of expressing the covariant version of Bernoulli equation i.e.:

$$u^a \nabla_a [\frac{\rho + P}{n}(g_{bc}u^b \xi^c)] = 0\,,$$

valid for any geometry admitting a Killing field ξ and any flow invariant under the action of the isometry. Assuming an equation of state $P = P(n, S)$ and introducing the adiabatic speed of sound a via $a^2 = \frac{dP}{d\rho}|_s$ Eqs. (8.10)-(8.12) can be recast as:

$$u^{'} = \frac{D_1}{D}\,, \tag{8.16}$$

$$n^{'} = -\frac{D_2}{D}\,, \tag{8.17}$$

$$u_o^{'} = -\frac{u_o a^2}{n}\frac{D_2}{D}\,, \quad \text{where} \tag{8.18}$$

$$D = \frac{u^2 - a^2(1 - \frac{2M}{r} + u^2)}{un}\,, \tag{8.19}$$

$$D_1 = -\frac{1}{n}[\frac{M}{r^2} - Aa^2(1 - \frac{2M}{r} + u^2)]\,, \tag{8.20}$$

$$D_2 = \frac{1}{u}[-\frac{M}{r^2} + Au^2]\,, \tag{8.21}$$

and A is defined by

$$A \equiv \frac{d}{dr}\ln \mid g(r) \mid = \frac{4\chi - \overline{a}}{2M\chi\,(2\chi - \overline{a})}\,.$$

Eqs. (8.16)-(8.21) are the basic equations describing the flow. We shall ignore here after Eq. (8.18) as redundant and concentrate on Eqs. (8.16), (8.17). An inspection of them shows that they reduce to the corresponding flow equations for Schwartzcild background provided $g(r) = r^2$. It is worth however to note the non trivial manner the parameter $\overline{a}$ enters the flow equations. A close look at D_1,D_2 shows whereas for the Schwarzschild case and near the event horizon, the first term within the square bracket in Eqs. (8.20), (8.21) dominates the rest, the situation is reversed for the class of dilatonic black holes approaching the extreme limit. In fact at the extreme limit the second term diverges. Following Bondi and others, any type of radiation losses will be initialy ignored and thus adopt the polytropic equation of state $P = P(n) = Kn^{\Gamma}$ as the relevant equation of state describing the accreting plasma. The parameter K is a constant and the polytropic index will satisfy $\Gamma < 5/3$. Such equation of state actually makes the flow to be isentropic and the first law implies the following expression for the speed of sound and energy density ρ:

$$a^2 = \frac{dP}{dn}\frac{n}{\rho + P} = \frac{\Gamma K n^{\Gamma-1}}{m + \Gamma K n^{\Gamma-1}/\,(\Gamma - 1)}\,, \tag{8.22}$$

$$\frac{dn}{d\rho} = \frac{n}{\rho + Kn^{\Gamma}} \Leftrightarrow \rho = mn + \frac{P}{\Gamma - 1}\,. \tag{8.23}$$

Thus a^2 and ρ are functions of the baryon density alone. For numerical purposes it is convenient to reformulate the above flow equations in a slightly different manner, a manner which also reveals that if critical point exists,then necessary are sonic horizons. Namely horizons defined by the property that outgoing sound waves emitted by the background flow interior to critical sphere are actually dragged inwards. Therefore any observer in the asymptotic region is soundly disconnected from the interior of the flow. Put it differently: the sound cone is tilted inwards for all points located interior to the critical sphere. This at least for the steady flows occurs, whenever a local orthonormal observer at rest relative to the coordinate system Eq. (8.1) find the speed of the flow being identical to that of sound. The importance of sonic horizons to accretion problems is well known. As we shall presently verify the requirement that the flow passes via the critical point, allows the determination of $\dot{M}$ in terms of the asymptotic quantities. Eliminating the baryon density n in favor of the sound speed a^2 and introducing the ordinary three velocity $v = \frac{d\overline{r}}{d\overline{t}}$ measured by a local orthonormal observer,related to u via

$$u^2 = v^2\frac{1}{(1 - v^2)}(1 - \frac{2M}{r})\,, \tag{8.24}$$

Eqs. (8.16), (8.17) transformed into the following equivalent system:

$$\frac{y(1-y)(v^2-a^2)}{v^2(1-v^2)^2}\frac{dv^2}{dy} = y - \frac{2a^2}{1-v^2}\frac{4-y\overline{a}}{2-y\overline{a}}(1-y) + \frac{y(v^2-a^2)}{1-v^2}\,, \tag{8.25}$$

$$\frac{2y(1-y)(v^2-a^2)}{(1-v^2)a^2(\Gamma-1-a^2)}\frac{da^2}{dy} = -y + 2\frac{4-y\overline{a}}{2-y\overline{a}}\frac{v^2(1-y)}{(1-v^2)}\,, \tag{8.26}$$

where $y = \frac{1}{\chi}$. Adding them together one obtains:

$$[\frac{a^2}{\Gamma-1-a^2}]^{\frac{2}{\Gamma-1}}\frac{v^2}{1-v^2}\frac{(1-y)(2-\overline{a}y)^2}{y^4} = \lambda_2 \tag{8.27}$$

while dividing the first one by a^2, the second one by v^2 and add them yield:

$$\frac{(1-v^2)(\Gamma-1-a^2)^2}{1-y} = \lambda_1 \tag{8.28}$$

where the right handsides of Eqs. (8.27)-(8.28) are constants. Imposing $v = 0$ at $y = 0$ one gets $\lambda_1 = \left(\Gamma - 1 - a_\infty^2\right)^2$ while λ_2 is in general a free parameter. Its relation with the accretion rate is

$$\lambda_2 = \left(\frac{K\Gamma}{m\,(\Gamma-1)}\right)^{\frac{2}{\Gamma-1}}\left(\frac{\dot{M}}{8\pi m M^2}\right)^2\,.$$

The above integrals of motion are just the conservation laws shown in Eqs. (8.13)-(8.14). Their usefulness in establishing numerically the uniqueness of a regular transonic flow will be discusses later on.

8.3 The determination of the critical points

In order to get a better feeling about the global behavior of the flow, we should know whether the dynamical equations (8.16)-(8.18) admit critical points, and if so their character i.e. whether they are saddles, nodes etc. On general grounds, smooth flows that are subsonic at infinity and regular over the horizon (a condition that as we shall see in the next section requires $u \neq 0$) are expected to pass via critical points. This can be inferred by noting that Eq. (8.19) indicates that at radial infinity $D < 0$ while for any equation of state satisfying the causality constraint i.e. $a^2 < 1$, it follows again from Eq. (8.19) that $D > 0$ at the horizon. Therefore there will be at least one point at the black hole exterior where $D(r) = 0$. Eqs. (8.16), (8.17) shows that flows reaching such points characterized by infinity gradients in the velocity and baryon density. Physically the flow turns over and its continuation is considered as being unphysical. Physically important flows reaching "turning over points" must simultaneously satisfy:

$$D = D_1 = D_2 = 0\,. \tag{8.29}$$

Extending the flow through the critical point may be a delicate issue. Whether an unambiguous extension is possible depends upon the character of the critical points. However, as we shall see in more details in the next section the critical points are saddles and for such cases the extension is free of ambiguities. In fact demanding the flow to pass via, as well as being regular over the event horizon, singles a unique solution determined solely by the boundary conditions at infinity. In view of the significance of the critical points, their proper identification is of prime importance. By definition potential critical points of the flow equations satisfy constraints (8.29). Note that if instead of (8.16), (8.17) the alternative set of equations (8.25), (8.26) is employed, one finds that at any critical point, an orthonormal observer measures the speed of the flow being equal to the local speed of sound. Thus the critical hypersurfaces are actually sonic horizons. In the subsequent analysis we shall employ equations (8.16), (8.17) for their determination. Starting from Eq. (8.29), one infers that u_s, a_s at the potential location of the critical points r_s satisfy:

$$u_s^2 = \frac{1}{A}\frac{M}{r_s^2}\,, \tag{8.30}$$

$$a_s^2 = u_s^2\left(1 - \frac{2M}{r_s} + \frac{M}{Ar_s^2}\right)^{-1}\,. \tag{8.31}$$

Combining Eqs. (8.30), (8.31) together with Bernoulli Eq. (8.14) and in view of (8.22) the coordinates of the critical points r_s and the corresponding baryon density, n_s satisfy the following algebraic system of equations:

$$\frac{u^2}{(1-\frac{2M}{r}+\frac{M}{r^2A})}|_s = \frac{dP}{dn}\frac{n}{\rho+P}|_s\,, \tag{8.32}$$

$$(\frac{\rho+P}{n})^2(1-\frac{2M}{r}+\frac{M}{r^2A})|_s = (\frac{\rho+P}{n})^2|_\infty\,. \tag{8.33}$$

In terms of the variable $\chi = \frac{r}{2M}$ defined earlier and

$$h = \frac{\rho+P}{n} = \frac{m\,(\Gamma-1)}{\Gamma-1-a^2}\,,$$

they can be rewritten in the following manner;

$$\frac{2\chi-\overline{a}}{2\chi(4\chi-\overline{a})} = (1-\frac{1}{\chi}+\frac{2\chi-\overline{a}}{2\chi(4\chi-\overline{a})})(\frac{dP}{dn})(\frac{n}{\rho+P})|_s\,, \tag{8.34}$$

$$1-\frac{1}{\chi}+\frac{2\chi-\overline{a}}{2\chi(4\chi-\overline{a})} = \frac{h^2|_\infty}{h^2|_s}\,. \tag{8.35}$$

Introducing the function

$$\Lambda \equiv a^2|_s\frac{h^2|_\infty}{h_s^2} = a_s^2[\frac{\Gamma-1-a_s^2}{\Gamma-1-a_\infty^2}]^2\,, \tag{8.36}$$

from the last equation we have

$$\frac{2\chi-\overline{a}}{2\chi(4\chi-\overline{a})}=\frac{\Lambda}{a^2}-1+\frac{1}{\chi}\,,$$

when Eq. (8.34) gives

$$\chi=\frac{a^2}{a^2-\Lambda\left(1-a^2\right)}\,. \tag{8.37}$$

From this last equation we see that $\chi>1$, thus the critical point lies outside the event horizon. Substituting the above expressions for χ,Λ in Eq. (8.34) after long algebraic computations, we get the following equation determining the sound speed at the critical points:

$$8\Lambda a^4-2\left(1+\overline{a}\Lambda\right)a^2\left[a^2-\Lambda\left(1-a^2\right)\right]+\overline{a}\left[a^2-\Lambda\left(1-a^2\right)\right]^2=0\,. \tag{8.38}$$

This equation has been studied numerically. We have found that for various values of a_∞^2 and $\Gamma=4/3$ there always exist a solution lying in the interval $[0,\Gamma-1)$. Note for any polytropic equation of state the speed of sound is bounded above by $\Gamma-1$ see Eq. (8.22). At the critical point, using

$$h^2=m^2\left(\frac{\Gamma-1}{\Gamma-1-a^2}\right)^2=m^2(1+\frac{2a^2}{\Gamma-1})+O(a^4)\quad\text{and} \tag{8.39}$$

$$\Lambda=a^2(1+\frac{2a_\infty^2}{\Gamma-1})+O(a^4)\,, \tag{8.40}$$

we get

$$a_s^2=2a_\infty^2\frac{1}{5-3\Gamma}+O(a_\infty^4,a^4\overline{a})\,, \tag{8.41}$$

$$\chi=\frac{1}{4}\frac{5-3\Gamma}{2a_\infty^2}+O(a_\infty^4,a^4\overline{a})\,. \tag{8.42}$$

Furthermore the numerical computations confirm the expressions (8.41), (8.42). In summary therefore there always exist one critical point whose coordinate location and speed of sound are given by equations (8.41), (8.42). Notice also that expressions (8.41), (8.42) are identical to those occurring for accretion taking place on a Schwarzschild background. Utilizing the information of the flow at the critical point one easily computes the accretion rate in terms of asymptotic quantities at infinity:

$$\dot{M}=4\pi\lambda\left(\frac{2}{5-3\Gamma}\right)^{\frac{5-3\Gamma}{2(\Gamma-1)}}M^2n_\infty a_\infty^{-3}\,, \tag{8.43}$$

i.e. the same rate as if the background would have been a Schwarzschild black hole with the same mass M. The parameter λ is combination of the various numerical factors, is of order unity and independent upon $\overline{a}$, while any contribution of $\overline{a}$ appears as correction term of the order $a_\infty^4\overline{a}$.

8.4 The nature of the critical points

Having established the existence of a critical point, we shall now examine its topological nature. This entails an understanding of the way various solutions curves of Eqs. (8.16), (8.17) behave in the neighborhood of the critical point. Ultimately one like to show that for a flow that is stationary at infinity a unique regular solution exists reaching the event horizon. For that is necessary that the critical point exhibit saddle like character, which by definition implies that only two at least C^1 solution pass through the critical point. One describing accretion and the other a "stellar wind". However outflows on a black hole background are consider as unphysical since as we shall discuss further later on, they are singular over a non singular horizon. In order unravel the nature of the critical point, it is convenient to turn Eqs. (8.16), (8.17) into a three dimensional dynamical system.Introducing a parameter l along the solution curves of the system (8.16), (8.17) and defining as one column vector: $\vec{x} = [r(l), u(l), n(l)]$ one gets the equivalent three dimensional system

$$(\dot{\vec{x}})^t = (D, D_1, D_2)^t \,, \tag{8.44}$$

where overdot signifies differentiation with respect to l, while t signifies transposition of the the row vectors. In this formulation the critical points appear as equilibrium points i.e. points where the right hand-side of Eq. (8.44) is vanishing. According to Hartmann-Grobmann theorem [Per91], in the vicinity of a critical point (equilibrium point) the solution curves of (8.44) are homeomorphically equivalent to its linearized version i.e.

$$\dot{\vec{x}} = F\vec{x} \,, \tag{8.45}$$

where F stands for the differential matrix of the vector valued function defined by the right hand side of (8.44) and computed at the critical point. Denoting by A_i, B_i, C_i with $i = 1, 2.3$ the partial derivatives of D, D_1, D_2 with respect to r, u, n respectively and taking into account Eq. (8.29) one finds the following expressions valid at the critical point:

$$\begin{aligned} A_1 = -\frac{2Aa^2u}{n} \,, A_2 = \frac{2(1-a^2)}{n} \,, A_3 = -\frac{u}{na^2}\frac{\partial a^2}{\partial n} \,, \\ B_1 = \frac{u^2}{n}[\frac{2A}{n} + \frac{\partial A}{\partial r} + 2A^2a^2] \,, B_2 = \frac{2Aa^2u}{n} \,, B_3 = \frac{Au^2}{na^2}\frac{\partial a^2}{\partial n} \,, \\ C_1 = -u(\frac{2A}{r} + \frac{\partial A}{\partial r}) \,, C_2 = -2A \,, C_3 = 0 \,. \end{aligned} \tag{8.46}$$

Furthermore in terms of the partial derivatives, the characteristic equation defined by F has the following form;

$$\begin{aligned} -[(A_1 - \lambda)(B_2 - \lambda)]\lambda + [B_3C_2 + A_2B_1 + A_3C_1]\lambda \\ +[-A_1B_3C_2 + A_2B_3C_1 + A_3B_1C_2 - A_3B_2C_1] = 0 \end{aligned} \tag{8.47}$$

A straightforward computation then shows that the last term in the characteristic equation is vanishing. Therefore one of the eigenvalues is zero while by noting that $A_1 = -B_1$ the remaining two non zero eigenvalues are given by:

$$\lambda_{\pm} = \pm[-(A_1^2 + B_3C_2 + A_2B_1 + A_3C_1)]^{\frac{1}{2}} . \tag{8.48}$$

Expanding out the quantity within the square root one finds that at the critical point the eigenvalues are real and of opposite sign. Diagonalizing the differential matrix F and following the standard procedure [Per91], one may show explicitly that only two solutions pass through the critical point. Therefore locally the solution curves exhibit a saddle type behavior, implying further the existence of two distinct solutions passing through the critical point. Thus the critical point is of the same nature as the one admitted by the corresponding flow equations on a Schwarzschild background. [1] We have established the existence a unique transonic flow, subsonic at infinity, passing trough the critical point and reaching the horizon, by resorting to numerical techniques. For that we found more convenient to employ equations (8.27), (8.28). They have been plotted for values of λ_1 appropriate to typical interstellar medium and various values of the parameter λ_2. Numerically we have found that for any choice of λ_1 there a exist a critical value of λ_2 (and thus a "critical" accretion rate $\dot{M}$) such that a flow subsonic at infinity, passes through a critical point and reaches the event horizon. The various solution curves for v, a are showing in Figures 8.1,8.2.

8.5 Asymptotic analysis

If for the moment we ignore the numerical results discussed in last paragraph, the analysis of the accretion flow presented so far is entirely independent upon the particular value of $\overline{a}$. The flow up to the critical point is uniquely determined for all values of $\overline{a}$ and irrespective whether $\overline{a}$ lies within [0,2].[2] However, its continuation from the critical point inward depends whether it is propagating on a black hole background or a naked singularity. The crucial element that differentiates between the two is the set of boundary conditions obeyed by the flow on the horizon and singularity respectively. For the first case, one can naturally infer a set of conditions obeyed by the flow at the horizon. According to the standard black hole physics, one demands that nothing peculiar takes place as the flow crosses the event horizon. In particularly at the crossing no physical scalars are allowed to diverge. This kind of regularity conditions have been introduced and discussed at some length by Thorne [Tho81] and Thorne et al [TFZ81]. However for flows running on naked singularities things are rather umbigious. It not clear what conditions are to be imposed on the

[1] Although attention has been restricted to the exterior critical point,the same conclusion valid for the other critical point.The analysis utilize only relations (8.29) and these are independent of the location of the critical point.

[2] For the case of naked singularities, $\overline{a}$ must constrained so that the critical point lies outside of singular "sphere".

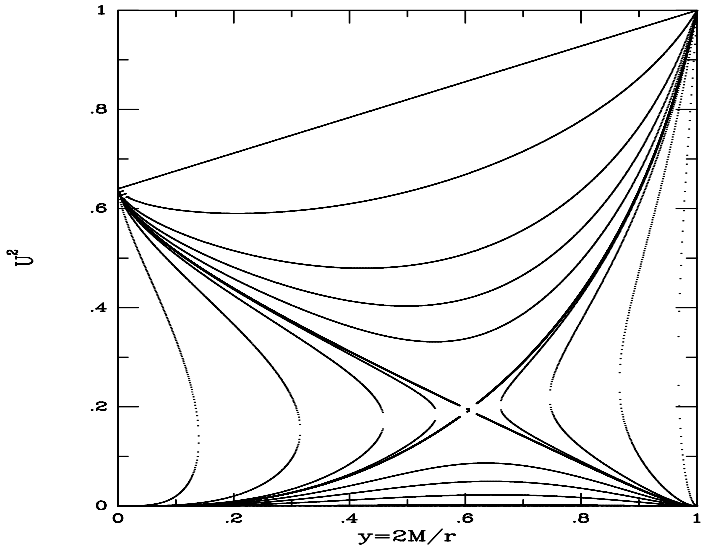

Figure 8.1: Figure shows the topology of the various solution curves for the v^2 obtained from plotting Eqs. (8.27), (8.28). In order exhibit clearly the saddle character of the critical point and the transonic solution we have taken $\Gamma = 4/3$, $\overline{a} = 1.8$, $a^2_\infty = 0.133$ and $v_\infty = 0$.

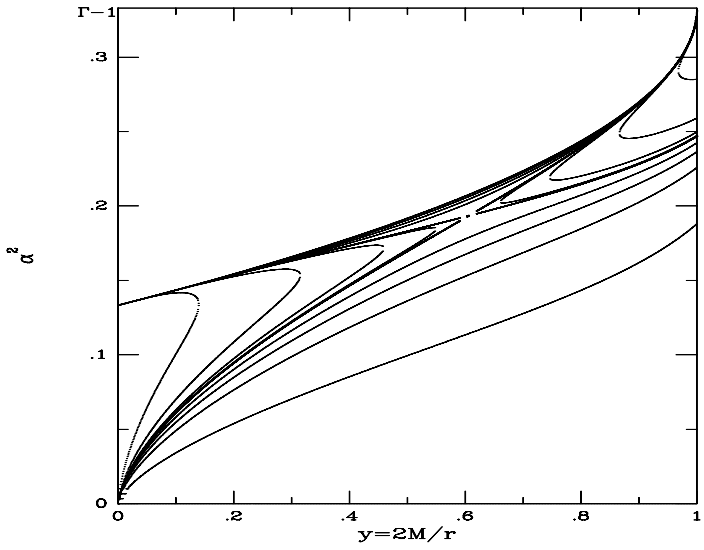

Figure 8.2: Figure shows the topology of the various solution curves for the a^2 obtained from plotting Eqs. (8.27), (8.28). The parameters are the same as in the previous figure.

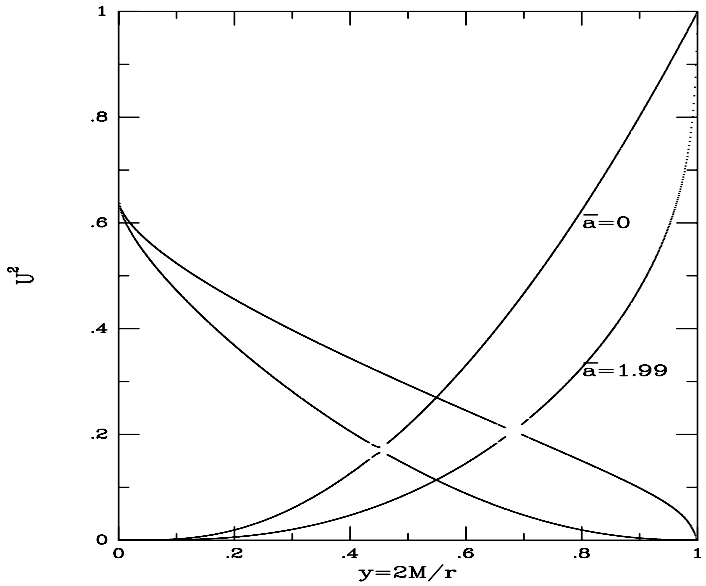

Figure 8.3: Critical solutions in the $y - v^2$ plane, for a Schwarzschild black hole $\overline{a} = 0$ and for an extreme dilatonic one $\overline{a} = 1.99$. The other parameters $\Gamma = 4/3$, $a^2_\infty = 0.133$ and $v_\infty = 0$. Note that for realistic boundary conditions $a^2_\infty \ll 1$, the critical point lies practically on the horizontal axis.

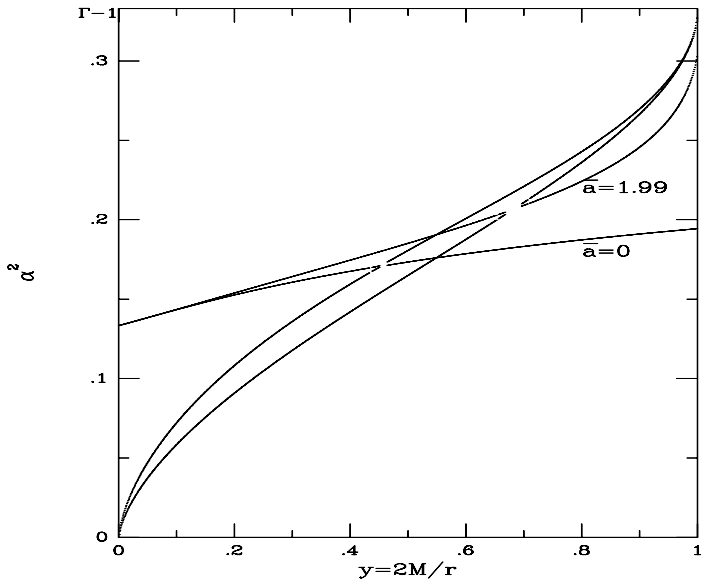

Figure 8.4: The same as in the previous figure but in the $y - a^2$ plane.

singularity. Note in particularly that for $\overline{a} = 2$ the saddle character of the critical point, at the space time singularity, implies that outflows are not a priori excluded. This point may interpreted as implying that space time singularities are totally unpredictable. Here after we shall concentrate on flows on black hole backgrounds. For our problem, it is sufficient to demand that the magnitude of the four-acceleration of the flow as well as the baryon density n are bounded at the horizon. The first condition implies that the non gravitational forces acting upon the flow are finite while a consequence of the second conditions is that all other flow parameters remain bounded as well. A straightforward calculation shows that the non vanishing components of the four acceleration vector a^μ are given by;

$$a_\mu = u^o \frac{\partial u_o}{\partial r} \delta^o_\mu + \left[u^r \frac{\partial u_r}{\partial r} + \frac{M}{r^2} \frac{1}{1 - \frac{2M}{r}} + \frac{2M}{r^2} \frac{u^r u_r}{1 - \frac{2M}{r}} \right] \delta^r_\mu \, .$$

In terms of the ordinary velocity velocity v and the parameter y introduced earlier, one finds the following expression for the magnitude $a^\mu a_\mu$:

$$a^\mu a_\mu = \frac{1}{4M} \frac{y^2}{(1-y)^{\frac{1}{2}}} \frac{1}{(1-v^2)^{\frac{1}{2}}} - \frac{y^2}{2M} (1-y)^{\frac{1}{2}} \frac{v}{(1-v^2)^{\frac{3}{2}}} \frac{dv}{dy} \, .$$

A close look at the right hand side of the above expression indicates that the magnitude of the four acceleration is unbounded on the horizon, unless $v(y)$ exhibits the following behavior;

$$v(y) = 1 + \frac{dv}{dy}|_{y=1}(1-y) + O((y-1)^2) \, .$$

In that case we find that

$$a^\mu a_\mu (y=1) \sim (\frac{dv}{dy})^{\frac{1}{2}}_{y=1} + O(y-1)^2 \, .$$

However from Eq. (8.25) one can easily infer $\frac{dv}{dy}|_{y=1}$ is non zero and bounded at the horizon. In turn equation (8.24) shows that a regular flow must have radial velocity $u = u^r$ non vanishing on the horizon. In the following the asymptotic behavior of the flow near the horizon compatible with $u \neq 0$ and bounded n will be determined for various values of the parameter $\overline{a}$ belonging to $[0, 2)$. From Eqs. (8.16), (8.17) one finds the following equations describing the flow near the horizon $\chi \approx 1^+$:

$$\frac{1}{u} \frac{du}{d\chi} \approx - \frac{\frac{1}{2\chi^2} - u^2 a^2 \frac{d}{d\chi} \ln \mid g \mid}{u^2 (1 - a^2)} \, , \tag{8.49}$$

$$\frac{1}{n} \frac{dn}{d\chi} \approx \frac{\frac{1}{2\chi^2} - u^2 \frac{d}{d\chi} \ln \mid g \mid}{u^2 (1 - a^2)} \, . \tag{8.50}$$

We shall look for asymptotic solutions describing regular flows over the event horizon. It is clear that the nature of the asymptotic solutions depends upon the

particular value of $\overline{a}$. We shall explicitly write down the closed form solutions for the two extreme cases of the $\overline{a}$, namely for $\overline{a}$ close to zero and the diametrically opposite case i.e. $\overline{a}$ extremely close to value 2. For the former case the second term in the numerator of Eq. (8.49) may be ignored. In that case demanding that u is non vanishing on the horizon, one arrives at

$$u^2(\chi) = \frac{1}{\chi}\,, \quad n(\chi) = \frac{C}{\chi^{\frac{3}{2}}}\,,$$

i.e. the well known free fall asymptotic solution on Shwarzchild background. However as we have argued earlier for a nearly extreme dilatonic black hole, the second term cannot any longer be ignored. In fact dominates the first term. In such case one finds

$$u(\chi) = A_1 g(\chi)^{\frac{a^2}{1-a^2}}\,, \quad n(\chi) = A_2 g(\chi)^{-\frac{1}{1-a^2}}\,, \tag{8.51}$$

where A_1, A_2 are arbitrary constants of integration. Demanding satisfaction of Eq. (8.13) near the horizon one finds that A_1, A_2 obey:

$$A_1 A_2 = \dot{M}\,, \tag{8.52}$$

while Bernoulli equation implies:

$$\frac{A_1}{A_2}(\rho + P) g(\chi)^{\frac{a^2+1}{1-a^2}} = [\frac{\rho + P}{n}]_\infty\,. \tag{8.53}$$

The solution are consistent provided $\rho + P = \frac{\Gamma}{\Gamma - 1} P$ i.e. $mn \approx 0$, or the rest masses are negligible. In such case we find that $a^2 = \Gamma - 1 = 1/3$ where we have taken the polytropic index to equal to 4/3. Manipulation of the above equations shows that near the horizon the baryon density is given by the following expression:

$$n(\chi) = [\frac{\Gamma K n(_\infty)}{(\Gamma - 1)(\rho + P)_\infty} \frac{\dot{M}}{g(\chi)}]^{\frac{3}{2}}\,. \tag{8.54}$$

8.6 Break down of the adiabaticity assumption

The above asymptotic solutions indicates that $n(\chi)$ became extremely high as the one allows the parameter $\overline{a}$ to get close to the extreme values. But high densities imply high temperatures. Assuming an ideal plasma then the temperature measured in the the local rest frame of the fluid is given by $T(r) = n(r)^{\Gamma - 1}$. In more realistic models of accreting interstellar medium onto a black hole, the inflowing plasma consists of a proton and an electron component of equal densities. Initially i.e. at radial infinity, both component are considered as non relativistic and thus $\Gamma = \frac{5}{3}$. Model calculations for the Schwarzschild hole show that the electron component barely becomes relativistic while the proton component remains non relativistic all the way down to the horizon. However for the dilatonic case,things may be different. The asymptotic solutions indicate

that for dilatonic black holes close to the extreme limit conditions are such that both components of the inflowing plasma become highly relativistic. Physically then one expects that many collisions such as thermal bremsstrahlung, pair creation, electron-positron annihilation and proton-proton collisions leading to pion production, to take place. Because of this important difference in the accretion near an extreme dilatonic black hole, it is natural to wonder whether the initially imposed adiabaticity assumption is still justified by the obtained solution. The large production of radiation may not any longer neglected. On the other hand adiabaticity would be consistent provided the outgoing luminosity due to various processes is negligible comparatively to the increase in the internal energy density of the plasma due to the work done by gravitational forces. As is known Bondi accretion on a Schwarzschild background indeed fulfill this requirement. To check the validity of the adiabaticity assumption for accretion on a a nearly extreme dilatonic black hole, one has to compute in details the production of photons due to various processes. This task however entails an element of uncertainty mainly due to ambiguities in the various cross sections particularly if one allows values of $\overline{a}$ that lead into pions production via proton colission. Fortunately we do not need to enter into such fine details. As we shall see taking into account only thermal bremsstrahlung it will be sufficient to conclude that indeed adiabaticity it is not consistent with the asymptotic solutions and thus treatment incorporating radiative transport is necessary. Since the sensitive region is near the event horizon we shall perform our theoretical experiment at the same region. In view of the fact that the plasma is highly relativistic, we may set without loss of generality $\Gamma = 4/3$. According to the calculations of Novikov and Thorne [NT73], a gram of the plasma in the local rest frame of the fluid losses radiation according to:

$$e_{ff} \approx T^{\frac{1}{2}} \approx n(\chi)^{\frac{\Gamma-1}{2}} \approx g(\chi)^{-\frac{1}{4}}$$

On the other hand the first law implies the rate of increase of the internal energy by the work done by gravity is given by

$$d(\frac{\rho}{n}) = K n^{\Gamma-2} g(\chi) \approx g(\chi)^{-\frac{1}{6}}$$

Comparing the two one concludes that the outgoing luminosity outweighs the internal energy gaining and thus Bondi adiabatic accretion strictly is not any longer consistent with a dilatonic black hole $\overline{a}$ approaching the extreme limit. In some sense this is rather understandable. The plasma due to the excessive heating emits much more free-free radiation in the case of extreme dilatonic black hole.

8.7 Discussion

In summary the results obtained so far, show that accretion on a dilatonic black hole may be of entirely different nature than accretion on a Schwarzschild one.

The crucial element is the value of $\overline{a}$. The breakdown of Bondi adiabatic accretion indicates the need of inclusion of radiative transport effects. However even with the inclusion of such effects we believe that outflowing luminosity would be much larger than the one would have emerged if the background was that of a Schwarzschild black hole. Since as is clear from the so far discussion is the geometry of the dilatonic black hole which causes large luminosity generation. The incorporation of radiative transport effects as well as the incorporation of the background monopole field, are currently under consideration.

This work has done in collaboration with Thomas Zannias [VZ].

Bibliography

[Bon52] H. Bondi, MNRAS **112** (1952), 195.

[GHS91] D. Garfinkle, G. Horowitz, and A. Strominger, Phys. Rev. D **43** (1991), 3140.

[Gib82] G. W. Gibbons, Nucl. Phys. B **207** (1982), 925.

[GM88] G. W. Gibbons and K. Maeda, Nucl. Phys. B **298** (1988), 741.

[Hol77] T. E. Holzer, J. Geophys. Res. **82** (1977), 23.

[HT83] S. R. Habbal and K. Tsinganos, J. Geophys. Res. **88** (1983), 1965.

[NT73] I. D. Novikov and K. Thorne, *in Black Holes*, Gordon and Breach, N. Y., 1973.

[Per91] L. Perko, *Differential Equations and Dynamical Systems*, Spring-Verlag, 1991.

[TFZ81] K. S. Thorne, R. A. Flammang, and A. N. Zytkow, MNRAS **194** (1981), 475.

[Tho81] K. S. Thorne, MNRAS **194** (1981), 439.

[VZ] N. Vlahakis and T. Zannias, unpublished.